

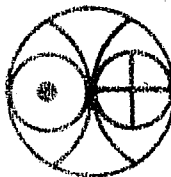
✓ 043
DHA
7527
✓

DEFORMED CONFIGURATION MIXING
SHELL MODEL STUDIES OF THE
1f_{7/2} 2p SHELL NUCLEI

BY
ASHOK KUMAR DHAR

A THESIS
SUBMITTED FOR THE DEGREE OF
DOCTOR OF PHILOSOPHY
OF THE
GUJARAT UNIVERSITY

JUNE 1976



043



B7527

PHYSICAL RESEARCH LABORATORY
AHMEDABAD
INDIA

TO MY PARENTS

SHRI MAKHAN LAL DHAR

AND

SHRIMATI RAJ DULARI DHAR

- WHO LIT IN ME THE TORCH OF LEARNING.

CERTIFICATE

I hereby declare that the work presented in this thesis is original and has not formed the basis for the award of any degree or diploma by any University or Institution.

Certified

Kumar H. Bhatt

Kumar H. Bhatt
Professor-in-Charge

Ashok

Ashok Kumar Dhar
Author

June 1, 1976.

STATEMENT

The atomic nucleus is an immensely complex system of strongly interacting fermions. It contains too many particles to be treated exactly yet too few for the adequate applicability of statistical methods. A theoretical description of such a system with a large number of degrees of freedom is possible only if these degrees of freedom are limited. This makes imperative the introduction of nuclear models. The extensive theoretical and experimental investigations to which nuclei have been subjected have often unfolded new and intriguing features of nuclear phenomena - the manifestations of strong, short range, attractive nuclear interactions.

The conventional nuclear shell model calculations in the chosen 'model' spaces using realistic and semiempirical effective interactions have successfully been performed for the description of low-lying states of nuclei in different regions of the periodic table.

The nuclei of the (fp) shell are not yet amenable to the exact (fp)ⁿ shell model calculations because of the enormously large matrix dimensionalities which are often greater than 20,000 for the angular momenta of interest.

Fortunately, the relative isolation of the $f_{7/2}$ single - particle state from the other fp shell states and the $1d_{3/2}$ state has prompted the shell model calculations in the truncated 'spherical' basis states within $(f_{7/2})^n$ or $(f_{7/2})^{n_1} (p_{3/2})^{n_2}$ with $n=n_1+n_2$ configurations. Such calculations take advantage of the importance of single particle energies in determining the dominant configurations important for the spectroscopy of the low-lying states. They however fail to take into account the coherent effects that arise due to the field producing tendency of the two body effective interactions. These effects require an enormously large basis space of the type $(f_{7/2})^{m_1} (p_{3/2})^{m_2} (p_{1/2})^{m_3} (f_{5/2})^{m_4}$ with $n=m_1+m_2+m_3+m_4$ for their description. Hence the description of a nucleus as provided by these shell model calculations is not adequate. On the other hand, the collective rotation-particle-coupling model which has been used for the studied of the fp shell nuclei includes in a collective way the role of coherent effects of the field producing part of the effective interaction. From a theoretical point of view, such calculations are not satisfactory since these collective effects are not deduced from the effective interactions between the nucleons by a microscopic calculations. Thus neither of these models provides a satisfactory description of the low-lying states of fp shell nuclei.

The present thesis describes a 'microscopic' study of nuclei using a different approach - the Deformed Configuration Mixing (DCM) calculations based on Projected Hartree-Fock theory. In this approach the effective interaction between the nucleons in presence of experimental single particle energies is allowed to generate within the full model space, in a self-consistent manner, the lowest energy intrinsic state of a nucleus. This results in the deformed basis of states which include simultaneously the coherent effects of both the single particle energies and of the various multipole field components of the effective interaction. It is, therefore, expected that the calculations based on such a deformed scheme would be more economical than the 'spherical' basis in the sense that smaller number of basis states would be required for describing the structure of the low-lying states of a nucleus. Thus the present model takes care of the limitations of the previous calculations.

The DCM calculation involves four stages:

- i) the generation of prolate and oblate Hartree-Fock intrinsic states and various other particle-hole excited intrinsic states upto a certain chosen excitation energy,

- ii) the evaluation of the expectation value of the Hamiltonian in the basis of states with definite angular momenta projected from different intrinsic states generated above,
- iii) the diagonalization of the Hamiltonian in the basis of orthonormalized projected states. This gives the energies and wave functions of the states of the composite spectrum.
- iv) These wave functions are used in the study of electromagnetic properties of the low-lying states.

Using this formalism, this thesis presents an extensive and thus far the most satisfying study of the spectra and electromagnetic properties of the low-lying states of the fp shell nuclei $^{45,47,49,51}\text{Ti}$, $^{47,48,49,51}\text{V}$ and ^{49}Cr . The deformed single particle basis states have been generated in the full $(\text{fp})^n$ configuration space. It may be mentioned that there does not exist any detailed microscopic study of these nuclei in which the effects of full fp shell are taken into account.

In all these studies, the effective interaction of Kuo and Brown modified by McGrory et al in an attempt to optimize the agreement with the experiment of the calculated

spectra of Ca isotopes has been used.

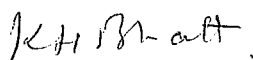
The agreement between the calculated and the experimental spectrum and electromagnetic properties of the low-lying states of the above mentioned nuclei is very good. An attempt has been made to suggest possible spin assignments to some of the observed states, on the basis of overall agreement with the experiment of the calculated energies and decay properties of these states.

The positions of the high-spin states and the decay modes of the Yrast cascades in these nuclei has been explained wherever experimental data exists and predicted otherwise.

The wave functions of the low-lying states of these nuclei have been analysed for possible band structures. Besides the ground state band, the existence of an excited low-lying collective band of states has been predicted in the spectra of the nuclei under consideration. For the nuclei $^{49,51}\text{Ti}$ and ^{51}V , there do not exist well defined ground state shapes and this is attributed to the tendency of the $(f_{7/2})^8$ neutron subshell closure that the chosen effective interaction leads to.

An interesting extension of the present detailed study has been with regard to the estimate of level densities.

of states upto about 5 MeV excitation in the nuclei. The level density of a nucleus increases with the excitation energy and above a few MeV, the experimental data indicates only the energies of these levels without much information about their parities etc. The present DCM calculations are, in principle, capable of describing these states adequately but become very time consuming. However, in view of scant experimental data, these complete DCM calculations are unnecessary. It is, however, possible to obtain an estimate of only the level density upto 5 to 6 MeV, by extrapolating the information obtained from the complete calculations for the low-lying states. The estimates of level density have usually been made by a combinatorial calculation in the basis of single particle intrinsic states which do not have a definite angular momentum. The approach presented in the thesis describes the estimate of level densities of the states of definite angular momenta and thus is an improvement over the usual methods.



K.H. Bhatt
(Professor-in-Charge)



A.K. Dhar
(Author)

ACKNOWLEDGEMENT

I feel privileged in having been given the opportunity of working at the Physical Research Laboratory, Ahmedabad. The excellent working facilities and the cordial and homely atmosphere prevailing in this institution have exerted a profound influence in my outlook and development.

Many staff members have helped me directly or indirectly whenever the occasion demanded. It is, however, almost impossible to thank them all individually. Nonetheless I wish to record with delight my explicit thanks to those who have given their generous time and assistance.

First of all, I wish to express my deep gratitude to Professor K.H. Bhatt for his invaluable guidance, supervision, inspiration and constant encouragement throughout the course of this study. His enormous patience, zeal and bubbling enthusiasm have always been a source of great stimulation to me in discussing with him various aspects of the present study over and over again. His sharp wit and comments have always provided lighter moments at the end of serious discussions.

I am also highly indebted to Professor J.C. Parikh for his continued and keen interest in this work right from the initial stages. Discussions with him have always been

illuminating and his suggestions constructive and beneficial.

For constant encouragement and interest in this work profound thanks are due to Professor S.P. Pandya. His critical comments at various stages of this work have led me to the better understanding of the subject.

Thanks are also due to Dr. S.B. Khadkikar and Dr. D.R. Kulkarni for their advice and help on some technical aspects. Their collaboration during some stages of this work has been fruitful. I acknowledge having learnt a great deal from the countless discussions with Dr. S.B. Khadkikar. Interesting discussions with my colleagues Dr. R. Haq, Mr. V. Satyan, Mr. J.J. Dikshit, Mr. V.B. Kamble and Mr. D.P. Ahalpara are also deeply acknowledged.

Dr. Dinesh Patel has been quite liberal in providing prompt and excellent facilities of the IBM360/44 computer. I express my deep appreciation to him and to the other personnel of the computing centre for their generous assistance. Special mention needs be made of Mr. P.S. Shah and Mr. H.B. Shah who helped me in the smooth and speedy running of various computer programs.

The excellent and pleasing co-operation of the library staff is delightfully acknowledged. The personnel of

the drafting and photography section have always undertaken the jobs with courtesy and cheerfulness.

Mr. V. Sahadevan has taken painstaking efforts in producing this neat thesis from my sketchy notes. He has typed till midnights the manuscript of this thesis and deserves my sincere thanks. Thanks are also due to Mr. K. Venugopalan for designing the first two pages of this thesis. Cyclostyling by Shri Ghanshyam Patel has been quite satisfactory.

The task of bringing this thesis to its present form was substantially lightened by the cheerful assistance of Dr. V.B. Sheorey, Mr. P.N. Guzdar, Mr. A.S. Sharma, Mr. S. Bujarbarua, Mr. V. Satyan and Miss S. Majmudar. They all deserve my deep appreciation.

One does not live by physics alone. My friends and colleagues have always provided an excellent and refreshing comradeship. The "adventures of ideas" with them have indeed been exciting.

Finally, I wish to express my deep gratitude to my parents for their constant encouragement and moral support.



A.K. Dhar.

CONTENTS

		Page Nos.
CERTIFICATE		iii
STATEMENT		iv
ACKNOWLEDGEMENTS		x
CONTENTS		xiii
LIST OF IMPORTANT TABLES AND FIGURES		xiv
PART I		1-32
Chapter	1 INTRODUCTION	1
PART II		37-69
Chapter	2 DEFORMED CONFIGURATION MIXING FORMALISM	37
Appendix	I Evaluation of Reduced Matrix Elements of a Tensor Operator	65
PART III	TITANIUM ISOTOPES	69-219
Chapter	3 Structure of ^{45}Ti	71
Chapter	4 Structure of ^{47}Ti	108
Chapter	5 Structure of ^{49}Ti	184
Chapter	6 Structure of ^{51}Ti	206
PART IV	VANADIUM ISOTOPES	220-317
Chapter	7 Structure of ^{47}V	221
Chapter	8 Structure of ^{48}V	240
Chapter	9 Structure of ^{49}V	266
Chapter	10 Structure of ^{51}V	295
PART V	CHROMIUM NUCLEUS	318-342
Chapter	11 Structure of ^{49}Cr	318
Appendix	II E2 Transitions in even-even Nuclei of 1f-2p Shell	343-349

LIST OF IMPORTANT TABLES AND FIGURES
(figures are given on the pages following the ones listed against them)

 ^{45}Ti

Page No.

Figure 5	Energy Spectrum	85
Figure 6	Branching Ratios and Lifetimes	99
Table 9	Static Moments	95
Table 10	B(E2) and B(M1) values within the ground state band	97
Table 11	(E2/M1) Mixing Ratios for transitions within the ground state band	98
Table 12	B(E2) and B(M1) values for the transitions within the excited K=1/2 predicted band and those to the ground state band	103

 ^{47}Ti

Ti

Figure 10	Energy Spectrum	126
Figure 11	Spectrum of High Spin States and of the K=1/2 Excited Band	128
Figure 12	Spectrum of J=1/2 and 3/2 States	132
Figure 13	Branching Ratios	145
Figure 14	B(E2) values within the K=1/2 Band	150
Figure 16	Plot of Level Density Curve	175
Table 23	B(E2) values within the ground state band	140
Table 24	B(M1) values within the ground state band	143
Table 25	(E2/M1) Mixing Ratios for transitions within the ground state band	145
Table 26	Mean Lifetimes of the members of the ground state band of states	148
Table 27	Static Moments	149

^{47}Ti

Page No.

Table 28	B(E2) and B(M1) values for Interband transitions between the members of the $K=1/2$ excited band and the members of the $K=5/2$ ground state band	153
----------	---	-----

 ^{49}Ti

Figure 19	Energy Spectrum	194
Figure 20	Branching Ratios and Lifetimes	199
Table 40	B(E2) and B(M1) values for the transition between the low-lying states	198
Table 41	Electromagnetic properties of the $K=1/2$ band.	200
Table 42	Interband Transitions	201

 ^{51}Ti

Figure 22	Energy Spectrum	212
Figure 23	Branching Ratios and Mean Lifetimes	217
Table 47	Electromagnetic properties of the ground state band	215
Table 48	B(E2) and B(M1) values within the 'hole' $K=7/2$ band	216
Table 49	Interband Transitions	217

 ^{47}V

Figure 26	Energy Spectrum	228
Figure 27	Branching ratios and Lifetimes	235
Table 53	B(E2) values for transitions within the ground state band	233

^{47}V

Table	54	B(M1) values for transitions within the ground state band	234
Table	55	(E2/M1) mixing ratios within the ground state band	234
Table	56	Static Moments	237

 ^{48}V

Figure	30	Energy Spectrum	248
Figure	31	Branching Ratios and Lifetimes	255
Table	60	B(E2) values within the ground state band	253
Table	61	B(M1) values within the ground state band	254
Table	62	(E2/M1) mixing ratios	255
Table	63	B(E2) values for transitions from states other than the ground state band	257
Table	64	B(M1) values for transition from other states	258
Table	65	Static Moments	259

 ^{49}V

Figure	34	Energy Spectrum	273
Figure	35	Branching Ratios and Mean Lifetimes	286
Table	69	B(E2) values within the ground state band	277
Table	70	B(E2) values for transitions from other states	278
Table	71	B(M1) values within the ground state band	280
Table	72	B(M1) values for transitions from other states	281 282
Table	73	(E2/M1) mixing ratios between low-lying states	284
Table	74	Mean Lifetimes of low-lying states	286
Table	75	Static Moments	290

^{51}V

Page No.

Figure 38	Energy Spectrum	307
Figure 39	Branching Ratios and Mean Life-times	311
Table 79	B(E2) values for transitions between the low-lying states	309
Table 80	B(M1) values for transitions between the low-lying states	310
Table 81	B(E2/M1) Mixing Ratios	311
Table 82	B(E2) and B(M1) values between the highly deformed excited K=3/2 band	313

 ^{49}Cr

Figure 40	Energy Spectrum	323
Figure 41	Branching Ratios	330
Figure 42	B(E2) and B(M1) values for the K=1/2 band	332
Table 85	B(E2) values within the ground state band	326
Table 86	B(M1) values within the ground state band	328
Table 87	(E2/M1) mixing ratios	329
Table 88	Mean Lifetime	331
Table 89	Static Moments	332
Table 90	Interband Transitions	334

PART I

CHAPTER 1

INTRODUCTION

INDEX

CHAPTER 1

1.	INTRODUCTION	1
	PREVIOUS STUDIES	2
2.	SHELL MODEL CALCULATIONS	2
2.1	The Model Spaces, Effective Interactions and Operators	2
2.2	The Dimensionalities	3
2.3	Truncated Shell Model Calculations	4
2.3.1	The Truncation Schemes	4
2.3.2	Calculations in the Truncated "Spherical" Basis	6
2.3.3	Calculations in the Truncated "Deformed" Basis	15
2.3.4	Deformed State Admixtures in fp Shell	17
3.	COLLECTIVE MODEL CALCULATIONS	18
3.1	Rotation-Particle-Coupling Model Calculations	18
3.2	Intermediate-Coupling Model Calculations	19
	PRESENT STUDIES	21
4.	MICROSCOPIC DEFORMED CONFIGURATION MIXING CALCULATIONS	21
4.1	The Motivation	21
4.2	Choice of Effective Interaction	24
4.3	Choice of Effective Operators	27
	REFERENCES	30

CHAPTER 1

1. INTRODUCTION

This thesis is concerned with the description of the spectra and electromagnetic properties of the low-lying collective states of the nuclei in the beginning of 1f-2p shell. The studies have been carried out in the frame work of deformed configuration mixing calculations based on projected Hartree-Fock theory.

No systematic and detailed microscopic studies taking into account the effects of full $(fp)^n$ space have thus far been performed for the study of nuclei in this region. However some of these nuclei have been studied¹⁾ with varying degrees of complexities according to the following prescriptions:

- i) The microscopic shell model calculations - mostly in the truncated spaces, and
- ii) The collective model calculations - mostly the ones based on rotation-particle-coupling model.

We shall first give briefly an over-view of these previous calculations, point out their successes and limitations and then see how the method adopted in the present study besides being satisfying takes care of the objection and limitations of the previous calculations.

PREVIOUS STUDIES

2. THE SHELL MODEL CALCULATIONS

2.1 The Model Spaces, Effective Interactions and Operators

The introduction of nuclear shell model has been one of the major triumphs in the studies of nuclear structure. The model envisages that the properties of nuclei can be described reasonably well by the interplay of a few valence particles outside a closed core nucleus - usually chosen to be the magic or semimagic nucleus. This notion of restricting the degrees of freedom of the nuclear system leads to the concept of "model" spaces and hence to "effective" interactions and operators defined for the chosen "model" space. The success of the shell model calculations in describing the properties of the low-lying states of a nucleus, hinges on the choice of the "model" space and the "proper" effective interactions and the effective electromagnetic operators.

In absence of the detailed knowledge about nuclear interactions, various prescriptions²⁾ have been followed to obtain these "effective" hamiltonians and operators. These involve their deduction either in a phenomenological manner from the observed properties of nuclei or in a realistic

manner by a microscopic calculation³⁾ starting with free nucleon-nucleon interaction. The effective electromagnetic operators have also been obtained⁴⁻⁷⁾ in a similar way.

It might be mentioned that the manner in which the various terms in the derivation of "realistic" effective interactions and operators, have been included, is not free from controversies^{4,8)}. It is for this reason that the semi-empirical modifications of these realistic interactions become necessary for the best overall agreement with the experiment.

2.2 The Dimensionalities

The nuclear shell model calculations within the full $(fp)^n$ configuration space are not feasible because of the enormously large matrices that are to be diagonalized. In the table given below, are presented the matrix dimensionalities⁹⁾ for the $T=1$, $J=0, 2, 4, 6, 8$ states of nuclei with a few

J	$d_{5/2} - s_{1/2} - d_{3/2}$			$f_{7/2} - p_{3/2} - p_{1/2} - f_{5/2}$		
	n = 6	8	12	6	8	12
0	148	481	1372	1514	17437	671159
2	525	1992	5768	6338	77907	3067868
4	502	2131	6562	8026	106132	4461696
6	255	1293	4434	6606	98092	4984885
8	67	460	1882	3896	68599	3745740

valence particles (n) in the fp shell space. For comparison, are also tabulated the corresponding dimensionalities for these states in the ds shell space.

It is seen than the matrix dimensionalities for a few particles tend to unmanageable numbers as the number of valence particles increases and the "model" space expands. For this reason complete shell model calculations have, thus far, been possible for the nuclei upto the ds shell. The ones that are performed in the $(fp)^n$ space are for the nuclei with $A \leq 44$.

2.3 Truncated Shell Model Calculations

Owing to the prohibitively large matrix dimensionalities the shell model calculations for fp shell nuclei have usually been performed in truncated spaces, differing from each other in the choice of configuration space and the effective interactions and operators.

2.3.1 The Truncation Schemes

Two types of truncation schemes have commonly been adopted. These are:

- i) those based on the one-body part of the Hamiltonian
- and ii) those based on also the two-body part of the Hamiltonian.

2.3.1.1 Scheme-1: The Truncated "Spherical" Basis

This scheme is based on the property of only the single particle part of the Hamiltonian. It exploits the relative isolation of the $f_{7/2}$ single-particle state from the $1d_{3/2}$ and $2p_{3/2}$ single particle states as a means of confining nucleons to the $1f_{7/2}$ state if N and $Z \leq 28$. For nuclei with N or $Z \geq 29$, the $1f_{7/2}$ subshell is regarded as full and extra nucleons confined to $p_{3/2}$, $f_{5/2}$ and/or $p_{1/2}$ single-particle states. Amongst the shell model calculations performed on the basis of this truncation scheme are the j - j coupled spherical shell model calculations in the $(f_{7/2})^n$ configuration and those which also include partially the effects of other fp shell single-particle states.

2.3.1.2 Scheme-2: The Truncated "Deformed" Basis

This type of truncation scheme while taking into account the relative isolation of the $f_{7/2}$ state also recognizes the dominant field producing tendency¹⁰⁾ of the two-body effective interaction. The studies of the f - p shell nuclei that have thus far been performed on the basis of this truncation scheme are in general the projected Hartree-Fock or projected Hartree-Fock-Bogoliubov calculations.

2.3.2 Calculations in the Truncated "Spherical" Basis

Such calculations take advantage of the importance of single-particle energies in determining the dominant configurations important for the spectroscopy of the low-lying states. They, however, fail to take into account the coherent effects that arise due to the field producing tendency of the two-body effective interaction since these effects require an enormously large basis space of the type $(f_{7/2})^{n_1} (p_{3/2})^{n_2} (p_{1/2})^{n_3} (f_{5/2})^{n_4}$ with $n = n_1 + n_2 + n_3 + n_4$ for their description.

We shall now discuss briefly the various calculations that have been performed in this truncated scheme.

2.3.2.1 The $(f_{7/2})^n$ Configuration Model Calculations

Nuclei with $20 \leq N$ and/or $Z \leq 28$ have been treated¹¹⁻¹⁷⁾ in this model. The low-lying states of these nuclei are described by the interplay of the valence nucleons in the isolated $f_{7/2}$ state.

A comprehensive calculation for most of the nuclei in the $(f_{7/2})^n$ model space has been performed by McCullen, Bayman and Zamick¹³⁾ (MBZ). Many of the observed properties of the low-lying states of nuclei in this region are reasonably accounted for. Calculations¹⁴⁻¹⁷⁾ within this model space have since

been performed or repeated for many of these nuclei in view of the availability of the new experimental data on the spectra of ^{42}Sc from which two-body matrix elements can be obtained. The energies of the low-lying high-spin states as predicted by this model are found to be generally in reasonable agreement¹⁸⁾ with the recent observations of heavy-ion induced reactions. However, there exist serious discrepancies¹⁹⁾ between the experiment and the $(f_{7/2})^n$ configuration calculations, as regards the energies of the excited states and the electromagnetic properties of the low-lying states of a nucleus. For example, in the nuclei ^{45}Ti , $^{47,49}\text{V}$ experimentally a ground state triplet of states with $J=(3/2, 5/2, 7/2)$ is observed. The $(f_{7/2})^n$ model calculation for these nuclei reproduces the first $J=3/2^+$ state above by about an MeV. Furthermore on the basis of such a model the spectra of nuclei having same number of particles or holes in the $1f_{7/2}$ shell are expected to have identical spectra. Such features, in general, are not observed in these particle-hole conjugate nuclei. Lawson¹⁴⁾ pointed out an interesting symmetry arising in the $(f_{7/2})^n$ model for the self-conjugate nuclei. According to this model the M1 transitions between the states having "opposite" signatures, should be forbidden. The experimental data¹⁶⁾, however, indicates the breakdown of this proposed selection rule. Another very remarkable disagreement of the $(f_{7/2})^n$ confi-

guration with the observed data concerns the level density in the low-excitation energy region. For example, in ^{45}Sc , ten levels below 1.6 MeV have been observed while as only one is expected on the basis of $(f_{7/2})^5$ model calculations.

Similarly, for the agreement with the observed E2 transitions between the low-lying states of a nucleus, large effective charges are required¹⁶⁾ in the $(f_{7/2})^n$ configuration model.

All these limitations point to the importance of the other fp shell configurations for the description of the low-lying states of nuclei in this region. It should, however, be mentioned that inspite of the many limitations of the $(f_{7/2})^n$ model calculations, they have been quite influential in the understanding of nuclei in the lower fp shell region.

2.3.2.2 Extended "Spherical" Shell Model Calculations

Such calculations include more than $(f_{7/2})^n$ configuration and are improvements over the pure $(f_{7/2})^n$ configuration model calculations. The configurations that have been considered are:

i) Those involving besides $(f_{7/2})^n$ configuration, the ones of the kind $(f_{7/2})^{n-m} (p_{3/2})^m$ with $m = 1$ or 2 , in which one or two $f_{7/2}$ neutrons are excited to the $p_{3/2}$ state. The

isotopes $^{42-47}\text{Ca}$ and $N=28$ isotones have been studied²⁰⁻²⁴⁾ in such a configuration space. Two body matrix elements were treated as fitting parameters.

ii) The $(f_{7/2} - p_{3/2})^n$ configuration. Raz and Soga²⁵⁾ performed shell model calculations in this space for the isotopes of Ca with $A=42-45$. The effective two-body interaction with seven free parameters was chosen to give best fit to the several sets of observed spectrum. This calculation showed the importance of the $p_{3/2}$ neutron orbit in the explanation of the low-lying $J=3/2^-$ state in $^{43,45}\text{Ca}$.

iii) The $(\pi f_{7/2})^{n_1} (\nu p_{3/2} - p_{1/2} - f_{5/2})^{n_2}$ with $n_1 + n_2 = n$ configurations. Such calculations regard ^{48}Ca as the closed core and consider a few valence neutrons outside the core nucleus. Nuclei with $Z \leq 28$ and $N > 28$ have been described²⁶⁻³⁰⁾ in such a configuration. Regarding ^{48}Ca as the closed core, Vervier²⁶⁾ and Horie and Ogawa²⁷⁾ treated $N=29$ nuclei while McGrory²⁸⁾ treated $N=30$ nuclei in this configuration space, and found good agreement with experiment for a large number of energy levels, spectroscopic factors and some β -decay and electromagnetic transition rates.

McGrory also performed a calculation in which ^{56}Co was regarded as ^{40}Ca core plus 14 or 15 nucleons in the $f_{7/2}$ orbit

and the remaining ones in the $p_{3/2}$, $f_{5/2}$ and $p_{1/2}$ orbits. For the E2 transition effective charges $e_p = 1.5e$, $e_n = 0.5e$ were used, while for M1 transition rates bare operators were used. An excellent description of the electromagnetic transitions in ^{56}Co was obtained.

2.3.2.3 $(p_{3/2} - f_{5/2} - p_{1/2})^n$ Configuration Model Calculations

Nuclei with N and $Z > 28$ have been studied³¹⁻³⁷⁾ in this configuration, regarding ^{56}Ni as the closed core. Calculations have been done mostly for the isotopes of Ni and for some of the isotopes of Cu.

Various authors have studied³¹⁻³⁶⁾ Ni isotopes in the $(p_{3/2} - f_{5/2} - p_{1/2})^n$ space with different effective interactions. Shimizu and Arima³⁵⁾ also included in their study of ^{58}Ni the excitations of particles resulting in 3p-1h and 4p-2h contributions from ^{56}Ni core. Reasonable agreement with the experiment was obtained.

A systematic study of the electromagnetic transitions in Ni isotopes has recently been made by Glaudemans et al³⁶⁾. The effective charge $e_n = (1.70 \pm 0.08)e$ has been found to give a best fit to the 33 measured E2 transition strengths and quadrupole moments in these nuclei. However, significant

discrepancy between the experiment and calculation is observed for the quadrupole moment of the 2^+ state of ^{60}Ni .

The large effective charge needed in this calculation shows that the deformation of ^{56}Ni 'core' is very important.

2.3.2.4 Restricted (fp)ⁿ Shell Model Calculations

Extensive shell model calculations for the $^{42-50}\text{Ca}$ isotopes have been carried out by McGrory et al.³⁸⁾ Assuming an inert ^{40}Ca core, two sets of basis vector spaces were considered:

- i) the basis space with $f_{7/2}$, $p_{3/2}$, $p_{1/2}$, $f_{5/2}$ single particle active states,
- ii) the space with $f_{7/2}$, $p_{3/2}$, $p_{1/2}$, $f_{5/2}$ and $g_{9/2}$ active neutron orbits.

The distributions of valence neutrons of the Ca isotopes in these basis spaces were governed by considering all Pauli allowed configurations of the form $(f_{7/2}^{n_1} p_{3/2}^{n_2} j_1^{n_3} j_2^{n_4})$ with $n = n_1 + n_2 + n_3 + n_4$ and $n_3 + n_4 \leq 2$. The orbits j_1 and j_2 could either be $p_{1/2}$, $f_{5/2}$ or $g_{9/2}$. The restriction $n_3 + n_4 \leq 2$ was made to reduce the matrix dimensionalities for heavier Ca isotopes. Kuo-Brown effective interaction³⁾ was employed. The calculations with this interaction showed that while the spectra of $^{42}\text{Ca} - ^{46}\text{Ca}$ could be explained successfully, the

spectra of the nuclei ^{47}Ca to ^{50}Ca , in contrast could not be reproduced. McGrory et al modified by least squares fit some of the $T=1$ matrix elements of the Kuo-Brown interaction, in an attempt to optimize the agreement between the experiment and the calculated spectra of all the $^{42}\text{Ca} - ^{50}\text{Ca}$ isotopes. The modifications were made in two stages:

i) The matrix elements $\langle f_{7/2}^2 J | V | f_{7/2}^2 J \rangle$ for $J=0$ and 2 were made more attractive by ~ 0.3 MeV and all the $T=1$, $\langle f_{7/2} p_{3/2} J | V | f_{7/2} p_{3/2} J \rangle$ matrix elements were made repulsive by about 0.3 MeV. All others were kept at the same value as Kuo-Brown matrix elements. This raised the Centre of Gravity (C.G) of $\langle f_{7/2} p_{3/2} J | V | f_{7/2} p_{3/2} J \rangle$ interaction from -0.1 MeV to $+0.2$ MeV. Calculation with these modified (called here MWH1) matrix elements showed that while the spectra of the nuclei $^{42-46}\text{Ca}$ were slightly improved in agreement than with the Kuo-Brown interaction, the spectra of the isotopes $^{47-50}\text{Ca}$ were still in disagreement with the experiment.

ii) To optimize the agreement for these heavier Ca isotopes, McGrory et al made further modification by adding $+250$ keV to all the diagonal matrix elements of the form

$$\langle f_{7/2} p_{1/2} J | V | f_{7/2} p_{1/2} J \rangle \text{ and } \langle f_{7/2} f_{5/2} J | V | f_{7/2} f_{5/2} J \rangle.$$

The effect of this change was to raise the C.G. of the

interaction of a nucleon in $f_{7/2}$ with that in $f_{5/2}$ and $p_{1/2}$ orbits. We label these modified matrix elements as MWH2.

The calculations with such a modified (MWH2) interaction showed that although the agreement for $^{42-46}\text{Ca}$ was not significantly different from that obtained with MWH1 interaction, the agreement for other Ca isotopes was considerably improved.

These calculations suggested that in the effective interaction of Kuo and Brown, the interactions of $f_{7/2}$ particles with $p_{1/2}$ and $f_{5/2}$ particles are too strong. The calculation further indicated that the effects of excitations of particles from the ^{40}Ca core into the fp shell spaces, are significant above about 2.5 MeV in ^{42}Ca though ^{50}Ca .

McGrory³⁹⁾ performed another shell model calculation for the nuclei with $A \leq 44$ ($^{42-44}\text{Ca}$, $^{42-44}\text{Sc}$) in the $(fp)^n$ space. Assuming that the most important matrix elements in the calculation were those involving $|f_{7/2}^2 JT\rangle$ states, McGrory treated eight matrix elements involving these states as free parameters to renormalize the Kuo-Brown effective interaction, given for $(fp-g_{9/2})$ space so as to be used in the fp space. The eight matrix elements were varied to optimize the agreement between the calculation and observation for the energies of 29 states and for seven ground state binding energies. The $\langle f_{7/2}^2 J T=1 | V | f_{7/2}^2 J T=1 \rangle$ matrix

elements obtained in this calculation are very similar to those of the MWH2 interaction of McGrory et al.

McGrory also studied the electromagnetic transition rates for these nuclei with $A \leq 44$. The E2 transitions were calculated using, in general, state independent effective charges $e_p = 1.2e$ and $e_n = 0.5e$. However for the transitions in ^{42}Ca and ^{42}Sc , the neutron effective charge was taken to be $e_n = e$. The calculated $B(E2)$ values were found to be smaller than the observed values even with the effective charges $e_n = e$. This discrepancy has been attributed to the admixture of the highly deformed states resulting from the excitation of the sd shell nucleons into the fp shell.

For M1 transitions various effective operators involving the corrections due to meson fields were considered. Reasonable agreement in some cases with the experiment was obtained.

An important feature that resulted from this calculation was that besides the modifications in the $T=1$ matrix elements of Kuo-Brown interaction, needed by McGrory et al.³⁸⁾, the changes in $T=0$ matrix elements were also found necessary.

The only other shell model calculation performed⁴⁰⁾ in the full $(fp)^n$ space is for the nucleus ^{44}Ti . Using Kuo-Brown effective interaction, a reasonable agreement with the experimental spectrum was obtained.

2.3.3 Calculations in the "Deformed" Basis

These calculations are not as common as the conventional shell model calculations. These calculations take into account the effects of the single-particle energies as well as the coherent effects of the field producing components of the effective interaction between the valence nucleons in determining the dominant configurations necessary for the description of the low-lying states.

In this approach the "deformed" basis states are obtained in the following way: The effective interaction between the nucleons is allowed to generate in a self consistent way a deformed intrinsic state by carrying out a Hartree-Fock or Hartree-Fock-Bogoliubov calculations for the valence nucleons in the full $(fp)^n$ space. The basis states for describing the low-lying states of the nucleus are then obtained by projecting out the states of definite angular momentum from the deformed intrinsic state.

The hope that this approach would be successful in describing the low-lying states of the comparatively less deformed fp shell nuclei arises from the following fact.

It has been shown^{11,12)} that the low-lying shell model states of nuclei in the $(f_{7/2})^n$ space are well projectable from the Hartree-Fock intrinsic state generated in this space.

This implies that even for "zero deformation" projected Hartree-Fock states correspond reasonably well to the collective states of these nuclei.

The absence^{10,41-43)} of the well developed rotational spectra for the nuclei in the beginning of fp shell indicates that these nuclei are not well deformed. However, because of the above fact, it is expected that even for small deformations, the low-lying collective states in the $(fp)^n$ space would be projectable, reasonably well from the corresponding HF intrinsic states generated in the $(fp)^n$ space. On the basis of such a model, the calculations that have thus far been made are mainly for the description of the "ground state bands" of even-even nuclei in the fp shell. These include the projected Hartree-Fock (HF) or Hartree-Fock-Bogoliubov (HFB) calculations⁴⁴⁻⁵¹⁾ with different choices of the effective interactions. HF and HFB calculations have also been done⁵²⁻⁵⁵⁾ for some of the even-even and odd-A nuclei in the beginning of fp shell. The agreement of these calculations with the experiment varies from quantitative in some cases to qualitative in most of the cases. The spectra are generally found to be compressed, but the electromagnetic transitions appear to be reasonably well described by the effective charges ranging from $e_p = (1.5 - 1.7)e$ and $e_n = (0.5 - 0.7)e$.

These reasonable effective charges needed in these deformed microscopic calculations imply that the chosen deformed configuration adequately takes into account the coherent effects of the dominant field producing components of the effective interaction.

2.3.4 Deformed State Admixtures in fp Shell

The presence of a number of low-lying states and large E2 enhancements, which do not arise in $(fp)^n$ space have been very well understood in terms of the deformed configuration mixing calculations of Gerace and Green⁵⁶⁾ and Flowers and Skouras^{57,58)}. The calculations involve the excitation of particles from the ^{40}Ca closed core to the f-p shell space.

The existence of mysterious low-lying states in ^{42}Ca and ^{42}Sc which could not be explained on the basis of $(fp)^n$ calculation prompted Flowers and Skouras⁵⁷⁾ to explain the energy spectrum of these $A=42$ nuclei by considering in their wave function of two particle states in the fp shell, the admixtures of 4p-2h states arising by the excitation of two particles from ^{40}Ca core. In general, there are a large number of $(ds)^{-2} (fp)^4$ states. Taking advantage of the field producing components of the effective interaction, they included in the calculation only those states of the four

nucleons in fp shell that were projected from the highly deformed $K=0$ ($K = \sum_i k_i$ with $k = \langle j_z \rangle$ the expectation value of angular momentum along the axis of symmetry) intrinsic state obtained by putting four particles in the lowest $k=1/2^-$ orbit of the fp shell. All $(sd)^{-2}$ states were included in the calculation. Yukawa-Rosenfeld interaction was used and the $d_{3/2}^- f_{7/2}$ single particle energy treated as a parameter to optimize the agreement between theory and experiment. Large number of E2 transitions between these deformed and "normal" $(fp)^2$ configuration states were found to be reproduced well with an effective charge $e_p = 1.75e$, and $e_n = 0.75e$.

A similar calculation for the explanation of "core excited" states in ^{46}Ti has been performed recently by Skouras⁵⁸⁾. A good agreement with the experiment for both energy levels and transition rates is obtained. Effective charges $e_p = 1.5e$, $e_n = 0.5e$ were found to give best overall fit for the observed E2 rates.

3. THE COLLECTIVE MODEL CALCULATIONS

3.1 Rotation-Particle-Coupling Model Calculations

Detailed calculations for odd-A nuclei in the lower fp shell have been performed by Malik and Scholz⁵⁹⁾ in the framework of strong coupling collective model. In this model all

but the odd nucleon are incorporated in the definition of the deformed "core". Axial symmetry for this "core" nucleus is assumed. The motion of the odd particle in such an axially symmetric potential leads to the coriolis term $(=\vec{I} \cdot \vec{j})$, where \vec{I} is angular momentum of the deformed "core" nucleus and \vec{j} of the odd particle) that couples the particle motion to the core nucleus. Various intrinsic states are obtained by varying the occupancies of the odd nucleon.

The model with all its simplicity has been quite successful in reproducing reasonably well the observed properties of many fp shell nuclei. The success of this model has enhanced the understanding and appreciation of the effects of the deformation on the structure of the low-lying states of these nuclei. Indeed, the dramatic consequences of deformation on the spectra of ^{45}Ti , $^{47,49}\text{V}$ were predicted by this model.

However, from a theoretical point of view, such calculations are not satisfactory since the collective effects are not deduced from the effective interaction between the nucleons by a microscopic calculation.

3.2 Intermediate Coupling Model Calculations

Some of the odd-A nuclei in the fp shell have also been studied⁶⁰⁻⁶⁴⁾ by the intermediate or weak coupling model

calculations. These calculations involve the coupling of the odd nucleon to the even-even core nucleus. The interaction between the core nucleus and the odd nucleon is usually considered⁶³⁾ to be of quadrupole-quadrupole form. Configurations involving upto three phonon excitations of the core nucleus have also been considered.

The calculations that have been performed in this model are for the isotopes of Mn, Fe, Cr, Zn and Ga. For the description of Cu isotopes with $A=59$ to 65 , Castei et al⁶¹⁾ considered also the effects of the observed anharmonicity in the "core" states of Ni isotopes. The resulting agreement for E2 and M1 transition was reasonably good. Dikshit and Singh⁶⁴⁾ performed a similar calculation for $^{55,57}\text{Fe}$ by considering the anharmonicity of $^{54,56}\text{Fe}$ and allowing the odd nucleon in ^{55}Fe to occupy $p_{3/2}$, $f_{5/2}$ and $p_{1/2}$ states. The calculated $B(M1)$ values are in significant disagreement with the observed values. However, E2 rates are well reproduced.

PRESENT CALCULATIONS

4. MICROSCOPIC DEFORMED CONFIGURATION MIXING CALCULATIONS

4.1 The Motivation

This thesis describes a microscopic study of odd-A nuclei in the 1f-2p shell in the framework of Deformed Configuration Mixing (DCM) calculations based on projected Hartree-Fock theory.

For the fp shell nuclei the projected HF and HFB calculations seem to provide an adequate description of the experimental ground state band of states. For the description of the states other than the ground state band, it is necessary to carry out, in the framework of the angular momentum projection scheme, the mixing of various excited HF states and of the bands resulting from different particle-hole (p-h) excitations from the lowest energy HF solution.

The axially symmetric HF solutions corresponding to prolate and oblate shapes of fp shell nuclei are usually close to each other in energy. Also, due to the antiquadrupole field sequence¹⁰⁾ of the single particle energies, the HF states of fp shell nuclei are likely to be less stable than those of the sd shell. It is expected therefore that

the Hamiltonian might appreciably mix the states projected from various p-h excited intrinsic states with those projected from the HF state.

The main advantages of performing such a configuration mixing calculation in the deformed basis generated in a self consistent manner according to the HF theory can be easily appreciated by comparing it with the "spherical" basis $\left[(j_1)^{n_1} (j_2)^{n_2} \dots \right]$ JT coupling scheme and with the SU(3) LSJT basis⁶⁵⁻⁶⁷).

The "spherical" basis takes advantage of the relative importance of the single particle energies in determining the dominant configurations which play an important part in the spectroscopy of the low-lying states. However, it does not anticipate the field producing tendency of the effective interaction. As a result, a large number of spherical basis states are needed to properly describe the structure of the low-lying states. On the other hand the SU(3) coupling scheme clearly recognizes the dominant quadrupole field tendency of the two-body interaction. It does not take into account the effects of the higher multipoles of the effective interaction as well as the highly significant role of the single-particle spin-orbit interaction in determining the structure of the low-lying states. The SU(3) basis is however more economical than the spherical basis in the sense that the

number of configurations needed to describe the states is much smaller than those needed in the spherical basis.

The DCM calculations⁶⁸⁾ based on projected HF theory takes into account partially the importance of the single particle energies as well as that of the various multipole field components which the interaction gives rise to. It is therefore expected that the deformed basis based on HF state would be more economical than the SU(3) basis for describing the structure of the low-lying states of nuclei. This choice of the basis states is also appropriate for the identification of band structure in nuclear spectra.

The DCM calculation involves four stages:

- i) the generation of prolate and oblate HF intrinsic states and various other p-h excited intrinsic states upto a certain chosen excitation energy.
- ii) the evaluation of the expectation value of the Hamiltonian in the basis of states with definite angular momenta projected from different intrinsic states generated above,
- iii) the diagonalization of the Hamiltonian in the basis of orthonormalized projected states. This gives the energies and wave functions of the states of composite spectrum.
- iv) These wave functions are used in the study of electro-

magnetic properties of the low-lying states.

Using this formalism, this thesis presents an extensive and thus far the most satisfying study⁶⁸⁻⁷⁸⁾ of the spectra and electromagnetic properties of the low-lying states of the fp shell nuclei $^{45,47,49,51}\text{Ti}$, $^{47,48,49,51}\text{V}$ and ^{49}Cr . The deformed single particle basis states have been generated in the full $(fp)^n$ configuration space. It may be mentioned that there does not exist any detailed microscopic study of these nuclei in which the effects of full fp shell are taken into account.

4.2 Choice of the Effective Interaction

In all the calculations presented in this thesis, Kuo-Brown³⁾ effective interaction modified by McGrory et al³⁸⁾ in an attempt to optimize the agreement with the experimental spectra of Ca isotopes has been used. This modification of Kuo-Brown interaction involves the 'sinking' of the C.G. of the interaction between two nucleons in the $1f_{7/2}$ state and 'raising' the C.G. of the interaction of a nucleon in $1f_{7/2}$ with a nucleon in $2p_{3/2}$, $2p_{1/2}$ and $1f_{5/2}$ states. We have labelled this modified Kuo-Brown interaction as MWH2 in subsec.2.3.2.4.

It is interesting to compare^{79,80)} the deformation producing tendency of this semi-empirical, semi-realistic MWH2

interaction with that of the "realistic" Kuo-Brown interaction.

The experimental data indicates a tendency for shell closure for nuclei with $N=28$. The MWH2 interaction is consistent⁷⁹⁾ with this trend. Except for ^{52}Cr , it gives rise to HF states for $N=28$ nuclei having a deformation smaller than those for the nuclei with $N=26$ and 30 . The $f_{7/2}$ neutron sub-shell is almost closed in the HF state of $N=28$ nuclei. The $f_{7/2}$ subshell is completely filled in the HF state of ^{56}Ni .

In contrast to MWH2 interaction, the Kuo-Brown effective interaction leads^{79,80)} to a HF state with large deformation for the nuclei with $N=28$ and hence is not consistent with the experimental observations. Thus the calculations with Kuo-Brown interaction, will not provide even a reasonable description of fp shell nuclei. It is for this reason that we have chosen MWH2 interaction in our calculations. However, this interaction too has the following limitations.

i) Although the MWH2 interaction reproduces well the spherical HF solution of ^{56}Ni , it does not reproduce⁸¹⁾ very well the single-particle or hole energies of ^{57}Ni and ^{55}Ni relative to closed ^{56}Ni . This interaction gives for ^{57}Ni the single-particle states with $p_{3/2}$ and $p_{1/2}$ at 0.54 and 0.67 MeV respectively relative to the $f_{5/2}$ single-particle

state. The observed single-particle energies for $p_{3/2}$, $f_{5/2}$ and $p_{1/2}$ states are 0, 0.78 and 1.08 MeV respectively.

Thus the calculations with MWH2 interaction for the nuclei with $N \geq 28$ would be in error and might become serious in the calculations of pick up or stripping strengths etc.

It is because of this inadequacy of the MWH2 interaction that we have restricted our calculations mainly for the nuclei with $N \leq 28$. For these nuclei the above limitation is not very serious.

ii) The HF calculations with MWH2 interaction lead⁷⁹⁾ to two distinct solutions with less and more deformation for the nuclei with $N=28$ and also⁸²⁾ for some of those with $N=26-29$ like $^{50-53}\text{Cr}$, $^{52,53}\text{Fe}$. As mentioned above, for the nuclei with $N=28$, the neutron $(f_{7/2})^8$ subshell is almost full in the less deformed HF solution. For all the nuclei the less deformed HF solution is lower in energy than the more deformed one except in the case of ^{52}Cr , for which the HF state with large quadrupole moment is the lowest. However, for this nucleus the less deformed HF intrinsic state is also very close in energy to the more deformed one.

There is some evidence^{83,84)} of the existence of such excited, 'deformed' bands in the spectra of $^{51,53}\text{Cr}$, ^{53}Fe .

The calculations with MWH2 interaction, for these nuclei, give very small energy separation between the ground state and these excited band heads compared to their observed separations. Thus the MWH2 interaction does not, in general, reproduce very well the band-head separations.

4.3 Choice of the Effective Operators

The description of electromagnetic properties of nuclei in a chosen model space requires the use of effective operators appropriate for the chosen space. Analogous to the microscopic derivation^{2,3,4)} of effective interactions various attempts have been made for obtaining⁴⁻⁷⁾ the effective charges for the description of E2 transition rates. There is a large uncertainty in the values of effective charges resulting from these microscopic calculations⁶⁾. However, the recent calculation of Kuo and Osnes⁷⁾, for fp shell nuclei, yields proton and neutron effective charges $e_p = 1.25e$, $e_n = 0.47e$. The effective charges e_p and e_n resulting from the macroscopic calculations of Bohr and Mottelson⁸⁵⁾ are 1.21e and 0.79e respectively.

In one of our calculations⁷²⁾ of $B(E2)$ values for the ground state band of states obtained by projected HF calculations for the even-even isotopes of Ti, Cr and Fe, the

isoscalar effective charges $e_p = 1.5e$ and $e_n = 0.5e$ were used. A reasonable agreement with the experiment was obtained. Similar effective charges were used by McGrory et al³⁹⁾ for the description of E2 transitions in nuclei with $A \leq 44$. The agreement of these calculations with the experiment was not good mainly because Ca isotopes are highly influenced by the "core" excited states.

We also attempted to determine⁸⁶⁾ the effective charges e_p and e_n by making a least squares fit between our calculated and experimental $B(E2, 2 \rightarrow 0)$ values for the even-even isotopes of Ti, Cr and Fe. The best values of e_p and e_n were found to be $(1.32 \pm 0.16)e$ and $(0.89 \pm 0.18)e$ respectively. These values are quite close to the values obtained by Bohr and Mottelson⁸⁵⁾ but slightly larger than those obtained by Kuo and Osnes⁷⁾.

In our calculation reported in this thesis we have used the effective charges $e_p = 1.32e$, $e_n = 0.89e$ as well as those of Kuo and Osnes. In some cases, calculations with effective charges $e_p = 1.5e$, $e_n = 0.5e$ are also done. For the magnetic transition, the free nucleon g -factors are used.

The present thesis is divided into five parts. In part II is described the Deformed Configuration Mixing formalism as applied to fp shell nuclei. In parts III to V are presented

the results of the DCM calculation on spectra and electromagnetic properties of the nuclei $^{45,47,49,51}\text{Ti}$, $^{47,48,49,51}\text{V}$ and ^{49}Cr . Each nucleus is discussed in a separate chapter. In an appendix at the end are presented some of the results on electromagnetic transitions in even-even isotopes of Ti, Cr and Fe.

REFERENCES

1. For a general reference to previous work, see:
 Proceedings of the Topical Conference on the Structure of $1f_{7/2}$ nuclei, Legnaro (Padova) 1971, ed. by R.A. Ricci (Editrice Compositori, Bologna, 1971).
 K.H. Bhatt, Invited talk, Proceedings of the International Conference on Gamma-ray Transition Probabilities, New Delhi, 1974, ed. by S.C. Pancholi and S.L. Gupta (Delhi University Press, to be published).
2. See Lecture notes in Physics (No.40): Effective Interactions and Operators in Nuclei, Proceedings of the Tucson International Conference on Nuclear Physics, Arizona, Tucson, 1975, ed. by B.R. Barrett (Springer Verlag, Berlin, Heidelberg, New York, 1975).
3. T.T.S. Kuo and G.E. Brown, Nucl. Phys. A114 (1968) 241.
4. B.R. Barrett and M.W. Kirson, Advances in Nuclear Physics, Vol.6, ed. by M. Baranger and E. Vogt (Plenum Press, New York, 1971), P.219; and references therein.
5. S. Yoshida and L. Zamick, Ann. Rev. Nucl. Sci. 22 (1972) 121; and references therein.
6. T.T.S. Kuo and E. Osnes, Nucl. Phys. A205 (1973) 1.
7. T.T.S. Kuo and E. Osnes, Phys. Rev. C12 (1975) 309.

8. M.W. Kirson, Proceedings of the International Conference on Nuclear Structure and Spectroscopy, Amsterdam, 1974, ed. by H.P. Blok and A.E.L. Dieperink (Scholar's Press, Amsterdam, 1974), Vol.II (Invited talks).
9. M. Harvey and T. Sebe, Atomic Energy of Canada Ltd., report AECL 3007 (1968).
10. K.H. Bhatt and J.C. Parikh, Phys. Lett. 24B (1967) 613.
11. R.D. Lawson, Phys. Rev. 124 (1961) 1500.
12. R.D. Lawson and B. Zeidman, Phys. Rev. 128 (1962) 821.
13. J.D. McCullen, B.F. Bayman and L. Zamick, Phys. Rev. 134 (1964) B515.
14. R.D. Lawson, Nucl. Phys. A173 (1971) 17.
15. F.J. Lynch, K.E. Nysten, R.E. Holland and R.D. Lawson, Phys. Lett. 32B (1970) 38.
16. E.A. Brown, D.B. Fossan, J.M. McDonald and K.A. Snover, Phys. Rev. C9 (1974) 1033; C11 (1975) 1122.
17. J.N. Black, Wm.C. McHarris, W.H. Kelly and B.H. Wildenthal, Phys. Rev. C11 (1975) 939.
18. See for example: J.J. Kolata, J.W. Olness and E.K. Warburton, Phys. Rev. C10 (1974) 1663.
19. L. Zamick, Proceedings of the Topical Conference on the Structure of $1f_{7/2}$ Nuclei, Legnaro (Padova) 1971, ed. by R.A. Ricci (Editrice Compositori, Bologna, 1971) p.9.
20. T. Engeland and E. Osnes, Phys. Lett. 20 (1966) 426.

21. N. Auerbach, Phys. Lett. 24B (1967) 260.
22. K. Lips and M.T. McEllistrem, Phys. Rev. C1 (1970) 1009.
23. E. Osnes and C.S. Warke, Nucl. Phys. A154 (1970) 331.
24. E. Osnes, Proceedings of the Topical Conference on the Structure of $1f_{7/2}$ Nuclei, Legnaro (Padova), 1971, ed. by R.A. Ricci (Editrice Compositori, Bologna, 1971), p.79.
25. B.J. Raz and M. Soga, Phys. Rev. Lett. 15 (1965) 924.
26. J. Vervier, Nucl. Phys. 78 (1966) 497.
27. H. Horie and K. Ogawa, Prog.Theor.Phys. 46 (1971) 439.
28. J.B. McGrory, Phys. Rev. 160 (1967) 915, Phys.Lett.26B (1968), 604. and Private communication to K.H. Bhatt.
29. K. Lips, Phys. Rev. C4 (1971) 482.
30. M.L. Rustgi, R.P. Singh, B. Barman Roy, R. Raj and C.C. Fu, Phys. Rev. C3 (1971) 2238.
31. S. Cohen, R.D. Lawson, M.H. Macfarlane, S.P. Pandya and M. Soga, Phys. Rev. 160 (1967) 903.
32. S.P. Pandya and B.P. Singh, Pramana 3 (1974) 61.
33. R.D. Lawson, M.H. Macfarlane and T.T.S. Kuo, Phys. Lett. 22 (1966) 168.
34. Y.K. Gambhir and R. Raj, Phys. Rev. 161 (1967) 1128.
35. K. Shimizu and A. Arima, Nucl. Phys. A227 (1974) 357.
36. P.W. Glaudemans, M.J.A. DeVoigt and E.F.M. Steffens, Nucl. Phys. A198 (1972) 609.
37. S.S.M. Wong, Nucl. Phys. A159 (1970) 235.

38. J.B. McGrory, B.H. Wildenthal and E.C. Halbert,
Phys. Rev. C2 (1970) 186.
39. J.B. McGrory, Phys. Rev. C8 (1973) 693.
40. K.H. Bhatt and J.B. McGrory, Phys. Rev. C3 (1971), 2293.
41. H. Rebel, G. Hauser, G.W. Schweimer, G. Nowicki, W.
Wiesner and D. Hartmann, Nucl. Phys. A218 (1974) 13.
42. G. Gneuss and W. Greiner, Nucl. Phys. A171 (1971) 449.
43. G. Ripka, Proceedings of the Topical Conference on the
Structure of $1f_{7/2}$ Nuclei, Legnaro(Padova), 1971, ed.by
R.A. Ricci (Editrice Compositori, Bologna, 1971), p.457.
44. S.B. Khadkikar and M.R. Gunye, Nucl. Phys. A110 (1968)
472.
45. A.K. Dhar, S.B. Khadkikar, D.R. Kulkarni and K.H. Bhatt,
Proceedings of the International Conference on Gamma-ray
Transition Probabilities, New Delhi, 1974, ed.by.S.C.
Pancholi and S.L. Gupta (Delhi Uni.Press, to be publi-
shed).
46. H. Chandra and M.L. Rustgi, Phys. Rev. C3 (1971) 1476;
C7 (1973) 180.
47. M.R. Gunye and S.B. Khadkikar, Phys. Lett. 30B (1969) 609.
48. K.R. Sandhya Devi, S.B. Khadkikar, J.K. Parikh and
B. Banerjee, Phys. Lett. 32B (1970) 179.
49. J.K. Parikh, Phys. Lett. 41B (1972) 271, Phys. Rev.C5
(1972) 153.

50. S.K. Sharma, ICTP, Preprint IC/74/58.
51. H.Muthur, K. Allart, K. Goeke and A. Faessler, Nucl. Phys. A248 (1975) 451.
52. J.C. Parikh and J.P. Svenne, Phys. Rev. 174 (1968) 1343.
53. J.K. Parikh, Phys. Rev. C6 (1972), 2177; C7 (1973) 1864.
54. T.S. Sandhu, M.L. Rustgi and A.L. Goodman, Phys. Rev. C12 (1975) 1340.
55. T.S. Sandhu and M.L. Rustgi, Phys. Rev. C12 (1975) 666.
56. W.J. Gerace and A.M. Green, Nucl. Phys. A93 (1967) 110.
57. B.H. Flowers and L.D. Skouras, Nucl. Phys. A116 (1968), 529; A136 (1969) 353.
58. L.D. Skouras, Joul.Phys. G4 (1975) 438.
59. F.B. Malik and W. Scholz, Phys. Rev. 150 (1966), 919; 153 (1967) 1071.
60. A. Arima and I. Hamamoto, Ann. Rev. Nucl. Sci. 21 (1971), 55.
61. B. Castel, I.P. Johnstone, B.P. Singh and K.W.C. Stewart, Can. Jou. Phys. 50 (1972) 1630.
62. V. Paar, Nucl. Phys. A147 (1970) 369.
63. A. Goswami, D.K. McDaniel and D. Nalcioglu, Phys. Rev. C7 (1973) 1263.
64. J.J. Dikshit and B.P. Singh, Pramana 3 (1974) 323 and Proceedings of the International Conference on Gamma-ray Transition Probabilities, New Delhi, 1974, ed.by.

S.C. Pancholi and S.L. Gupta (Delhi Uni.Press, to be published).

65. J.P. Elliot, Proc.Roy.Soc.A245 (1958), 128,562.
66. J.P. Elliot and M. Harvey, Proc. Roy. Soc. A272 (1963) 557.
67. M.K. Banerjee, C. Levinson and S. Meshkov, Phys. Rev.130 (1963) 1064.
68. A.K. Dhar, D.R. Kulkarni and K.H. Bhatt, Nucl. Phys. A238 (1975) 340.
69. A.K. Dhar, D.R. Kulkarni and K.H. Bhatt, Phys. Lett. 47B (1973) 133.
70. A.K. Dhar, D.R. Kulkarni and K.H. Bhatt, Nucl. Phys.and Solid State Phys.(India), 16B(1973) 146.
71. A.K. Dhar, D.R. Kulkarni and K.H. Bhatt, Proceedings of the International Conference on Nuclear Structure and Spectroscopy, Amsterdam (1974), ed. by H. Blok and A.E.L. Dieperink (Scholar's Press, Amsterdam, 1974) Vol.I, p.59.
72. A.K. Dhar, D.R. Kulkarni, S.B. Khadkikar and K.H. Bhatt, Proceedings of the International Conference on Gamma-ray Transition Probabilities, Delhi, 1974 ed.by. S.C.Pancholi and S.L. Gupta (Delhi Uni.Press, to be published).
73. A.K. Dhar, S.B. Khadkikar, D.R. Kulkarni and K.H. Bhatt, Nucl. Phys. and Solid State Phys.(India), 17B (1974) 246.
74. A.K. Dhar, D.R. Kulkarni and K.H. Bhatt, Nucl. Phys. and Solid State Phys.(India), 17B (1974) 243.

75. A.K. Dhar, S.B. Khadkikar, D.R. Kulkarni and K.H. Bhatt, Self-consistent field theories in Nuclear Physics, ed.by G. Ripka (1975) p.83.
76. A.K. Dhar, D.R. Kulkarni and K.H. Bhatt, Nucl. Phys. and Solid State Phys.(India), 18B (1975).
77. A.K. Dhar and K.H. Bhatt, Nucl. Phys. and Solid State Phys. (India), 18B (1975).
78. A.K. Dhar and K.H. Bhatt - sent for publication.
79. A.K. Dhar, D.R. Kulkarni and K.H. Bhatt, Phys. Lett. 50B (1974) 323.
80. S.K. Sharma and K.H. Bhatt, Phys. Rev. Lett.30(1973) 620.
81. A.K. Dhar and K.H. Bhatt, Proceedings of the International Topical Conference on Effective Interactions and Operators in Nuclei, Tucson (1975) ed. by B.R. Barrett, Vol.I,p.8.
82. A.K. Dhar - unpublished.
83. W. Gullholmer and Z.P. Sawa, Nucl. Phys. A204 (1973) 561.
84. Z.P. Sawa, Phys. Scrip. 7 (1973) 5.
85. A. Bohr and B.R. Mottelson, Nuclear Structure (Benjamin, New York, to be published), Vol.II, Chap.6: as quoted in Ref.16.
86. A.K. Dhar - unpublished; see also K.H. Bhatt (Ref.1).

INDEX

CHAPTER 2

DEFORMED CONFIGURATION MIXING FORMALISM

1.	THE SPECTRUM	37
1.1	Intrinsic States	38
1.1.1	HF Intrinsic States	38
1.1.2	Excited Intrinsic States	44
1.1.3	Isospin Mixing in the Intrinsic States	46
1.2	Projected Spectra	47
1.2.1	Evaluation of Kernels	49
1.3	Orthonormalization of the Projected States and Mixing due to Hamiltonian	54
2.	BAND STRUCTURE	57
3.	ELECTROMAGNETIC PROPERTIES	58
3.1	E2 Transitions	60
3.2	M1 Transitions	61
3.3	Decay Rates and (E2/M1) Mixing Ratios	62
3.4	Lifetime and Decay Intensity	63
APPENDIX I		
	Evaluation of the Reduced Matrix Elements of a Tensor Operator	65
	REFERENCES	68

CHAPTER 2

DEFORMED CONFIGURATION MIXING FORMALISM

In this chapter we shall present the details of the deformed configuration mixing formalism based on projected Hartree-Fock theory for the study of spectrum and electromagnetic properties of the fp shell nuclei.

1. THE SPECTRUM

This involves the following three stages of calculations:

A. Generation of the HF and other low-lying particle-hole excited intrinsic states, upto a certain chosen excitation energy, in the $(fp)^n$ configuration space;

B. The evaluation of the energies of the states of definite angular momentum, projected from each of the intrinsic states generated above,

C. Orthonormalization of the states projected from different intrinsic states and the diagonalization of the Hamiltonian in the basis of these orthonormalized states.

We shall now discuss these three stages of the calculation.

1.1 Intrinsic States

1.1.1 Hartree-Fock Intrinsic States

We shall give here the calculational details for the generation¹⁾ of an axially symmetric HF intrinsic state of a nucleus with n valence particles in the fp shell space. The Schrodinger equation for such a system is

$$H\Psi = E\Psi \quad (1)$$

where the Hamiltonian

$$H = \sum_{\alpha, \beta}^n \langle \alpha | h_0 | \beta \rangle a_{\alpha}^{\dagger} a_{\beta} + \frac{1}{4} \sum_{\alpha \beta \gamma \delta} \langle \alpha \beta | \tilde{v} | \gamma \delta \rangle a_{\alpha}^{\dagger} a_{\beta}^{\dagger} a_{\delta} a_{\gamma} \quad (2)$$

The first term on the right side in eq.(2) is the one-body part of the Hamiltonian consisting of kinetic energy and potential energy including \vec{l}^2 and $\vec{l} \cdot \vec{s}$ interactions etc., describing the single particle shell model states. The second term

$$\langle \alpha \beta | \tilde{v} | \gamma \delta \rangle = \langle \alpha \beta | v | \gamma \delta \rangle - \langle \alpha \beta | v | \delta \gamma \rangle$$

is an antisymmetric matrix element of the two-body force. a^{\dagger} and a are the usual fermion creation and annihilation operators respectively.

According to HF theory, the approximate description of the ground state of the fp shell nuclei can be obtained by

replacing in eq.(1) the wave function ψ by a variationally determined Slater determinantal wave function χ of single particle states $|\lambda\rangle$, i.e.,

$$\psi \simeq \chi = \prod_{\lambda=1}^n b_{\lambda}^{+} |^{40}\text{Ca}\rangle \quad (3)$$

such that

$$\delta \frac{\langle \chi | H | \chi \rangle}{\langle \chi | \chi \rangle} = 0 \quad (4)$$

For an axially symmetric HF solution, the angular momentum is not a good quantum number while its projection along the axis of symmetry is conserved. Thus we can label the wave function

$$\chi \equiv \chi_{K_0} \text{ and } |\lambda\rangle \equiv |\lambda, k\rangle$$

where $K_0 = \sum_{i=1}^n k_i$ with $k = \langle j_z \rangle$ the expectation value of the projection of \vec{j} along the axis of symmetry. In the single particle wave function $|\lambda, k\rangle$, λ refers to quantum numbers other than those labelled by k .

The energy of the state χ_{K_0} is given by:

$$\begin{aligned} E_{K_0} &\equiv \langle \chi_{K_0} | H | \chi_{K_0} \rangle \\ &= \sum_{\lambda=1}^n \langle \lambda | h_0 | \lambda \rangle + \frac{1}{2} \sum_{\lambda, \mu}^n \langle \lambda \mu | \tilde{v} | \lambda \mu \rangle \end{aligned} \quad (5)$$

The orbitals $|\lambda\rangle$ are expanded in the basis of fp shell states as:

$$|\lambda\rangle \equiv |\lambda, k\rangle = \sum_j c_{jk}^\lambda |jk\rangle \quad (6)$$

with $j = f_{7/2}, p_{3/2}, p_{1/2}$ and $f_{5/2}$.

This eq.(5) can be expressed as:

$$\begin{aligned} \langle \chi_{K_0} | H | \chi_{K_0} \rangle = & \sum_{\lambda=1}^n \sum_{j_1, j_3} c_{j_1 k_1}^{*\lambda} \langle j_1 k_1 \tau_1 | h_0 | j_3 k_1 \tau_1 \rangle c_{j_3 k_1}^\lambda \\ & + \frac{1}{2} \sum_{\lambda, \mu} \sum_{\substack{j_1, j_3 \\ j_2, j_4}} c_{j_1 k_1}^{*\lambda} c_{j_2 k_2}^{*\mu} \langle j_1 k_1 \tau_1, j_2 k_2 \tau_2 | \tilde{v} | j_3 k_1 \tau_1, j_4 k_2 \tau_2 \rangle \\ & \times c_{j_3 k_1}^\lambda c_{j_4 k_2}^\mu \end{aligned} \quad (7)$$

The variational eq.(4) implies the variation in single particle orbits $|\lambda\rangle$. Thus c_{jk} become variational parameters. This leads to the eigenvalue equation:

$$\sum_{j_3} \langle j_1 k_1 \tau_1 | h | j_3 k_1 \tau_1 \rangle c_{j_3 k_1}^\lambda = e_{k_1}^\lambda c_{j_1 k_1}^\lambda \quad (8)$$

where h is the Hartree-Fock hamiltonian and e_k is the corresponding energy of the single-particle orbit $|\lambda\rangle$. The matrix element:

$$\langle j_1 k_1 \tau_1 | h | j_3 k_1 \tau_1 \rangle =$$

$$\langle j_1 k_1 \tau_1 | h_o | j_3 k_1 \tau_1 \rangle + \sum_{\mu=1}^{\eta} \langle j_1 k_1 \tau_1, \mu | \tilde{v} | j_3 k_1 \tau_1, \mu \rangle \quad (9)$$

Equations (8) and (9) define the Hartree-Fock equations which are solved iteratively until a self-consistent solution is reached. At this stage, the HF solution is defined and the HF energy:

$$E_{\text{HF}} = \langle \chi_{K_o} | H | \chi_{K_o} \rangle = \sum_{\lambda=1}^{\eta} e^{\lambda} - \frac{1}{2} \sum_{\lambda=1}^{\eta} \langle \lambda | U | \lambda \rangle \quad (10)$$

where $\langle \lambda | U | \lambda \rangle$ is the matrix element of the HF self-consistent potential.

In our calculations of HF hamiltonian matrix, we use for the first term on right side in eq.(9) the experimental single particle energies of ^{41}Ca nucleus.

The solution of eq.(8) leads to a complete set of single particle orbits $|\lambda, k\rangle$. In the HF state of a nucleus the nucleons occupy the lowest energy orbits according to the Pauli Principle. In fig.1, we have sketched, for later use some of the occupied and unoccupied HF orbitals of a $N \neq Z$ nucleus.

The dashed line separates the neutron occupied orbits from those of the unoccupied ones. We refer to the occupied

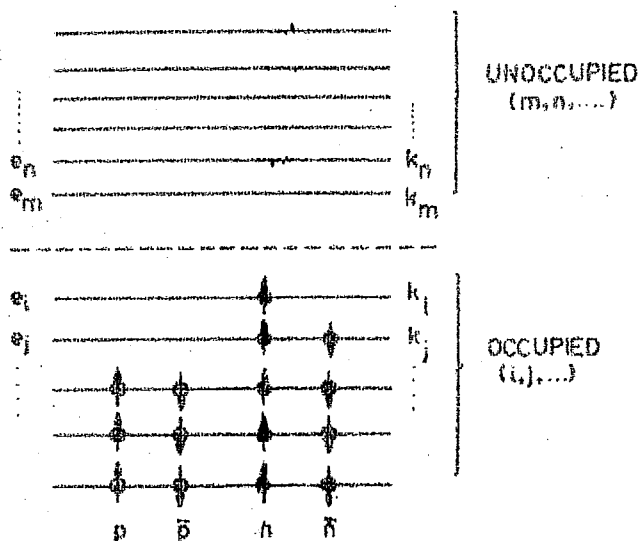


Fig.1

orbits by the label i, j, \dots and to unoccupied ones by m, n, \dots .

If the HF single particle orbits $|\lambda, k\rangle$ are invariant under a particular unitary transformation for which H is invariant, then, the HF hamiltonian h also possesses that symmetry. For even-even $N=Z$ nuclei, both time reversal and isospin symmetries are conserved and this leads to the four-fold degeneracy of the single particle orbitals. For even-even $N \neq Z$ nuclei, only time reversal symmetry is good, while for odd- A nuclei both these are broken. Thus for odd- A and odd-odd nuclei the HF single particle states are not degenerate in energy. In drawing the sketch above, we have, however, ignored

these differences in energies.

The intrinsic quadrupole moment of these single particle states labelled by $|k\rangle$ in fig.1, are given by the expectation value:

$$q_k = \langle k | \hat{q}_0^2 | k \rangle \quad (11)$$

where the single nucleon mass quadrupole moment operator

$$\hat{q}_0^2(i) = \int \frac{16\pi}{5} r_i^2 y_0^2(\theta_i, \phi_i)$$

with $y_0^2(\theta_i, \phi_i)$ as the spherical harmonic of rank 2.

The total mass quadrupole moment of the HF intrinsic state χ_{K_0} is then given by:

$$Q_{K_0} = \langle \chi_{K_0} | \hat{Q}_0^2 | \chi_{K_0} \rangle \quad (12)$$

where $\hat{Q}_0^2 = \sum_{i=1}^n \hat{q}_0^2(i)$.

Equation (12) can be rewritten in terms of proton (pr) and neutron (nu) contributions as:

$$Q_{K_0} = \sum_{\alpha=1}^P [q_k(\alpha)]_{pr} + \sum_{\beta=1}^N [q_k(\beta)]_{nu}$$

where P and N refer to protons and neutrons and $n=P+N$.

1.1.2 Excited Intrinsic States

The excited intrinsic states used in the calculations described in this thesis have been obtained by various p-h excitations from the HF states.

As seen from fig.1, the 1p-1h excited intrinsic state can be expressed as:

$$|\chi_{K}(1p-1h)\rangle = b_m^+ b_i |\chi_{K_0}\rangle$$

where $K = K_0 - k_i + k_m$.

In a similar manner, the wave function for the 2p-2h excited intrinsic state can be written as:

$$|\chi_{K'}(2p-2h)\rangle = b_m^+ b_n^+ b_i b_j |\chi_{K_0}\rangle$$

with $K' = K_0 + k_m + k_n - k_i - k_j$ and so on.

In general, we designate various intrinsic states by $\chi_K(\gamma)$ where γ distinguishes between the intrinsic states with the same K . The energies of these states are then given by:

$$E_K(\gamma) = \langle \chi_K(\gamma) | H | \chi_K(\gamma) \rangle \quad (13)$$

In order to know which p-h excited intrinsic states should be included in the calculation, it is necessary to have some rough estimate of the energies of these excited intrinsic states relative to the HF intrinsic state.

The energy of the 1p-1h excited intrinsic state is given by:

$$\begin{aligned} E_K(1p-1h) &= \langle \chi_K(1p-1h) | H | \chi_K(1p-1h) \rangle \\ &= E_{K_0} + e_m - e_i - \langle mi | \tilde{v} | mi \rangle \end{aligned}$$

Thus the excitation energy of the 1p-1h excited intrinsic state relative to the HF state is:

$$E_{K_0}(HF) - E_K(1p-1h) = e_i - e_m + \langle mi | \tilde{v} | mi \rangle \quad (14)$$

and that of the 2p-2h excited intrinsic state is:

$$E_{K_0}(HF) - E_K(2p-2h) = e_i + e_j - e_m - e_n + \text{Interaction terms} \quad (15)$$

It is thus seen that the p-h excited intrinsic states would lie higher from the HF intrinsic state by about the differences in the HF single-particle energies of the orbitals between which the excitations are considered. It is generally observed that the interaction terms in these expressions do not modify this estimate significantly.

The essential question is what is the minimum number of intrinsic states which should be included in the calculation to obtain a reasonable description of the spectrum of a nucleus upto a given energy? The prescription we would like to suggest is that if we want to calculate the spectrum of the n lowest states with a given J we must at least include $n+1$ lowest intrinsic states which can give rise to a state with that J value.

1.1.3 Isospin Mixing in the Intrinsic States

As already mentioned in subsec.1.1.1, for an odd- A or an odd-odd nucleus both proton-neutron and time-reversal symmetries are broken in their HF intrinsic states. Hence in such intrinsic states protons and neutrons occupy single-particle orbits that are not identical in structure. Therefore even the HF intrinsic states of odd- A or odd-odd nuclei have admixtures of various isospin components. Usually, however, the differences in the structure of the proton and neutron HF orbitals are not very large. Therefore the isospin component with $T=M_T$ is dominant in the HF intrinsic state. Similar features occur for the intrinsic states involving the excitation of a neutron from an occupied to an unoccupied orbit if the corresponding proton orbits are unoccupied. However, the intrinsic states in which the neutrons do not occupy orbits which are similar

to those occupied by the protons, have large isospin mixing. In order to obtain in the final spectrum states of definite isospin T , we include intrinsic states with mixed isospin having similar excitation of the protons and neutrons. It is hoped that a linear combinations of such configurations would lead to states with definite isospin T .

1.2 Projected Spectra

The deformed intrinsic states $\chi_K(\eta)$ generated above do not have a definite angular momenta. In order to make comparison with the experiment it is necessary to extract out from the intrinsic state χ_K the states of good angular momentum.

The state $\chi_K(\eta)$ can be expanded in terms of the eigenfunctions of J^2 as:

$$\chi_K(\eta) = \sum_J a_{JK}(\eta) \psi_K^J(\eta) \quad (16)$$

where $a_{JK}(\eta)$ is the amplitude of the state $\psi_K^J(\eta)$ in the intrinsic state $\chi_K(\eta)$.

The states with definite angular momentum J are then given by:

$$\psi_{MK}^J(\eta) = \frac{2J+1}{8\pi^2 \sqrt{N_{JK}}} \int d\Omega D_{MK}^{*J}(\Omega) R(\Omega) |\chi_K(\eta)\rangle \quad (17)$$

where ψ_{MK}^J is the normalized projected state and the rotational operator.

$$R(\Omega) = e^{-i\alpha J_z} e^{-i\beta J_y} e^{-i\gamma J_z}$$

with $\Omega = (\alpha, \beta, \gamma)$ corresponding to Euler angles. N_{JK} is the normalization constant and is given by:

$$N_{JK} = \frac{2J+1}{8\pi} \int d\Omega D_{KK}^{*J}(\Omega) \langle \chi_K(\eta) | R(\Omega) | \chi_K(\eta) \rangle \quad (18)$$

The matrix element of the Hamiltonian in the basis of these normalized states projected from different intrinsic states $\chi_K(\eta)$ is given by:

$$H_{K\eta, K'\eta'}^J = \langle \psi_{MK}^J(\eta) | H | \psi_{MK'}^J(\eta') \rangle \quad (19)$$

As seen from appendix I, at the end of this chapter, eq.(19) can be written as:

$$H_{K\eta, K'\eta'}^J = \frac{2J+1}{2\sqrt{N_{JK}N_{JK'}}} \int_0^\pi d\beta \sin\beta d_{KK'}^J(\beta) \langle \chi_K(\eta) | e^{-i\beta J_y} H | \chi_{K'}(\eta') \rangle$$

with

$$N_{JK} = \frac{2J+1}{2} \int_0^\pi d\beta \sin\beta d_{KK}^J(\beta) \langle \chi_K(\eta) | e^{-i\beta J_y} | \chi_K(\eta) \rangle \quad (20)$$

The diagonal matrix element gives the energy of a state projected from a particular intrinsic state.

$$E_{JK}(\eta) \equiv H_{K\eta, K\eta}^J = \langle \psi_{MK}^J(\eta) | H | \psi_{MK}^J(\eta) \rangle \quad (21)$$

The matrix elements $\langle \chi_K | e^{-i\beta J_Y} H | \chi_{K'} \rangle$ and $\langle \chi_K | e^{-i\beta J_Y} | \chi_{K'} \rangle$ in eq.(20) are called the energy and overlap kernels respectively.

1.2.1 Evaluation of Kernels

1.2.1.1 Overlap Kernel

Since $J_Y = \sum_{i=1}^n (j_Y)_i$, the operator $e^{-i\beta J_Y} | \chi_{K'} \rangle$ causes the rotation of each of the single particle states $|\lambda'\rangle$ of $| \chi_{K'} \rangle$ by an angle β about y-axis. Thus the function $e^{-i\beta J_Y} | \chi_{K'} \rangle$ is a determinant of the rotated single particle wave functions and its overlap with the determinant $| \chi_K \rangle$ is the determinant of the matrix of scalar products of the rotated orbit $e^{-i\beta J_Y} | \lambda' \rangle$ with the unrotated orbit $|\lambda\rangle$. Thus:

$$O_{KK'}(\beta) \equiv \langle \chi_K | e^{-i\beta J_Y} | \chi_{K'} \rangle = \det [M_{\lambda\lambda'}(\beta)] \quad (22)$$

where

$$M_{\lambda\lambda'}(\beta) = \langle \lambda | e^{-i\beta J_Y} | \lambda' \rangle = \sum_j c_{jk}^{*\lambda} c_{jk}^{\lambda'} d_{kk'}^j(\beta) \delta_{\lambda\lambda'} \quad (23)$$

For $\beta \rightarrow 0$, $M_{\lambda\lambda'}(\beta) \rightarrow \delta_{\lambda\lambda'}$.

Decomposing into proton and neutron parts:

$$O_{KK'}(\beta) = D^P(M_{\lambda\lambda'}) D^N(M_{\mu\mu'})$$

where P and N refer to ranks of proton and neutron determinants (D) with their matrix elements $M_{\lambda\lambda'}$ given by eq.(23).

1.2.1.2 Energy Kernel

The energy kernel is

$$H_{KK'}(\beta) \equiv \langle \chi_K | e^{-i\beta J_Y} H | \chi_{K'} \rangle$$

where the Hamiltonian

$$H = T + V$$

$T = \sum_{i=1}^{\eta} t_i$ is the one-body operator and $V = \sum_{i < j}^{\eta} v_{ij}$ is the two-body interaction term. Thus the energy kernel can be decomposed into kernels corresponding to one-body and two-body kernels as:

$$H_{KK'}(\beta) = \langle \chi_K | e^{-i\beta J_Y} T | \chi_{K'} \rangle + \langle \chi_K | e^{-i\beta J_Y} V | \chi_{K'} \rangle$$

One-body Energy Kernel

This can be expressed²⁾ as:

$$\begin{aligned} & \langle \chi_K | e^{-i\beta J_Y} T | \chi_{K'} \rangle \\ &= \sum_{\lambda, \lambda'}^{\eta} (-)^{\lambda + \lambda'} \langle \lambda | e^{-i\beta J_Y} t | \lambda' \rangle D_{\lambda, \lambda'}^{n-1} \end{aligned} \quad (24)$$

where the sum is over the occupied orbits. $D_{\lambda, \lambda'}^{n-1}$ is the determinant of rank $(n-1)$ of the matrix elements given by eq.(23) obtained from the $n \times n$ determinant given in eq.(22) by removing λ^{th} and λ'^{th} row and column respectively. The orbits $|\lambda\rangle$ are expanded in the basis states

$$|\lambda\rangle = \sum_j c_{jk}^\lambda |jk\tau\rangle$$

For the sake of convenience we abbreviate this to the form

$$|\lambda\rangle = \sum_\alpha c_\alpha |\alpha\rangle \text{ with } |\alpha\rangle = |jk\tau\rangle$$

where the sum is considered only over j . With this choice eq.(24) becomes:

$$\begin{aligned} & \langle \chi_K | e^{-i\beta J_Y T} | \chi_{K'} \rangle \\ &= \sum_{\lambda, \lambda'} (-)^{\lambda+\lambda'} D_{\lambda, \lambda'}^{n-1} \sum_{\alpha, \alpha'} \langle \alpha | e^{-i\beta J_Y t} | \alpha' \rangle c_\alpha^* c_{\alpha'} \end{aligned}$$

We call

$$\sum_{\lambda, \lambda'} (-)^{\lambda+\lambda'} c_\alpha^* c_{\alpha'} D_{\lambda, \lambda'}^{n-1} = D_{\alpha, \alpha'}^{n-1} \quad (26)$$

Using eq.(26) we can rewrite eq.(25) as:

$$\langle \chi_K | e^{-i\beta J_Y T} | \chi_{K'} \rangle = \sum_{\alpha, \alpha'} \langle \alpha | e^{-i\beta J_Y t} | \alpha' \rangle D_{\alpha, \alpha'}^{n-1} \quad (27)$$

With the matrix element

$$\langle \alpha | e^{-i\beta j_y t} | \alpha' \rangle = \sum_{k_y} d_{\alpha k_y}^{j_{\alpha}}(\beta) \langle j_{\alpha} k_y | t | j_{\alpha} k_{\alpha'} \rangle \delta_{\tau_{\alpha} \tau_{\alpha'}} \quad (28)$$

It may be noted that in eq.(27) the summation is over the basis states, in our case $f_{7/2}, p_{3/2}, p_{1/2}, f_{5/2}$ and does not depend on the number of nucleons. The nucleon number information is stored according to eq.(26) which under isospin decomposition involved in eq.(28) reduces to storing $D_{\alpha, \alpha'}^{N-1}, D_{\alpha, \alpha'}^{P-1}, D^N$ and D^P . The matrix elements of all these determinants are calculated according to eq.(23).

Two-Body Energy Kernel

In a manner similar to the one-body kernel, the interaction energy kernel can be written²⁾ as:

$$\langle \chi_K | e^{-i\beta J_y V} | \chi_{K'} \rangle = \sum_{\substack{\lambda, \mu \\ \lambda', \mu'}} (-)^{\lambda + \lambda' + \mu + \mu'} \langle \lambda \mu | e^{-i\beta j_y V} | \lambda' \mu' \rangle D_{\lambda \mu, \lambda' \mu'}^{n-2} \quad (29)$$

where $D_{\lambda \mu, \lambda' \mu'}^{n-2}$ is the determinant with λ^{th} and μ^{th} rows and λ'^{th} and μ'^{th} columns absent. Expressing in basis states, we have

$$\langle \chi_K | e^{-i\beta J_y V} | \chi_{K'} \rangle = \sum_{\substack{\alpha, \gamma \\ \alpha', \gamma'}} \langle \alpha \gamma | e^{-i\beta j_y V} | \alpha' \gamma' \rangle D_{\alpha \gamma, \alpha' \gamma'}^{n-2} \quad (30)$$

where

$$D_{\alpha\gamma, \alpha'\gamma'}^{n-2} = \sum_{\substack{\lambda, \mu \\ \lambda', \mu'}}^n (-)^{\lambda+\lambda'+\mu+\mu'} c_{\alpha}^* c_{\gamma}^* c_{\alpha'} c_{\gamma'} D_{\lambda\mu, \lambda'\mu'}^{n-2} \quad (31)$$

and the matrix element

$$\langle \alpha\gamma | e^{-i\beta j_Y} | \alpha'\gamma' \rangle = \sum_{m_{\delta}, m_{\delta'}} d_{k_{\alpha} k_{\beta}}^{j_{\alpha}}(\beta) d_{k_{\gamma} k_{\delta'}}^{j_{\gamma}}(\beta) \langle j_{\alpha} k_{\delta} \tau_{\alpha}, j_{\gamma} k_{\delta} \tau_{\gamma} | j_{\alpha} k_{\alpha} \tau_{\alpha}, j_{\gamma} k_{\gamma} \tau_{\gamma} \rangle \quad (32)$$

The isospin couplings in eq.(32) would involve storing of

$$D_{\alpha\gamma, \alpha'\gamma'}^{P-2}, D_{\alpha\gamma, \alpha'\gamma'}^{N-2}, D^P, D^N, D_{\alpha, \alpha'}^{P-1}, \text{ and } D_{\gamma, \gamma'}^{N-1}$$

The last two determinants are needed for the computation of proton-neutron energy kernel and are given by:

$$\begin{aligned} D_{\alpha, \alpha'}^{P-1} &= \sum_{\lambda, \lambda'} (-)^{\lambda+\lambda'} c_{\alpha}^* c_{\alpha'} D_{\lambda, \lambda'}^{P-1} \\ D_{\gamma, \gamma'}^{N-1} &= \sum_{\mu, \mu'} (-)^{\mu+\mu'} c_{\mu}^* c_{\mu'} D_{\mu, \mu'}^{N-1} \end{aligned} \quad (33)$$

Using eq.(30), proton-proton and neutron-neutron energy kernels can be simultaneously computed. The determinant D^{n-2} in these have to be replaced by the product $D^{P-2} D^N$ and $D^{N-2} D^P$ for the proton-proton and neutron-neutron interaction energy kernels respectively. The proton-neutron energy kernel on the other hand becomes:

$$E_{JK}(\gamma) \equiv H_{K\gamma, K\gamma}^J = \langle \psi_{MK}^J(\gamma) | H | \psi_{MK}^J(\gamma) \rangle \quad (21)$$

The matrix elements $\langle \chi_K | e^{-i\beta J_Y} H | \chi_{K'} \rangle$ and $\langle \chi_K | e^{-i\beta J_Y} | \chi_{K'} \rangle$ in eq.(20) are called the energy and overlap kernels respectively.

1.2.1 Evaluation of Kernels

1.2.1.1 Overlap Kernel

Since $J_Y = \sum_{i=1}^n (j_Y)_i$, the operator $e^{-i\beta J_Y} | \chi_{K'} \rangle$ causes the rotation of each of the single particle states $| \lambda' \rangle$ of $| \chi_{K'} \rangle$ by an angle β about y-axis. Thus the function $e^{-i\beta J_Y} | \chi_{K'} \rangle$ is a determinant of the rotated single particle wave functions and its overlap with the determinant $| \chi_K \rangle$ is the determinant of the matrix of scalar products of the rotated orbit $e^{-i\beta J_Y} | \lambda' \rangle$ with the unrotated orbit $| \lambda \rangle$. Thus:

$$O_{KK'}(\beta) \equiv \langle \chi_K | e^{-i\beta J_Y} | \chi_{K'} \rangle = \det [M_{\lambda\lambda'}(\beta)] \quad (22)$$

where

$$M_{\lambda\lambda'}(\beta) = \langle \lambda | e^{-i\beta J_Y} | \lambda' \rangle = \sum_j c_{jk}^{*\lambda} c_{jk}^{\lambda'} d_{kk'}^j(\beta) \delta_{\lambda\lambda'} \quad (23)$$

For $\beta \rightarrow 0$, $M_{\lambda\lambda'}(\beta) \rightarrow \delta_{\lambda\lambda'}$.

Decomposing into proton and neutron parts:

$$O_{KK'}(\beta) = D^P(M_{\lambda\lambda'}) D^N(M_{\mu\mu'})$$

where P and N refer to ranks of proton and neutron determinants (D) with their matrix elements $M_{\lambda\lambda'}$ given by eq.(23).

1.2.1.2 Energy Kernel

The energy kernel is

$$H_{KK'}(\beta) \equiv \langle \chi_K | e^{-i\beta J_{YH}} | \chi_{K'} \rangle$$

where the Hamiltonian

$$H = T + V$$

$T = \sum_{i=1}^{\eta} t_i$ is the one-body operator and $V = \sum_{i<j}^{\eta} v_{ij}$ is the two-body interaction term. Thus the energy kernel can be decomposed into kernels corresponding to one-body and two-body kernels as:

$$H_{KK'}(\beta) = \langle \chi_K | e^{-i\beta J_Y} T | \chi_{K'} \rangle + \langle \chi_K | e^{-i\beta J_Y} V | \chi_{K'} \rangle$$

One-body Energy Kernel

This can be expressed²⁾ as:

$$\begin{aligned} & \langle \chi_K | e^{-i\beta J_Y} T | \chi_{K'} \rangle \\ &= \sum_{\lambda, \lambda'}^{\eta} (-)^{\lambda + \lambda'} \langle \lambda | e^{-i\beta J_Y} t | \lambda' \rangle D_{\lambda, \lambda'}^{n-1} \end{aligned} \quad (24)$$

where the sum is over the occupied orbits. $D_{\lambda, \lambda'}^{n-1}$ is the determinant of rank $(n-1)$ of the matrix elements given by eq.(23) obtained from the $n \times n$ determinant given in eq.(22) by removing λ^{th} and λ'^{th} row and column respectively. The orbits $|\lambda\rangle$ are expanded in the basis states

$$|\lambda\rangle = \sum_j c_{jk}^\lambda |jk\tau\rangle$$

For the sake of convenience we abbreviate this to the form

$$|\lambda\rangle = \sum_\alpha c_\alpha |\alpha\rangle \text{ with } |\alpha\rangle = |jk\tau\rangle$$

where the sum is considered only over j . With this choice eq.(24) becomes:

$$\begin{aligned} & \langle \chi_K | e^{-i\beta J_{Y_T}} | \chi_{K'} \rangle \\ &= \sum_{\lambda, \lambda'}^n (-)^{\lambda+\lambda'} D_{\lambda, \lambda'}^{n-1} \sum_{\alpha, \alpha'} \langle \alpha | e^{-i\beta J_{Y_T}} | \alpha' \rangle c_\alpha^* c_{\alpha'} \end{aligned}$$

We call

$$\sum_{\lambda, \lambda'}^n (-)^{\lambda+\lambda'} c_\alpha^* c_{\alpha'} D_{\lambda, \lambda'}^{n-1} = D_{\alpha, \alpha'}^{n-1} \quad (26)$$

Using eq.(26) we can rewrite eq.(25) as:

$$\langle \chi_K | e^{-i\beta J_{Y_T}} | \chi_{K'} \rangle = \sum_{\alpha, \alpha'} \langle \alpha | e^{-i\beta J_{Y_T}} | \alpha' \rangle D_{\alpha, \alpha'}^{n-1} \quad (27)$$

With the matrix element

$$\langle \alpha | e^{-i\beta j_Y t} | \alpha' \rangle = \sum_{k_Y} d_{k_Y}^{j_\alpha}(\beta) \langle j_\alpha k_Y | t | j_\alpha k_{\alpha'} \rangle \delta_{\alpha \alpha'} \quad (28)$$

It may be noted that in eq.(27) the summation is over the basis states, in our case $f_{7/2}, p_{3/2}, p_{1/2}, f_{5/2}$ and does not depend on the number of nucleons. The nucleon number information is stored according to eq.(26) which under isospin decomposition involved in eq.(28) reduces to storing $D_{\alpha, \alpha'}^{N-1}, D_{\alpha, \alpha'}^{P-1}, D^N$ and D^P . The matrix elements of all these determinants are calculated according to eq.(23).

Two-Body Energy Kernel

In a manner similar to the one-body kernel, the interaction energy kernel can be written²⁾ as:

$$\langle \chi_K | e^{-i\beta j_Y V} | \chi_K \rangle = \sum_{\substack{\lambda, \mu \\ \lambda', \mu'}} (-)^{\lambda+\lambda'+\mu+\mu'} \langle \lambda \mu | e^{-i\beta j_Y V} | \lambda' \mu' \rangle D_{\lambda \mu, \lambda' \mu'}^{n-2} \quad (29)$$

where $D_{\lambda \mu, \lambda' \mu'}^{n-2}$ is the determinant with λ^{th} and μ^{th} rows and λ'^{th} and μ'^{th} columns absent. Expressing in basis states, we have

$$\langle \chi_K | e^{-i\beta j_Y V} | \chi_K \rangle = \sum_{\substack{\alpha, \gamma \\ \alpha', \gamma'}} \langle \alpha \gamma | e^{-i\beta j_Y V} | \alpha' \gamma' \rangle D_{\alpha \gamma, \alpha' \gamma'}^{n-2} \quad (30)$$

where

$$D_{\alpha\gamma, \alpha'\gamma'}^{n-2} = \sum_{\substack{\lambda, \mu \\ \lambda', \mu'}}^n (-)^{\lambda+\lambda'+\mu+\mu'} c_{\alpha}^* c_{\gamma}^* c_{\alpha'} c_{\gamma'} D_{\lambda\mu, \lambda'\mu'}^{n-2} \quad (31)$$

and the matrix element

$$\langle \alpha\gamma | e^{-i\beta j_y} | \alpha'\gamma' \rangle = \sum_{m_{\delta}, m_{\delta'}} d_{k_{\alpha} k_{\beta}}^{j_{\alpha}}(\beta) d_{k_{\gamma} k_{\delta}}^{j_{\gamma}}(\beta) \langle j_{\alpha} k_{\delta} \tau_{\alpha}, j_{\gamma} k_{\delta} \tau_{\gamma} | v | j_{\alpha} k_{\alpha} \tau_{\alpha}, j_{\gamma} k_{\gamma} \tau_{\gamma} \rangle \quad (32)$$

The isospin couplings in eq.(32) would involve storing of

$$D_{\alpha\gamma, \alpha'\gamma'}^{P-2}, D_{\alpha\gamma, \alpha'\gamma'}^{N-2}, D^P, D^N, D_{\alpha, \alpha'}^{P-1}, \text{ and } D_{\gamma, \gamma'}^{N-1}$$

The last two determinants are needed for the computation of proton-neutron energy kernel and are given by:

$$\begin{aligned} D_{\alpha, \alpha'}^{P-1} &= \sum_{\lambda, \lambda'} (-)^{\lambda+\lambda'} c_{\alpha}^* c_{\alpha'} D_{\lambda, \lambda'}^{P-1}, \\ D_{\gamma, \gamma'}^{N-1} &= \sum_{\mu, \mu'} (-)^{\mu+\mu'} c_{\mu}^* c_{\mu'} D_{\mu, \mu'}^{N-1} \end{aligned} \quad (33)$$

Using eq.(30), proton-proton and neutron-neutron energy kernels can be simultaneously computed. The determinant D^{n-2} in these have to be replaced by the product $D^{P-2} D^N$ and $D^{N-2} D^P$ for the proton-proton and neutron-neutron interaction energy kernels respectively. The proton-neutron energy kernel on the other hand becomes:

$$\begin{aligned}
\langle \chi_K | e^{-i\beta J_Y} V^{PN} | \chi_{K'} \rangle = \\
\sum_{\alpha_P, \gamma_N} \sum_{\alpha'_P, \gamma'_N} \langle \alpha_P \gamma_N | e^{-i\beta j_Y} V^{PN} | \alpha'_P \gamma'_N \rangle D_{\alpha_P, \alpha'_P}^{P-1} D_{\gamma_N, \gamma'_N}^{N-1}
\end{aligned}
\tag{34}$$

1.3 Orthogonalization of the Projected States and Mixing due to Hamiltonian

The states $\psi_{MK}^J(\gamma)$ with definite angular momentum J projected from various intrinsic states $\chi_K(\gamma)$ are, in general, not orthogonal to each other. A set of orthogonal vectors can be obtained by following the usual Schmidt's procedure. This procedure, however, becomes tedious to work out for more than two or three vectors. We have followed³⁾ a simple alternative prescription which makes use of standard matrix diagonalization routines.

Consider the overlap matrix

$$N_{K\gamma, K'\gamma'}^J = \langle \psi_{MK}^J(\gamma) | \psi_{MK'}^J(\gamma') \rangle \tag{35}$$

between the normalized states $\psi_{MK}^J(\gamma)$ of definite angular momentum J . For an orthonormal set of vectors the matrix N^J with its elements given by eq.(35) would be a unit matrix,

whereas in case of nonorthogonal basis, it is not diagonal. Since N^J is Hermitean, it can be diagonalized by a unitary transformation. Thus

$$U^+ N^J U = n^J$$

$$U^+ U = I$$

where n^J is the eigenvalue of the matrix N^J . The corresponding eigenvectors can be written as:

$$\phi_M^J(\nu) = \sum_{K\gamma} C_{K\gamma}^J(\nu) \psi_{MK}^J(\gamma) \quad (36)$$

where

$$C_{K\gamma}^J(\nu) = \left[n^J(\nu) \right]^{-1/2} U_{K\gamma}(\nu) \quad (37)$$

with $U_{K\gamma}$ corresponding to the element of the unitary transformation that diagonalizes N^J . Parameter ν distinguishes different states with same J .

The functions $\phi_M^J(\nu)$ constitute an orthonormal set of vectors. From eq.(37) it is clear that if any of the eigenvalue $n^J(\nu)$ of the overlap matrix N^J is vanishing, then the corresponding vector is spurious and should be eliminated.

Having obtained the orthonormal set of projected states,

it is necessary for the mixing due to Hamiltonian, to transform the Hamiltonian matrix given by eq.(19) between the nonorthogonal projected states, into the matrix between the orthonormal basis states. These can be expressed as:

$$\langle \phi_M^J(\nu) | H | \phi_M^J(\nu') \rangle = \sum_{K\eta} \sum_{K'\eta'} C_{K\eta}^{*J}(\nu) C_{K'\eta'}^J(\nu') \langle \psi_{MK}^J(\eta) | H | \psi_{MK'}^J(\eta') \rangle \quad (38)$$

The composite spectrum of a nucleus is obtained by diagonalizing this Hamiltonian matrix in the basis of orthonormalized projected states. The resulting eigen-functions are:

$$\Phi_M^J(\alpha) = \sum_{\nu} A_{M\nu}^J(\alpha) \phi_M^J(\nu)$$

which according to eq.(36) become:

$$\Phi_M^J(\alpha) = \sum_{K\eta} S_{K\eta}^J(\alpha) \psi_{MK}^J(\eta) \quad (39)$$

where

$$S_{K\eta}^J(\alpha) = \sum_{\nu} C_{K\eta}^J(\nu) A_{M\nu}^J(\alpha)$$

and label α distinguishes different eigenstates with the same angular momentum.

In the following sections we shall first examine these wave function for possible band structures and then for the calculation of the electromagnetic properties.

2. BAND STRUCTURE

We shall now describe the procedure which we have adopted to determine the extent to which the low-lying states $\Phi_M^J(\alpha)$ obtained in the above DCM calculation, can be grouped into bands of states projected from the lowest few intrinsic states included in a particular calculation.

The various eigen functions $\Phi_M^J(\alpha)$ as given by eq.(39) are:

$$\Phi_M^J(\alpha) = \sum_{K\eta} S_{K\eta}^J(\alpha) \psi_{MK}^J(\eta)$$

Thus the overlap

$$\begin{aligned} B_K^J(\eta, \alpha) &\equiv \langle \psi_{MK}^J(\eta) | \Phi_M^J(\alpha) \rangle \\ &= \sum_{K'\eta'} S_{K'\eta'}^J(\alpha) N_{K\eta, K'\eta'}^J \end{aligned} \quad (40)$$

gives the amplitude that the eigenstate $\Phi_M^J(\alpha)$ contains the state $\psi_{MK}^J(\eta)$ projected from the intrinsic state $\chi_K(\eta)$.

The larger the amplitude $B_K^J(\eta, \alpha)$ the more pronounced will

be the memory of that band in the state $\bar{\Phi}_M^J(\alpha)$.

A set of states has been recognized as a band of states if in the wave functions of all these states comprising the set, the intensity $\left| B_K^J(\gamma, \alpha) \right|^2$ of a state $\psi_{MK}^J(\gamma)$ projected from a given intrinsic state $\chi_K(\gamma)$ is large, for all the states of the group.

Using this prescription, the DCM wave functions of the states of the composite spectrum, of each of the nuclei described in this thesis have been analysed for possible band structures.

3. ELECTROMAGNETIC PROPERTIES

In this section we shall discuss the calculations of reduced electric quadrupole and magnetic dipole transition probabilities, life times, the (E2/M1) mixing ratios and branching ratios for the transitions between the states $\bar{\Phi}_M^J(\alpha)$ of the final composite spectrum obtained in the above DCM calculation.

The calculations of electric and magnetic transition probabilities between the states $\bar{\Phi}_M^J(\alpha)$ involve the evaluation of the matrix elements of the appropriate transition operators O_m^J of rank J between these states. Thus using eq.(39), we have

the matrix elements

$$\langle \Phi_M^J(\alpha) | \hat{O}_m^1 | \Phi_{M'}^{J'}(\alpha') \rangle =$$

$$\sum_{K, \gamma} \sum_{K', \gamma'} S_{K\gamma}^{*J}(\alpha) S_{K'\gamma'}^{J'}(\alpha') \langle \psi_{MK}^J(\gamma) | \hat{O}_m^1 | \psi_{M'K'}^{J'}(\gamma') \rangle \quad (41)$$

The reduced electromagnetic transition probability of multipolarity 1 between the states $\Phi_{M'}^{J'}(\alpha')$ and $\Phi_M^J(\alpha)$ is given by:

$$B(EM1; J' \rightarrow J) = \sum_{m, m'} |\langle \Phi_M^J(\alpha) | \hat{O}_m^1 | \Phi_{M'}^{J'}(\alpha') \rangle|^2 \quad (42)$$

Using Wigner-Eckart theorem and following deShalit and Talmi⁴⁾ phase convention, eq.(42) reduces to:

$$B(EM1; J' \rightarrow J) = \frac{1}{2J' + 1} |\langle \Phi^J(\alpha) | \hat{O}_0^1 | \Phi^{J'}(\alpha') \rangle|^2 \quad (43)$$

Our definition of the reduced matrix element differs from that of Rose and Brink⁵⁾ by a factor $(2J'+1)^{\frac{1}{2}}$ but has the same phase. In our convention, in the matrix element the initial state always stands on the right and the final state always to the left. Rose and Brink have it the other way round. Therefore our ratio of the reduced matrix elements for the electric and magnetic transitions between a given set of states differs from Rose and Brink convention, by a phase factor $(-)^{\bar{l}-1}$ where \bar{l} is the lowest order multipolarity in the transition e.g. in case of E2 and M1 transitions between

the states of angular momentum J and J' , $l = 2$ and $\bar{l} = 1$.

3.1 E2 Transitions

The operator corresponding to the electric quadrupole ($l = 2$) transition is:

$$\hat{Q}_M^2 = \sum_{i=1}^Z [e_i r_i^2 Y_M^2(\theta_i, \phi_i)]_p + \sum_{j=1}^N [e_j r_j^2 Y_M^2(\theta_j, \phi_j)]_n$$

where $Y_M^2(\theta, \phi)$ are the usual spherical harmonics of rank 2. p and n stand for proton and neutron and e 's are the corresponding effective charges. We have followed Condon and Shortly phase convention for the definition of $Y_M^L(\theta, \phi)$. With this choice:

$$Y_M^{*L}(\theta, \phi) = (-)^M Y_{-M}^L(\theta, \phi)$$

The reduced electric quadrupole transition probability as given by eq. (43) between the eigenstates $\Phi_M^J(\alpha)$ and $\Phi_{M'}^{J'}(\alpha')$ can be written as:

$$B(E2, J' \rightarrow J) = \frac{1}{2J'+1} \left| M_p e_p + M_n e_n \right|^2 \quad (44)$$

where M_p and M_n are the reduced proton and neutron matrix element and are defined as:

$$M_p = \sum_{K\gamma} \sum_{K'\gamma'} S_{K\gamma}^{*J}(\alpha) S_{K'\gamma'}^J(\alpha') \sum_{i=1}^Z \langle \psi_K^J(\gamma) || r_i^2 y^2(e_i, \theta_i) || \psi_{K'}^{J'}(\gamma') \rangle_p \quad (45)$$

M_n can be obtained from eq.(45) by replacing p by n and Z by N . The matrix element of r^2 needed in the evaluation of eq.(45) have been obtained by calculating oscillator length parameter from the relation $\hbar\omega = 41A^{-1/3}$ MeV.

The static electric quadrupole moment Q of the state $\Phi_M^J(\alpha)$ is given by the diagonal matrix element of the operator \hat{Q}_0^2 defined above and is defined for the state with $M=J$. Thus:

$$Q(J, \alpha) = \sqrt{\frac{16\pi}{5}} \sum_{\substack{K\gamma \\ K'\gamma'}} S_{K\gamma}^{*J}(\alpha) S_{K'\gamma'}^J(\alpha) \langle \psi_K^J(\gamma) || \hat{Q}_0^2 || \psi_{K'}^J(\gamma') \rangle \quad (46)$$

3.2 M1 Transitions

The reduced magnetic dipole ($l=1$) transition probability from the state J' to J as given by eq.(43) can be written as:

$$B(M1, J' \rightarrow J) =$$

$$\frac{1}{2J'+1} \left| \sum_{K\gamma} \sum_{K'\gamma'} S_{K\gamma}^{*J}(\alpha) S_{K'\gamma'}^J(\alpha') \langle \psi_K^J(\gamma) || \hat{\mu} || \psi_{K'}^{J'}(\gamma') \rangle \right|^2 \quad (47)$$

where the magnetic dipole transition operator:

$$\hat{\mu} = \sqrt{\frac{3}{4\pi}} \left[\sum_{i=1}^Z (g_l \vec{l}_i + g_s \vec{s}_i)_p + \sum_{j=1}^N (g'_s \vec{s}_j)_n \right]$$

where \vec{l} and \vec{s} are the single nucleon orbital angular momentum and spin operators. g_l and g_s are the corresponding gyromagnetic ratios. The free g-factors $g_l=1$, $g_s=5.596$ for the proton and $g'_s = -3.826$ for the neutron have been used in all the calculations reported herein.

The magnetic dipole moment is given by:

$$\mu(J, \alpha) = \int \frac{4\pi}{3} \sum_{\substack{KK' \\ \gamma\gamma'}} S_{K\gamma}^{*J}(\alpha) S_{K'\gamma'}^J(\alpha) \langle \psi_K^J(\gamma) \| \hat{\mu} \| \psi_{K'}^J(\gamma') \rangle \quad (48)$$

The reduced matrix elements in eqs.(45)-(48) are evaluated by the usual procedure⁶⁾. However, for completeness, their final form is given in appendix I.

3.3 Decay Rates and (E2/M1) Mixing Ratios

The magnetic decay rates $T(E2)$ and $T(M1)$ are related⁷⁾ to $B(E2)$ and $B(M1)$ as:

$$T(E2) = 1.22 \times 10^9 E^5 B(E2)$$

$$T(M1) = 1.76 \times 10^{13} E^3 B(M1)$$

where E is the energy difference (in MeV) between the states for which transition is considered. $B(E2)$ is in $e^2 \text{fm}^4$ and $B(M1)$ is in $(\text{n.m.})^2$ units.

The $(E2/M1)$ mixing ratios for the transitions between the states $\Phi_M^J(\alpha)$ and $\Phi_{M'}^{J'}(\alpha')$ is defined as:

$$\delta = \text{Sg} \sqrt{\frac{T(E2, J' \rightarrow J)}{T(M1, J' \rightarrow J)}} \quad (49)$$

where Sg is the sign resulting from the ratio of the reduced matrix elements for the $E2$ and $M1$ transitions. As mentioned earlier our sign of the $(E2/M1)$ mixing ratio is opposite to that of Rose and Brink.

The phases of the observed mixing ratios are given according to Rose and Brink convention. Hence to make the comparison with the observed data on $(E2/M1)$ mixing ratios, we have multiplied our values of δ given by eq.(49) by a negative sign.

3.4 Lifetime and Decay Intensity

The lifetime τ of a transition from the state $\Phi_{M'}^{J'}(\alpha')$ to the state $\Phi_M^J(\alpha)$ is given by:

$$\tau = \frac{1}{T} \quad (50)$$

where T is the total decay rate between the states labelled by J' and J and is defined as:

$$T(J' \rightarrow J) = T(E2, J' \rightarrow J) + T(M1, J' \rightarrow J)$$

The mean lifetime τ_m of a state $\Phi_M^{J'}(\alpha')$ is then given by:

$$\frac{1}{\tau_m} = \frac{1}{\tau_1} + \frac{1}{\tau_2} + \dots \quad (51)$$

where τ_1, τ_2, \dots are the lifetimes of the various transitions from the state $\Phi_M^{J'}(\alpha')$ to the other states.

The relative decay intensity I for the transitions from a state $\Phi_M^{J'}(\alpha')$ to the state $\Phi_M^J(\alpha)$ can be defined as:

$$I(J' \rightarrow J) = \frac{T(J' \rightarrow J)}{\sum_{J''} T(J' \rightarrow J'')} \times 100 \quad (52)$$

where the summation in the denominator is over all the states to which the transition from the state J' are considered.

APPENDIX I

We shall give here a general expression for the evaluation of the reduced matrix elements of an operator T_M^L of rank L between the states projected from different intrinsic states.

Following Wigner-Eckart theorem and deShalit and Talmi⁴⁾ phase convention the matrix element:

$$\langle \psi_{M_1 K_1}^{J_1} | T_M^L | \psi_{M_2 K_2}^{J_2} \rangle = (-)^{J_1 - M_1} \begin{pmatrix} J_1 & L & J_2 \\ -M_1 & M & M_2 \end{pmatrix} \langle J_1 K_1 || T^L || J_2 K_2 \rangle \quad (\text{A.1})$$

The matrix element on the left hand side can also be expressed in terms of the matrix elements between the intrinsic states χ_K as:

$$\begin{aligned} \langle \psi_{M_1 K_1}^{J_1} | T_M^L | \psi_{M_2 K_2}^{J_2} \rangle = & \frac{2J_2 + 1}{2 \int N_{J_1 K_1} N_{J_2 K_2}} C_{M_2}^{J_2 L} C_{M_1}^{J_1} \sum_{\nu} C_{K_2}^{J_2 L} C_{K_2 + \nu}^{J_1} \\ & \times \int_0^\pi d\beta \sin\beta d_{K_1, K_2 + \nu}^{J_1}(\beta) \langle \chi_{K_1} | e^{-i\beta J_Y} T_M^L | \chi_{K_2} \rangle \end{aligned} \quad (\text{A.2})$$

The Clebsch-Gordon and 3-J coefficients are related by

$$C_{M_2}^{J_2 \quad L \quad J_1} = \sqrt{2J_1+1} \quad (-)^{J_1-M_1} \begin{pmatrix} J_1 & L & J_2 \\ -M_1 & M & M_2 \end{pmatrix} \quad (A.3)$$

Substituting this in eq.(A.2) and comparing the right hand side with eq.(A.1) we obtain for the reduced matrix element:

$$\begin{aligned} \langle J_1 K_1 || T^L || J_2 K_2 \rangle = & \frac{2J_2+1}{2} \sqrt{\frac{2J_1+1}{N_{J_1 K_1} N_{J_2 K_2}}} \sum_{\nu} C_{K_2}^{J_2 \quad L \quad J_1} \nu \quad K_2 + \nu \\ & \times \int_0^{\pi} d\beta \sin\beta d_{K_1, K_2+\nu}^{J_1}(\beta) \langle \chi_{K_1} | e^{-i\beta J_Y} T_{\nu}^L | \chi_{K_2} \rangle \end{aligned} \quad (A.4)$$

If $T^L = \sum_{i=1}^n t^L(i)$ is a one-body operator, then its kernel reduces to the form:

$$\begin{aligned} \langle \chi_{K_1} | e^{-i\beta J_Y} T_{\nu}^L | \chi_{K_2} \rangle = & \sum_{i,k=1}^n (-)^{i+k} D_{i,k}^{n-1} \sum_{j_i, j_k} \frac{(-)^{3j_i-j_k-\nu-2m_k}}{(2j_k+1)^{1/2}} C_{j_i m_i}^* C_{j_k m_k} d_{m_i, m_{k+\nu}}^{j_i}(\beta) \\ & \times C_{m_k+\nu}^{j_i \quad L \quad j_k} \langle n_i 1_i j_i || t^L || n_k 1_k j_k \rangle \end{aligned} \quad (A.5)$$

The study of the electromagnetic properties thus involves the evaluation of the single-particle^{matrix} elements, in eq.(A.5), of the appropriate operator. Their evaluation for the operators of interest is given in ref.6.

REFERENCES

1. G. Ripka, *Advances in Nuclear Physics*, Vol.I, ed.by M. Baranger and E. Vogt (Plenum Press, New York, 1968) P.183.
2. C.S. Warke and M.R. Gunye, *Phys. Rev.* 155(1967) 1084.
3. D.J. Rowe, *Joul.Math.Phys.* 19 (1969) 1774.
4. A. deShalit and I. Talmi, *Nuclear Shell Theory* (Academic Press, New York, 1963).
5. H.J. Rose and D.M. Brink, *Rev. Mod. Phys.* 39 (1967) 306.
6. M.R.Gunye and C.S. Warke, *Phys. Rev.* 159 (1967) 885.
7. A. Bohr and B.R. Mottelson, *Nuclear Structure* (Benjamin, New York, 1966) Vol.I, p.382.

PART III

TITANIUM ISOTOPES

Chapter 3: STRUCTURE OF ^{45}Ti

Chapter 4: STRUCTURE OF ^{47}Ti

Chapter 5: STRUCTURE OF ^{49}Ti

Chapter 6: STRUCTURE OF ^{51}Ti

INDEX

TITANIUM ISOTOPES

	SECTION HEADINGS	Page Nos.			
	CHAPTERS	3	4	5	6
1.	INTRODUCTION	71	108	184	206
1.1	Experimental Data	71	108	184	206
1.2	Previous Calculations	73	109	185	206
2.	PRESENT CALCULATIONS	73	110	185	207
2.1	Calculation of the Energy Spectrum	74	111	185	207
2.2	Comparison of the Calculated and Experimental Spectrum	85	128	194	212
2.3	Band Structure	89	133	195	213
2.4	Electromagnetic Properties	93	138	197	214
2.5	Level Density		171		
	REFERENCES	105	181	204	219

illustrated. The comparison of the calculated spectrum and electromagnetic properties of each of these nuclei with the experimental data and also with the $(f_{7/2})^n$ and RPC calculations shall be presented.

CHAPTER 3

THE NUCLEUS ^{45}Ti

1. INTRODUCTION

1.1 Experimental Data

The nucleus ^{45}Ti has been mainly studied by five types of reactions at different incident beam energies. The ground state band of states upto $J=(15/2)$ in this nucleus has been observed by Sawa et al¹⁾ in (α, n) reaction induced by 14.2 MeV α -beam. Jett et al²⁾ provided an evidence for the existence of the ground state triplet at 0.37 and 40 keV in ^{45}Ti by γ -ray measurements following $^{45}\text{Sc}(p, n) ^{45}\text{Ti}$ reaction. They further showed that the internal conversion coefficient for the 37 keV transition has a value consistent with that for an E2 transition. Lynch et al³⁾ observed the mean lifetime of $4.5 \pm 0.5 \mu\text{s}$ for the 37 keV state excited in their (p, n) experiment at 7.5 MeV. Using this observed value together with the value of 17.8 for the internal conversion of the 37 keV transition, Lynch et al deduced the radiative lifetime of $85 \pm 10 \mu\text{s}$ for the $3/2 \rightarrow 7/2$, 37 keV transition. This corresponds to a six fold enhancement of the E2 transition rate. Lynch et al³⁾ also performed $^{45}\text{Sc}(p, n)$ and $^{42}\text{Ca}(\alpha, n)$ reactions at $E_p = 6$ MeV and $E_\alpha = 10$ MeV and measured the mean lifetime of 17.2 ± 1.0 ns for the 40 keV transition. Using the internal

conversion coefficient of 0.25, they inferred the M1 radiative lifetime of 21.5 ± 1.35 ns for this level. There, however, exists a discrepancy between the lifetimes for the 40 keV state as measured by Lynch et al³⁾ and by Blasi et al⁴⁾. Blasi et al have observed the value of 11.5 ± 1.5 ns for this state in contrast to 17.2 ± 1.0 ns observed by Lynch et al.

The spectrum of ^{45}Ti upto about 2 MeV has been observed by Iyengar et al⁵⁾ using (p,n γ) reaction and neutron time-of-flight technique. Earlier similar studies were also made by Brugger et al⁶⁾ and McCallum et al⁷⁾. Iyengar et al⁵⁾, Zuk et al⁸⁾ and Iyengar and Robertson⁹⁾ also studied (p,n γ) reaction at $E_p = 2.8 - 5.6$ MeV, $3.35 - 4.50$ MeV and $4.45 - 5.90$ MeV respectively; and observed spins, parities and decay properties of the low-lying states of ^{45}Ti . Six states upto about 6 MeV excitation in ^{45}Ti have been observed by L'Ecuyer and St-Pierre¹⁰⁾ and Lutz and Bohn¹¹⁾ by employing ($^3\text{He},d$) reactions at about 10 and 18.2 MeV energies. Recently ^{46}Ti (p,d) ^{45}Ti reaction at 34.78 MeV has been performed by Plauger and Kashy¹²⁾ and about four $J=7/2^-$ and three $J=3/2^-$ states upto about 5 MeV in ^{45}Ti are observed. Earlier (p,d) measurements of Kashy and Conlon¹³⁾ and Jones et al¹⁴⁾ had given information only about the orbital angular momentum of the transferred neutron. The ground state moments of ^{45}Ti have been measured by atomic beam resonance method by Cornwell and McCullen¹⁵⁾.

1.2 Previous Calculations

For the nucleus ^{45}Ti , the $(f_{7/2})^5$ calculation¹⁶⁾ had predicted near degeneracy of its ground state with $J=7/2$ and the $J=5/2$ state. The latter being lower in energy. The first $J=3/2$ state was predicted to lie above 2 MeV.

The RPC model calculation¹⁷⁾ had predicted the ground state $(7/2 - 3/2 - 5/2)$ triplet in ^{45}Ti , the dramatic confirmation of which was provided by Jett et al²⁾. However, the description of the excited states of ^{45}Ti as obtained by these calculations is not satisfactory.

Johnstone¹⁸⁾ performed for the study of ^{45}Ti , the band mixing calculation using projected HF theory. He used s-state Kallio-Kolltveit two body effective interaction¹⁹⁾ and considered the mixing of the states projected from the intrinsic states obtained by $1p-1h$ excitations from the HF state of ^{45}Ti . The triplet of states with the right sequence is reproduced within about 200 keV compared to 40 keV spread in the observed spectrum. However, such a close agreement has been found to be force dependent.

2. PRESENT CALCULATIONS

We shall now present the results of our DCM calculations described in chapter 2 for the nucleus ^{45}Ti . First we shall

discuss the details of the energy spectrum and then those of the electromagnetic transitions between the low-lying states of this nucleus.

2.1 THE CALCULATION OF THE ENERGY SPECTRUM

2.1.1 Generation of Intrinsic States

2.1.1.1 Hartree-Fock Intrinsic States

Both axially symmetric prolate and oblate HF states of ^{45}Ti have been obtained using MWH2 interaction. The prolate $K=3/2$ HF state has the energy $E_K = -11.7$ MeV while the oblate $K=5/2$ state occurs at -10.5 MeV.

In tables 1 and 2, are given the single particle energies e_k (eq.8), the quadrupole moments q_k (eq.11) and the amplitudes c_{jk} with $j=1/2, 3/2, 5/2$ and $7/2$ in the occupied and the lowest few unoccupied single proton and neutron orbitals of the prolate and oblate HF states of ^{45}Ti . The dashed line separates the occupied orbitals from the unoccupied ones. It is seen from tables 1 and 2 that although the chosen effective interaction leads to single particle orbits with dominant $f_{7/2}$ component, the admixture of other fp shell states $f_{5/2}$, $p_{3/2}$ and $p_{1/2}$ is sizeable and corresponds to deformation $^{20)}\delta \simeq 0.20$ for the prolate HF state and $\delta \simeq -0.31$ for the oblate state. It may be pointed out at this stage that in the RPC model calculations³⁾ of Malik and Scholz,

Table 1

Structure of the occupied and some of the unoccupied proton and neutron orbits of the prolate $K=3/2$ HF state of ^{45}Ti . The dashed line separates the occupied orbitals from the unoccupied ones. e_k and q_k are the energies and quadrupole moments of the single particle orbits k . c_{jk} is the amplitude of the state $|jk\rangle$ in the orbit k . ($E_{\text{HF}} = -11.7$ MeV, $Q_{\text{HF}} = 29.82 \text{ b}^2$; $b^2 = \hbar/m\omega$).

	k	e_k MeV	q_k b^2	$c_{\frac{1}{2}k}$	$c_{\frac{3}{2}k}$	$c_{\frac{5}{2}k}$	$c_{\frac{7}{2}k}$
P R O T O N S	1/2	-6.58	4.70	0.195	-0.399	-0.212	0.871
	-1/2	-6.13	4.73	-0.200	-0.402	0.217	0.866
	3/2	-3.78	2.20		-0.170	-0.179	0.969
	-3/2	-3.08	2.12		-0.158	0.156	0.975
	5/2						
	7/2						
N E U T R O N S	1/2	-5.65	4.48	0.174	-0.365	-0.196	0.893
	-1/2	-5.86	4.84	-0.217	-0.217	0.250	0.850
	3/2	-2.41	2.07		-0.146	-0.144	0.979
	5/2	-0.40	-0.31			-0.061	0.998
	7/2	0.51	2.45				1.0
	9/2						

Table 2

Structure of the occupied and some of the unoccupied proton and neutron orbits of the OBLATE HF state of ^{45}Ti . ($E_{\text{HF}} = -10.5$ MeV, $Q_{\text{HF}} = -13.07$ b 2). For other details see caption of table 1.

	k	e_k MeV	q_k b 2	$c_{\frac{1}{2}k}$	$c_{\frac{3}{2}k}$	$c_{\frac{5}{2}k}$	$c_{\frac{7}{2}k}$
P	7/2	-5.37	-3.0				1.0
R	-7/2	-4.89	-3.0				1.0
O							
T							
O	5/2	-3.36	-1.0			0.232	0.973
N	-5/2	-2.67	-1.09			-0.256	0.967
S							
	7/2	-4.35	-3.0				1.0
N	-7/2	-4.70	-3.0				1.0
E							
U	5/2	-2.16	-1.07			0.248	0.969
T							
R							
O	-5/2	-2.59	-1.04			-0.240	0.971
N	3/2	-1.20	-0.44		0.343	0.095	0.935
S	1/2	-0.55	0.58	0.107	0.254	0.056	0.960

single particle orbitals with $\delta = -0.34$ have been found to give an optimum agreement with the experimental data.

2.1.1.2 Excited Intrinsic States

For the description of the low-lying states of ^{45}Ti , we have considered all the intrinsic states $\chi_K(\eta)$ upto about 3 MeV relative excitation energy. The details of these various excited intrinsic states are given below.

One particle-One hole Excited Intrinsic States

Nine intrinsic states obtained by various 1p-1h excitations from the prolate and oblate HF states have been found to lie within 3 MeV excitation from the lowest energy HF state. In table 3 are presented the specific excitations, the K-values and the energies $E_K(\eta)$ (eq.13) of these intrinsic states along with the energies and K-values of their parent HF states from which they were obtained. For example, the state with $K=5/2$ at -9.82 MeV is obtained from the prolate HF state by exciting the odd neutron from the $k=3/2$ orbital to the unoccupied $k=5/2$ orbital and so on. Thus in all eleven intrinsic states upto about 3 MeV excitation are obtained. From these intrinsic states, four states with $J=1/2$, seven states with $J=3/2$, ten states with $J=5/2$ and eleven states with $J \geq 7/2$ can be obtained.

Table 3

Energies and K-values of the prolate and oblate HF states of ^{45}Ti and of the intrinsic states obtained by 1p-1h excitations from the HF states. k_i and k_m are the k-values of the hole and particle orbitals. The labels p and n refer to the proton and neutron respectively.

Shape	Hole k_i	Particle k_m	K	E_K (MeV)
Prolate	(HF State)		3/2	-11.64
	n 3/2	n 5/2	5/2	-9.82
	n 3/2	n 7/2	7/2	-8.90
	p 1/2	p 3/2	5/2	-8.66
	n -1/2	n -3/2	1/2	-8.57
	n 3/2	n 1/2'	1/2	-8.55
	p -1/2	p -3/2	1/2	-8.43

Oblate	(HF State)		5/2	-10.53
	n 5/2	n 3/2	3/2	-9.45
	n 5/2	n 1/2	1/2	-9.13
	p 7/2	p 5/2	3/2	-8.38

It is seen from table 3 in conjunction with tables 1 and 2, that the energies of the excited intrinsic states relative to their corresponding prolate and oblate HF states, are about the differences in the energies of the single-particle states between which the excitations are considered.

Two Particle-Two Hole Excited Intrinsic States

According to eq.(15) and tables 1 and 2 such states are expected to lie above 4 MeV relative excitation energy and thus are not included in the present calculation. In order to verify this expectation, we have computed the energies of some of the intrinsic states resulting from 2p-2h excitations to the lowest unoccupied HF orbitals. The information regarding these states in ^{45}Ti is given in table 4.

Table 4

Details of the 2p-2h excited intrinsic states in ^{45}Ti

Shapes	Holes k_i	Particles k_m	K	E_K (MeV)
Prolate	p $+1/2$, n $-1/2$	p $+3/2$, n $-3/2$	3/2	-7.24
	p $\pm 1/2$	p $\pm 3/2$	3/2	-6.82
	p $+1/2$, n $+3/2$	p $-3/2$, n $+5/2$	1/2	-6.25
Oblate	p $+7/2$, n $+5/2$	p $+5/2$, n $+3/2$	1/2	-7.38
	p $\pm 7/2$	p $\pm 5/2$	5/2	-6.60
	p $+7/2$, n $-7/2$	p $+5/2$, n $-5/2$	5/2	-6.08

2.1.1.3 Isospin Mixing in the Intrinsic States

For the intrinsic states listed in table 3, isospin $T=1/2$

is the dominant component. In table 5 are given the amplitudes of the isospin $T=1/2$ and $3/2$ in these intrinsic states. The isospins with $T \geq 5/2$ are extremely small and are not given in the table.

Table 5

Shape	K	E_K (MeV)	Amplitudes	
			$T=1/2$	$T=3/2$
Prolate	3/2	-11.64	0.999	0.036
	5/2	-9.82	0.999	0.036
	7/2	-8.90	0.999	0.036
	5/2	-8.66	0.999	0.034
	1/2	-8.57	0.816	0.577
	1/2	-8.55	0.999	0.023
	1/2	-8.43	0.816	0.577
Oblate	5/2	-10.53	1.0	0.0
	3/2	-9.45	1.0	0.0
	1/2	-9.13	1.0	0.0
	3/2	-8.38	0.999	0.009

For the intrinsic states with $K=1/2$ at -8.57 and -8.43 MeV the $T=3/2$ admixture is about 33 percent. Of these intrinsic state the former is obtained by the excitation of a paired neutron from the occupied $k = -1/2$ orbit to that with $k = -3/2$. Such an intrinsic state is sketched at 2(a). In a similar

^{45}Ti

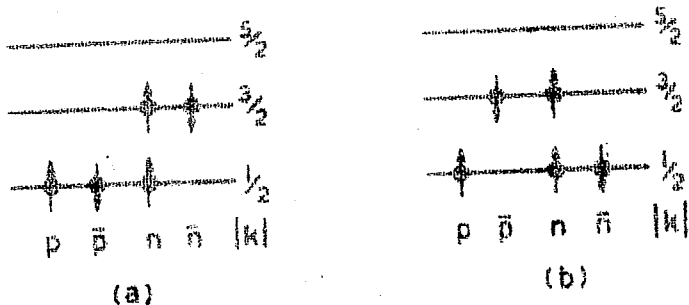


Fig.2

A sketch of the $K=1/2$ intrinsic states of ^{45}Ti obtained by the excitation of a paired neutron (a) and a paired proton (b) from the occupied $k = -1/2$ orbit to the corresponding unoccupied $k = -3/2$ orbit. These $K=1/2$ intrinsic states have substantial isospin mixing. A linear combination of these configurations is expected to lead in the final spectrum of states with definite isospin.

manner the intrinsic state at -8.43 MeV is obtained by the corresponding excitation of the paired proton and is sketched at 2(b). It is clear from table 5 that the states projected from any of these intrinsic states alone would not have good isospin T . It is, however, hoped that by including both such intrinsic states in the calculation, the interaction would lead to states which are linear combination of these two configurations (a) and (b) with definite isospin.

2.1.2 Energy Spectra of the Angular Momentum Projected States

Using the procedure described in chapter 2, sec.1.2, states $\psi_{MK}^J(\gamma)$ with definite angular momenta J have been projected from each of the eleven intrinsic states of table 3. The energy spectra of these states are plotted in figs.3 and 4 according to the appearance of their intrinsic states at 3A and 4A. Thus in fig.3, the states projected from the HF prolate (P) $K=3/2$ intrinsic state are plotted under the column labelled P:3/2 and so on. The intensity $|a_{JK}(\gamma)|^2$ (eq.16), of a projected state $\psi_{MK}^J(\gamma)$ in the intrinsic state $\chi_K(\gamma)$ is also given on top of each of the states in figs.3 and 4. Thus, as shown in fig.3, the angular momentum distribution in the lowest energy $K=3/2$ prolate intrinsic state is peaked around $J=7/2$ with 17 percent intensity. It is seen from figs. 3 and 4 that the projected spectra show a considerable departure from the rotational sequence. This is in contrast to the

^{45}Ti

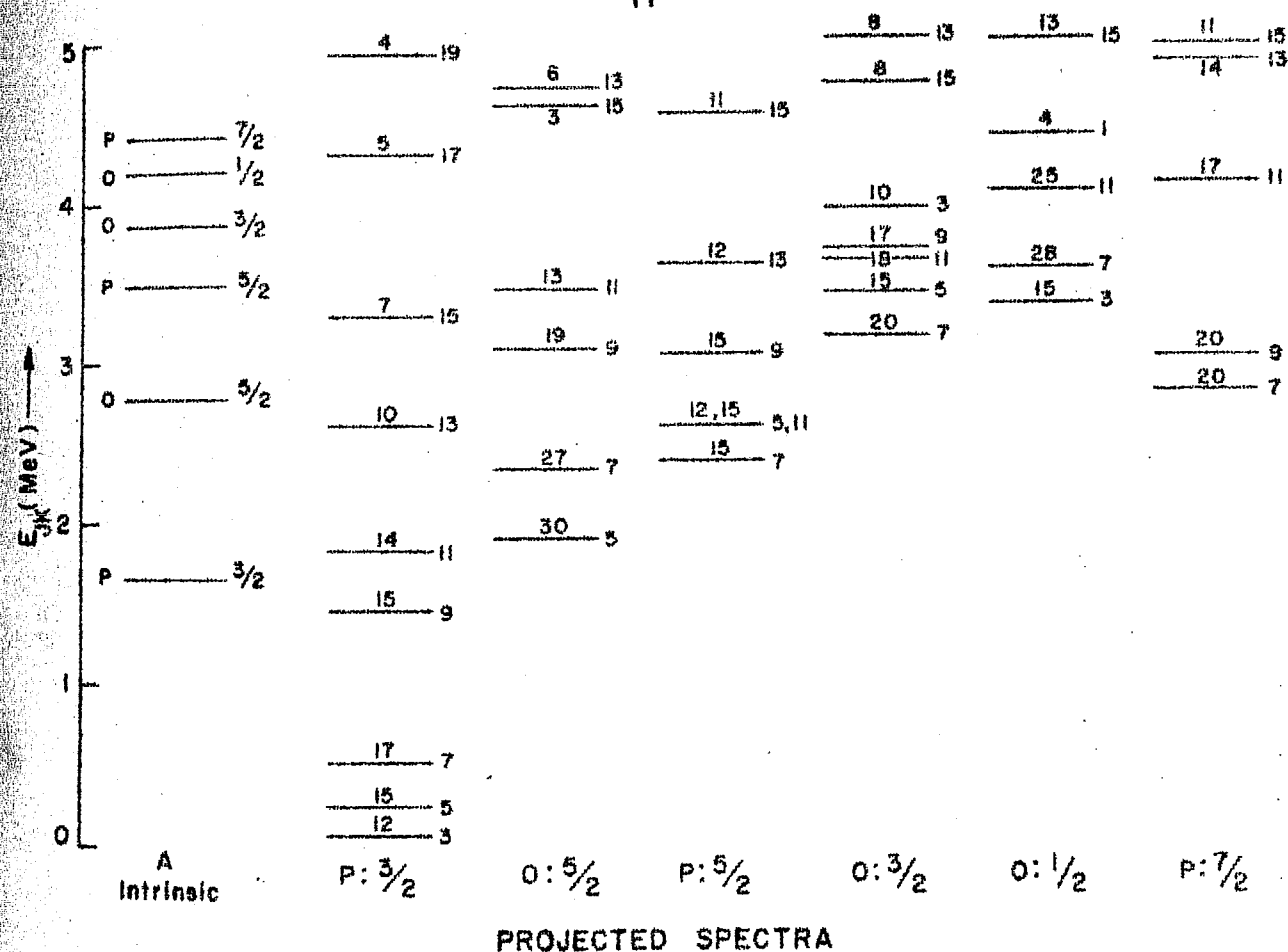
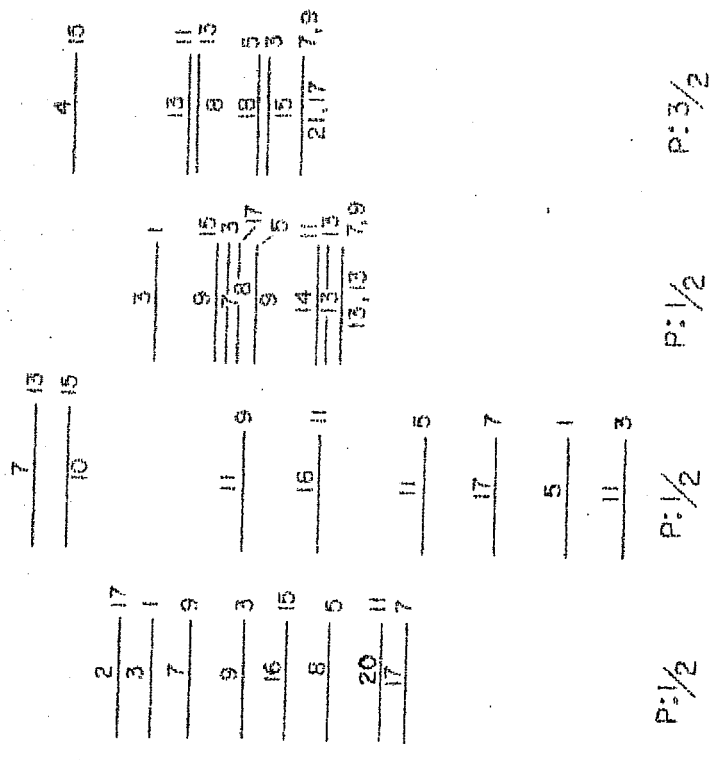
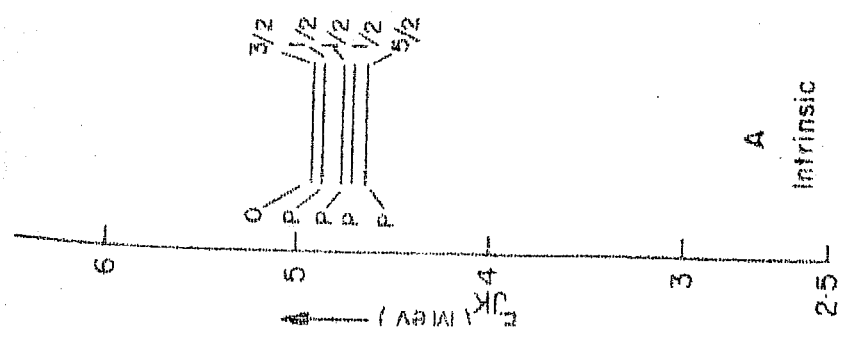


Fig.3

Energy spectrum of the prolate(P) and oblate(O) intrinsic states of ^{45}Ti and of the states with definite angular momentum projected from them. The energies of the intrinsic states are plotted under A, where the numbers on the right indicate their K-values. Projected spectra are plotted according to the sequence of the intrinsic states under A. The numbers on the right give $2J$ values while those on the top are the intensities of those projected states in their corresponding intrinsic states.

⁴⁵Ti



PROJECTED SPECTRA

Fig.4

Energy spectrum of the prolate (P) and oblate (O) intrinsic states of ⁴⁵Ti and of the states with definite angular momentum projected from them. All these spectra are plotted relative to the energies of the states in fig.3. For other details see the caption of Fig.3.

RPC model calculations¹⁷⁾ including coriolis-coupling between different bands, in which the spectra of all $K \neq 1/2$ bands are assumed to have a $J(J+1)$ sequence. It is thus clear that this assumption built in the RPC model does not emerge out of the microscopic calculations using effective interactions between the nucleons.

2.1.3 Nonorthogonality of the Projected States

We shall now illustrate the extent of the nonorthogonality of the states $\psi_{MK}^J(\gamma)$ projected from the different intrinsic states $\chi_K(\gamma)$ of ^{45}Ti . In table 6 are given the overlaps $N_{K\gamma, K'\gamma'}^J$ given by eq.(35) of the normalized projected states with $J=7/2$ projected from the intrinsic states with $K \leq 7/2$ of ^{45}Ti . Thus the overlaps of the $J=7/2$ state projected from the prolate HF $K=3/2$ intrinsic state (labelled $P \frac{3}{2}$) at -11.64 MeV, with the $J=7/2$ states projected from other intrinsic states listed in table 3, are given in the top most row of table 6. Similarly, the overlaps of the $J=7/2$ state projected from the oblate $K=5/2$ ($O \frac{5}{2}$) intrinsic state with the other projected $J=5/2$ states are given in the second row and so on.

It is seen from table 6, that the overlap of the $J=7/2$ projected from the prolate HF $K=3/2$ intrinsic state ($P \frac{3}{2}$), with

Table 6

The overlap matrix of the $J=7/2$ states projected from the eleven intrinsic states $\chi_K(\gamma)$ at energies $E_K(\gamma)$ (in MeV) of ^{45}Ti . P and O refer to the prolate and oblate shapes respectively.

K	$P \frac{3}{2}$	$O \frac{5}{2}$	$P \frac{5}{2}$	$O \frac{3}{2}$	$O \frac{1}{2}$	$P \frac{7}{2}$	$P \frac{5}{2}$	$P \frac{1}{2}$	$P \frac{1}{2}$	$P \frac{1}{2}$	$O \frac{3}{2}$
E_K	-11.64	-10.53	-9.82	-9.45	-9.13	-8.90	-8.66	-8.57	-8.55	-8.43	-8.38
$P \frac{3}{2}$	1.0	0.47	0.44	0.32	0.37	0.08	-0.45	-0.49	0.11	0.44	0.23
$O \frac{5}{2}$		1.0	0.38	0.69	0.32	0.24	-0.08	-0.36	-0.02	0.18	0.52
$P \frac{5}{2}$			1.0	0.49	0.35	0.23	0.36	-0.25	0.01	0.17	-0.03
$O \frac{3}{2}$				1.0	0.67	0.44	0.13	-0.34	-0.10	0.06	-0.14
$O \frac{1}{2}$					1.0	0.35	-0.06	-0.35	-0.06	0.08	-0.35
$P \frac{7}{2}$						1.0	0.10	-0.07	-0.007	0.02	-0.18
$P \frac{5}{2}$							1.0	0.21	-0.05	-0.23	-0.32
$P \frac{1}{2}$								1.0	0.08	0.34	-0.10
$P \frac{1}{2}$									1.0	-0.04	-0.01
$P \frac{1}{2}$										1.0	0.21
$O \frac{3}{2}$											1.0

almost all the other projected states except for those projected from the prolate $K=1/2$ (P_2^1) intrinsic state at -8.55 MeV are large, yet not too large to give rise to spurious states. Thus a $J=7/2$ state projected from any of the excited intrinsic states would not by itself describe well an excited state of ^{45}Ti nucleus.

The overlap matrices for other angular momenta have a similar pattern.

As a consequence of this nonorthogonality of the states $\psi_{MK}^J(\eta)$ the energy spectra of the orthonormalized states $\phi_M^J(\eta)$ would be shifted relative to the spectra of the states $\psi_{MK}^J(\eta)$ shown in figs.3 and 4. These energy shifts are different from the shifts produced by the mixing of various orthonormalized projected states by the Hamiltonian.

Of particular interest in table 6 are the values of the overlaps of the states projected from the prolate $K=1/2$ intrinsic state at -8.55 MeV with all the other projected states. These overlaps are quite small for all the J -values (upto $19/2$). This indicates the possibility of a well defined band of states, projected from this $K=1/2$ state, all of which might correspond to the eigenstates of the Hamiltonian if the mixing due to the Hamiltonian turns out to be small.

2.1.4 The Composite Spectrum

The composite spectrum of ^{45}Ti has been obtained by diagonalizing the Hamiltonian in the basis of orthonormalized projected state $\phi_M^J(\nu)$.

In order to verify our expectation that the low-lying states of ^{45}Ti would be adequately described by the states projectable from few of its lowest energy intrinsic states listed in table 3, we have diagonalized the Hamiltonian in the basis of orthonormalized projected states, in two stages:

- A) only lowest five intrinsic states of table 3 were considered²¹⁾ for the calculation of spectrum of ^{45}Ti .
- B) All the eleven intrinsic states were included.

The spectra resulting from these two calculations are plotted at (A) and (B) in fig.5. The calculation B containing the larger number of basis states, does not change much the spectrum of ^{45}Ti upto about 3 MeV excitation obtained in calculation A. However, the additional states included in calculation B appear and modify the spectrum above 3 MeV.

2.2 COMPARISON OF THE CALCULATED AND EXPERIMENTAL SPECTRUM

In fig.5 is also plotted the experimental spectrum of ^{45}Ti . The calculated ground state band of states with $J=7/2, 9/2, 11/2, 13/2$

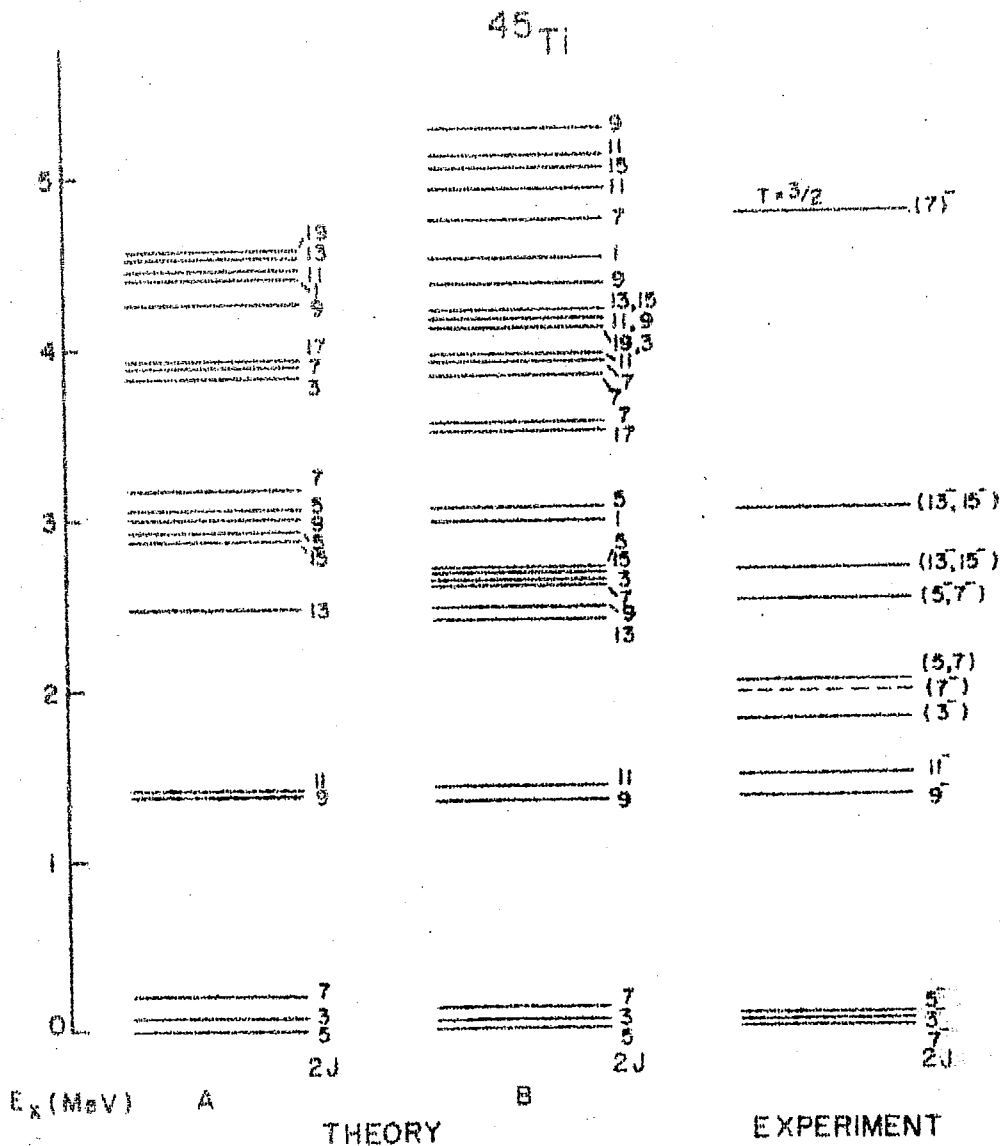


Fig.5

The calculated spectra of ^{45}Ti are compared with its observed spectrum. A and B denote the spectra obtained in calculations A and B with successively increasing number of basis states as discussed in subsec.2.1.4.

and $15/2$ occur at 0.13, 1.34, 1.47, 2.40 and 2.64 MeV. These agree well with the spectrum of high-spin states observed by Sawa et al¹⁾. The calculated $J=17/2$ and $19/2$ members of the ground state band are calculated to be at 3.49 and 4.09 MeV respectively and do not yet have experimental counterparts.

The ground state triplet observed by Jett et al²⁾ in $(p,n\gamma)$ reaction is very well reproduced, except that the $J=5/2$ and $7/2$ states have interchanged. Such an interchange, however, is not serious for near degenerate states. Zuk et al⁸⁾ have assigned $J=7/2^-$ or $9/2^-$ rather than $5/2^-$ to 40 keV level. Our calculations do not favour the existence of a second $J=7/2^-$ or $9/2^-$ level among the members of the observed ground state triplet.

The experimental data regarding the only other states observed at 1.80 ($3/2^-$), 1.95 ($7/2^-$), 2.016 ($5/2$, $7/2$) and 2.50 ($5/2^-$, $7/2^-$) MeV levels is not very specific. The 1.80 MeV level has been excited in (p,n) , (p,d) and (γ,α) reaction studies^{5,9,12,22)}. Plauger and Kashy¹²⁾ report the existence of a probable ($7/2^-$) level at 1.95 MeV from their (p,d) reaction measurements. Iyengar and Robertson⁹⁾ have not seen this state in their (p,n) and $(p,n\gamma)$ reaction studies. Instead, in this region they have seen a level with positive parity at 1.958 MeV and a level at 2.016 MeV. The positive parity assignment to the former level is also consistent with the

(π, α) reaction measurements²²⁾ wherein a state with $l=2$ transfer is observed at 1.96 MeV. For the 2.016 MeV state, Iyengar and Robertson⁹⁾ have assigned $J=(5/2 \text{ or } 7/2)$ of either parity. They further suggest that the 1.95 MeV level observed by Plauger and Kashy¹²⁾ may be the one observed at 2.016 MeV in their experiment. It is however not very clear from the data whether the 1.95 MeV and the 2.016 MeV levels are one and the same. It is likely that the level at 1.95 MeV may be a doublet of states: 1.958 MeV state of positive parity and 1.95 MeV of negative parity. The 2.50 MeV level has been assigned $J=(5/2^- \text{ or } 7/2^-)$ on the basis of $l=2$ transfer in the (π, α) reaction measurements²²⁾.

In the calculated spectrum at 5B, a triplet of states with $J=7/2-3/2-5/2$ occurs at 2.60, 2.63 and 2.72 MeV respectively. We associate these calculated states with the observed triplet at 1.80, 1.95 and 2.016 MeV. This association is supported by the similarities of the observed and calculated decay properties of these states. The mean lifetimes and branching ratios for the transitions from the states at 1.80 and 2.016 MeV have been observed by Iyengar and Robertson⁹⁾.

1.80 MeV Level

We shall show later that the calculated decay properties of the $J=3/2$ state at 2.63 MeV are similar to the observed

($3/2^-$) state at 1.80 MeV. It is therefore likely that the 2.63 MeV $3/2^-$ state corresponds to the 1.80 MeV observed state.

1.95 MeV Level

No data on decay properties of this level is available. However, the probable spin assignment of $7/2^-$ is suggested on the basis of (p,d) reaction measurements¹²⁾. It is likely that our calculated $J=7/2^-$ state at 2.60 MeV corresponds to this observed level.

2.016 MeV Level

This level is assigned $J=(5/2 \text{ or } 7/2)$ of either parity by Iyengar and Robertson⁹⁾. Both of our calculated $J=7/2$ and $5/2$ states at 2.60 and 2.72 MeV have decay properties similar to those observed for this 2.016 MeV level. In view of this agreement and the likely existence of the 1.95 MeV ($7/2^-$) level with which we have associated our calculated $J=7/2$ at 2.60 MeV, we suggest that our calculated $J=5/2$ state be regarded as that corresponding to this 2.016 MeV observed level.

It would be of interest to ascertain whether the levels at 1.95 and 2.016 MeV are the one and the same or that the 1.95 MeV is a doublet of states with the observed 1.958 MeV state of positive parity ($3/2^+$, $5/2^+$) and the 1.95 MeV ($7/2^-$) state.

If this triplet ($3/2-7/2-5/2$) exists, our calculated $J=5/2$ state at 3.07 MeV is then likely to correspond to the observed 2.50 MeV level with $J=5/2^-$ or $7/2^-$. For other calculated states no experimental counterparts are seen thus far. It would be of interest to investigate the high spin states predicted by our calculations.

It is interesting that although the ground state band is well reproduced by our calculation, the second excited set of states with $J=3/2, 5/2, 7/2$ are too high (~ 800 keV) in energy compared to the experimental spectrum. Similar discrepancies also occur²³⁾ for other fp shell nuclei and were a common feature of the calculated shell model spectra of the sd shell nuclei²⁴⁾. These probably reflect the inadequacies of the chosen effective interaction.

2.3 BAND STRUCTURE

The states $\Phi_M^J(\alpha)$ of the final composite spectrum of ^{45}Ti have been analysed for the possible band structures according to the procedure illustrated in sec.2 of chapter 2.

For each of the states $\Phi_M^J(\alpha)$ we have compared the overlaps $B_K^J(\gamma, \alpha)$ given by eq.(40) with the states $\psi_{MK}^J(\gamma)$ projected from each of the intrinsic states $\chi_K(\gamma)$ included in the calculation. The state $\Phi_M^J(\alpha)$ is considered to be belonging to a particular intrinsic state $\chi_K(\gamma)$ if the corresponding

intensity $|B_K^J|^2$ of the state $\psi_{MK}^J(\eta)$ is large. The quantity $(1 - |B_K^J|^2)$ gives the intensity in the state $\Phi_M^J(\alpha)$ of all the states orthogonal to $\psi_{MK}^J(\eta)$ and thus provides a measure of 'band mixing'.

If the intensity $|B_K^J|^2$ of the various states projected from a single intrinsic state is consistently large for a set of states $\Phi_M^J(\alpha)$ of the composite spectrum, then that set has been regarded as the 'band' of states.

According to this criterion, two bands of states:

(i) the ground state $K=3/2$ band and (ii) an excited $K=1/2$ band of states are likely to exist in the spectrum of ^{45}Ti . The other states of ^{45}Ti are found to have a complex structure in the sense that the intensities $|B_K^J|^2$ of the states projected from different intrinsic states are almost similar.

We shall now discuss these two bands of states.

2.3.1 The Ground State Band

The states with $J=3/2$ upto $19/2$ at energies E_J given in table 7, of the composite spectrum at 5B, are found to have consistently large intensities $|B_{3/2}^J|^2$ of the states projected from the prolate HF $K=3/2$ intrinsic state. These dominant intensities are given in table 7. It is seen from table 7 that the calculated $J=3/2$ state at 0.07 MeV is just the state projected from the prolate HF $K=3/2$ state. In a similar manner,

Table 7

Intensity of the states projected from the prolate HF $K=3/2$ intrinsic state, in the final 'ground state band' of states in ^{45}Ti , shown in fig.5B

J	$\frac{3}{2}$	$\frac{5}{2}$	$\frac{7}{2}$	$\frac{9}{2}$	$\frac{11}{2}$	$\frac{13}{2}$	$\frac{15}{2}$	$\frac{17}{2}$	$\frac{19}{2}$
E_J (MeV)	0.07	0.0	0.13	1.34	1.47	2.40	2.64	3.49	4.09
$ B_{3/2}^J ^2$	1.0	0.92	0.86	0.96	0.86	0.94	0.85	0.86	0.79

the $J=7/2$ state calculated at 0.13 MeV has the 86 percent intensity of the $J=7/2$ state projected from the prolate $K=3/2$ intrinsic state. In other words, this state has 14 percent admixture of all the other $J=7/2$ states orthogonal to that projected from the prolate HF $K=3/2$ intrinsic state. Thus we observe that compared to the states with $J=3/2, 5/2, 9/2$ and $13/2$ the band mixing in other states of table 7 is somewhat large (about 15 percent). The average band-mixing in all these states is about 11 percent.

2.3.2 $K=1/2$ Excited Band

As already mentioned the states projected from the $K=1/2$ excited intrinsic state at -8.55 MeV in ^{45}Ti are almost orthogonal to the states projected from the other intrinsic states of table 3. These states are thus likely to correspond to the

eigenstates of the Hamiltonian and are not expected to be altered much from their unperturbed positions (fig.4, col.4, p: $\frac{1}{2}$), if the mixing due to Hamiltonian is weak. As mentioned above, we have analysed the states of the composite spectrum in terms of the overlaps of the states projected from different intrinsic states. Of these, we give in table 8 the energies E_J of the states $\Phi_M^J(\alpha)$ for which the intensities $|B_{\frac{1}{2}}^J|^2$ of the states projected from the prolate $K=1/2$ intrinsic state at -8.55 MeV, is large. It is seen that the average band mixing in all these states is about 18 percent. The $J=13/2$ state at 4.14 MeV has about 62 percent band mixing, if regarded as a member of this band. It may be noted that there does not exist any other $J=13/2$ state in the calculated spectrum that has a large intensity of the $J=13/2$ state projected from this prolate $K=1/2$ intrinsic state. It is in this sense that the $J=13/2$ state at 4.14 MeV is only a weak member of this band.

Table 8

Intensity of the states projected from the prolate $K=1/2$ excited intrinsic state in the states of angular momentum J at energies E_J in the composite spectrum of ^{45}Ti .

J	$\frac{3}{2}$	$\frac{1}{2}$	$\frac{7}{2}$	$\frac{11}{2}$	$\frac{5}{2}$	$\frac{9}{2}$	$\frac{13}{2}$
E_J (MeV)	2.63	2.97	3.56	4.14	4.19	5.24	6.55
$ B_{1/2}^J ^2$	0.85	0.86	0.74	0.38	0.79	0.83	0.83

Experimental information about this band of states in ^{45}Ti is not available. It would be interesting to undertake an investigation of this band of states.

It is seen from table 3 that the structure of this $K=1/2$ band involves the excitation of the odd neutron from the occupied $k=3/2$ orbital to the unoccupied $k=1/2$ orbital. It is thus the only intrinsic state included in the present calculation in which the effects of the single particle states other than the $f_{7/2}$ state become dominant. The small **overlap** of the states projected from such an intrinsic state, with those projected from other intrinsic states included in the calculation is because of the structural differences in the orbit occupied by the odd nucleon. It is because of this reason that the excited states involving the excitation of a particle from the $f_{7/2}$ shell to the other fp shell states, would result in the existence of excited bands. Similarly excited bands, occur^{23,25,26,27)} in other fp shell nuclei with $Z, N \leq 28$.

2.4 ELECTROMAGNETIC PROPERTIES

We shall now discuss the electromagnetic properties of the low-lying states of ^{45}Ti , obtained in the DCM calculation. Experimental data^{3,4,5,8,9)} is available only for the lifetimes and branching ratios for transitions between the members of

the ground state band upto $J=11/2$ at 1.47 MeV and from the states at 1.80 and 2.016 MeV. Cornwell and McCullen¹⁵⁾ have measured the static moments of the $J=7/2$ ground states of ^{45}Ti .

In the calculations of the electric transitions we have used the effective charges $e_p=1.32e$ and $e_n=0.89e$. These charges were obtained²⁸⁾ in a least squares fit between the experimental and calculated²⁹⁾ $B(E2, 2 \rightarrow 0)$ transitions in even-even isotopes of Ti, Cr and Fe. For the description of magnetic properties values of free nucleon g-factors of the proton and neutron are used. We shall also give some of the results of $B(E2)$ values obtained with $e_p=1.5e$ and $e_n=0.5e$.

We shall first discuss the results of the static moments and then the transitions between the states of the ground state band followed by those between the other excited states of ^{45}Ti .

2.4.1 Static Moments

In table 9 are given the DCM calculated static electric quadrupole and magnetic dipole moments of the ground state triplet in ^{45}Ti . Also tabulated are the results of the $(f_{7/2})^5$ configuration calculations of Lynch et al³⁾ and the RPC results of Malik and Scholz as given by Lynch et al.

Table 9

Static electric quadrupole and magnetic dipole moments of the ground state triplet in ^{45}Ti

J	Q (e barn)			μ (n.m.)		
	7/2	5/2	3/2	7/2	5/2	3/2
Expt ^a	$\pm 0.015 \pm 0.015$			$\pm 0.095 \pm 0.002$		
DCM ^b	-0.13	-0.08	+0.18	-0.02	-0.22	-0.41
$(f_{7/2})^5$ ^c	-0.068			-0.59		
RPC ^d	+0.092			-0.66		

a. Ref. 15 b. $e_p = 1.32e$, $e_n = 0.89e$ c. Ref. 3 d. Quoted in ref. 3.

The $(f_{7/2})^5$ shell model calculation of Lynch et al have been performed using the $(f_{7/2})^2_{JT}$ matrix elements as obtained from the measurements of ^{42}Sc spectrum by Moinester et al⁽³⁰⁾. In this calculation $e_p = 1.97e$ and $e_n = 1.87e$ and $g_p = 1.499 \text{ n.m.}$ and $g_n = -0.39 \text{ n.m.}$ have been used.

The RPC model calculations assume deformation $\delta = -0.35$ the collective gyromagnetic ratio $g_R = Z/A$ and the magnetic moment of the odd nucleon to be 75 percent of its free particle value.

It is seen from table 9 that the quadrupole moment of

the $J=7/2$ ground state in ^{45}Ti as obtained by DCM calculation is higher than the experimental¹⁵⁾ value. The RPC value as well as the $(f_{7/2})^5$ configuration calculation value is also higher but smaller than our DCM value. In contrast the value of the magnetic moment as obtained in DCM calculation is in much better agreement with the experiment than those obtained by Lynch et al or Malik and Scholz.

In spite of the small value of these observed ground state moments, there is an interesting experimental measurement¹⁵⁾ for ^{45}Ti according to which the ratio $\mu_J/Q > 0$ for the ground state. Our DCM results and the $(f_{7/2})^5$ shell model results obey this relation while the RPC result does not.

2.4.2 Transitions in the Ground State Band

2.4.2.1 B(E2) and B(M1) Values

In table 10 are given the DCM calculated B(E2) and B(M1) values for the transitions between the members of the ground state band. Experimental data on these transitions is not available. In order to ascertain the effects of the configuration mixing on B(E2) and B(M1) values, we have also tabulated in columns, labelled PHF, the B(E2) and B(M1) values obtained for the transitions between the states projected from the prolate $K=3/2$ HF intrinsic state

Table 10

The calculated $B(E2)$ and $B(M1)$ values for the transitions from the initial state J_i to the final state J_f of the ground state band in ^{45}Ti . The results obtained by using full deformed configuration mixed wave functions are listed under the column DCM while those obtained by using only the projected Hartree-Fock states are given under the column PHF.

J_i	J_f	$B(E2) \text{ e}^2 \text{ fm}^4$			$B(M1) \text{ (n.m.)}^2$	
		PHF ^a	DCM ^a	DCM ^b	PHF	DCM
3/2	7/2	224	165	124		
5/2	3/2	268	223	169	0.20	0.07
	7/2	232	228	174	0.39	0.07
9/2	5/2	161	130	103		
	7/2	104	90	74	0.31	0.22
11/2	7/2	190	158	122		
	9/2	78	65	51	0.40	0.26
13/2	9/2	195	187	144		
	11/2	50	49	43	0.33	0.24
15/2	11/2	200	164	129		
	13/2	43	33	26	0.47	0.51
17/2	13/2	185	159	121		
	15/2	27	28	25	0.33	0.19
19/2	15/2	179	88	71		
	17/2	26	17	12	0.49	1.17

a. $e_p = 1.32e$, $e_n = 0.89e$

b. $e_p = 1.5e$, $e_n = 0.5e$

alone. The latter $B(E2)$ values are calculated with the effective charges $e_p = 1.32e$ and $e_n = 0.89e$. It is seen that compared to $B(E2)$ values the $B(M1)$ values are quite sensitive to the slight admixture in the wave functions.

2.4.2.2 (E2/M1) Mixing Ratios

The (E2/M1) mixing ratios calculated by using eq.(49) for the transitions between the members of the ground state band are given in table 11. Experimentally the value of only the mixing ratio for $9/2 \rightarrow 7/2$ transition is available. Unfortunately different measurements have led to different

Table 11

(E2/M1) mixing ratios for ground state band in ^{45}Ti

J_i	J_f	(E2/M1)	
		cal.	expt ^b
5/2	7/2	0.02	
	3/2	0.02	
9/2	7/2	0.23	$+0.34 \pm 0.12$
11/2	9/2	0.02	
13/2	11/2	0.14	
15/2	13/2	0.02	
17/2 ^a	15/2	0.05	
19/2 ^a	17/2	0.02	

a. Theoretical excitation energy
b. Ref.9

values. Sawa et al¹⁾ have given $\delta(9/2 \rightarrow 7/2) = 0.51_{-0.08}^{+0.18}$ while that by Zuk et al⁸⁾ ranges between 0.466 to 0.885 and that by Iyengar and Robertson⁹⁾ is 0.34 ± 0.12 . Our calculated values of 0.23 for the $(9/2 \rightarrow 7/2)$ transition is in close agreement with the latter measurements. For other transitions the experimental data does not exist.

2.4.2.3 Mean Lifetimes and Branching Ratios

The mean lifetimes τ_m and the branching ratios for the transitions between the low-lying states of ^{45}Ti are given in fig.6. Effective charges $e_p = 1.32e$ and $e_n = 0.89e$ are used. We have associated our calculated members of the ground state band with the high-spin states observed by Sawa et al¹⁾. These are indicated by thick lines in the fig.6. The vertical lines in this figure indicate the transitions originating from a state with a filled circle to the states where the arrows end. The numbers on top of the states are the calculated branching intensities while those below are the corresponding experimental values.

The experimental values of the mean life time are summarized from the observations of Iyengar et al⁵⁾, Lynch et al³⁾ and Blasi et al⁴⁾. As already mentioned in sec.1, the observed mean lifetime of the 40 keV level is not very certain. For this level Blasi et al⁴⁾ have measured $T_{1/2} = 11.5 \pm 1.5$ ns while Lynch et al⁵⁾ have observed $T_{1/2} = 17.2 \pm 1.0$ ns.

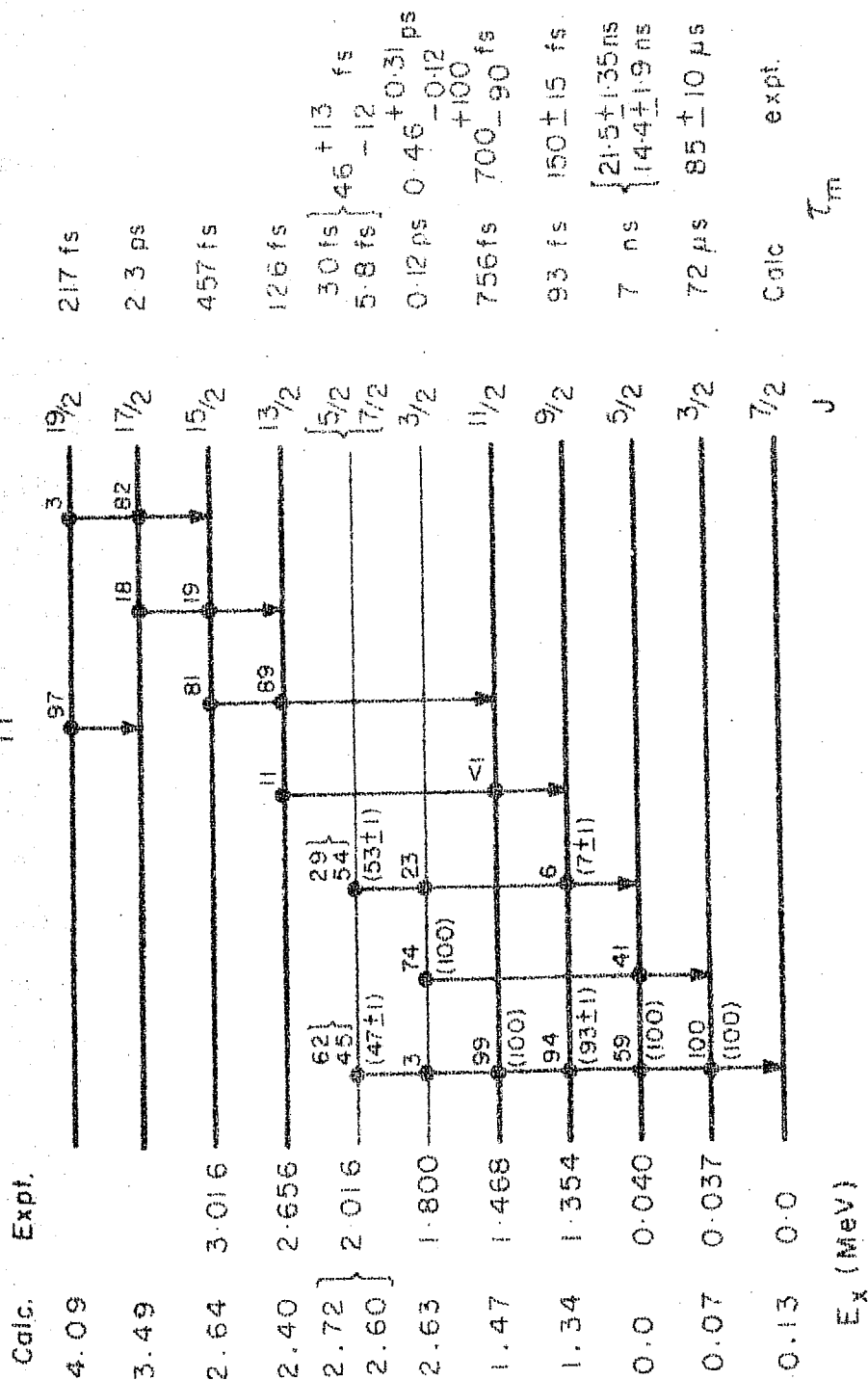


Fig. 6

Mean lifetimes and Branching ratios in 45-Ti. The states drawn in thick line belong to the ground state band. The numbers on the top of the states are the calculated branching intensities. Those below in parenthesis are the corresponding observed values. Both the calculated $J=7/2$ and $5/2$ states at 2.60 and 2.72 MeV are associated with the observed 2.016 MeV level. For discussion of this level see subsec. 2.4.3.

Using the internal conversion coefficient³⁾ of 0.25 for the decay of this 40 keV level, these values correspond to the radiative mean lifetime of 14.4 ± 1.9 ns and 21.5 ± 1.35 ns respectively.

The agreement between the theory and the experiment upto $J=11/2$ state at 1.47 MeV is good. The discrepancy occurs for the $J=5/2$ state at 40 keV. For this state the calculated lifetime is shorter than both the experimental values. Also this state is observed²⁾ to decay only to the $J=7/2$ ground state, while the calculation predicts 59:41 percent branches to the $J=7/2$ ground state and $J=3/2$ state at 37 keV. However, because of the energy difference of only 3 keV between the $5/2$ and $3/2$ states, it appears very hard to measure the $5/2 \rightarrow 3/2$ transition. In this sense, it seems that the departure in the measured and calculated branching ratios is not serious. For the members of the ground state band no experimental data is available. The calculation predicts a dominant M1 decay for the states with $J=13/2, 17/2$ and $19/2$. It would be interesting to measure the branching intensities for the decays between these high spin states in ^{45}Ti .

2.4.3 Other States

In this section we shall present the results of our $B(E2)$ and $B(M1)$ values for the transitions between the members

of the $K=1/2$ band of states and also for the transitions from these states to the members of the ground state band.

In the first half of table 12 are given the calculated $B(E2)$ and $B(M1)$ values for the intra-band transitions. These transitions are strong and in some cases similar to those calculated for the ground state band. Because of the strong $B(M1)$ value, these states are likely to have an $M1$ decay mode. In the second half of table 12 are given the corresponding values for the inter-band transitions from some of the members of the $K=1/2$ band to those of the ground state band. All these interband transitions are hindered, except for the $7/2$ (3.56 MeV) \rightarrow $7/2$ (gs) transition. Because of the large energy difference and a $B(M1)$ value of 0.19, this state has a fast $M1$ decay mode.

Iyengar and Robertson⁹⁾ have identified a state at 1.80 MeV. This state has been observed to decay only to $J=3/2$ of the ground state triplet with a lifetime of 460^{+310}_{-120} fs. Jones et al¹⁴⁾ and Plauser and Kashy¹²⁾ have suggested $J=3/2^-$ for this level.

The calculated $J=3/2$ member of the $K=1/2$ band occurs at 2.63 MeV. If this state is associated with the 1.80 MeV observed level, then as shown in fig.6, this state decays dominantly (74 percent) to the $J=3/2$ state at 0.037 MeV. The calculated mean lifetime of this state is also in reasonable

Table 12

Calculated $B(E2)$ and $B(M1)$ values for transitions between the members of the excited $K=1/2$ band of states in ^{45}Ti (above the dotted line) and those from the members of this $K=1/2$ band to the members of the ground state band (below the dotted line). For the members of the excited band, calculated energies while for the ground state band experimental energies are given.

$2J_i$	$2J_f$	E_i (MeV)	E_f (MeV)	$B(E2)$ $e^2 \text{fm}^4$	$B(M1)$ (n.m.) ²
1	3	2.97	2.63	280	1.11
7	3	3.56	2.63	136	
11	7	4.14	3.56	89	
5	1	4.19	2.97	108	
	3		2.63	32	0.003
	7		3.56	11	0.60
9	7	5.24	3.56	13	0.05
	11		4.14	0.03	0.24
	5		4.19	177	
<hr/>					
3	7	2.63	0.0	9	
	5		0.037	7	0.01
	3		0.040	3	0.06
1	5	2.97	0.037	0.01	
7	7	3.56	0.0	0.0003	0.19
	5		0.037	0.74	0.01
	3		0.040	0.04	
11	9	4.14	1.35	7	0.03
	11		1.47	28	0.01

agreement with the experiment. On the basis of the similarity in the decay modes of the calculated $J=3/2$ state at 2.63 MeV and the observed 1.80 MeV state, it appears tempting to identify the 1.80 MeV observed state as the band head of the $K=1/2$ band of state. Apart from this $J=3/2^-$ state there is no experimental information for the other states of this $K=1/2$ band.

Among the other states for which the experimental data⁹⁾ on decay modes is available is the state observed at 2.016 MeV. Probable spins $J=(5/2, 7/2)$ have been suggested. Iyengar and Robertson⁹⁾ have measured its decay branches 47:53 for the 2.016 \rightarrow 0.0 and 0.040 MeV transitions respectively. In the calculated spectrum at 5B, we have $J=5/2$ and $7/2$ states at 2.72 and 2.60 MeV. We have associated both these calculated $J=5/2$ and $7/2$ states in turn with the 2.016 MeV observed level and calculated the decay modes at that energy. The resulting values for lifetimes and branching ratios corresponding to each of these assignments, are given in fig.6. The calculated $J=7/2$ state has almost identical branching ratios as the observed ones but the lifetime is too short compared to what is measured. On the other hand, the $J=5/2$ state at 2.016 MeV decays with 62 and 29 percent branches to the $J=7/2$ and $5/2$ states of the ground state triplet, with a mean lifetime of 30 fs. Thus the lifetime of the

calculated $J=5/2$ state agrees with the observed value while the branching ratios do not.

It is clear therefore that both the $J=5/2$ and $7/2$ states provide an equivalent description of the observed decay modes of the 2.016 MeV level. However, Plauser and Kashy¹²⁾ have excited in (p,d) reaction a state at 1.95 MeV with tentative $J=7/2^-$ assignment. Earlier, we have associated our calculated $J=7/2^-$ state at 2.60 MeV with this state. It is therefore likely that our $J=5/2^-$ state at 2.72 MeV corresponds to the 2.016 MeV level.

It would be interesting to verify these assignments experimentally and also to resolve whether 1.95 MeV and 2.016 MeV levels are one and the same or that 1.95 MeV is a doublet, as suggested in this investigation.

REFERENCES

1. Z.P. Sawa, J. Blomqvist and W. Gullholmer, Nucl. Phys. A205 (1973) 257.
2. J.H. Jett, G.D. Jones and R.A. Ristinen, Phys. Lett. 28B (1968) 111.
3. F.J. Lynch, K.E. Nysten, R.E. Holland and R.D. Lawson, Phys. Lett. 32B (1970) 38.
4. P. Blasi, P.R. Maurenzig and N. Taccetti, Nuovo Cim. Lett. 2 (1969) 174.
5. K.V.K. Iyengar, E. Wong and G.C. Neilson, Nucl. Phys. A155 (1970) 582.
6. R.M. Brugger, T.W. Bonner and J.B. Marion, Phys. Rev. 100 (1955) 84.
7. G.J. McCallum, A.T.G. Ferguson and G.S. Mani, Nucl. Phys. 17 (1960) 116.
8. W.M. Zuk, W.F. Davidson, L.E. Carlson and M.R. Najam, Nucl. Phys. A187 (1972) 501.
9. K.V.K. Iyengar and B.C. Robertson, Nucl. Phys. A171 (1971) 73.
10. J. L'Ecuyer and C. St-Pierre, Nucl. Phys. A100 (1967) 401.
11. H.F. Lutz and T.S. Bohn, Nucl. Phys. A116 (1968) 112.
12. P.J. Plauger and E. Kashy, Nucl. Phys. A152 (1970) 609.
13. E. Kashy and T.W. Conlon, Phys. Rev. 135 (1964) B389.

14. G.D. Jones, R.R. Johnson and J.H. Jett, Nucl. Phys. A111 (1968) 449.
15. R.G. Cornwell and J.D. McCullen, Phys. Rev. 148 (1966) 1157.
16. J.D. McCullen, B.F. Bayman and L. Zamick, Phys. Rev. 134 (1964) B515.
17. F.B. Malik and W. Scholz, Phys. Rev. 150 (1966) 919.
18. I.P. Johnstone, Phys. Lett. 28B (1969) 643.
19. A. Kallio and K. Kolltveit, Nucl. Phys. 53 (1964) 87.
20. B.E. Chi, Nucl. Phys. 83 (1966) 97.
21. A.K. Dhar, D.R. Kulkarni and K.H. Bhatt, Nucl. Phys and Solid State Phys. (India) 16B (1975) 146.
22. M.B. Lewis, Nucl. Data Sheets 4 (1970) 237.
23. A.K. Dhar and K.H. Bhatt, Nucl. Phys. and Solid State Phys. (India) 18B (1975) and to be published.
24. D.R. Kulkarni and S.P. Pandya, Nucl. Phys. and Solid State Phys. (India) 16B (1973) 153.
25. A.K. Dhar and K.H. Bhatt, sent to Phys. Rev.
26. A.K. Dhar, S.B. Khadkikar, D.R. Kulkarni and K.H. Bhatt, Nucl. Phys. and Solid State Phys. (India) 17B (1974) 246.
27. A.K. Dhar, D.R. Kulkarni and K.H. Bhatt, Nucl. Phys. A238 (1975) 340.
28. A.K. Dhar - unpublished.
29. A.K. Dhar, D.R. Kulkarni, S.B. Khadkikar and K.H. Bhatt,

Proc. Int. Conf. on Gamma-ray Trans. Prob., New Delhi (1974), ed. by S.C. Pancholi and S.L. Gupta (Delhi Univ. Press, to be published).

30. M. Moinester, J.P. Schiffer and W.P. Alford, Phys. Rev. 179 (1969) 984.

CHAPTER 4

THE NUCLEUS ^{47}Ti

1. INTRODUCTION

1.1 Experimental Data

A considerable amount of experimental information¹⁻¹⁴⁾ regarding the nucleus ^{47}Ti has been recently obtained. The ground state band of states upto $J=17/2$ and the other high-spin states of this nucleus have been observed by Sawa et al²⁾ in (α, n) reaction measurements. Rapaport et al³⁾, Alty et al⁴⁾, Kocher and Haeberli⁵⁾ and more recently Chowdhury and SenGupta⁶⁾ performed (d, p) reactions on ^{46}Ti at about 10 MeV incident beam energy and identified low-lying low-spin states of ^{47}Ti . Some of the low-spin states upto about 9 MeV excitation in ^{47}Ti have also been observed by Plauser and Kashy in ^{48}Ti (p, d) reaction at 35.15 MeV proton beam energy. A detailed experimental investigation on the electromagnetic decay properties, lifetimes, branching ratio and $(E2/M1)$ mixing ratios of some of the low-lying states of ^{47}Ti have been made by Weaver et al⁸⁾ using Doppler-shift-attenuation method. Interesting data about the decay properties of some of these states has also been provided by Fifield et al⁹⁾ in their study of the β -decay of ^{47}V by Meyer-Schutzmeister et al¹⁰⁾, by

performing $^{45}\text{Sc}(^3\text{He}, p\gamma)$ reaction. Sawa et al²⁾ have also given (E2/M1) mixing ratios for the transitions between the high-spin states of this nucleus. Rao et al¹¹⁾ have investigated the structure of ^{47}Ti by employing the reactions $^{48}\text{Ti}(^3\text{He}, \alpha)$, $^{47}\text{Ti}(p, p'\gamma)$ and $^{45}\text{Sc}(^3\text{He}, p)$ at 13.0, 6.5 and 12 MeV bombarding energies and deduced spins, parities and transition strengths of the levels upto about 3.5 MeV excitation energy.

1.2 Previous Calculations

In the full fp shell space, the number of states¹⁵⁾ of seven particles with $T=3/2$ and $J=1/2, 3/2, 5/2, 7/2$ and $9/2$ are 8793, 16464, 22071, 25141 and 25600 respectively. For this reason complete shell model calculations have not been done. The $(f_{7/2})^7$ configuration calculations of McCullen, Bayman and Zamick with its extreme truncation of the configuration space does not adequately describe the structure of this nucleus. The RPC model calculations for this nucleus have been performed by Malik and Scholz¹⁷⁾, Weaver et al and recently by Haas et al¹⁸⁾. These calculations, however, are not microscopic.

In the next section we shall describe the microscopic DCM calculations that we performed for the study of ^{47}Ti .

2. PRESENT CALCULATIONS

The configuration mixing calculations for ^{47}Ti have been performed in the basis of states projected from the prolate and oblate HF intrinsic states and from the determinantal states obtained by various elementary excitations from these HF states. MWH2 effective interaction¹⁹⁾ is used.

In subsec.2.1 - 2.3 we shall describe the results of the DCM calculations for the spectrum of ^{47}Ti . The electromagnetic properties of its low-lying states are described in subsec.2.4. An attempt has been made to assign spin-values to the various observed states, on the basis of the agreement with the experiment of the calculated energies and decay properties of these states. In subsec.2.5 we shall present a simple method of extrapolating results of the band-mixing calculations to obtain an estimate of the level density upto an excitation of 6 MeV in ^{47}Ti . The estimates of level density have usually been made by a combinatorial calculation in the basis of single particle intrinsic states which do not have a definite angular momentum. Our approach differs from this conventional method, in that the estimate of level density of the states of definite angular momentum is obtained and is thus an improvement over the usual methods.

2.1 THE CALCULATION OF THE ENERGY SPECTRUM

2.1.1 Generation of Intrinsic States

2.1.1.1 Hartree-Fock Intrinsic States

Using MWH2 interaction, prolate and oblate HF solutions have been obtained for the nucleus ^{47}Ti . The single particle states with $|k| = 1/2, 3/2$ and $5/2$ are occupied for the prolate $K=5/2$ state. The energy E_K and the quadrupole moment Q_K of this state is -15.54 MeV and $21.12 b^2$ (with $b^2 = \hbar/m\omega$). For the oblate HF state with energy -14.46 MeV and quadrupole moment $-14.11 b^2$, the state with $|k| = 7/2, 5/2$ and $3/2$ are occupied.

In tables 13 and 14 are given the structural details of the HF prolate and oblate single particle proton and neutron occupied and a few lowest unoccupied orbitals. The corresponding energies e_k (eq.8) and quadrupole moments q_k (eq.11) of these orbits are also given. The dashed line separates the information regarding the occupied orbits from that of the unoccupied ones. The energy spectrum of some of these orbits is sketched in fig.7 where the small difference in the energies of the proton-neutron and their time-reversed orbits has been ignored in drawing the figure. The structure of these orbitals indicates a deformation $^{20)} \delta \sim 0.15$ for the prolate HF state and -0.10 for the oblate HF state.

Table 13

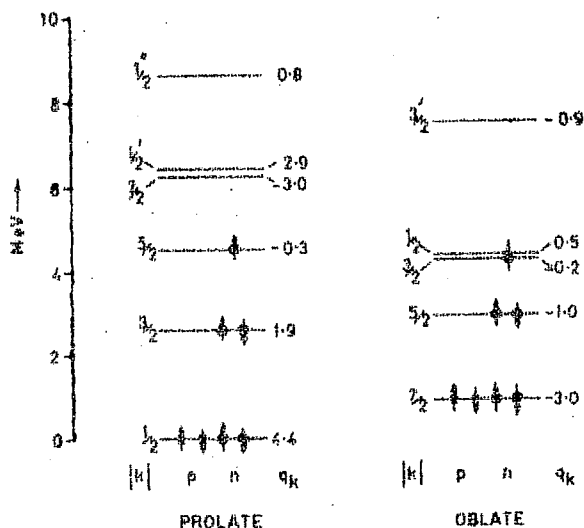
Structural and spectral details of the occupied and a few lowest unoccupied proton and neutron orbitals of the PROLATE $K=5/2$ HF intrinsic states of ^{47}Ti . ($E_K = -15.54$ MeV, $Q_K = 21.12$ b²). For other details see caption of table 1

	k	e_k MeV	q_k b ²	$c_{\frac{1}{2}k}$	$c_{\frac{3}{2}k}$	$c_{\frac{5}{2}k}$	$c_{\frac{7}{2}k}$
P R O T O N S	1/2	-7.45	4.39	0.153	0.359	-0.177	0.903
	-1/2	-7.35	4.32	-0.146	-0.350	0.164	0.910
	3/2	-5.44	2.18		-0.173	-0.157	0.972
	-3/2	-5.06	2.19		-0.173	0.167	0.971
	5/2	-3.56	-0.22			-0.116	0.993
N E U T R O N S	1/2	-5.54	4.34	0.150	-0.349	-0.176	0.908
	-1/2	-5.95	4.29	-0.164	-0.326	0.209	0.907
	3/2	-2.91	1.91		-0.119	-0.104	0.987
	-3/2	-3.38	2.13		-0.156	0.166	0.974
	5/2	-1.03	-0.26			0.086	0.996
	-5/2	-1.49	-0.25			0.096	0.995
	7/2	0.69	-3.0				1.0
	1/2'	0.87	2.88	-0.490	0.646	0.417	0.410
	1/2''	3.05	0.80	-0.426	-0.670	0.604	-0.070

Table 14

Structural and spectral information of the occupied and a few lowest unoccupied proton and neutron orbitals of the OBLATE $K=3/2$ HF intrinsic state of ^{47}Ti . ($E_K = -14.46$ MeV and $Q_K = -14.11 \text{ b}^2$). For other details see caption of table 1.

	k	e_k MeV	q_k b^2	$c_{\frac{1}{2}k}$	$c_{\frac{3}{2}k}$	$c_{\frac{5}{2}k}$	$c_{\frac{7}{2}k}$
P							
R	7/2	-6.72	-3.0				1.0
O	-7/2	-6.47	-3.0				1.0
T							
O	5/2	-4.73	-0.95			0.209	0.978
N							
S	-5/2	-4.42	-1.04			-0.238	0.971
	7/2	-4.67	-3.0				1.0
	-7/2	-5.12	-3.0				1.0
N							
E	6/2	-2.70	-1.0			0.227	0.974
U	-5/2	-2.74	-0.95			-0.207	0.978
T							
R	3/2	-1.34	-0.16		0.289	0.078	0.954
O	-3/2	-1.67	-0.04		0.261	-0.066	0.963
N							
S	1/2	-1.24	0.45	0.112	0.275	0.071	0.952
	3/2	1.99	-0.89		0.947	-0.151	-0.275



Fi.7

As shown in table 13 and fig.7 for the prolate shape, the first neutron unoccupied orbital with $k=7/2$ is at 1.72 MeV from the last occupied $k=5/2$ orbit. At only 180 keV from it is the second orbital with $k=1/2$. The neutron 1p-1h excitations to these unoccupied orbitals are expected to give intrinsic states lower in energy than the ones obtained by excitation to the higher unoccupied orbitals. The first proton unoccupied orbital with $k=3/2$ is at about 1.91 MeV. Similar information regarding the structure of the oblate intrinsic state is summarized in table 14.

2.1.1.2 One Particle-One Hole Excited Intrinsic States

We have considered in our calculation intrinsic states upto 3 MeV excitation relative to the prolate HF state. Eight intrinsic states obtained by various 1p-1h excitations from

Table 15

Energies and K-values of the prolate and oblate HF states of ^{47}Ti and of the intrinsic states obtained by 1p-1h excitations from these HF states.

Shape	Hole k_i	Particle k_m	K	E_K (MeV)
Prolate	(HF STATE)		5/2	-15.54
	n 5/2	n 7/2	7/2	-14.17
	n -3/2	n -5/2	3/2	-13.78
	n 5/2	n 1/2'	1/2	-13.76
	p -1/2	p -3/2	3/2	-12.97
Oblate	(HF STATE)		3/2	-14.46
	n 3/2	n 1/2	1/2	-13.91
	n -5/2	n -3/2	5/2	-13.30
	n -5/2	n -1/2	1/2	-13.19
	p -7/2	p -5/2	5/2	-12.25

the lowest prolate and oblate HF states are found to be within the above energy interval. These states are listed above in table 15 along with their HF states from which they were obtained. It may be pointed out that the intrinsic state with $K=1/2$ at -13.19 MeV is obtained by the 1p-1h excitation from the oblate HF state with the odd neutron in the $k = -3/2$ orbit. Thus the proton and neutron occupied orbitals in this $K=1/2$ intrinsic state are:

$$\pi(\pm 7/2)^2 \nu(\pm 7/2, +5/2, -3/2, -1/2)^5$$

In table 15, except for the first two 1p-1h excitations from the prolate shape and first 1p-1h excitation from the oblate shape, all other 1p-1h excitations would correspond to the 'core' excitations in the language of RPC model in which all but the last odd particle are incorporated in the definition of the deformed 'core'.

It is seen from table 15 that there exist three $K=1/2$ intrinsic states upto about 3 MeV excitation from the prolate HF state. The energy spread of these $K=1/2$ states is only 0.72 MeV. Kocher and Haeberli⁵⁾ and Chowdhury and SenGupta⁶⁾ have reported seven $J=1/2$ states within 6 MeV in the spectrum of ^{47}Ti . All these $J=1/2$ states are spread within 4 MeV relative separation energy. It is clear therefore that the inclusion of only three $K=1/2$ intrinsic states would not be adequate to describe the low-lying $J=1/2$ states. In view of this, the configuration space of $J=1/2$ states has been extended by including other 1p-1h and also some 2p-2h excited $K=1/2$ intrinsic states. In all ten $K=1/2$ states with an energy spread of around 2.6 MeV have been obtained. The structure and energies of these $K=1/2$ intrinsic states are given in table 16. For example, the prolate $K=1/2$ state at -11.38 MeV is a 2p-2h excited state obtained by exciting a

proton in $k = -1/2$ and a neutron in $k = -3/2$ orbits to the orbits with $k = -3/2$ and $-5/2$ respectively.

Table 16

Energies of the lowest ten $K=1/2$ intrinsic states obtained by $1p-1h$ and $2p-2h$ excitations from the lowest prolate and oblate HF states. These states were used in the calculation of only the $J=1/2$ states in ^{47}Ti .

Shape	Hole k_i	Particle k_m	E_K (MeV)
Prolate	n $5/2$	n $1/2'$	-13.76
	n $-3/2$	n $-7/2$	-12.61
	n $3/2$	n $-1/2$	-11.96
	n $5/2$	n $1/2''$	-11.56
	p $-1/2, n -3/2$	p $-3/2, n -5/2$	-11.38
	n $-1/2$	n $-5/2$	-11.35

Oblate	n $3/2$	n $1/2$	-13.91
	n $-5/2$	n $-1/2$	-13.19
	n $\pm 5/2$	n $+1/2, n -3/2$	-11.91
	p $-7/2, n -3/2$	p $-5/2, n -1/2$	-11.66

Similarly, the configuration space involving the intrinsic states of table 15 can give only six $J=3/2$ states. Vector polarization measurements of (d,p) reaction⁵⁾ have shown the existence of six $J=3/2$ states within an energy spread of 2.36 MeV in ^{47}Ti . To obtain a reasonably adequate description of these low-lying low-spin states, we have also

expanded the configuration space of the $J=3/2$ states, by including five other p-h excited $K=1/2$ and $3/2$ states. The details of these eleven intrinsic states are given in table 17. Of these the structure of the oblate $K=1/2$ intrinsic state at -13.19 MeV is already explained above

Table 17

Energies and K-values of the intrinsic states used for the description of only the $J=3/2$ states in ^{47}Ti . The oblate $K=1/2$ and $3/2$ intrinsic states at -13.19 and -12.14 MeV respectively, have the odd neutron in the $k = -3/2$ orbital.

Shape	Hole k_i	Particle k_m	K	E_K (MeV)
Prolate	n $-3/2$	n $-5/2$	$3/2$	-13.78
	n $5/2$	n $1/2$	$1/2$	-13.76
	p $-1/2$	p $3/2$	$3/2$	-12.97
	n $-3/2$	n $-7/2$	$1/2$	-12.61
	n $-3/2, 5/2$	n $\pm 7/2$	$3/2$	-12.10
	n $3/2$	n $-1/2$	$1/2$	-11.96

Oblate			$3/2$	-14.46
	n $3/2$	n $1/2$	$1/2$	-13.91
	n $-5/2$	n $-1/2$	$1/2$	-13.19
	n $-5/2$	n $1/2$	$3/2$	-12.14
	n $\pm 5/2$	$\left\{ \begin{array}{l} n \ 1/2 \\ n \ -3/2 \end{array} \right\}$	$1/2$	-11.91

while that of the oblate $K=3/2$ intrinsic state at -12.24 MeV is:

$$\pi(\pm 7/2)^2 \gamma(\pm 7/2, +5/2, -3/2, +1/2)^5$$

It may be noted that the $K=1/2$ states used here for the description of the $J=3/2$ states, have also been included in the ten states used for obtaining the spectrum of $J=1/2$ states.

2.1.1.3 Two particle-Two hole Excited Intrinsic States

Such intrinsic states would be expected to be higher in energy than the $1p-1h$ excited states. It is likely however, that some of the $2p-2h$ excited states may have an energy lower than the $1p-1h$ intrinsic states discussed above. They might then be important for determining the structure of the low-lying states of the nucleus. To ensure that we do not miss these low-lying $2p-2h$ excited states, the energies of some of the intrinsic states resulting from the $2p-2h$ excitations to the lowest unoccupied HF orbitals have been computed. The information regarding these states is provided in table 18. Of these the $2p-2h$ excited intrinsic states with $K=1/2$ have been included in the calculation of the spectrum of only the $J=1/2$ states while as those with $K=3/2$ and $1/2$ at -12.10 and -11.91 MeV respectively have been used for the

Table 18

Structural information of some of the low-lying 2p-2h excited intrinsic states in ^{47}Ti .

Shape	Holes k_i	Particles k_m	K	E_K (MeV)
Prolate	n $-3/2, n$ 5/2	n $\bar{7}/2$	3/2	-12.10
	p $\pm 1/2$	p $\pm 3/2$	5/2	-12.04
	p $-1/2, n$ 5/2	p $-3/2, n$ 7/2	5/2	-11.62
	p $-1/2, n$ $-3/2$	p $-3/2, n$ $-5/2$	1/2	-11.38
	n $\pm 3/2$	n 7/2, n $-5/2$	7/2	-11.10
	n $\pm 3/2$	n $\pm 7/2$	5/2	-10.78

Oblate	n $-5/2, n$ 3/2	n $\bar{1}/2$	5/2	-12.63
	n $\pm 5/2$	n $+1/2, n$ $-3/2$	1/2	-11.91
	n $\pm 5/2$	n $\pm 1/2$	3/2	-11.83
	p $-7/2, n$ 3/2	p $-5/2, n$ 1/2	3/2	-11.70
	p $-7/2, n$ $-3/2$	p $-5/2, n$ $-1/2$	1/2	-11.66
	p $-7/2, n$ $-5/2$	p $-5/2, n$ $-3/2$	5/2	-11.18
	p $\pm 7/2$	p $\pm 5/2$	3/2	-10.75

spectrum of only the $J=3/2$ states. For other J states, there is an adequate number of 1p-1h excited intrinsic states which are lower than the 2p-2h excited states. Hence the latter are not included in the calculation of the full spectrum. Their inclusion would however improve the level density at higher excitations.

2.1.1.4 Isospin Mixing in the Intrinsic States

The intrinsic states listed above in tables 15, 16 and 17 have a small admixture of different isospins T . In table 19 we give the amplitudes of the isospin components with $T=3/2$ and $5/2$, in the intrinsic states of table 15. The

Table 19

The amplitudes of the $T=3/2$ and $5/2$ isospin components in the intrinsic states of ^{47}Ti , given in table 15.

Shape	K	E_K (MeV)	$T=3/2$	$T=5/2$
Prolate	5/2	-15.54	0.999	0.025
	7/2	-14.17	0.999	0.015
	3/2	-13.78	0.999	0.025
	1/2	-13.76	0.999	0.024
	3/2	-12.97	0.999	0.009
<hr/>				
Oblate	3/2	-14.46	1.0	0.0
	1/2	-13.91	1.0	0.0
	5/2	-13.30	1.0	0.0
	1/2	-13.19	1.0	0.0
	5/2	-12.25	0.999	0.014

amplitudes of isospin $T \geq 5/2$ are negligibly small and are hence not given in the table. It is seen from table 19 that $T=3/2$ is the dominant isospin. The maximum amplitude

of $T=5/2$ admixture is only 0.025 for the lowest energy intrinsic state with $K=5/2$. It is hoped that this feeble isospin mixing in these intrinsic state would not alter the structure of the low-lying states in any significant manner.

2.1.2 Energy Spectra of the Angular Momentum Projected States

The states $\psi_{MK}^J(\gamma)$ with definite angular momenta J have been projected from the ten intrinsic states $\chi_K(\gamma)$, listed in table 15. The spectra (eq.21) projected from prolate and oblate intrinsic states are given in figs.8 and 9 respectively, and are plotted according to the order of the appearance of their corresponding intrinsic states at 8A and 9A. The intensity $|a_{JK}(\gamma)|^2$, given by eq.16 of a projected state $\psi_{MK}^J(\gamma)$ in the intrinsic state $\chi_K(\gamma)$ is also given in figs.8 and 9. Except for the states projected from the lowest prolate intrinsic state all other projected spectra show a considerable departure from a rotational sequence. This is in contrast to the assumptions of the RPC model calculations.

2.1.3. Non-orthogonality of the Projected States

We illustrate here the extent of the non-orthogonality

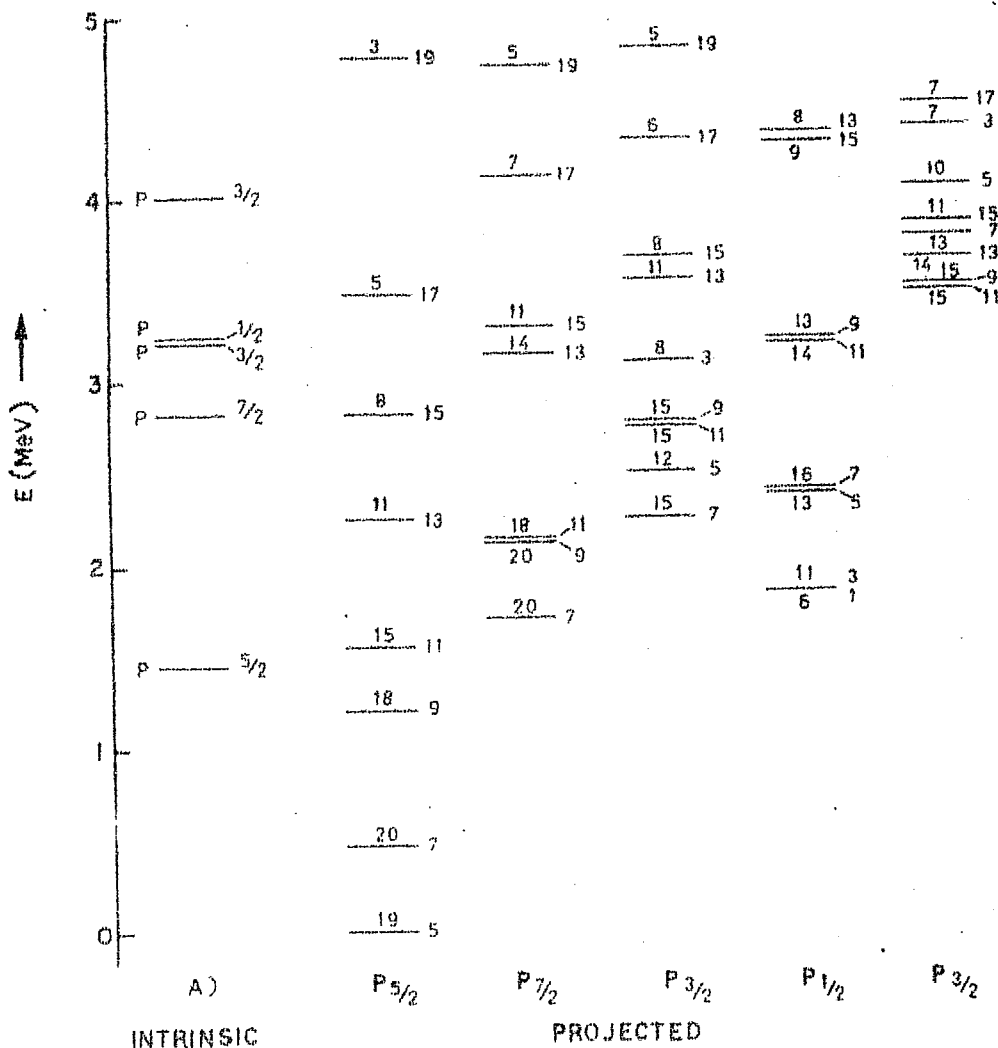


Fig.8

Energies of the prolate (P) intrinsic states and of the states of definite angular momentum in ^{47}Ti . The energies of the intrinsic states are plotted under A, where the numbers on the right indicate their K-values. Projected states are plotted according to the sequence of their intrinsic states at A. The numbers on the right give the $2J$ values while those on the top are their intensities in their intrinsic state.

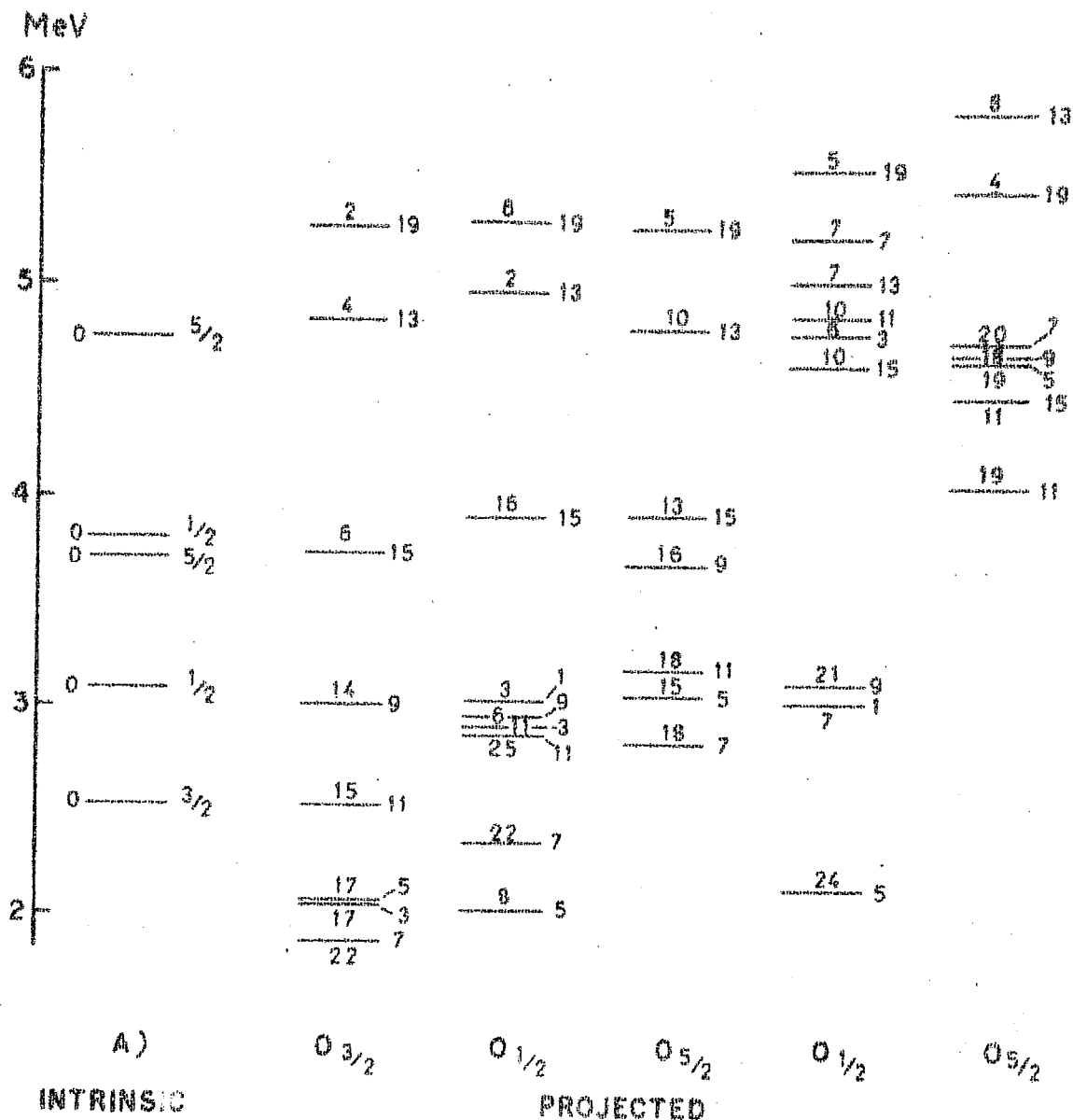


Fig.9

Energy spectra of the states projected from the oblate(O) intrinsic states of ^{47}Ti . All these spectra are plotted relative to the energies of the prolate states in fig.8. For other details see caption of fig.8.

of the states $\psi_{MK}^J(\gamma)$. For each of the states with $J \geq 7/2$, ten projected states are obtained while for $J=1/2, 3/2$ and $5/2$ only three, six and nine states respectively can be projected from the ten intrinsic states listed in table 15.

In table 20 are listed the overlaps (eq.35) of the various normalized projected states with $J=5/2$ obtained from the intrinsic states with $K \leq 5/2$ of table 15.

For $J=5/2$, the overlap of the state projected from the lowest energy prolate $K=5/2$ intrinsic state with almost all other projected states except for those projected from the prolate $K=1/2$ intrinsic state at -13.76 MeV is large enough to give rise to nonspurious orthogonal set of states. Therefore a $J=5/2$ state projected from any of the excited intrinsic states would not by itself describe well an excited state of ^{47}Ti nucleus. The overlap matrices for the other J states have a similar structure.

The non-orthogonality of the projected states leads to a slight overcompleteness of the basis states for $J \geq 7/2$. This is seen from the fact that all the eigenvalues of the overlap matrix (table 20) for the $J=5/2$ state are positive. Hence all the orthogonalized states are independent. This is also true for the states with $J < 9/2$. For the high spin states with $J=9/2, 13/2$ and $17/2$ one of the ten eigenvalues of the corresponding overlap matrix (eq.35) have been found

Table 20

The overlap matrix of the $J=5/2$ state projected from the nine intrinsic states of table 15 with $K=5/2$ at energies E_K (in MeV) in ^{47}Ti . P and O refer to the Prolate and Oblate deformations respectively.

K	$P \frac{5}{2}$	$O \frac{3}{2}$	$O \frac{1}{2}$	$P \frac{3}{2}$	$P \frac{1}{2}$	$O \frac{5}{2}$	$O \frac{1}{2}$	$P \frac{3}{2}$	$O \frac{5}{2}$
E_K	-15.54	-14.46	-13.91	-13.78	-13.76	-13.30	-13.19	-12.97	-12.25
$P \frac{5}{2}$	1.0	0.55	0.70	-0.36	-0.01	-0.27	-0.65	0.34	0.10
$O \frac{3}{2}$		1.0	0.68	-0.44	0.04	-0.51	-0.48	-0.00	0.29
$O \frac{1}{2}$			1.0	-0.27	-0.05	-0.25	-0.85	0.26	0.23
$P \frac{3}{2}$				1.0	-0.05	0.53	0.31	0.50	0.19
$P \frac{1}{2}$					1.0	-0.06	0.05	0.04	0.01
$O \frac{5}{2}$						1.0	0.09	0.26	0.25
$O \frac{1}{2}$							1.0	-0.21	-0.24
$P \frac{3}{2}$								1.0	0.35
$O \frac{5}{2}$									1.0

to be zero. Thus according to eq.37 for these states one of the states is spurious. Similarly for the states with $J=11/2$, $15/2$ and $19/2$ two states have been found to be spurious.

As a result of this non-orthogonality of the states $\psi_{MK}^J(\gamma)$ the energy spectra given by eq.(38) of the orthogonalized state $\phi_M^{\bar{J}}(\nu)$ would be shifted relative to the spectra of the states $\psi_{MK}^J(\gamma)$ shown in figs.8 and 9. These energy shifts are different from the shifts produced by the mixing of various orthogonalized projected states by the Hamiltonian.

Of particular interest in table 20 are the values of the overlaps of the states projected from the prolate $K=1/2$ intrinsic state at -13.76 MeV with all the other projected states. These overlaps are quite small for all the J -values (upto $19/2$). This indicates the possibility of a well defined band of states, projected from this $K=1/2$ state, all of which may reasonably correspond to the eigenstates of the Hamiltonian. Since this $K=1/2$ state is obtained by exciting a neutron from the highest occupied $k=5/2$ orbit to the unoccupied $k=1/2$ orbit (see table 15), it is likely that the band of states projected from this $K=1/2$ state would be preferentially observed in reactions involving neutron excitations from the ground state.

2.1.4 Composite Spectrum

The composite spectrum of ^{47}Ti was obtained by diagonalizing the Hamiltonian (eq.38) in the basis of the orthonormalized projected states $\phi_M^J(\gamma)$.

It is expected that the low-lying states of a nucleus would be described in terms of the mixing of the states projected from a few of the low-lying intrinsic states. To test this expectation we first carried^{21,22,23} out the calculation of the energy spectra with three choices of successively larger number of the basis states.

A) The basis states were chosen to be only the states projected from the five intrinsic states $P_{5/2}$, $P_{7/2}$, $P_{1/2}$, $O_{3/2}$ and $O_{1/2}$ (-13.91 MeV) listed in table 15.

B) This configuration space was expanded to include also the states projected from the intrinsic states $P_{3/2}$ (-13.78 MeV), $P_{3/2}$ (-12.97 MeV) and the oblate $K=5/2$ state at -12.25 MeV.

C) The calculation was further extended to incorporate also the states projected from the remaining intrinsic states listed in table 15.

The energy spectra resulting from the mixing of the above, five, eight and ten bands of projected states are

shown in figs.10A,10B and 10C respectively.

Comparison of these three calculated spectra show that the relative energy of the states upto about 2.5 MeV obtained in the first calculation is not altered much by expanding successively the configuration space to include various "core" excited 1p-1h states (calculation B and C).

For comparison we have shown the energy levels of ^{47}Ti observed in $(\alpha, n)^2$, $(d, p)^{5,6)}$, $(p, p'\gamma)^8)$ and $(^3\text{He}, p\gamma)^{10)}$ reactions. The calculated spectra upto 2.5 MeV in figs.10A, B and C are all quite similar to the experimental spectrum. This confirms the expectation that only a few p-h excited intrinsic states are needed for a reasonable description of the low-lying states of the nucleus ^{47}Ti .

Additional states appearing at about 3 MeV in calculation B and not reproduced in calculation A correspond to the "core" excited configurations listed in table 15. Although the spectra shown in A, B and C look similar, the calculation C containing the largest number of basis states, improves upon the states beyond 2.5 MeV obtained in calculation A and B. For example, the second $J=1/2$ state around 3.37 MeV obtained in calculation A and B is pushed down to around 3 MeV in the last calculation, and corresponds possibly to the $J=1/2$ state observed^{5,6)} at 2.79 MeV. Also the $J=5/2$ state at 3.07 MeV obtained in calculation B

comes down to 2.85 MeV in calculation C and thus lines up with the experimental $J=5/2$ states observed⁵⁾ tentatively at 2.85 MeV.

2.2 COMPARISON OF THE CALCULATED AND OBSERVED SPECTRUM

The experimental as well as calculated spectra are quite complex. It is convenient therefore to consider separately the set of high-spin states $J \geq 7/2$ observed primarily by Sawa et al²⁾ in (α, n) reaction and by Weaver et al⁸⁾ in $(p, p'\gamma)$ reaction and the low spin states $J \leq 7/2$ observed by Kocher et al⁵⁾ in (d, p) reaction.

2.2.1 High-spin States

In figure 11A we compare the experimental spectrum of the high spin states with the ones obtained above in calculation C.

In the experimental spectrum the states drawn in long lines are observed by Sawa et al²⁾. Of these, the states shown in heavy lines are connected by strong transitions. The ones drawn in thin line decay weakly. The states shown by short lines were observed in $(p, p'\gamma)$ reaction⁸⁾.

In the calculated spectrum the states drawn in long lines are ones we think correspond to the states observed by

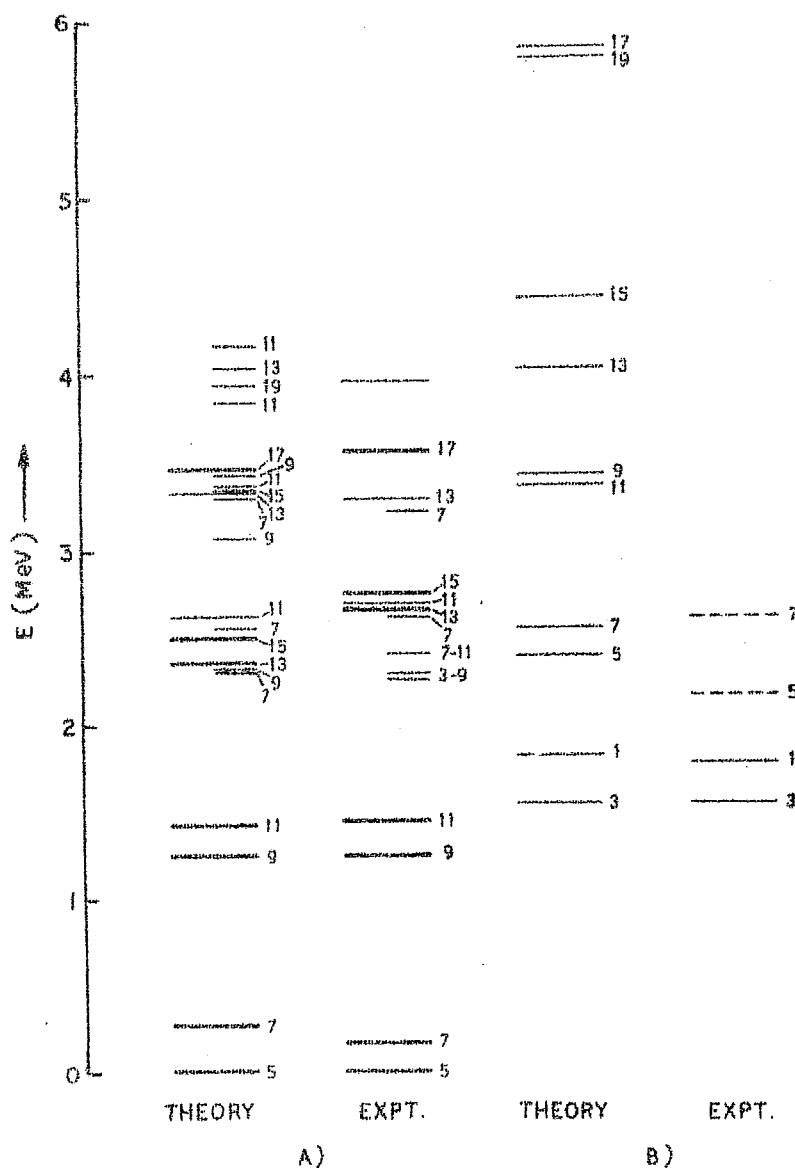


Fig.11

(A) The spectra of the calculated and observed high-spin states in ^{47}Ti . In the experimental spectrum the states drawn in long lines are observed by Sawa et al (Ref.2). Those drawn in short lines have been taken from ref.8. For other details see subsec.2.2.1. (B) The calculated band of states belonging to the prolate $K=1/2$ intrinsic state are compared with a few experimental states which might belong to this band. See subsec.2.3.2 for a discussion of these states.

Sawa et al²⁾. Amongst these the ones drawn in heavy lines are predominantly the states projected from the $K=5/2$ ground state HF band. The states drawn in thin lines do not belong to this ground state band. The states drawn in short lines are the ones which do not have a counterpart in the spectrum observed in (α, n) reaction and may correspond to those observed in $(p, p'\gamma)$ experiment.

The three main discrepancies between the experimental and calculated high spin spectra are the following:

- i) The states with $J=13/2$ and $15/2$ are significantly lower than their experimental counterparts at about 2.75 MeV.
- ii) The calculated high-spin states drawn in short lines with $J=15/2$, $11/2$ and $9/2$ at around 3.4 MeV and the states with $J=11/2$, $19/2$, $13/2$ and $11/2$ at around 4 MeV do not yet have experimental counterparts.

It might appear tempting to associate the calculated $J=19/2$ state at 3.95 MeV with the experimental state at 3.98 MeV. But, because of the observed²⁾ decay (though weak) of the level at 3.98 MeV to the $J=13/2$ state at 3.29 MeV, the $J=19/2$ assignment to the 3.98 MeV level is ruled out. Also, it is not likely to correspond to the calculated $J=13/2$ state at 4.05 MeV, since as will be shown in the next section, that state belongs to the $K=1/2$ band, drawn separately in fig.11B for clarity. If the experimental state at

3.98 MeV were the $J=13/2$ state of the $K=1/2$ band, it would have decayed strongly to the $J=9/2$ or $11/2$ states obtained at about 3.40 MeV. Such a strong decay has not been observed. It is therefore likely that the observed state at 3.98 MeV may correspond only to one of the $J=11/2$ states at about 4 MeV.

iii) There are two states with $J=7/2$ and $9/2$ at about 2.30 MeV in the calculated spectrum. In the experimental spectrum, Weaver et al⁸⁾ have obtained three states with a possible spin assignment of $J=3/2$ to $9/2$ and $J=7/2$ to $11/2$. Thus experimentally there is one extra state around 2.30 MeV compared to the calculated spectrum.

The calculated state with $J=7/2$ at 2.56 MeV matches well with 2.62 MeV state observed in the stripping reaction⁵⁾.

It is interesting to note that the observed as well as calculated "ground state band" of states terminates at the $J=17/2$ state. The calculated $J=19/2$ state at 3.95 MeV does not belong to this band. The excited $J=19/2$ states have considerable "band mixing". This will be discussed in next section.

It would be of interest to identify the high-spin states above 4 MeV shown in fig.10C.

2.2.2 Low-Spin States

Kocher and Haeberli⁵⁾ and Chowdhury and Sen Gupta⁶⁾ have observed seven $J=1/2$, six $J=3/2$, one $J=5/2$ and two $J=7/2$ states in (d,p) reaction.

The basis space of calculation C contains only three $J=1/2$ states and six $J=3/2$ states projected from the $K=1/2$ and $3/2$ intrinsic states. The calculated spectrum of low spin states in figure 10C is not in good agreement with the experimental one.

In order to obtain a reasonable description of the low-lying states of a nucleus in a truncated configuration space, it is clear that the configuration space should at least contain a few more states than the number of observed states in the chosen energy range. From this point of view the configuration space chosen in calculation C is adequate for the description of states with $J \geq 5/2$ for which ten states for each $J \geq 5/2$ are included in the calculation. For $J=5/2$, nine states are obtained. Thus the number of states in the configuration space is sufficiently greater than the number of observed low-lying states with $J \geq 5/2$.

For the low-spin states with $J=1/2$ and $3/2$ the configuration space of calculation C is clearly too small for the description of the observed states. The configuration space

for these states was therefore extended by including additional 1p-1h and some 2p-2h excited intrinsic states (see tables 16 and 17) with $K=1/2$ and $K=3/2$. Ten $J=1/2$ states were included in the expanded configuration space, whereas for $J=3/2$ eleven states were obtained.

The spectrum of the $J=1/2$ and $3/2$ states obtained from this expanded configuration space is compared in fig.12 with the spectrum observed⁵⁾ in the (d,p) reaction. For completeness we have also included the two excited states with $J=5/2$ and $7/2$ observed by Kocher et al⁵⁾. The first $J=7/2$ state is reproduced well by the calculation and is not included in fig.12. The experimental state at 5.01 MeV is not observed by Kocher et al, but is included in Nuclear Data Sheets¹⁾ and is also observed recently by Chowdhury and Sen Gupta⁶⁾.

Excellent agreement is obtained for the low-spin spectrum upto 3 MeV excitation. Above 3 MeV the agreement between the experimental and calculated spectrum for the $J=1/2$ state is quite good. For the $J=3/2$ state there are significant deviations above 3 MeV.

The calculation C is adequate for the description of the states with $J \geq 5/2$ and a comparison of the experimental and calculated spectra for the $J=5/2$ and $7/2$ states can be made from fig.10C. The calculated $J=5/2$ states occur at

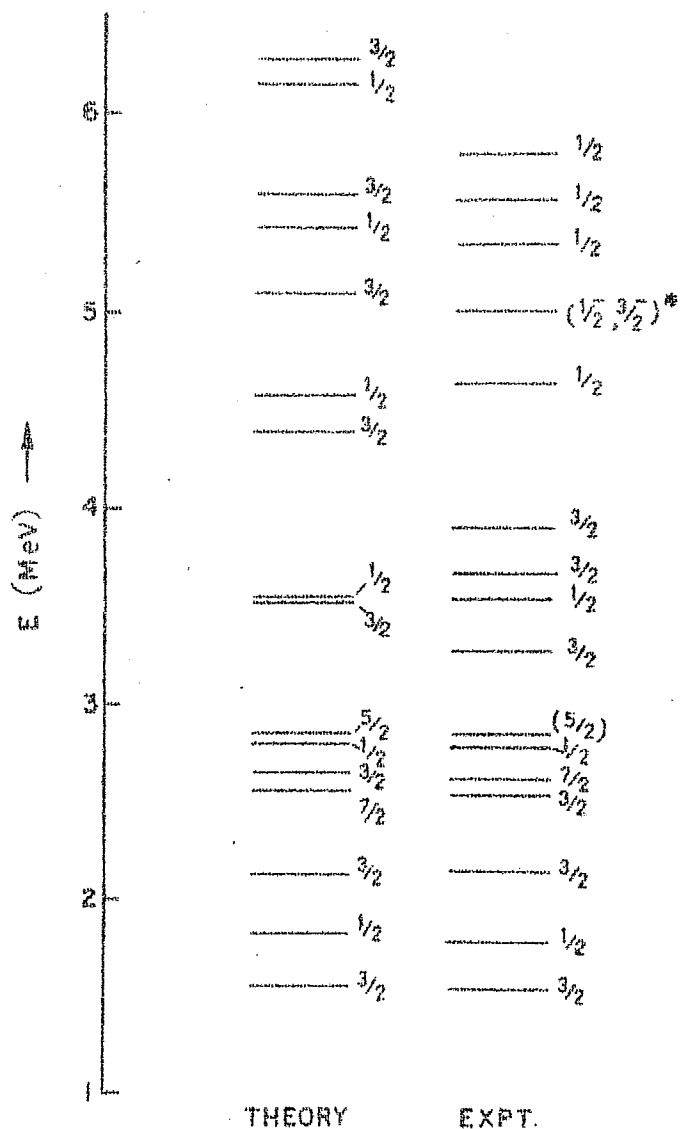


Fig.12

The calculated spectrum of low-spin states in ^{47}Ti are compared with the observed states of Kocher et al (ref.5). The starred state in the experimental spectrum is adopted from refs.1 and 6.

0, 2.40, 2.85 and 4.40 MeV. These compare well with the experimental states with definite $J=5/2$ assignment at 0, 2.17 and 2.85 MeV. The state at 2.17 MeV was observed by Fifield et al⁹⁾ in the β -decay of ^{47}V . The one at 2.85 MeV was seen in (d,p) reaction^{5,6)}.

The calculated states with $J=7/2$ occur at 0.27, 2.30, 2.56, 3.32 and 4.30 MeV. The observed states with definite $J=7/2$ assignment occur at 0.16, 2.62, and 3.22 MeV. The first two are observed in the (d,p) reaction^{5,6)}. The $J=7/2$ assignment for the 3.22 MeV state was made by Meyer-Schulzmeister et al¹⁰⁾ on the basis of the pure $L_{np}=0$ angular distribution in ($^3\text{He},p$) reaction. They have suggested it to be an antianalog state. In the neighbourhood of calculated 2.30 MeV $J=7/2$ state, there are three experimental states observed by Weaver et al⁸⁾ with possible spin assignments of $J=7/2$. One of these may have $J=7/2$ and would correspond to the calculated state at 2.30 MeV. It would be of interest to identify the experimental counterpart of the 4.30 MeV $J=7/2$ state.

2.3

BAND STRUCTURE

In the following we have analysed the structure of the various states of the composite spectrum plotted at 10C in terms of the states projected from the various intrinsic states of table 15.

2.3.1 Ground State Band

The spectrum of states (fig.8, col.2) projected from the HF prolate $K=5/2$ intrinsic state at -15.54 MeV is already in reasonable agreement with the spectrum of ground state band observed by Sawa et al.²⁾. In the final spectrum shown in fig.10C, the ground state obtained by diagonalization of the Hamiltonian is depressed by only 170 keV relative to the energy of the $J=5/2$ state projected from the $K=5/2$ HF state. The shifts in the other members of the "ground state band" due to the mixing of the states by the Hamiltonian are also similarly small. It is expected therefore that the "ground state band" obtained in fig.10C will still be predominantly the band projected from the $K=5/2$ HF state.

In table 21, we list the probabilities $\left| B_{5/2}^J \right|^2$ (eq.(40)) for states of the "ground state band" with angular momenta $J=5/2$ to $19/2$. It is seen that the intensity of the $J=5/2$ state projected from the $K=5/2$ HF state is 96 percent. Thus the total contribution of the part of the eight other $J=5/2$ states orthogonal to the one projected from the HF state is only 4 percent. It is clear from the table 21 that the lowest $J=19/2$ state is not predominantly the $J=19/2$ state projected from the HF state. Thus the ground state band extends upto $J=17/2$ and is predominantly the band projected from the $K=5/2$ HF state.

Table 21

Intensity of the states projected from the prolate HF $K=5/2$ intrinsic state in the final "ground state band" of states of ^{47}Ti shown in fig.10C.

J	$\frac{5}{2}$	$\frac{7}{2}$	$\frac{9}{2}$	$\frac{11}{2}$	$\frac{13}{2}$	$\frac{15}{2}$	$\frac{17}{2}$	$\frac{19}{2}$
E_J (MeV)	0.0	0.27	1.25	1.42	2.35	2.50	3.46	3.95
$ B_{5/2}^J ^2$	0.96	0.85	0.94	0.77	0.98	0.71	0.90	0.35

The strong transition between the states corresponding to the calculated "ground state band" observed by Sawa et al.²⁾ strongly indicates that these states form a band. It is very significant that Sawa et al have not observed the $J=19/2$ state although it is not ruled out by the energetics of the (α, n) reaction populating these states. It may be concluded from this that the transition probability from the $J=19/2$ to the $J=17/2$ state is small and thus the $J=19/2$ state is not a good member of the ground state band. This conclusion is also supported by the calculated decay properties of this state which we shall discuss later.

2.3.2 A $K=1/2$ Band

As mentioned in subsec.2.1.3 the states projected from the prolate $K=1/2$ intrinsic state at -13.76 MeV are almost

orthogonal to all the other projected states. The energies of the states projected from the $K=1/2$ intrinsic state are shown in fig.8, col.4. A comparison of this pure $K=1/2$ spectrum with the composite spectrum resulting from calculation 10C described above shows that Hamiltonian mixes the states projected from the $K=1/2$ intrinsic state with those projected from the other intrinsic states only weakly. It is of interest therefore to identify in the final spectrum of fig.10C states which belong predominantly to this $K=1/2$ band.

Table 22

Intensity of the states projected from the prolate $K=1/2$ intrinsic state in the states of angular momentum J and energies E_J of the composite spectrum in fig.10C.

J	$\frac{3}{2}$	$\frac{1}{2}$	$\frac{5}{2}$	$\frac{7}{2}$	$\frac{11}{2}$	$\frac{9}{2}$	$\frac{13}{2}$	$\frac{15}{2}$	$\frac{19}{2}$	$\frac{17}{2}$
E_J (MeV)	1.65	1.85	2.40	2.56	3.38	3.44	4.04	4.46	5.80	5.84
$\left B_{\frac{1}{2}}^J \right ^2$	0.60	0.92	0.72	0.98	0.98	0.74	0.64	0.77	0.79	0.96

We have plotted separately in fig.11B the energy spectrum of the states of fig.10C which correspond to this $K=1/2$ band. The probability that these states in fig.11B contains the state projected from the $K=1/2$ intrinsic state at -13.76 MeV is given above in table 22. Although these states are

still predominantly the ones projected from the $K=1/2$ band, the admixture of other bands is significantly higher than that seen for the ground state band. The average admixture in the final "band" of components other than that projected from the $K=1/2$ intrinsic state is about 20 percent. In fig. 11B, we have also plotted the experimental spectrum of the states which might correspond to this band.

2.3.3 Structure of Other States

The structure of some of the other states upto 4 MeV of the final composite spectrum at 10C is complex. An evidence for the complex nature of some of these excited states is provided by the $J=5/2$ and $3/2$ states observed at 2.83 and 3.22 MeV. The present calculation reproduces their energies well at 2.85 and 3.32 MeV respectively. These states have been strongly excited in $^{45}\text{Sc} (^3\text{He}, p\gamma) ^{47}\text{Ti}$ reaction, but their γ -decay patterns have not been established¹⁰⁾ because of many decay branches of equal intensities.

It is interesting to note that although the oblate $K=3/2$ intrinsic state is the first excited intrinsic state, there does not exist in the final spectrum, a set of states which have a large amplitude for belonging to the $K=3/2$ band of states projected from this intrinsic state. Also most of the states which have a predominant (~ 30 percent) oblate

$K=3/2$ component are quite high in energy. This implies that the effective interaction does not allow the existence of a coherent oblate shape in ^{47}Ti .

2.4 ELECTROMAGNETIC PROPERTIES

We present here the results of the E2 and M1 transitions in ^{47}Ti . We have also attempted to compare our results with all the available experimental information and with the results of RPC calculations^{8,18)}. For the calculation of electric properties the effective charges $e_p=1.32e$, $e_n=0.89e$ and $e_p=1.5e$, $e_n=0.5e$ have been used. For M1 transitions the values of free nucleon g-factors for the proton and neutron have been employed.

We shall first discuss the transitions within the ground state band and then present some electromagnetic evidence for the existence of the $K=1/2$ 'band'. This will be followed by a level-by-level comparison of the calculated and experimental decay properties of the more complex states. We have attempted to make some spin assignments on the basis of this comparison.

2.4.1 Transitions in the Ground State Band

States with $J=5/2$ to $17/2$ have been identified²⁾.

Our calculated ground state band shown by thick lines in fig.11A consists, to a large extent, of the states of definite J projected from the lowest energy HF intrinsic state with $K=5/2$. The admixtures of the other bands is about 12 percent to the states with $J=5/2$ to $17/2$. In order to investigate the effects of band mixing on the transition rates we shall compare the results of our DCM calculations with those obtained by using only the pure wave function projected from the $K=5/2$ HF state. The latter results have been labelled as PHF in the tables.

2.4.1.1 B(E2) Values

These are given in table 23. The experimental $B(E2)$ values between the first four members of this band are of Weaver et al.⁸⁾. An earlier and probably the only direct observation of the $5/2 \rightarrow 9/2$ E2 transition is the Coulomb excitation measurement of Afonin et al.¹⁴⁾ on ^{47}Ti by ^{12}C ions at 38.6 MeV. The $B(E2)$ value for this transition has been given to be $62 \pm 12 \text{ e}^2 \text{ fm}^4$. This implies the $B(E2)$ value of 103 ± 7 for the $9/2 \rightarrow 5/2$ transition in reasonable agreement with the value of Weaver et al.⁸⁾. Weaver et al.⁸⁾ and Haas et al.¹⁸⁾ have also computed the spectrum and $B(E2)$ values for the transitions between some of the low-lying states of ^{47}Ti using RPC model. For comparison their results on $B(E2)$ values are also given in table 23.

Table 23

$B(E2, J_i \rightarrow J_f)$ values in ($e^2 \text{fm}^4$) for the transitions within the ground state band in ^{47}Ti . Results obtained by using Deformed Configuration Mixed wave functions and the projected HF states are listed under the columns DCM and PHF respectively.

J_i	J_f	Expt. ^a	Present			RPC	
			DCM [*]	PHF [*]	DCM ⁺	Haas ^b et al	Weaver ^a et al
7/2	5/2	232 \pm 33	223	288	157	171	219
9/2	5/2	126 \pm 64	73	81	55	51	74
	7/2	51 $^{+46}_{-20}$	176	236	131	148	222
11/2	7/2	149 \pm 40	127	134	95	88	136
	9/2		128	179	92	111	
13/2	9/2		156	162	118	113	
	11/2		93	135	72	86	
15/2	11/2		153	176	115	131	
	13/2		56	102	40	64	
17/2	13/2		169	178	120	142	
	15/2		53	81	43	51	
19/2	15/2		98	174	72		
	17/2		20	63	15		

* $e_p = 1.32e$, $e_n = 0.89e$

+ $e_p = 1.5e$, $e_n = 0.5e$

a. Ref. 8

b. Ref. 18

A comparison of the DCM and PHF calculated $B(E2)$ values given in columns 4 and 5 respectively shows that compared to the PHF values the DCM values are on an average depleted by about 20 percent. This reduction in $B(E2)$ values is quite significant in view of the average band mixing of only about 12 percent in the ground state band. In general, the $B(E2)$ values for the pure $E2$ transitions are not significantly changed, in going from PHF to DCM calculations. The exception is the $19/2 \rightarrow 15/2$ transition for which 40 percent reduction occurs. The other transitions for which drastic reduction in $B(E2)$ values occurs are from the $J=15/2 \rightarrow 13/2$ and from $19/2 \rightarrow 17/2$. This is because the $J=15/2$ and $19/2$ states calculated at 2.50 and 3.95 MeV have about 29 and 65 percent admixture of the states other than the ones projected from the HF $K=5/2$ intrinsic state.

The DCM calculated values in column 4 are somewhat large compared to the RPC values of Haas et al¹⁸⁾ but are similar to those obtained by Weaver et al⁸⁾.

The agreement of the calculated and the experimental⁸⁾ $B(E2)$ values for the $7/2 \rightarrow 5/2$ and $11/2 \rightarrow 7/2$ transitions is fairly good. However, deviations occurs for the $9/2 \rightarrow 5/2$ and $9/2 \rightarrow 7/2$ transitions. For the $9/2 \rightarrow 5/2$ transitions the DCM as well as RPC calculations predict small $B(E2)$ value (though within errors) compared to the experimental value of

Weaver et al⁸⁾. In contrast the theories predict a consistently large $B(E2)$ value for the $9/2 \rightarrow 7/2$ transition compared to its observed value.

The reduction in $B(E2)$ value for the $9/2 \rightarrow 5/2$ transition compared to the $7/2 \rightarrow 5/2$ transition can be understood as a consequence of the fact that these states belong to the $K=5/2$ band. The $B(E2)$ value can be written approximately

$$B(E2, J \rightarrow J') \simeq \frac{5}{16\pi} \left[C_{5/2, 0}^{J, 2, J'} \right]^2 (Q_0)^2$$

where Q_0 is the intrinsic quadrupole moment. The $9/2 \rightarrow 5/2$ transition is weak because the corresponding Clebsch-Gordon coefficient is very small. Unfortunately this reasoning does not help us in understanding the small observed $B(E2)$ value of $9/2 \rightarrow 7/2$ transition. For this transition however the experimental value in itself is quite uncertain. A careful remeasurement of the $9/2 \rightarrow 7/2$ transition and also between other members of the band would be helpful.

In table 23, col.6, are given the $B(E2)$ values obtained in our DCM calculation by using effective charges $e_p=1.5e$ and $e_n=0.5e$. Compared to the $B(E2)$ values obtained with effective charges $e_p=1.32e$ and $e_n=0.89e$ values given in column 6 are about 25 percent smaller. The $B(E2)$ values in column 6 are in general agreement with the RPC values and in qualitative

agreement with the experimental values.

2.4.1.2 B(M1) Values

These are given in table 24. Also tabulated are the experimental B(M1) values given by Weaver et al⁸⁾ and the RPC calculated values of Haas et al¹⁸⁾ and of Weaver et al⁸⁾.

Table 24

B(M1, $J_i \rightarrow J_f$) values in (n.m.)² for transitions within the ground state band in ⁴⁷Ti.

J_i	J_f	Expt ^a	Present		RPC	
			DCM	PHF	Haas ^b et al	Weaver ^a et al
7/2	5/2	0.56 ^{+0.34} -0.26	0.04	0.36	0.13	0.03
9/2	7/2	0.18 \pm 0.02	0.28	0.58	0.22	0.11
11/2	9/2	0.32 \pm 0.16	0.34	0.74	0.36	0.34
13/2	11/2		0.54	0.81	0.31	
15/2	13/2		0.51	0.87	0.51	
17/2	15/2		0.66	0.84	0.33	
19/2	17/2		0.32	0.87		

a. Ref.8

b. Ref.18

We shall first compare the B(M1) values for the transition obtained in our PHF and DCM calculations. Compared to PHF values a drastic reduction on an average of about 50 percent occurs in the DCM calculations. This is signifi-

cantly large compared to the corresponding decrease of only about 20 percent for the $B(E2)$ values. This indicates the extreme sensitivity of $M1$ transitions to even slight admixtures in the wave function. An extreme reduction in the $B(M1)$ value occurs for the $7/2 \rightarrow 5/2$ transition.

Except for the $7/2 \rightarrow 5/2$ transition the agreement with the observed $B(M1)$ values is good. The experimental $B(M1)$ value for the $7/2 \rightarrow 5/2$ transition is quite uncertain. Our DCM result for the $7/2 \rightarrow 5/2$ transition agrees with the RPC result of Weaver et al.⁸⁾ but not of Haas et al.¹⁸⁾. For other transition upto $J=11/2$ the agreement between DCM and RPC result is reasonably good. The $B(M1)$ values for the transitions between the high spin states as obtained by Haas et al.¹⁸⁾ are, in general, weak compared to our values.

2.4.1.3 (E2/M1) Mixing Ratios

In table 25 are compared the results of our DCM calculated mixing ratios with the experimental²⁾ values and with the RPC model values of Haas et al.¹⁸⁾. The agreement between the theory and experiment is very good except for the mixing ratios for the transitions $11/2 \rightarrow 9/2$ and $17/2 \rightarrow 15/2$ for which wrong signs are obtained. The reason for these discrepancies is not clear. Our calculated value of $\delta = +0.23$ for $9/2 \rightarrow 7/2$ transitions is more in agreement with the experimental value

of $+0.15 \pm 0.06$ observed by Weaver et al⁸⁾, than with the value $+0.32 \pm 0.03$ measured by Sawa et al²⁾.

Table 25

(E2/M1) mixing ratios for the transitions between the members of the ground state band in ⁴⁷Ti.

J_i	J_f	(E2/M1) mixing ratios		
		Expt ^b	DCM ⁺	RPC ^d
7/2	5/2	$+0.07 \pm 0.03$	$+0.10$	$+0.05$
		$+0.027 \pm 0.007^c$		
9/2	7/2	$+0.32 \pm 0.03$	$+0.23$	$+0.24$
		$+0.15 \pm 0.06^c$		
11/2	9/2	-0.03 ± 0.02	$+0.03$	$+0.03$
13/2	11/2	$+0.14 \pm 0.02$	$+0.13$	$+0.17$
15/2	13/2		$+0.004$	$+0.01$
17/2	15/2	-0.03 ± 0.03	$+0.06$	$+0.08$
19/2 ^a	17/2		$+0.01$	

+ $e_p = 1.32e$, $e_n = 0.89e$. a. Theoretical excitation energy.

b. Ref.2. c. Ref.8. d. Ref.18.

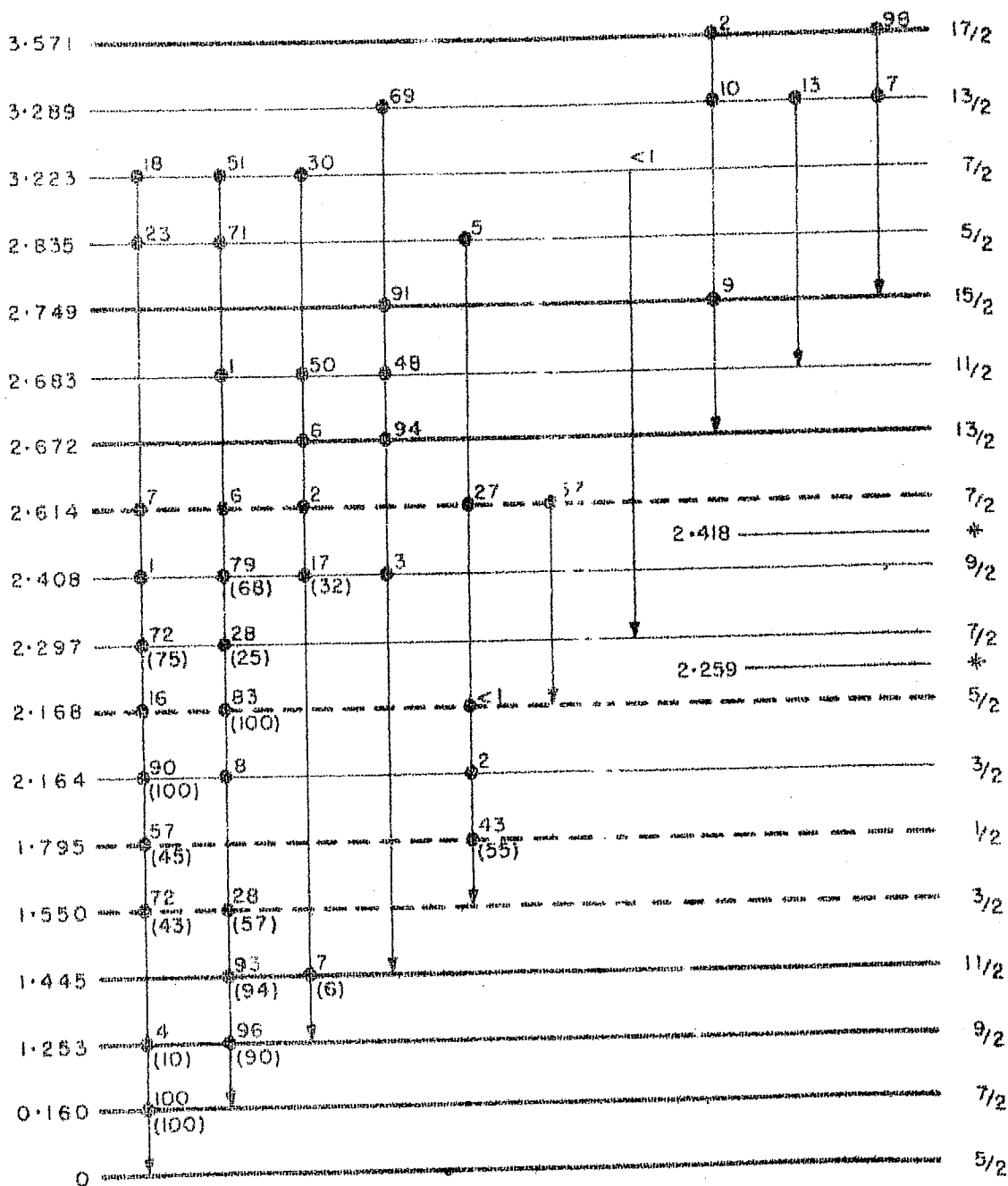
2.4.1.4 Branching Ratios

The branching ratios for various transitions between some of the low-lying states of ⁴⁷Ti are given in fig.13. The states drawn therein by thick lines belong to the ground state band. Weaver et al⁸⁾ have given the branching figures for the transitions between the states upto $J=11/2$ belonging

CAPTION FOR FIGURE 13

Branching intensities in ^{47}Ti . The states drawn in thick lines belong to the ground state band. Those shown by dotted lines are the possible low-lying members of the $K=1/2$ excited band predicted by our calculations. The vertical lines indicate the transitions originating from the state with a filled circle to the state where the arrow ends. The numbers on top of these states are the corresponding calculated decay intensities. Those below in parenthesis are the experimental values. The observed states at energies 2.259 and 2.418 MeV with astrisk mark have many probable spin values. Our calculations do not reproduce states with decay properties similar to these two observed states.

^{47}Ti



E_x (MeV)

Fig.13

to the ground state band, and for other low-lying states of ^{47}Ti . Their values for the various transitions between the members of the ground state band are given in parenthesis just below the state from which the corresponding γ -ray is emitted. The observed values of branching figures for the transitions from $J=9/2$ and $11/2$ states at 1.253 and 1.445 MeV have an error of about 4. To avoid the complexity of the figure these errors are not given here. Our calculated branching figures, are given on top of the state from which the decays are considered. $B(E2)$ values obtained with $e_p = 1.32e$, $e_n = 0.89e$ are used.

The agreement between the calculated and observed branching figures for the states upto $J=11/2$ at 1.445 MeV is very good. Values of the branching ratios for the decays of other high-spin states of the ground state band are not yet measured. For the ground state band of states upto $J=17/2$ at 3.57 MeV the values of branching ratios obtained by Haas et al.¹⁸⁾ are in agreement with our values. Our calculations predict a dominant M1 decay mode for all the high-spin states of the ground state band. This prediction is consistent with the recent heavy-ion reaction measurements on fp shell nuclei. In the studies of ^{51}V and ^{53}Mn by Gogelein et al.²⁹⁾ and of ^{49}Cr by Blasi et al.²⁵⁾, it was found that in the cascades along the Yrast states in the nuclei the transitions are of fast M1 mode. In yet another experi-

ment, Huber et al²⁶⁾ studied the high-spin states of ^{50}Cr by $^{40}\text{Ca}(^{16}\text{O}, 2p\alpha)$ reaction and found that the angular distribution of γ -rays emitted from the $J=12^+$ at 7.611 MeV and $J=11^+$ at 6.946 MeV are of dipole character.

It is interesting to compare the branching ratios of the transition from the $J=9/2$ and $11/2$ states at 1.25 and 1.45 MeV. The $J=9/2$ state decays mostly to the $J=7/2$ state by M1 transition. The $J=11/2$ state also has large $B(M1)$ to the $J=9/2$ state. However, it decays mostly to the $J=7/2$ state through E2 transition mainly because of the large energy difference.

Similarly the $J=13/2$ state at 2.67 MeV decays by a fast M1 mode to the $J=11/2$ state at 1.45 MeV. This explains the non-observation of the $13/2 \rightarrow 9/2$ transition by Sawa et al²⁾.

The relative branching intensities for the transitions from the first $J=19/2$ state calculated at 3.95 MeV are not given in fig.13. This state decays with a 55 percent branch to the $J=17/2$ state at 3.57 MeV and with a 45 percent E2 branch to the $J=15/2$ state at 2.75 MeV.

2.4.1.5 Mean Lifetimes

Weaver et al⁷⁾ have also measured the lifetime of some of the low-lying states of ^{47}Ti . In table 26 are compared

Table 26

Mean lifetimes of the members of the ground state band in ^{47}Ti .

J	τ_m (ps)		
	Expt ^a	DCM	RPC ^c
7/2	320 \pm 100 ^b	343	106
9/2	0.21 \pm 0.02	0.15	0.19
11/2	1.5 $^{+0.5}_{-0.3}$	1.71	2.4
13/2		0.053	0.09
15/2		0.22	1.6
17/2		0.15	0.3

a. Ref.8.

b. Direct timing measurements of R.E. Holland and F.J. Lynch, Phys. Rev. 121, 1464 (1961).

c. Ref.18.

the calculated and observed lifetimes of the members of the ground state band upto J=17/2 at 3.57 MeV in ^{47}Ti . The agreement between the calculated and observed values is good.

The RPC calculated¹⁸⁾ value of 106 ps for the lifetimes of the J=7/2 state is in disagreement with both the experimental and our DCM values. Also the lifetimes of the high-spin states of the ground state band as calculated by Haas et al¹⁸⁾ are quite different from our corresponding values mainly because of the large differences in the RPC and our DCM calculated B(M1) values given in table 24.

2.4.1.6 Static Moments

The static electric quadrupole and magnetic dipole moments of the first three states of ^{47}Ti are given in table 27. Our DCM calculated values for the $J=5/2$ ground state are in excellent agreement with the observed values^{27,28)}. The RPC value¹⁸⁾ for the ground state magnetic moment is quite different from the DCM and observed values. It would be interesting to measure the moments of other low-lying states of ^{47}Ti .

Table 27

Static moments of some of the low-lying states in ^{47}Ti .

J	E_J (MeV)	$Q(\text{efm}^2)$			μ (n.m.)		
		Expt ^a	DCM	RPC ^b	Expt ^c	DCM	RPC ^c
5/2	0.0	29 \pm 1	28	25	-0.79 \pm 0.01	-0.80	-1.22
7/2	0.16		9	4.3		-0.60	-0.95
9/2	1.25		-6			0.81	

a. Ref.27.

b. Ref.18.

c. Ref.28.

2.4.2 Transitions in the $K=1/2$ Band

The calculated DCM energy spectrum of the states with $J=1/2$ upthrough $J=19/2$ is plotted in fig.11B. These states

are predominantly the ones projected from the prolate $K=1/2$ 1p-1h excited intrinsic state. The average band mixing in these states is about 20 per cent. However, as seen from table 22, for $J=3/2$ and $13/2$ states calculated at 1.65 and 4.04 MeV, the admixture of the states projected from the intrinsic states other than the above $K=1/2$ intrinsic state is as large as 40 percent. In other words, these states are not very good members of this band.

On the basis of the definite spin assignments $3/2$, $1/2$, $5/2$ and $7/2$ to the states observed at 1.55, 1.79, 2.17 and 2.61 MeV respectively, we associated in subsec.2.3.2 our calculated $J=3/2$, $1/2$, $5/2$ and $7/2$ states at 1.65, 1.85, 2.40 and 2.56 MeV of the $K=1/2$ band with the above observed states.

In this section, we shall present electromagnetic evidence that supports this identification.

The $B(E2)$ values obtained in our DCM calculations for the E2 transitions between the members of the $K=1/2$ band are given under the column DCM in fig.14. In this figure the members of the band have been grouped in two sets on the basis of their pure E2 transitions. The $B(E2)$ and $B(M1)$ values for the cross over transition indicated by thin arrows between the two sets of states of the band are also given in the figure. The numbers above these arrows are the $B(E2)$

CAPTION FOR FIGURE 14

Spectrum and transitions within the $K=1/2$ band in ^{47}Ti . This band is separated into two sub-bands on the basis of their pure E2 transitions indicated by thick arrows. The numbers by the side of these arrows in the column labelled PHF are the $B(E2)$ values (in $e^2\text{fm}^4$) for the transitions between the states projected from only the prolate $K=1/2$ excited intrinsic state. $B(E2)$ values obtained in the band mixed calculations are given in the column DCM. The $B(E2)$ and $B(M1)$ (in $(\text{n.m.})^2$) values for transitions between these sub-bands are given above and below thin arrows respectively.

^{47}Ti

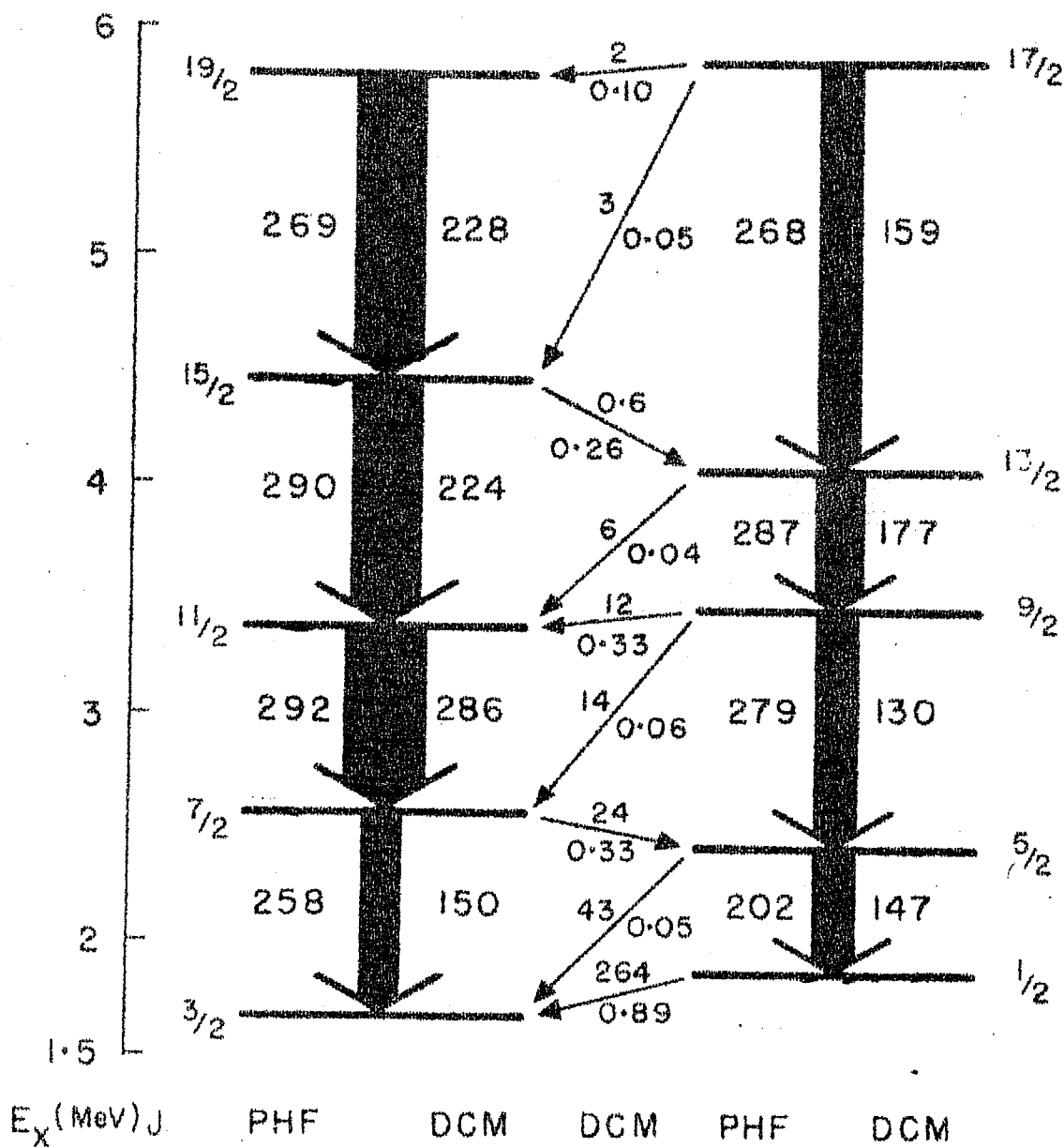


Fig.14

values, while those below are the corresponding $B(M1)$ values. We have also given in column PHF of fig.14 the $B(E2)$ values obtained for the pure $E2$ transitions between the states projected from the $K=1/2$ intrinsic state alone. The results of the electric transitions are given for the effective charges $e_p = 1.32e$ and $e_n = 0.89e$.

A comparison of PHF and DCM results shows that the band mixing has a considerable effect on both the $B(E2)$ and $B(M1)$ values. For the $1/2 \rightarrow 3/2$ transition the $B(M1)$ value resulting from DCM calculation is 0.89 (n.m.)^2 . The corresponding PHF value is only 0.32 (n.m.)^2 .

The RPC calculated $B(E2)$ and $B(M1)$ values for the $1/2 \rightarrow 3/2$ transition obtained by Haas et al.¹⁸⁾ are $208 \text{ e}^2 \text{ fm}^4$ and 0.92 (n.m.)^2 . These are in reasonable agreement with our DCM results. The $(E2/M1)$ mixing ratios obtained in our calculation for the $1/2 \rightarrow 3/2$ and $5/2 \rightarrow 3/2$ transitions of the $K=1/2$ band are $+0.03$ and $+0.15$. The corresponding RPC values¹⁸⁾ are $+0.03$ and -0.13 . Thus the RPC value of δ for $5/2 \rightarrow 3/2$ transition is opposite to our value.

The $B(E2)$ values given in fig.14 are large and comparable to the values given in table 23 for the ground state band. Also most of the $B(E2)$ and $B(M1)$ values for transitions between the members of the $K=1/2$ band and the ground state band are very small because of the $\Delta K=2$ selection

rule. It may therefore be possible to identify some of the members of this band by their preferential decay within the band.

So far the only transition observed^{8,9)} within this band is that from the $J=1/2 \rightarrow 3/2$ state. In spite of the small energy difference of only 244 keV, the $J=1/2$ state decays to the $J=3/2$ state with a 55 percent (Weaver et al⁸⁾ or 66 percent (Fifield et al⁹⁾) branch. The rest of the decay occurs to the $J=5/2$ ground state with an energy difference of about 1.80 MeV. This implies a large hinderance in the $B(E2)$ value for the $1/2 \rightarrow 5/2$ ground state transition. The calculated branching ratios for these $1/2 \rightarrow 3/2$ and $1/2 \rightarrow 5/2$ transitions given in fig.13 are in reasonable agreement with the observed values of Fifield et al⁹⁾.

The experimental data about the intraband decays of the other members of the $K=1/2$ band does not exist. Nevertheless some information⁸⁾ about the decay properties of the states observed in the energy interval 2 to 2.4 MeV is known. Most of these states decay to the ground state band of states. In the following we shall therefore attempt to identify the states in the experimental spectrum that can be associated with the members of the $K=1/2$ band, on the basis of the comparison between the electromagnetic transition properties of the calculated and observed states.

In table 28 are given the $B(E2)$ and $B(M1)$ values for transitions between some of the members of the $K=1/2$ band to the members of the ground state band. Except for the $B(M1)$ value of 0.34 (n.m.)^2 for the $5/2 \rightarrow 7/2$ (0.16 MeV) transition, all these values are small. For transitions involving higher members of the $K=1/2$ band and the ground state band, both the $B(E2)$ and $B(M1)$ values are extremely small and are hence not given in the table. The small $B(M1)$

Table 28

$B(E2)$ and $B(M1)$ values for interband transition from some of the members of the $K=1/2$ band to those of the ground state band in ^{47}Ti .

E_i^{cal} (MeV)	E_f^{expt} (MeV)	J_i	J_f	$B(E2)$ ($e^2 \text{ fm}^4$)	$B(M1)$ (n.m.) ²
1.65	0.0	3/2	5/2	21.8	0.0036
	0.16		7/2	30	
1.85	0.0	1/2	5/2	13	
2.40	0.0	5/2	5/2	12	0.05
	0.16		7/2	3.5	0.34
	1.25		9/2	9.3	
2.56	0.0	7/2	5/2	0.0002	0.0002
	0.16		7/2	0.30	0.0001
3.38	0.16	11/2	7/2	0.05	
	1.25		9/2	0.02	0.00003

value of 0.0036 (n.m.)^2 for the $3/2 \rightarrow 5/2$ ground state transition is in agreement with the retardation of about 10^{-3} for this transition observed by Weaver et al⁸⁾. The RPC model calculation of Weaver et al⁸⁾ fails to reproduce this retarded $B(M1)$ value and instead gives the value 0.68 (n.m.)^2 for the $3/2 \rightarrow 5/2$ ground state transition.

The observed⁸⁾ branching ratio for the $J=3/2$ state at 1.55 MeV are 43:57 for the $3/2 \rightarrow 5/2$ and $3/2 \rightarrow 7/2$ decays. Our calculated ratios as given in fig.13 are 72:28. These differences, however, are not too serious since the transitions are retarded. The same reason explains the differences in the calculated $(E2/M1)$ mixing ratios of -0.95 compared to the experimental ratio of -0.47 ± 0.10 or $-4.4^{+1.2}_{-2.6}$ both given by Weaver et al⁸⁾. Haas et al¹⁸⁾ have obtained $\delta = +0.01$ for the $3/2 \rightarrow 5/2$ ground state transition.

The $J=5/2$ state observed⁸⁾ at 2.17 MeV decays only to the first excited $J=7/2$ state with a lifetime of 25 ± 6 fs. If the $J=5/2$ state were a good member of the $K=1/2$ band, one would have expected it to decay to the $J=3/2$ and $1/2$ members of this band with a significant intensity. However, our calculations show that as a consequence of the band mixing the 2.40 MeV $J=5/2$ state of the $K=1/2$ band has a large $B(M1)$ value of 0.34 (n.m.)^2 for the $5/2 \rightarrow 7/2$ transition. As a result the calculated $J=5/2$ state decays dominantly

to the $J=7/2$ state of the ground state band. The calculated lifetime for the $5/2 \rightarrow 7/2$ transition is 20 fs. The $(E2/M1)$ mixing ratios as obtained in our DCM calculation for the $5/2 \rightarrow 7/2$ transition is -0.05 . The experimental value is 0 ± 0.17 .

It is thus seen that the decay properties of the calculated $J=5/2$ state at 2.40 MeV are consistent with the experimental decay properties of the observed $J=5/2$ state at 2.17 MeV. We shall show later that these decay properties of the calculated $J=5/2$ state do not fit the decay modes of any other state observed in about 2 to 2.4 MeV energy interval and also that none of the other $J=5/2$, $7/2$ or $9/2$ states calculated about that energy interval is consistent with the decay properties of the $J=5/2$ state at 2.17 MeV. From this, it may be concluded that inspite of the non-observation of the intraband transition, the $J=5/2$ state at 2.17 MeV may belong to the $K=1/2$ band.

Experimentally a state with definite $J=7/2$ is observed^{6,7,8)} at 2.61 MeV. Meyer-Schutzmeister et al¹⁰⁾ have observed a strong transition from this $J=7/2$ state to the first excited $J=7/2$ state at 0.16 MeV. No branching intensity is known.

Our calculated $J=7/2$ state at 2.56 MeV of the $K=1/2$ band is close in energy to the above observed state. In

the next section, we shall show, that on the basis of the decay properties of this calculated $J=7/2$ state, its identification with any of the observed states in the energy interval 2 to 2.5 MeV can be ruled out.

If the calculated $J=7/2$ state at 2.56 MeV is associated with the observed $J=7/2$ state at 2.61 MeV, it is found, as shown in fig.13 that this state decays mostly to the $J=3/2$ and $5/2$ members of the band. This, then is in contrast to the observed¹⁰⁾ decay mode of the $J=7/2$ state at 2.61 MeV. Hence there is a difficulty in identifying the calculated $J=7/2$ state with the one observed at 2.61 MeV.

We, however, feel that this difference in the decay properties of the calculated and the observed $J=7/2$ states may be because of the extreme retardation of about 10^{-4} of the calculated $B(M1)$ value for the transitions between the $J=7/2$ state at 2.56 MeV to the $J=5/2$ and $7/2$ states of the ground state band.

It is likely that the magnitude of small $B(M1)$ value may depend strongly on the wave functions and our calculations would not reproduce these small $B(M1)$ values very accurately. To illustrate this point, for example, a small $B(M1)$ value of 0.02 (n.m.)^2 would make this $J=7/2$ state decay more strongly to the $J=7/2$ state at 0.16 MeV than to the $J=3/2$ and $5/2$ members of the $K=1/2$ band.

It is thus likely that the calculated $J=7/2$ state observed at 2.61 MeV may be the member of the $K=1/2$ band. We hasten to add that this identification is very tentative and experimental studies of the properties of this state might throw some light.

All the other higher members of the $K=1/2$ band have extremely retarded transitions to the ground state band. Their experimental identification is very much desirable.

2.4.3 Other States

So far we have discussed:

i) The states with $J=5/2$ upto $J=17/2$ of the ground state band and ii) The states with $J=3/2, 1/2, 5/2$ and $7/2$ at 1.55, 1.80, 2.17 and 2.61 MeV of the $K=1/2$ band.

Sawa et al²⁾ have observed a state at 3.98 MeV whose J -value is not specified. They also observed some of the other high-spin states of ⁴⁷Ti shown by thin lines in fig. 11A which we have not discussed so far. Among other states, the $J=7/2, (5/2)$ and $(7/2)$ at 2.61, 2.84 and 3.22 MeV respectively have been observed by Meyer-Schutzmeister et al¹⁰⁾. Decay properties of the latter states are not fully known.

In the DCM calculated spectrum shown in fig.10, we have almost the same number of states in the energy interval

2 to 3 MeV as in the observed spectrum. The agreement of the calculated and the observed states is quite good.

Both the experimental and DCM calculated spectra of ^{47}Ti plotted in fig.10 are complex. We have redrawn these spectra, in fig.15 in a manner suitable for the identification of the various levels that we wish to study now.

Note that in the calculated spectra in fig.15, the states are not all drawn according to increasing energy. We have lined up the calculated states with the experimental ones to which they seem to correspond, on the basis of their decay properties.

We shall now undertake a level-by-level discussion of the states observed above 2 MeV, but exclude those drawn in thick lines in fig.13. Such states are already discussed. We shall attempt to assign J-values to the observed levels with uncertain spins. Our assignments are based on an overall agreement of the calculated and experimental values of the energies, branching ratios and lifetimes of the various transitions from the state under consideration.

2.164 MeV Level

This state has been observed in $(p,p'\gamma)^{8)}$, $(d,p)^{3-6)}$, $(^3\text{He},p\gamma)^{10)}$ and in β -decay $^{9)}$ of ^{47}V experiments. Weaver et al $^{8)}$ have assigned $J=3/2$ or $(1/2)$ to this level and observed

CAPTION FOR FIGURE 15

Comparison of the experimental and calculated spectrum of ^{47}Ti . For the states with $J = 5/2$, ten intrinsic states are considered while for $J=1/2$ and $3/2$ eleven intrinsic states are included. The resulting energies are given on the left of each state in the calculated spectrum. The above ten intrinsic states used for the description of $J = 5/2$ states contained only three $K=1/2$ and $3/2$ states. The energies of the low-lying $J=1/2$ and $3/2$ states resulting from this smaller calculation are indicated in square brackets. Notice that in the calculated spectrum, the states are not drawn according to increasing energies, but are levelled up with the experimental states on the basis of the agreement with the experiment of the calculated energies and decay properties.

$^{47}_{\text{Ti}}$

3.571	17	3.46	17
3.550	1	3.55	1
		3.44	9
		3.38	11
		3.36	15
3.289	13	3.34	13
3.280	3	3.52	3
3.223	(7)	3.30	7
		3.07	9
2.835	(5)	2.85	5
2.790	1	2.81	1
2.749	15	2.50	15
2.683	11	2.62	11
2.672	13	2.35	13
2.613	7	2.56	7
2.540	3	2.65	3
2.416	(1,3,5,7)		
2.408	(7,9,11)	2.32	9
2.297	(3,5,7,9)	2.30	7
2.260	(3,5,7,9)		
2.168	(5,7,9)	2.40	5
2.164	3	2.13	[2.27] 3
1.795	1	1.82	[1.85] 1
1.550	3	1.56	[1.65] 3
1.445	11	1.42	11
1.252	9	1.25	9
0.160	7	0.27	7
0	5	0	5
E_J (MeV) EXPT.	2J	E_J (MeV) THEORY	2J

Fig.15

the lifetime of 31 ± 8 fs for its 100 percent decay to the $J=5/2$ ground state. The (d,p) reaction^{3,6)} and β -decay measurements⁹⁾ have led to $J=3/2$ assignment for this state. Fifield et al⁹⁾ have also observed 95 ± 1 and 5 ± 1 percent branches respectively for the transitions from this level to the ground state and first excited state at 0.16 MeV.

Our calculated $J=3/2$ at 2.27 MeV is in reasonable agreement with the level at 2.164 MeV. It should be mentioned that in our extended DCM calculation for the description of only the low-lying states of ^{47}Ti , the $J=3/2$ state at 2.27 MeV is pushed down to 2.13 MeV in very good agreement with the observed state.

The calculated $J=3/2$ state at 2.27 MeV, if regarded as the one corresponding to the 2.164 MeV observed state decays (fig.13) to the $J=5/2$ ground state with 90 percent intensity and to the first excited $J=7/2$ state with 8 percent branch. This is in agreement with the measurements of Fifield et al⁹⁾. The calculated mean lifetime of 18 fs of this state is also in reasonable agreement with the observed value.

2.168, 2.259, 2.297, 2.408 and 2.416 MeV Levels.

These levels have been observed⁸⁾ in $(p,p'\gamma)$ reaction. J -values ranging from $1/2$ to $11/2$ have been assigned to this

bunch of levels. Corresponding to these, in the calculated spectrum, shown in fig.10C, we have two $J=5/2$ states at 2.40 and 2.84 MeV, two $J=7/2$ states at 2.29 and 2.56 MeV, one $J=9/2$ state at 2.32 MeV and a $J=11/2$ state at 2.61 MeV. The $J=5/2$ state at 2.40 MeV is the member of the $K=1/2$ band and as discussed above may be associated with the observed state at 2.168 MeV.

In the first row of table 29 are given the energies of these observed levels along with their suggested J -values. The available experimental data about their branching ratios and lifetimes is tabulated in the second row of the table.

We have ruled out $J=1/2$ and $3/2$ assignments to these levels on the assumption that in our DCM calculation for the $J=1/2$ and $3/2$ states of ^{47}Ti , a very good agreement was obtained for all the $J=1/2$ and $3/2$ states observed upto about 6 MeV excitation. Our calculation did not give any additional $J=1/2$ or $3/2$ state in the energy interval 2 to 3 MeV, which could be associated with the levels for which such possible J -values have been suggested. We have therefore associated our calculated $J=5/2$, $7/2$ and $9/2$ states obtained in the energy interval 2 to 2.85 MeV, with the observed levels of table 29.

The energies and J -values of these calculated states are listed in column 1 of table 29. We have calculated bran-

CAPTION FOR TABLE 29

Comparison of the calculated and experimental branching ratios and lifetimes and possible spin assignments in ^{47}Ti . The observed energies of the levels with probable spin values are given in the topmost row. The observed branching ratios and lifetimes of the transitions from each of these levels are given in the second row. Each of the states J_i calculated at energies E_i , listed in column 1, is, in turn, associated with each of the observed levels in first row. Using the experimental level energy, the branching ratios (%) and lifetimes (τ) for the transitions from the corresponding associated state J_i to the states J_f observed at energies E_f (listed in column 1) are calculated. The table gives the matrix of the branching ratios and lifetimes so calculated. The decay properties of the calculated states J_i , which are in optimum agreement with the decay properties of the observed levels are shown by a rectangular box, indicating thereby that spin assignment for the particular observed level.

LEVEL ENERGY (MeV)		2.168		2.259		2.297		2.408		2.416	
POSSIBLE J :		$\frac{5}{2}, \frac{7}{2}, \frac{9}{2}$		$\frac{3}{2}, \frac{5}{2}, \frac{7}{2}, \frac{9}{2}$		$\frac{3}{2}, \frac{5}{2}, \frac{7}{2}, \frac{9}{2}$		$\frac{7}{2}, \frac{9}{2}, \frac{11}{2}$		$\frac{1}{2}, \frac{3}{2}, \frac{5}{2}, \frac{7}{2}$	
AVAILABLE EXPERIMENTAL DATA		2.168→0.16 MeV 100 $\tau = 25 \pm 6$ fs		2.259→0.0 MeV: 85 →0.16 MeV: 15 τ (85%) = $1.2^{+0.5}_{-0.3}$ ps		2.297→0.0 MeV: 75 →0.16 MeV: 25 $\tau = 11 \pm 7$ fs		2.408→0.16 MeV: 68 →1.25 MeV: 32 τ (68%) = 31^{+13}_{-10} fs		2.416→0.0 MeV: 25 →1.55 MeV: 25 →1.83 MeV: 50 $\tau > 2$ ps	
CALCULATED BRANCHING RATIOS AND LIFETIMES											
J _i	E _i ^{cal} MeV	J _f	E _f ^{expt} MeV	τ		τ		τ		τ	
				%	%	%	%	%	%	%	%
$\frac{5}{2}$	2.40	$\frac{5}{2}$	0.0	104 fs		16	91 fs	16	86 fs	14	74 fs
				83	21 fs						
$\frac{5}{2}$	2.85	$\frac{5}{2}$	0.0	23 fs		25	20 fs	25	19 fs	20	16 fs
				73	8 fs						
$\frac{7}{2}$	2.30	$\frac{5}{2}$	0.0	5 fs		72	4 fs	72	4 fs	71	3 fs
				27	13 fs						
$\frac{7}{2}$	2.56	$\frac{5}{2}$	0.0	27 ps		48	24 ps	45	23 ps	36	20 ps
				26	59 ps						
$\frac{9}{2}$	1.25	$\frac{3}{2}$	1.25	87 ns		3	38 ns	3	33 ns	4	20 ns
				17	88 ps						
$\frac{9}{2}$	2.32	$\frac{5}{2}$	0.0	1.8 ps		2	1.2 ps	2	1.1 ps	2	0.8 ps
				84	25 fs						
$\frac{9}{2}$	1.25	$\frac{3}{2}$	1.25	170 fs		14	125 fs	15	113 fs	17	84 fs
				12	170 fs						

Table 29

ching ratios and lifetimes for the various allowed decays by associating each of our calculated $J=5/2$, $7/2$ or $9/2$ state with the observed level under consideration. The results of these calculations are given in table 29. For example, we first associate the calculated $J=5/2$ state at 2.40 MeV with the observed one at 2.168 MeV. We then use the experimental energy differences to calculate the branching ratios and lifetimes for the transition from this $J=5/2$ level to the $J=5/2$ and $7/2$ states at 0.0 and 0.16 MeV. The calculated branching ratios (16:83) and lifetimes $\tau = 104$ fs and 21 fs are listed at the top of column 2 corresponding to the 2.168 MeV level. Similarly the other calculated states with spins J_i are associated in turn with each of the observed states. The corresponding branching ratios and lifetimes for transitions to the states J_f at energies E_f are listed in the column under each of the observed state. For emphasizing the association between a calculated and observed state the decay properties of the calculated levels which are in optimum agreement with the observed ones have been enclosed in a box in table 29. We shall now follow up these levels individually.

2.168 MeV Level

The available experimental data on the decay properties of this level are summarized in the second row of table 29.

It is clear from this table that except for the calculated $J=5/2$ state at 2.40 MeV and possibly the $J=9/2$ state at 2.32 MeV, none of the other states provides agreement with the observed branching ratios and lifetimes of this level. This makes $J=5/2$ and $9/2$ assignments equally probable for this level. We would however like to associate our calculated $J=9/2$ state at 2.32 MeV with the observed state at 2.408 MeV with $J=(7/2, 9/2, 11/2)$ spin assignments. The reason for this is that, as we shall soon show, it is the only state having the decay properties similar to the 2.40 MeV observed level.

2.259 and 2.297 MeV Levels

As shown in table 29, the measured branching ratios for the decays of these states to the ground and first excited state are similar but their lifetimes are different.

It is seen that none of the calculated states with $J=5/2, 7/2$ or $9/2$ provides a reasonable agreement with the observed decay properties of the 2.259 MeV level. The $J=7/2$ state calculated at 2.30 MeV gives a reasonable agreement for the branching ratios of this level but is ruled out by extremely short resulting lifetime. In contrast, as shown in column 4 of table 29, the decay properties of the calculated $J=7/2$ state at 2.30 MeV are in excellent agreement with the observed decay properties of the 2.297 MeV level. We

therefore suggest that the observed state at 2.297 MeV has $J=7/2$ and corresponds to the calculated one at 2.30 MeV.

In view of the overall agreement between our calculated and experimental energy spectra, it is surprising that there is no calculated state corresponding to the 2.259 MeV observed level. It is perhaps likely that this state may not arise from the $(fp)^n$ configuration, and may be a member of a 'core excited band' of states. On the other hand it would be of interest to re-examine the decay properties of this state more carefully.

2.408 MeV Level

As shown in table 29, the $J=9/2$ state calculated at 2.32 MeV provides a unique description of the observed properties of this state. We have also compared the decay properties of the calculated $J=11/2$ state at 2.61 MeV with those of the 2.408 MeV state. The agreement between these two is very poor. We propose therefore $J=9/2^+$ for the observed 2.408 MeV level.

2.416 MeV Level

Experimentally⁸⁾, this state decays with 50 percent branch to a positive parity state with $J=3/2$ observed at 1.825 MeV. No parity assignments have been made though

possible spins of $1/2$ to $7/2$ have been suggested. Our calculations do not describe positive parity states of ^{47}Ti .

This level has equal branching ratio for the decays to the $5/2^-$ and $3/2^-$ states at 0 and 1.55 MeV. Our calculated $J=7/2$ state at 2.56 MeV has a decay mode somewhat similar to that of the 2.416 MeV level. However, the agreement is poorer than for the other three states discussed above. We therefore do not suggest any spin assignment for this level.

In view of its strong decay to the positive parity state at 1.825 MeV inspite of the smaller energy difference, this level may be a member of the positive parity band of states arising due to $1p-1h$ excitation from the sd to fp shell.

2.614 and 2.835 MeV Levels

These levels have been strongly excited¹⁰⁾ in (^3He , $p\gamma$) reaction and have been found to decay strongly to the $J=7/2$ state at 0.16 MeV. The level at 2.835 MeV has also a decay branch to the $J=3/2$ state at 1.548 MeV. Spins $7/2^-$ and $(5/2^-)$ respectively have been suggested^{5,6,10)} for these levels. In contrast the (^3He , α) measurements by Rao et al¹¹⁾, L'Ecuyer et al¹²⁾ and Lutz et al¹³⁾ have assigned $J=7/2$ to the 2.835 MeV level. Of these (^3He , α)

reaction studies, only Rao et al have seen the 2.61 MeV level and have assigned $J=(5/2^-, 7/2^-)$ to this level.

Our calculated state with $J=7/2$ and $5/2$ at 2.56 and 2.85 MeV are in very good agreement with the observed levels under discussion. The $J=7/2$ state at 2.56 MeV is the member of the $K=1/2$ band. In our discussion on the transitions in the $K=1/2$ band, we have suggested that the $J=7/2$ state observed at 2.61 MeV may be regarded as the one corresponding to our calculated 2.56 MeV $J=7/2$ state of the $K=1/2$ band.

The calculated branching ratios for various transitions from the $J=5/2$ state at 2.85 MeV, when associated with the observed state at 2.835 MeV are given in fig.13. In agreement with the qualitative observations¹⁰⁾, this state decays predominantly (71 percent) to the $J=7/2$ state at 0.16 MeV with a mean lifetime of 2.3 fs. The calculated $B(M1)$ values for the $5/2 \rightarrow 7/2$ and $5/2 \rightarrow 3/2$ transitions are 0.90 and 0.61 (n.m.)² respectively.

3.223 MeV Level

This level is excited strongly in the ($^3\text{He}, p\gamma$) reaction¹⁰⁾ and is also observed in the $(d, p)^{5,6)}$ and $(^3\text{He}, \alpha)$ reactions¹¹⁾. The $J=7/2$ has been suggested for this level. In spite of its strong excitation, this level has been

indicated¹⁰⁾ to decay weakly to the second excited state of ^{47}Ti . Our calculated $J=7/2$ state at 3.30 MeV has decay properties in qualitative agreement with this observed data.

The calculated mean lifetime is 1.6 fs.

2.683 and 3.289 MeV Levels

The decay modes of these high-spin state with $J=11/2$ and $13/2$ respectively have been studied by Sawa et al²⁾. The $J=11/2$ at 2.683 MeV decays to the $J=9/2$ member of the ground state band. The $J=13/2$ state decays to the above $J=11/2$ state and to the $J=11/2$ at 1.45 MeV. The latter transition has been found to be of very low intensity. Sawa et al have also given $(E2/M1)$ mixing ratios for the transitions $11/2 \rightarrow 9/2$ and $13/2 \rightarrow 11/2$ at 2.68 MeV.

The calculated states with $J=11/2$ and $13/2$ at 2.62 and 3.34 MeV shown by thin lines in fig.11A are in very good agreement with the experimental states. These states have large band-mixing (63 percent and 45 percent respectively) compared to the $J=11/2$ and $13/2$ states of the ground state band. The $B(E2)$, $B(M1)$ and $(E2/M1)$ mixing ratios for the transitions between these states and from them to the members of the ground state band are given in table 30.

Table 30

Electromagnetic properties of the calculated $J=11/2$ and $13/2$ states at 2.62 and 3.34 MeV respectively, when associated with the corresponding observed states at 2.68 and 3.29 MeV.

J_i	J_f	E_i (MeV)	E_f	$B(E2)$ $e^2 \text{fm}^4$	$B(M1)$ (n.m.) ²	(E2/M1)	
						DCM	Expt ^a
11/2	9/2	2.68	1.25	7.7	0.50	+0.05	0 \pm 0.02
	11/2		1.45	5.0	0.74	+0.03	
13/2	11/2	3.29	1.45	6.0	0.09	-0.12	
	13/2		2.67	0.18	0.35	+0.004	
	11/2		2.68	66.3	0.52	-0.06	0 \pm 0.04
	15/2		2.75	3.7	0.41	+0.01	

a. Ref.2.

It is seen that the $B(E2)$ values for the transitions between the calculated $J=11/2$ state at 2.62 MeV and the $J=9/2$ and $11/2$ members of the ground state band are small. However, the $B(M1)$ values for these transitions are significantly large. The calculated branching ratios for the transitions given in fig.13 show that this state decays with almost equal intensity to the $J=9/2$ and $11/2$ states of the ground state band. The corresponding lifetime is about 19 fs. Experimentally, however, no decay to the $J=11/2$ state at 1.45 MeV has been seen. It would be of interest to look for this decay. The calculated mixing ratio for the 2.168 \rightarrow 1.25

MeV transition is in reasonable agreement with the experiment.

The $B(E2)$ values for various transitions from the calculated $J=13/2$ state at 3.34 MeV are, in general, small. The exception is the $13/2 \rightarrow 11/2$ (2.68 MeV) transition which has a relatively large $B(E2)$ value. The $B(M1)$ values however are in general large. It is seen from fig.13 that this calculated $J=13/2$ state at 3.34 MeV when identified with the observed 3.29 MeV $J=13/2$ state, decays predominantly (69%) to the $J=11/2$ state at 1.45 MeV, mainly due to the large energy difference between these states. The corresponding mean lifetime is 68 fs. The calculated mixing ratio for the $13/2 \rightarrow 11/2$ (2.68 MeV) transition agrees with the observations of Sawa et al.

3.98 MeV Level

In the experimental spectrum (fig.11A) Sawa et al.²⁾ have observed a state at 3.98 MeV. No spin assignment has been made. However in their experiment a weak γ -ray from this state to the $J=13/2$ at 3.29 MeV has been seen.

Corresponding to this observed level we have in the calculated spectrum, shown in fig.11A, four high spin states with $J=11/2, 19/2, 13/2$ and $11/2$ at 3.84, 3.95, 4.04 and

4.18 MeV respectively. These are drawn in fig.11 by half lines.

The observation of the $3.98 \text{ MeV} \rightarrow J=13/2$ (3.289 MeV) decay, rules out $J=19/2$ assignment to the 3.98 MeV level. The $J=13/2$ state calculated at 4.04 MeV is a member of the $K=1/2$ band of states. Had the observed 3.98 MeV state been this $J=13/2$ state, it would have preferentially decayed strongly to the other members of the band. Such strong transitions have not been seen. Thus it is unlikely that 3.98 MeV state is the calculated $J=13/2$ state. The only other candidate for this state could be one of the $J=11/2$ state obtained at 3.84 and 4.18 MeV.

In table 31 are given the $B(E2)$, $B(M1)$, $(E2/M1)$ mixing ratios, lifetimes and branching ratios, for decays from these two calculated $J=11/2$ states, when associated, in turn, with the 3.98 MeV observed level. It is seen that both the calculated states decay predominantly to the $J=11/2$ state observed at 1.45 MeV. In view of the paucity of the experimental data, on the transitions under investigation, it is not possible to pinpoint the particular $J=11/2$ state that might correspond to the 3.98 MeV level.

Table 31

Calculated decay properties of the $J=11/2$ states at 3.84 and 4.18 MeV when associated with the 3.98 MeV observed level.

J_i	E_i^{cal} MeV	J_f	E_f^{expt} MeV	$B(E2)$ $e^2 \text{fm}^4$	$B(M1)$ (n.m.) ²	δ	τ_m (fs)	I (%)
11/2	3.84	11/2	1.45	14	0.59	+0.10	4.5	79
		13/2	2.67	18	0.71	+0.05		13
		11/2	2.68	5	0.34	+0.04		6
11/2	4.18	11/2	1.45	10	0.32	-0.12	8.1	77
		9/2	2.41	0.01	0.18	-0.003		10
		13/2	2.67	6	0.15	-0.07		5

2.5 LEVEL DENSITY

The calculations for the ^{47}Ti nucleus described above show that the low-lying states of this nucleus upto ~ 3 MeV excitation energy are reproduced very well by our model. However, the level density for this nucleus increases very rapidly beyond 3 MeV excitation energy. Lewis¹⁾ has given around 113 levels upto 6 MeV in the spectrum of ^{47}Ti nucleus. Of these the spin and parity assignments for only about 27 levels has been made. The success of our model in describing the states of ^{47}Ti upto 3 MeV excitation energy

suggests that it might be able to yield the correct number of states (corresponding to excitations within the f-p shell) upto about 6 MeV since that amount of energy does not appear to be too large for our truncated configuration model to break down.

Extension of the complete band mixing calculation, described above, to include all the intrinsic states upto 6 MeV excitation relative to the HF state is quite cumbersome. Since in absence of spin parity assignments our only aim is to obtain an estimate of the level density, such a detailed calculation is not necessary. The calculation of the level density was guided by the results of the complete band mixing calculation. It was performed in the following stages:

(a) Intrinsic States

Various intrinsic state were obtained by 1p-1h, 2p-2h etc. excitations from the HF state of ^{47}Ti . The energies of the occupied as well as unoccupied single-particle orbits were taken to be those corresponding to the HF state. These energies depend upon the chosen effective interaction. In table 32 we list the single-particle energies ϵ_k of the 20 fp shell orbits of the protons and neutrons. In the HF states of ^{47}Ti , only the first two proton and the first five

Table 32

The energies and k -values of the proton and neutron single particle states of the lowest prolate Hartree-Fock field. The states above the dashed line are occupied in the prolate Hartree-Fock state. Those below are unoccupied.

PROTONS		NEUTRONS	
k	e_k (MeV)	k	e_k (MeV)
0.5	0.0	-0.5	1.499
-0.5	0.096	0.5	1.915
<hr/>			
1.5	2.009	-1.5	3.975
-1.5	2.395	1.5	4.542
2.5	3.893	-2.5	5.962
<hr/>			
-2.5	4.847	2.5	6.428
0.5	6.057	-3.5	7.279
-0.5	6.073	3.5	8.138
3.5	6.130	-0.5	8.174
-3.5	6.618	0.5	8.325
-0.5	8.188	-1.5	10.285
0.5	8.191	0.5	10.506
1.5	8.608	-0.5	10.577
-1.5	8.889	1.5	10.596
-0.5	10.052	0.5	11.787
1.5	10.188	-0.5	11.995
0.5	10.297	1.5	12.697
-1.5	10.561	-1.5	13.192
-2.5	12.445	2.5	14.434
2.5	12.586	-2.5	14.838

neutron orbits are occupied. The total single particle energy of the HF state is then defined as

$$\epsilon_0 = \sum_{i=1}^2 e_n^{(p)} + \sum_{j=1}^5 e_j^{(n)}$$

All intrinsic states with total single particle energy ϵ within 6 MeV relative to ϵ_0 are obtained. There are 121 such states. Of these, 27 are 1p-1h, 71 are 2p-2h, 20 are 3p-3h and 2 are 4p-4h excited states. Thus most of the intrinsic states arise due to comparatively small excitations from the HF state.

The $K = \sum_i k_i$ values of the intrinsic states range from $\pm 1/2$ to $\pm 19/2$. The number of states with definite K values are listed in table 33. For an even-even nucleus, the single particle states with $\pm K$ values are degenerate in energy due to the time reversal invariance of the HF state. In that case the number of states with $\pm K$ values in any energy interval are equal. For an odd- A nucleus, time reversal symmetry is broken. Therefore the single particle orbits with $\pm k$ are not degenerate. As a result the number of states with $\pm K$ values within a given energy range are not equal.

The intrinsic states listed in table 33 are all deformed and a number of states with definite angular momenta

Table 33

K values.	$\frac{1}{2}$	$\frac{3}{2}$	$\frac{5}{2}$	$\frac{7}{2}$	$\frac{9}{2}$	$\frac{11}{2}$	$\frac{13}{2}$	$\frac{15}{2}$	$\frac{17}{2}$	$\frac{19}{2}$	Total States.
+K	14	13	8	4	5	2	2	1	0	0	49
-K	13	16	12	10	7	8	3	1	1	1	72

can be projected from them. For an even-even nucleus, the states projected from an intrinsic state χ_K are identical to those projected from the state χ_{-K} . For an odd-A nucleus this is not strictly true, but is true to a large extent. Hence the states with either positive or negative K should be considered while calculating the total number of independent projected states. For this reason, we consider only the 72 intrinsic states with negative K-values which lie within 6 MeV of the HF energy ϵ_0 of ^{47}Ti . The states projected from the positive K intrinsic states would already be included in those projected from the 72 states with negative K values.

The distribution in energy of the 72 intrinsic states with negative K values is shown in fig.16 by the dotted line. The minimum in the density of the intrinsic states around 3 MeV is interesting. It occurs at an energy where the density of the observed states has a peak. This minimum arises due to particular distribution of the single particle

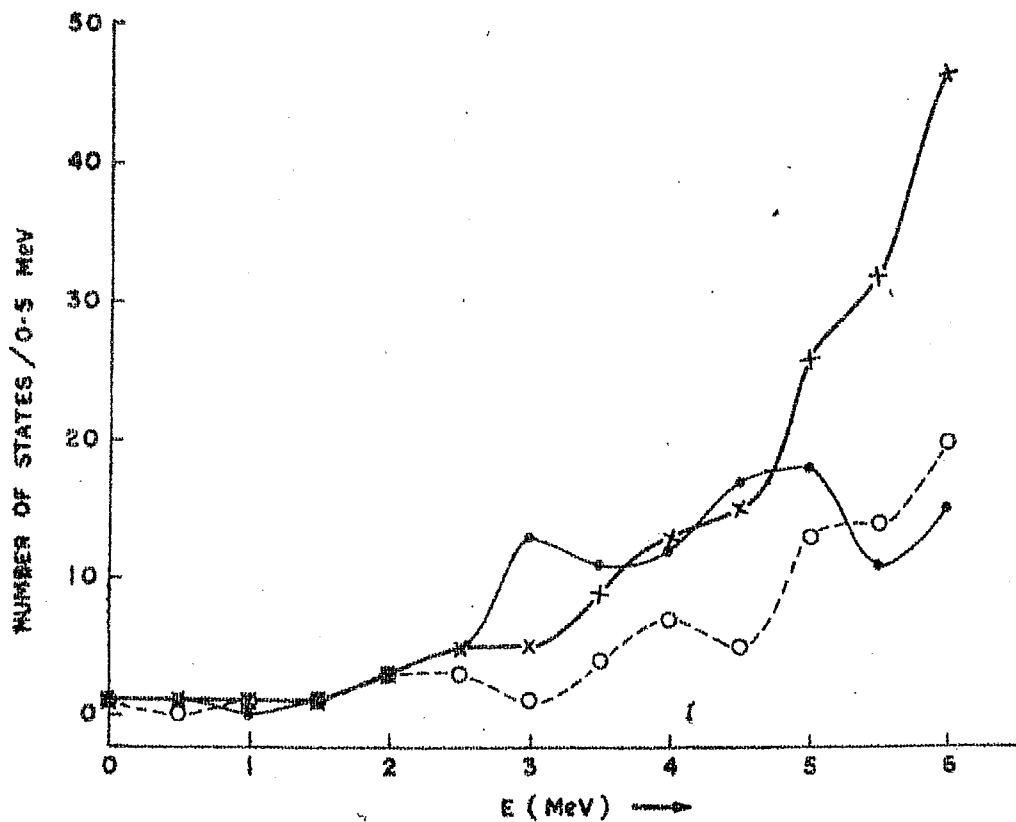


Fig.16

Density of states upto 6 MeV in the spectrum of ^{47}Ti . The dotted curve gives the number of intrinsic states per 1/2 MeV. The thick curve (shown by crosses) is the calculated distribution curve, while the thin curve is the experimental level density curve.

energies which the chosen interaction gives rise to.

It is clear that the total number of intrinsic states obtained upto 6 MeV are significantly smaller than the number of observed energy levels. It appears to us that this must be true for any nucleus. In the usual combinatorial computation²⁹⁾ of the level densities one just counts the number of intrinsic states within a given energy interval. It is likely therefore that if realistic single particle energies (HF energies?) appropriate for the particular nucleus are chosen, these combinatorial calculations should underestimate the level densities.

(b) Projected States

Having obtained the 72 intrinsic states that span a range of 6 MeV, the next question is to determine the range of energy within which will lie all the states with definite angular momentum projected from these intrinsic states. A clue for this has been taken from the description of the low-lying states of ⁴⁷Ti nucleus for which 19 different intrinsic states listed in tables 15 and 17 have been used. All these states occur within 4.2 MeV relative separation energy. The spectrum projected from all these intrinsic states are on the average spread over 3.5 MeV. This spread of the spectrum projected from a particular intrinsic state, we refer to as the "width" of the intrinsic state.

For the level density calculation we have assumed that on an average each of the 72 intrinsic states upto 6 MeV energy has a "width" of 3.5 MeV. Therefore the total span of the states projected from all the 72 intrinsic states becomes 9.5 MeV.

The next question therefore is to determine how many states with definite angular momenta can be projected from these 72 intrinsic states. To answer this question without actually carrying out the projection calculation, we use the information obtained from the detailed projection calculation for the ten intrinsic states listed in table 15.

It is observed that states with $J=K$ upto $J=19/2$ are projectable from an intrinsic state with a given K . Thus ten J -states can be projected from the intrinsic state with $K=1/2$ and so on. From the distribution of the K -values of the 72 intrinsic states listed in table 33, we estimate that in all 540 states can be projected from all these intrinsic states. Thus on an average about 7 to 8 states can be projected from each of the intrinsic states.

(c) Orthogonalization and Hamiltonian Mixing

All the 540 states projected from the 72 intrinsic states, are not orthogonal to each other. The main effect, as far as level densities are concerned, of orthogonalizing these states would be to reduce the number of states within

the energy interval of 9.5 MeV spanned by the nonorthogonal states. The reduction factor that would take into account the effects of orthogonalization and mixing due to Hamiltonian, has been adopted from that obtained in detailed calculation for ^{47}Ti nucleus.

From the ten intrinsic states of table 15, which are spread over 3 MeV, around 80 projected states have been obtained. Since each intrinsic state has an average width of about 3.5 MeV all the 80 projected states lie within an energy interval of about 6.5 MeV. After the orthogonalization and Hamiltonian mixing effects are taken care of, the final composite spectrum plotted at 10C contains only about 50 states upto 6.5 MeV. This implies therefore that for the low-lying states of ^{47}Ti , the number of orthogonal states within an energy interval in which all the projected (non-orthogonal) states lie is about $5/8$ of the total number of the nonorthogonal states in that energy range.

From this result of the complete band mixing calculation we assume that about 5 orthogonal states can be projected from each of the 72 intrinsic states considered above. For the sake of simplicity we assume that these five states are centred around the energy of their intrinsic states and are equally spaced within the energy spread of 3.5 MeV. This assumption is, of course, not strictly true but as can be

seen from the projected spectra in figs.8 and 9, is better than assuming a $J(J+1)$ spacing for the projected states.

With these assumptions we get about 360 states upto 9.5 MeV excitation energy in the spectrum of ^{47}Ti nucleus. Of these only 158 states lie within 6 MeV excitation.

The distribution curve indicating the number of states within every $1/2$ MeV energy interval has been shown in fig.16 by a thick line. The corresponding observed density for the same energy interval has been shown by the thin line. Since the present calculation attempts to estimate only the level density corresponding to nuclear excitations within the f-p shell, the so far identified positive parity states have been omitted while plotting the observed density distribution curve.

Upto 2.5 MeV, the calculated and the observed level densities, are in fairly good agreement. At around 2.5 to 3 MeV the calculated curve shows a "valley" in contrast to the "bunching" of levels observed in that energy interval. It may be pointed out, however, that for the observed states at around 3 MeV excitation energy the spins and parities are not known. Our calculation can reproduce only negative parity states. It is likely therefore that some of the levels observed around 3 MeV have positive parities.

It would be interesting to identify the parities of these states. Barring this deviation at 3 MeV excitation energy range, the calculated and experimental spectrum seem to be in a fairly good agreement upto 4.75 MeV. It may be mentioned that the level densities in nuclei increase almost exponentially with increase in excitation energy. Therefore, the dip seen in the experimental density distribution curve beyond 4.75 MeV may be because of some technical difficulties in resolution etc. The large differences in the theoretical estimate of 158 levels and the observed level density of 108 levels (excluding so far identified five positive parity levels) arise mainly due to the fall in the observed level density beyond 4.75 MeV. It would be of interest to obtain an improved experimental estimates of level density of ^{47}Ti beyond 4.5 MeV.

The procedure adopted here for calculating the level densities of a nucleus in the neighbourhood of the fermi surface seems to us more appropriate than the usual combinatorial procedure wherein the effect of the two-body interactions on the level densities are taken care of by choosing the single-particle level densities at the fermi surface to fit the observed level densities.

REFERENCES

1. M.B. Lewis, Nucl. Data Sheets, B4 (1970) 313.
2. Z.P. Sawa, J. Blomqvist and W. Gullholmer, Nucl. Phys. A205 (1973) 257.
3. J. Rapaport, A. Sperduto and W.W. Buechner, Phys. Rev. 143 (1966) 808.
4. J.L. Alty, L.L. Green, G.D. Jones and J.F. Sharpey-Schafer, Nucl. Phys. A100 (1967) 191.
5. D.C. Kocher and W. Haeberli, Nucl. Phys. A196 (1972) 225.
6. M.S. Chowdhury and H.M. Sen Gupta, Nucl. Phys. A229 (1974) 484.
7. P.J. Plauger and E. Kashy, Nucl. Phys. A152 (1970) 609.
8. J.J. Weaver, M.A. Grace, D.H. F. Start, R.W. Zurmuhle, D.P. Balamuth and J.W. Noe, Nucl. Phys. A196 (1972) 269.
9. L.K. Fifield, J.W. Noe, D.P. Balamuth and R.W. Zurmuhle, Nucl. Phys. A204 (1973) 516.
10. L. Meher-Schutzmeister, J.W. Smith, G. Hardie, H. Siefken, K.T. Knopfle, M. Rogge and C. Mayer-Boricke, Nucl. Phys. A199 (1973) 593.
11. M.N. Rao, J. Rapaport, T.A. Belote and W.E. Dorenbusch, Nucl. Phys. A151 (1970) 351.
12. J. L'Ecuyer and C. St-Pierre, Nucl. Phys. A100 (1967) 401.

13. H.F. Lutz and T.S. Bohn, Nucl.Phys. A116 (1968) 112.
14. O.F. Afonin, A.P. Grinberg, I.kh.Lemberg and I.N. Chogunov, Sov.Jou.Nucl.Phys. 6 (1968) 160.
15. T. Sebe and M. Harvey, Atomic Energy of Canada Ltd, Report AECL 3007 (1968) P.14.
16. J.D. McCullen, B.F. Bayman and L. Zamick, Phys.Rev. 134 (1964) B515.
17. F.B. Malik and W. Scholz, Phys. Rev. 150 (1969) 919; 153 (1967) 1071.
18. B. Haas, P. Taras and J. Styczen, Nucl. Phys. A246 (1975) 241.
19. J.B. McGrory, B.H. Wildenthal and E.C. Halbert, Phys. Rev. C2 (1970) 86.
T.T.S. Kuo and G.E. Brown, Nucl.Phys.A114 (1968) 241.
20. B.E. Chi, Nucl.Phys. 83 (1966) 97.
21. A.K. Dhar, D.R. Kulkarni and K.H. Bhatt, Phys. Lett. 47B (1973) 132.
22. A.K. Dhar, D.R. Kulkarni and K.H. Bhatt, Nucl. Phys. and Solid State Phys.(India), 16B (1973) 146.
23. A.K. Dhar, D.R. Kulkarni and K.H. Bhatt, Nucl. Phys. A238 (1975) 340.
24. H. Gogelein, R.B. Huber and C. Signorini, Proc. Int. Conf. on Nucl. Phys, Munich, 1973 edited by J.de Boer and H.J. Mang (North Holland, Amsterdam/American Elsevier, New York, 1973), Vol.I, P.176.

25. P. Blasi, R.B. Huber, W. Kutschera and C. Signorini,
Proc. Int. Conf. on Nucl. Phys., Munich, 1973, ed.
J.de Boer and H.J. Mang (North Holland, Amsterdam/
American Elsevier, New York, 1973) Vol.I, P.211.
26. R.B. Huber, W. Kutschera, H. Morinaga and C. Signorini,
Proc. Int. Conf. on Nucl. Phys., Munich, 1973, ed.
J.de Boer and H.J. Mang (North Holland, Amsterdam/
American Elsevier, New York, 1973), Vol.I, P.174.
27. V.S. Shirley, Hyperfine Structure and Nuclear Radiati-
ons, ed. E. Matthias and D.A. Shirley (North Holland,
1968), P.985.
28. V.S. Shirley, Table of Nuclear Moments in Hyperfine
Interactions in Excited Nuclei, edited by G. Goldring
and R. Kalish (Gordon and Beach Science Publishers
Inc., New York, 1971) P.1255.
29. J.R. Huizenga and L.C. Moretto, Ann. Rev. Nucl. Sci.
22 (1972) 427.

CHAPTER 5

THE NUCLEUS ^{49}Ti

1.

INTRODUCTION

1.1

Experimental Data

The experimental data on ^{49}Ti is less extensive¹⁾ than $^{45,47}\text{Ti}$ inspite of the several reactions performed at a variety of incident energies for the investigations of its level structure. The information about this nucleus exists mainly from the (d,p) reaction measurements of Kocher and Haeberli²⁾ and Ball et al³⁾. In other⁴⁻⁸⁾ earlier (d,p) reaction measurements, levels upto about 6 MeV were excited but the spins and parities were not known. Plauger and Kashy⁹⁾ made spin assignments to some of the level of ^{49}Ti excited in (p,d) reaction studies at 45.05 MeV. The other experimental investigations for the study of this nucleus include¹⁰⁻¹³⁾ $^{48}\text{Ti}(n,\gamma)$, $^{49}\text{Ti}(p,p')$, $^{50}\text{Ti}(d,t)$, $^{50}\text{Ti}(^3\text{He},\alpha)$, $^{50}\text{V}(t,\alpha)$ and $^{51}\text{V}(d,\alpha)$ reactions. No definite information is available for the high-spin states in this nucleus. However, possible spin assignments ranging from 5/2 to 19/2 are suggested to some of the low-lying states on the basis of $l_p=3$ transfer in $^{50}\text{V}(t,\alpha)$ reaction studied by Anderson et al¹¹⁾. No data is available

on the electromagnetic properties of this nucleus. However, the values of ground state moments are known^{14,15)}.

1.2 Previous Calculations

No detailed theoretical study of ^{49}Ti has been made. The $(f_{7/2})^9$ shell model calculation choosing proton and neutron configurations $\pi(f_{7/2})^2 \nu(f_{7/2})^{-1}$ has been performed¹⁶⁾. The RPC model calculations of Malik and Scholz¹⁷⁾ consider intrinsic states corresponding to $\beta=0.15$ for the optimum agreement with the experimental spectrum. Recently the spectrum of this nucleus has also been studied by Abecasis et al¹⁸⁾ on the basis of intermediate-coupling-model calculations. The spectrum of the low-lying states of ^{49}Ti as obtained in these calculations is in qualitative agreement with the experiment. No calculations have been reported on the study of the electromagnetic properties of this nucleus.

We shall present in the next section the results^{19,20)} of our DCM calculations on the spectrum and electromagnetic properties of the low-lying states of ^{49}Ti .

2. PRESENT CALCULATIONS

2.1 CALCULATION OF THE ENERGY SPECTRUM

2.1.1 Generation of Intrinsic States

For the nucleus ^{49}Ti , deformed HF calculations lead to

the prolate $K=7/2$ HF state with an energy $E_K = -17.28$ MeV, almost degenerate in energy with the oblate $K=1/2$ HF state. The corresponding intrinsic quadrupole moments Q_K are 14.2 b^2 and -12.3 b^2 .

It is seen by comparing the energies of the HF calculations of the nuclei ^{45}Ti , ^{47}Ti and ^{49}Ti , that the prolate-oblate energy separation goes on decreasing with the increase in neutron number and becomes almost degenerate for ^{49}Ti (and also for ^{51}Ti which we shall show later). This degeneracy is due to the lack of collectivity for the nuclei with $N \sim 28$ corresponding to the $(f_{7/2})^8$ neutron sub-shell closure. It may be mentioned that the chosen effective interaction gives small energy gaps at the fermi surface as a result of which the oblate solution of ^{49}Ti does not converge in the usual HF iterative procedure. We obtained the above $K=1/2$ oblate HF state by a specific choice of the single particle occupancies. Thus, in the oblate $K=1/2$ HF intrinsic state of ^{49}Ti , the occupied single particle states were constrained to have the following k values

$$\pi(\pm 7/2)^2 \quad \nu(\pm 7/2, \pm 5/2, \pm 3/2, + 1/2)^7.$$

The structural and spectral information about the occupied (above the dashed line) and the lowest unoccupied (below the dashed line) proton and neutron single particle

states or the prolate and oblate HF states of ^{49}Ti are given in tables 34 and 35. It is seen from these tables that the single particle energy gaps at the fermi surface are not very large. It is therefore expected that the inclusion of p-h excited intrinsic states would be necessary for the description of the low-lying states of ^{49}Ti .

We have included in our calculations all the intrinsic states that lie within about 2 MeV relative to the prolate HF state. Nine excited intrinsic states obtained by 1p-1h excitations from the prolate and oblate HF states have been found to lie within this chosen energy interval of 2 MeV excitation. The details of these intrinsic states are presented in table 36, along with the energies and K-values of the HF states from which they are generated. The 2p-2h excited intrinsic states were found to lie above 2 MeV relative excitation energy and were not thus included in the present calculation.

In all, therefore, eleven intrinsic states listed in table 36 were considered. Out of these, four states with $J=1/2$, seven states with $J=3/2$, ten states with $J=5/2$ and eleven states with $J \geq 7/2$ can be obtained.

For all the intrinsic states of table 36, $T=5/2$ is the dominant isospin. The maximum amplitude of isospin $T=7/2$ in some of these intrinsic states is 0.022. The isospin

Table 34

Structural and spectral details of the occupied and a few lowest unoccupied proton and neutron orbitals of the PROLATE $K=7/2$ HF intrinsic state of ^{49}Ti . For this HF state, the energy $E_K = -17.28$ MeV and quadrupole moment $Q_K = 14.20 \text{ b}^2$. For other details see caption for table 1.

	k	e_k (MeV)	q_{k2} (b^2)	$c_{\frac{1}{2}k}$	$c_{\frac{3}{2}k}$	$c_{\frac{5}{2}k}$	$c_{\frac{7}{2}k}$
P	1/2	-7.53	3.54	0.083	-0.222	-0.141	0.961
R	-1/2	-7.43	3.53	-0.081	-0.224	0.123	0.963
O							
T	3/2	-6.31	1.89		-0.111	-0.110	0.988
N	-3/2	-6.10	1.88		-0.114	0.095	0.989
S	5/2	-5.23	-0.27			-0.082	0.997
	1/2	-4.95	3.61	0.109	-0.231	-0.128	0.958
N	-1/2	-5.14	3.62	-0.094	-0.229	0.172	0.954
E	3/2	-3.06	1.78		-0.102	-0.062	0.993
U	-3/2	-3.50	1.75		-0.073	0.110	0.991
T	5/2	-1.55	-0.37			-0.027	0.999
R	-5/2	-2.34	-0.25			0.092	0.996
O	7/2	-0.34	-3.0				1.0
N							
S	-7/2	-1.30	-3.0				1.0
	1/2	1.64	3.26	-0.447	0.740	0.414	0.285
	1/2	3.44	0.66	0.560	0.632	-0.536	0.016

Table 35

Structural and spectral details of the occupied and a few lowest unoccupied proton and neutron orbitals of the OBLATE $K=1/2$ HF intrinsic state of ^{49}Ti . For this HF state, the energy $E_K = -17.27$ MeV and quadrupole moment $Q_K = -12.23$ b². For other details see caption for table 1.

	k	e_k (MeV)	q_k (b ²)	$c_{\frac{1}{2}k}$	$c_{\frac{3}{2}k}$	$c_{\frac{5}{2}k}$	$c_{\frac{7}{2}k}$
P R O T O N S	7/2	-7.47	-3.0				1.0
	-7/2	-7.41	-3.0				1.0
	5/2	-5.77	-0.90			0.189	0.981
	-5/2	-5.78	-0.89			-0.187	0.982
	3/2	-5.05	0.36		0.189	0.052	0.981
N E U T R O N S	7/2	-4.86	-3.0				1.0
	-7/2	-4.85	-3.0				1.0
	5/2	-2.66	-0.85			0.173	0.985
	-5/2	-3.08	-0.84			0.169	0.986
	3/2	-2.19	0.27		0.211	0.036	0.977
	-3/2	-1.59	0.28		0.208	-0.045	0.977
	1/2	-1.15	0.87	0.082	0.212	0.045	0.973
	-1/2	-1.78	1.16	-0.073	0.165	-0.020	0.983
	3/2	2.26	-1.25		0.967	-0.152	-0.203
	-3/2	2.22	-1.29		0.967	-0.158	-0.198
	1/2	2.270	-1.11	0.714	0.656	0.131	-0.209

Table 36

Energies and K-values of the prolate and oblate HF states of ^{49}Ti and of the intrinsic states obtained by 1p-1h excitations from the HF states. For the oblate $K=1/2$ intrinsic states at -15.96 and -15.31 MeV the odd neutron is in the $k = -1/2$ orbital.

Shape	Hole k_i	Particle k_m	K	E_K (MeV)
Prolate	(HF STATE)		7/2	-17.28
	n -5/2	n -7/2	5/2	-16.60
	n 7/2	n 1/2'	1/2	-15.68
	p -1/2	p -3/2'	5/2	-15.58
	n -3/2	n -7/2	3/2	-15.41
Oblate	(HF STATE)		1/2	-17.27
	n 1/2	n 3/2	3/2	-17.01
	n -5/2	n -1/2	5/2	-16.14
	p -7/2	p -5/2	1/2	-15.96
	p -7/2	p -5/2	3/2	-15.58
	p 7/2	p 5/2	1/2	-15.31

mixing due to the components with $T > 7/2$ is negligibly small. It is, however, hoped that this extremely small isospin impurity would not alter in any significant manner the structure of the low-lying states of ^{49}Ti .

2.1.2 Projected Spectra

The states $\psi_{MK}^J(\gamma)$ with definite angular momenta have been projected from each of the eleven intrinsic states of ^{49}Ti listed in table 36. The energy spectra of these states are plotted in figs.17 and 18.

In view of the near degeneracy of the prolate and oblate HF states and the $(f_{7/2})^8$ sub-shell closure, it is hoped that the states projected from either of these two intrinsic states would be almost equivalent. However, as seen from first two columns $P: \frac{7}{2}$ and $O: \frac{1}{2}$ in fig.17, this expectation is not borne out. The $J=9/2$ and $13/2$ states belonging to the oblate HF state occur high in energy and have a small intensity (3 and 10% respectively) of being contained in this HF intrinsic state. On the other hand, these states occur lower in energy when projected from the prolate HF state. In contrast, the $J=11/2$ state is better described by the oblate HF state. It is thus seen that the projections from a HF state alone is not sufficient to provide a reasonable description of the 'ground state band' of ^{49}Ti .

It is also observed from fig.18 that the band of states projected from the prolate $K=1/2$ ($P:1/2$) intrinsic state at -15.68 MeV, has a peculiar structure involving the clustering into doublets of states with $J=(1/2, 3/2)$, $(5/2, 7/2)$,

49Ti

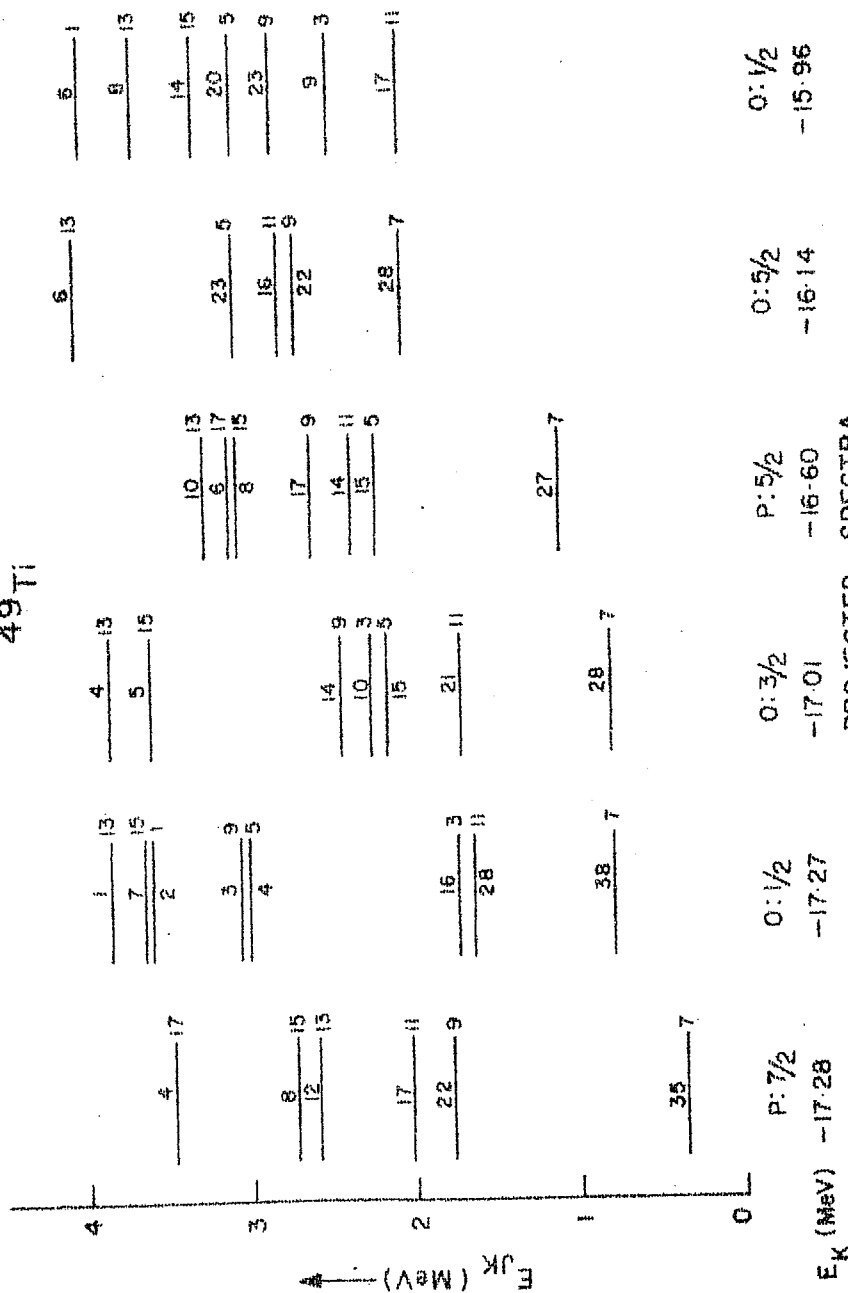
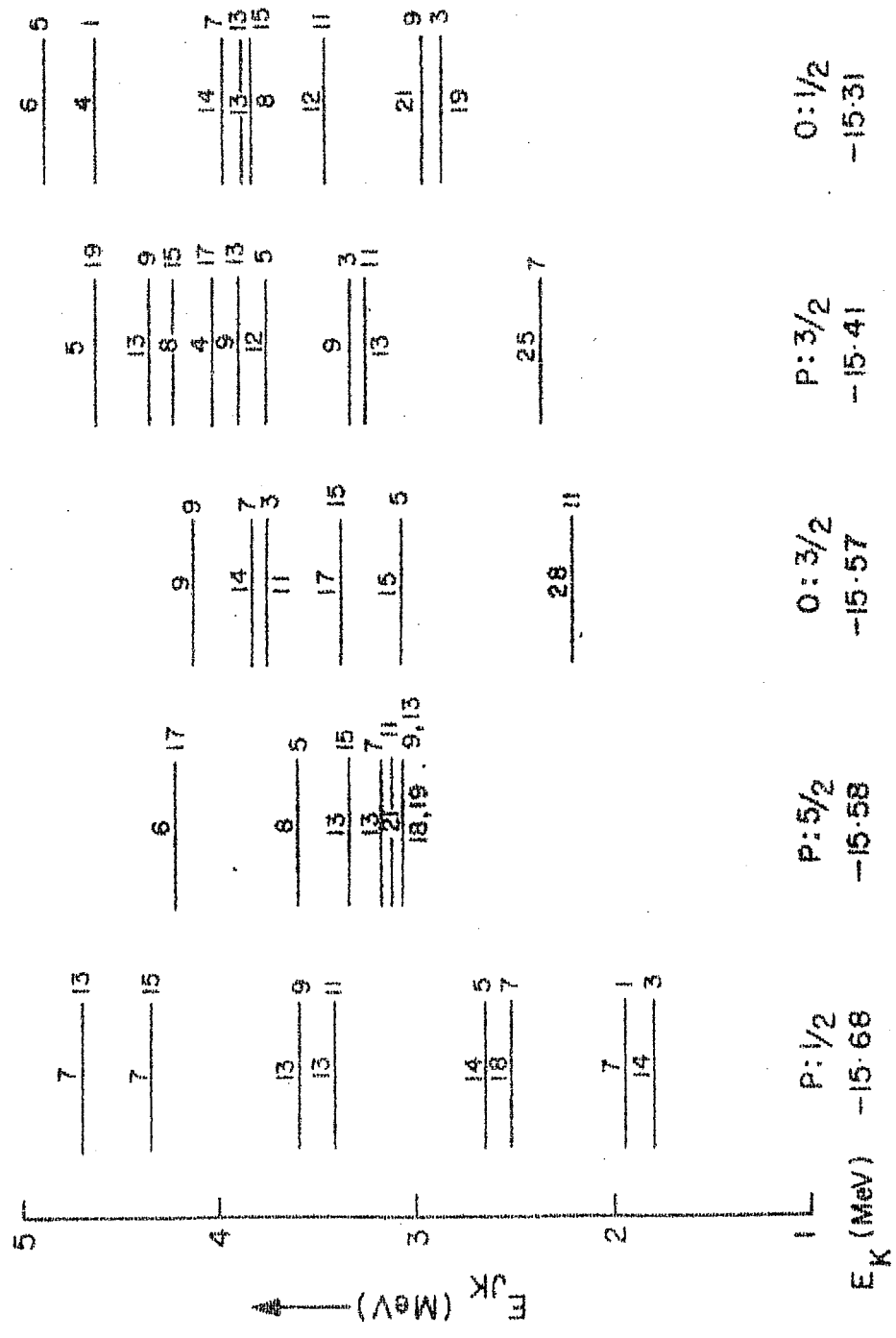


Fig.17

Energy spectra of the states with definite angular momentum projected from the prolate (P) and oblate (O) intrinsic states in ^{49}Ti . The K-values and energies of these intrinsic states are given at the bottom. For the projected states the numbers on the right are their 2J values while those on the top are their intensities in their intrinsic states.

^{49}Ti



PROJECTED SPECTRA
Fig. 18

Energy spectra of the states projected from the prolate (P) and oblate (O) intrinsic states of ^{49}Ti . The energies and K-values of the corresponding intrinsic states are given at the bottom of the figure. For other details see caption of fig. 17.

(9/2,11/2) and (13/2,15/2). Similar features, in general, occur for the $K=1/2$ band of states in the RPC calculation and are interpreted in terms of the decoupling parameter $a \approx -1$. For the $K=1/2$ band of ^{49}Ti , under discussion, we have calculated the decoupling parameter:

$$a = - \sum_j (-)^{j+\frac{1}{2}} (j+\frac{1}{2}) \left| c_{j1/2} \right|^2 \text{ with } j = \frac{1}{2}, \frac{3}{2}, \frac{5}{2}, \frac{7}{2}$$

by considering the wave function ($c_{j1/2}$) of the odd neutron in the $K=1/2$ orbital, to be that obtained in our HF calculation (table 34), the value of 'a' turns out to be -0.85.

Similar features were also observed for the excited $K=1/2$ band in ^{47}Ti .

2.1.3 Nonorthogonality of the Projected States

In table 37, are presented the mutual overlaps of the $J=7/2$ states projected from the eleven intrinsic states. It is seen that these overlaps of the $J=7/2$ states projected from the prolate and oblate HF states and the oblate $K=3/2$ state at -17.01 MeV are very large. This is the consequence of the small deformation and the tendency of the $f_{7/2}$ neutron subshell closure. The overlap matrices for other angular momentum states also have a similar structure.

Of interest in table 37 are the overlaps of the $J=7/2$

Table 37

The overlap matrix of the $J=7/2$ states projected from the eleven intrinsic states of ^{49}Ti . The K-values and energies E_K (in MeV) of these intrinsic states are given on the top of the table. P and 0 refer to Prolate and Oblate deformations respectively.

K	P $\frac{7}{2}$	0 $\frac{1}{2}$	0 $\frac{3}{2}$	P $\frac{5}{2}$	0 $\frac{5}{2}$	0 $\frac{1}{2}$	P $\frac{1}{2}$	P $\frac{5}{2}$	0 $\frac{3}{2}$	P $\frac{3}{2}$	0 $\frac{1}{2}$
E_K	-17.28	-17.27	-17.01	-16.60	-16.14	-15.96	-15.68	-15.58	-15.58	-15.41	-15.31
P $\frac{7}{2}$	1.0	0.902	-0.838	-0.540	0.484	0.017	0.007	0.499	0.404	0.389	0.412
0 $\frac{1}{2}$		1.0	-0.893	-0.567	0.492	0.096	0.022	0.424	0.494	0.467	0.460
0 $\frac{3}{2}$			1.0	0.821	-0.763	-0.073	0.026	-0.132	-0.123	-0.610	-0.092
P $\frac{5}{2}$				1.0	-0.866	-0.020	0.018	0.320	0.265	-0.660	0.287
0 $\frac{5}{2}$					1.0	0.055	-0.021	-0.275	-0.301	0.841	-0.333
0 $\frac{1}{2}$						1.0	0.020	0.034	0.289	0.045	-0.199
P $\frac{1}{2}$							1.0	-0.003	0.011	0.001	0.024
P $\frac{5}{2}$								1.0	-0.794	0.169	0.727
0 $\frac{3}{2}$									1.0	-0.104	0.726
P $\frac{3}{2}$										1.0	-0.134
0 $\frac{1}{2}$											1.0

state projected from the prolate $K=1/2$ intrinsic state at -15.68 MeV, with all the other $J=7/2$ states projected from other intrinsic states. These overlaps are consistently small for all the states upto $J=17/2$ projected from this $K=1/2$ intrinsic state. Earlier we have shown the existence²¹⁾ of similar features for the nuclei $^{45,47}\text{Ti}$, wherein a similarly excited $K=1/2$ band was predicted to exist. It is therefore likely that in the spectrum of ^{49}Ti there also might exist an excited $K=1/2$ band of states, if the mixing due to Hamiltonian of the states projected from this band, with the other projected states is weak.

2.2 COMPOSITE SPECTRUM AND COMPARISON WITH THE EXPERIMENT

The composite spectrum of ^{49}Ti has been obtained by diagonalizing the Hamiltonian matrix in the basis of orthonormalized projected states obtained from the eleven intrinsic states of table 36. In fig.19 is compared this final composite calculated spectrum with the experimental spectrum compiled from the available data.

The agreement between theory and experiment upto about 3 MeV is very good. The observed bunching of states at about 1.5 and 2.5 MeV is very well reproduced. The information about the high-spin states in ^{49}Ti does not exist. However, in (t, α) reaction studies of Anderson et al¹¹⁾ possibility of the existence of states with tentative J values ranging

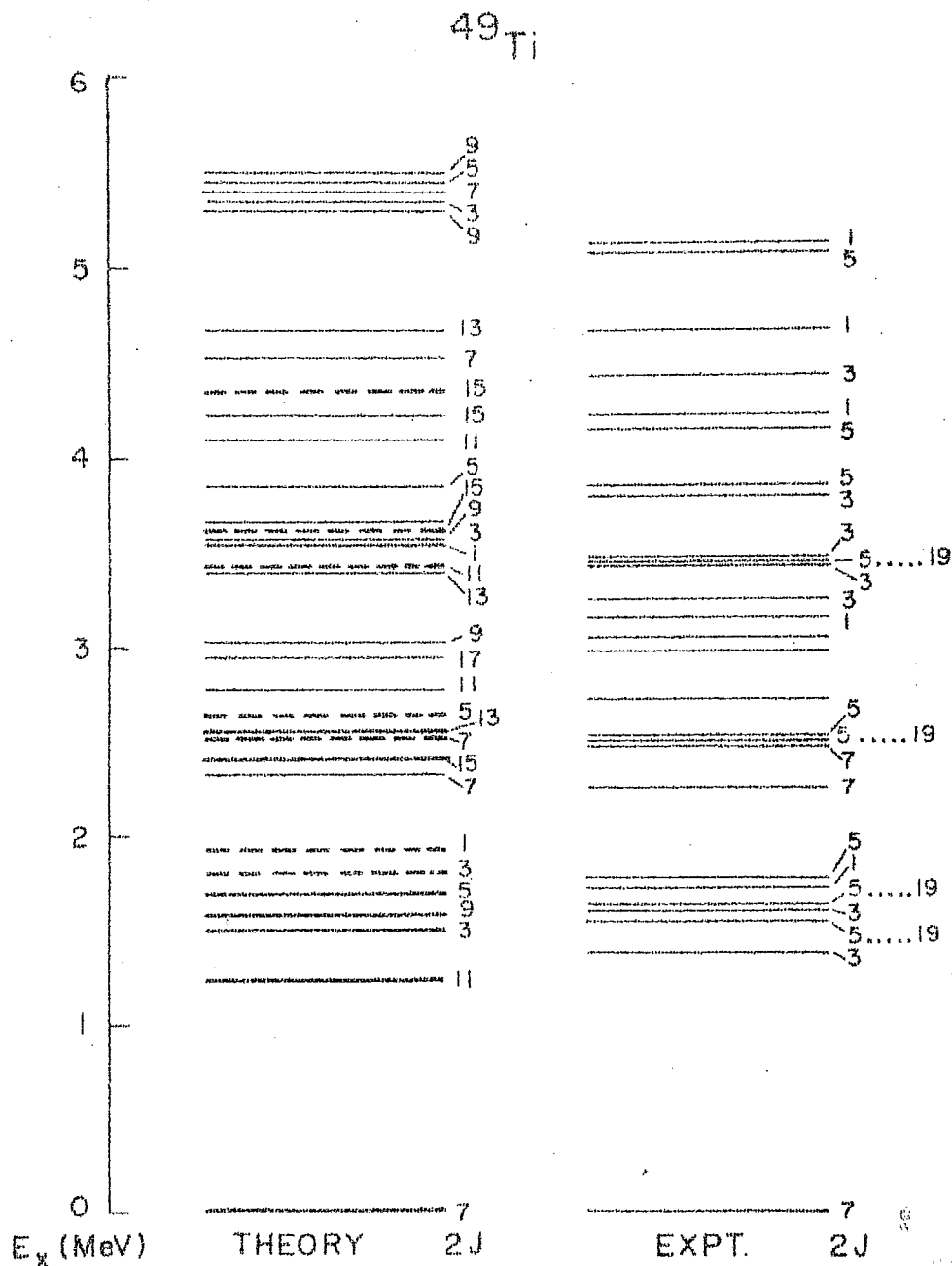


Fig.19

Comparison of the theoretical and experimental spectrum of ^{49}Ti . In the theoretical spectrum the states drawn in full thick lines belong dominantly to those projected from the prolate and oblate HF states. The states indicated by thick dotted lines are the members of the $K=1/2$ band that is predicted to exist. More complex states are indicated by thin lines.

from $5/2$ to $19/2$ have been suggested in the neighbourhood of our calculated high-spin states. There are more states with $J=3/2$ in the experimental spectrum above 3 MeV than in the calculated spectrum. Inclusion of additional p-h excited intrinsic states would be necessary to account for these low-spin states. On the other hand, the high-spin states predicted by the present calculations need be identified.

2.3

BAND STRUCTURE

Because of the similarities of the states projected from the prolate and oblate HF states the "ground state band" of ^{49}Ti does not have a well defined shape. In fig. 19 the states indicated by thick lines are, to a large extent, those projected from the prolate and oblate HF states. The extent to which these states can be regarded as those projected from the prolate $K=7/2$ and oblate $K=1/2$ intrinsic states, is illustrated in table 38. We have presented in this table the intensities $\left| B_K^J \right|^2$ in these states, of the composite spectrum, of the states projected from either the prolate $K=7/2$ or oblate $K=1/2$ HF states.

Table 38

Intensity of the states projected from the prolate $K=7/2$ and oblate $K=1/2$ HF intrinsic states in the states of angular momentum J at energies E_J in the composite spectrum of ^{49}Ti .

J	E_J MeV	B_K^J	
		$K=7/2$	$K=1/2$
7/2	0.0	0.88	0.83
11/2	1.22	0.54	0.91
3/2	1.50		0.91
9/2	1.58	0.92	0.64
5/2	1.69		0.89
15/2	2.41	0.87	0.49
13/2	2.56	0.98	0.50
17/2	2.94	0.89	0.25
1/2	3.57		0.99

It is seen from table 38 that the states with $J=1/2$, $3/2, 5/2, 7/2$ and $11/2$ belong dominantly to the oblate HF state while those with $J=7/2, 9/2, 13/2, 15/2$ and $17/2$ to the prolate $K=7/2$ intrinsic state. The $J=7/2$ ground state has equal probability of being described by either of these states.

It is thus clear that the 'ground state band' of ^{49}Ti does not have a unique interpretation in terms of the projections from a single HF intrinsic state.

As already mentioned, there exists the possibility of the occurrence of a $K=1/2$ excited band of states in the spectrum of ^{49}Ti . The energies and the J -values of the states that were found to have the large intensity $|B_{\frac{1}{2}}^J|^2$ of the states projected from this prolate $K=1/2$ intrinsic state are given in table 39. It is clear that this is an almost pure band of states.

Table 39

Intensity of the states projected from the prolate $K=1/2$ intrinsic state at -15.68 MeV, in the states of angular momentum J at energies E_J (in MeV) of the composite spectrum of ^{49}Ti .

J	$\frac{3}{2}$	$\frac{1}{2}$	$\frac{7}{2}$	$\frac{5}{2}$	$\frac{11}{2}$	$\frac{9}{2}$	$\frac{15}{2}$	$\frac{13}{2}$	$\frac{17}{2}$
E_J	1.81	1.92	2.54	2.65	3.42	3.60	4.34	4.68	5.95
$ B_{\frac{1}{2}}^J ^2$	0.98	0.99	0.94	0.98	0.99	0.98	0.96	0.98	0.95

2.4 ELECTROMAGNETIC PROPERTIES

Experimental data on the decay modes in ^{49}Ti is not available. However, the $(E2/M1)$ mixing ratio of +0.055 for the $1/2_1 \rightarrow 3/2_1$ transition is measured²²⁾. Afonin et al²³⁾ have given the $B(E2)$ value of $< 30e^2\text{fm}^4$ for the $7/2_1 \rightarrow 3/2_1$ transition from their Coulomb excitation measurements. This implies a $B(E2)$ value of less than $60e^2\text{fm}^4$ for

the $3/2_1 \rightarrow 7/2_1$ transition.

No previous results are available for the electromagnetic properties of the low-lying states in this nucleus. For the study of E2 transitions effective charges $e_p = 1.32e$ and $e_n = 0.89e$ are used, while for M1 transitions values of free nucleon g-factors for the proton and neutron are employed.

Table 40

Calculated $B(E2)$, $B(M1)$ and $(E2/M1)$ mixing ratios for the transitions between the members of the "ground state band" in ^{49}Ti .

$2J_i$	$2J_f$	$B(E2)$ $e^2 \text{fm}^4$	$B(M1)$ $(\text{n.m.})^2$	$E2/M1$
11_1	7_1	65		
3_1	7_1	77 (< 60)		
9_1	7_1	104	0.33	+0.24
	11_1	23	1.77	+0.003
5_1	7_1	39	0.57	-0.12
	3_1	38	1.99	+0.014
15_1	11_1	38		
13_1	11_1	50	0.43	+0.12
	9_1	57		
	15_1	79	2.71	+0.007

In table 40 are summarized the calculated decay properties of the members of the ground state band drawn in thick lines in fig.19. We have also given in parenthesis in this table the measured value of $B(E2, 7/2_1 \rightarrow 3/2_1)$. This is in reasonable agreement with our calculated value. The $B(E2)$ values are significantly smaller in ^{49}Ti compared to those in ^{47}Ti since the intrinsic quadrupole moment of ^{49}Ti is about $14 b^2$ whereas that for ^{47}Ti is $21 b^2$. The interesting effect of this small deformation for ^{49}Ti is that the calculation does not give a well defined ground state band within which the $B(E2)$ values are significantly large compared to those for other transitions as observed in ^{47}Ti .

In contrast the $B(E2)$ values given in table 41 for the transitions between the members of the calculated $K=1/2$ band are quite large. For this band of states, we have also presented in table 41 the values of $B(E2)$, $B(M1)$ and $(E2/M1)$ mixing ratios. It is seen from this table that this band splits into two sub-bands: $(3/2-7/2-11/2-15/2)$ and $(1/2-5/2-9/2-13/2-17/2)$ on the basis of the large $B(E2)$ values for the pure $E2$ transitions. The crossover transitions between these two sub-bands are small, except for the $1/2_1 \rightarrow 3/2_2$ and $5/2_2 \rightarrow 7/2_3$ transitions. For the $1/2_1 \rightarrow 3/2_2$ decay both the $B(E2)$ and $B(M1)$ values are large

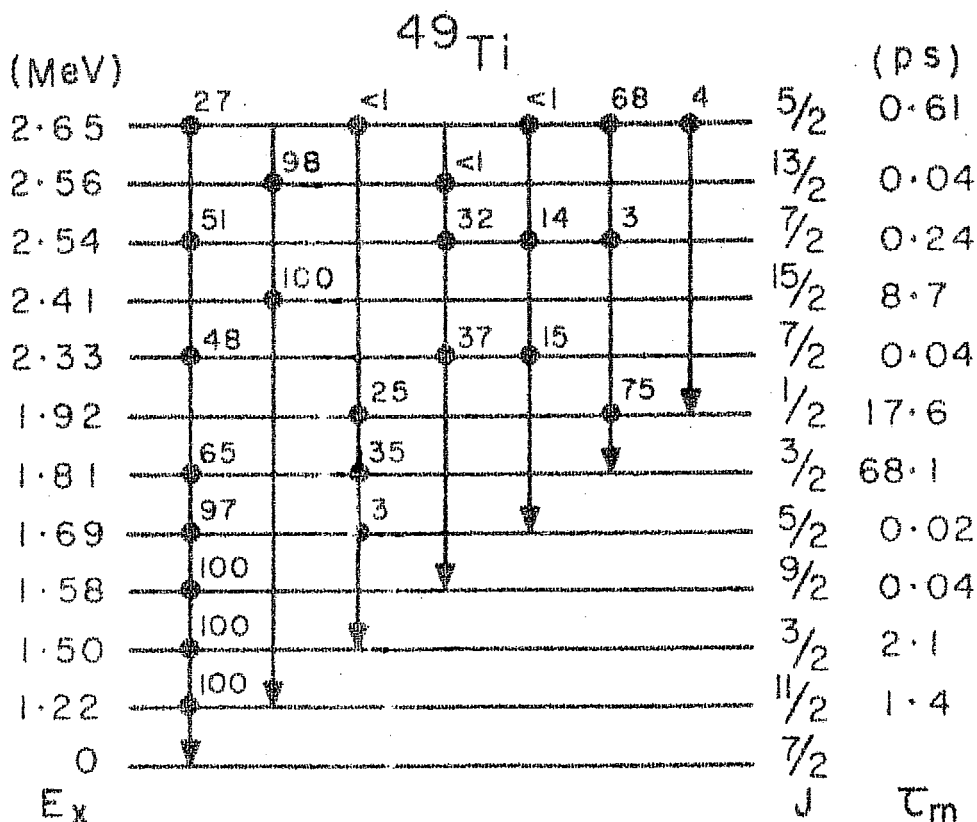


Fig.20

The calculated mean lifetimes and branching ratios for the transitions between the low-lying states in ^{49}Ti . The vertical lines indicate the transitions originating from the state marked with a filled circle to the state where the arrow ends. The numbers on the top of the states are the decay intensities.

while for the $5/2_2 \rightarrow 7/2_3$ decay only $B(M1)$ value is large.

Table 41

Calculated $B(E2)$, $B(M1)$ and $(E2/M1)$ mixing ratios for the transitions within the $K=1/2$ band of states in ^{49}Ti .

$2J_i$	$2J_f$	$B(E2)$ $e^2_{fm}{}^4$	$B(M1)$ (n.m.) 2	$E2/M1$
1_1	3_2	291	0.93	+0.0004
7_3	3_2	174		
5_2	3_2	44	0.08	-0.19
	1_1	152		
	7_3	25	0.75	+0.01
11_3	7_3	201		
9_3	7_3	14	0.05	-0.22
	5_2	206		
15_4	11_3	208		

The members of this $K=1/2$ calculated band have hindered $B(E2)$ and $B(M1)$ values for transitions to the members of the 'ground state band' and to other low-lying states. In table 42 are displayed these values. The dotted line separates $B(E2)$, $B(M1)$ values of the transitions from some of the members of the $K=1/2$ band to those of the 'ground state band' (above the dotted line) from those from the $J=7/2$ state calculated at 2.33 MeV.

Table 42

Calculated $B(E2)$ and $B(M1)$ values for the transitions from some of the members of the $K=1/2$ band to the members of the ground state band in ^{49}Ti . Similar values for transitions from the $J=7/2$ state calculated at 2.33 MeV are given below the dotted line.

$2J_i$	$2J_f$	$B(E2)$ $e^2_{\text{fm}}^4$	$B(M1)$ $(\text{n.m.})^2$
3_2	7_1	0.79	
	3_1	7.03	0.03
	5_1	0.71	0.06
1_1	3_1	7.5	0.02
	5_1	0.58	
7_3	7_1	0.46	0.008
	9_1	0.002	0.12
	5_1	3.6	0.28
	7_2	11.3	0.009
5_2	7_2	0.00009	0.002
	3_1	0.44	0.0001
	5_1	0.22	0.0004
<hr/>			
7_2	7_1	20.3	0.05
	11_1	1.20	
	9_1	0.92	1.99
	3_1	3.86	
	5_1	67.22	1.71

It is thus likely that the members of the calculated $K=1/2$ band may be identified on the basis of these hindered decays. In fig.20 are given the calculated branching intensities and the mean lifetimes between some of the low-lying states of ^{49}Ti upto 2.65 MeV. The observed²²⁾ mixing ratio of +0.053 for the $1/2$ (1.92 MeV) \rightarrow $3/2$ (1.50 MeV) is in good agreement with the calculated value of +0.055 for this transition.

The observed^{14,15)} and our calculated ground state static moments of ^{49}Ti are:

$$\begin{aligned} Q \text{ (efm}^2\text{)} & : \text{calc.} = 26, \quad \text{expt.} = 24 \\ \mu \text{ (n.m.)} & : \text{calc.} = -1.03, \text{expt.} = -1.10 \end{aligned}$$

The intermediate-coupling-model calculations of Abecasis et al¹⁸⁾ give the corresponding values of $14e \text{ fm}^2$ and -0.95 n.m. In this calculation the effective charges $e_p = 2e$ and $e_n = 0.5e$ and the spin gyromagnetic ratios $0.6 g_s(\text{free})$ and $0.5 g_s(\text{free})$ for the proton and neutron respectively were found to give optimum agreement with the experimental values.

To summarize, the present study of ^{49}Ti has been quite successful in reproducing the experimental spectrum upto about 3 MeV and also the available data on electromagnetic properties. It is hoped that this study would

motivate interest in the identification of the high spin states and the members of the $K=1/2$ band and also the study of electromagnetic properties in ^{49}Ti .

REFERENCES

1. S. Raman, Nucl. Data Sheets B4 (1970) 397.
2. D.C. Kocher and W. Haerberli, Nucl. Phys. A196 (1972) 225.
3. A.E. Ball, G. Brown and A. Denning, Nucl. Phys. A183 (1972) 472.
4. J.L. Yntema, Phys. Rev. 131 (1963) 811.
5. J.L. Alty, L.L. Green, G.D. Jones and J.F. Sharpey-schafer, Nucl. Phys. A100 (1967) 191.
6. P.P. Barnes, J.R. Comfort, C.K. Bockelman, O. Hansen and A. Sperduto, Phys. Rev. 159 (1967) 920.
7. J.H. Bjerregaard, P.F. Dahl, O. Hansen, G. Sidenius, Nucl. Phys. 51 (1964) 641.
8. P. Wilhjel'm, O. Hansen, J.R. Comfort, C.K. Bockelman, P.D. Barnes and A. Sperduto, Phys. Rev. 166 (1968) 1121.
9. P.J. Plauger and E. Kashy, Nucl. Phys. A152 (1970) 609.
10. P. Fettweis and M. Saidane, Nucl. Phys. A139 (1969) 113.
11. S.A. Anderson, O. Hansen, L. Vistisen, R. Chapman, S. Hinds, Nucl. Phys. A125 (1969) 65.
12. J. Lecuyer, C.St-Pierre, Nucl. Phys. A100 (1967) 401.
13. H.F. Lutz and T.S. Bohn, Nucl. Phys. A116 (1968) 112.
14. G.H. Fuller and V.W. Cohen, Nucl. Data Tables A5 (1969) 433.

15. V.S. Shirley, Tables of Nuclear Moments in Hyperfine Interactions in Excited Nuclei, edited by G. Goldring and R. Kalish (Gordon and Beach Science Publishers, Inc., New York, 1971) P.1255.
16. J.D. McCullen, B.F. Bayman and L. Zamick, Phys. Rev. 134 (1964) B515.
17. F.B. Malik and W. Scholz, Phys. Rev. 150 (1966) 919.
18. S.M. Abecasis, C.A. Heras and F. Krmpotic, Phys. Rev. C11 (1975) 1015.
19. A.K. Dhar and K.H. Bhatt, Nucl. Phys. and Solid State Physics (India) 18B (1975).
20. A.K. Dhar and K.H. Bhatt, Sent to Nuclear Physics.
21. A.K. Dhar, D.R. Kulkarni and K.H. Bhatt, Nucl. Phys. A238 (1975) 740.
22. J. Honzatko, J. Kajfosz and J. Kopecky, Czech. J. Phys. 18B (1968) 34.
23. O.F. Afonin, A.P. Grinberg, I.Kh.Lemberg and I.N. Chugunov, Sov. Jou. Nucl. Phys. 6 (1968) 160.

CHAPTER 6

THE NUCLEUS ^{51}Ti

1. INTRODUCTION

1.1 Experimental Data

Experimental data on ^{51}Ti is, in general, sparse. Arnell et al.²⁾ populated the high-spin states of this nucleus in $^{48}\text{Ca}(\alpha, n) ^{51}\text{Ti}$ reaction. Some of the low-spin states upto about 5 MeV excitation have been observed³⁻⁵⁾ in (d,p) and in the vector-polarized (d,p) reactions⁶⁾ studied at 6 and 10 MeV respectively. Glover et al.⁷⁾ performed $^{49}\text{Ti}(t, p)$ reaction at $E_t=12$ MeV, for the study of the low-lying states in ^{51}Ti .

1.2 Previous Calculations

The nucleus ^{51}Ti has been of considerable⁸⁻¹³⁾ theoretical interest. Regarding ^{48}Ca as the closed core, shell model calculations have been performed with different choices of the effective interactions. Qualitative agreement with the experiment was obtained. Considering ^{48}Ca as the core the structure of ^{51}Ti has also been studied by Divadeenam and Beres¹²⁾ in terms of: i) single neutron states, ii) 2p-1h neutron states and iii) excited ^{50}Ti core plus neutron states. Larner¹³⁾ performed the intermediate coupling model calculations for ^{51}Ti and calculated the spectrum and $B(E2)$

values for the transitions from some of the low-lying states to the ground state.

2. PRESENT CALCULATIONS

It is already mentioned in chapter 1 that although the chosen MWH2 effective interaction reproduced very well the shell closure for nuclei with $N, Z=28$, it does not reproduce¹⁴⁾ the single particle or hole energies relative to ^{56}Ni core. Thus MWH2 interaction is somewhat inconsistent near the region with Z or $N \geq 28$. In view of this, our present DCM calculations for ^{51}Ti are not as extensive as for other odd isotopes of Ti.

2.1 CALCULATION OF ENERGY SPECTRUM

2.1.1 Generation of Intrinsic States

For the nucleus ^{51}Ti , the MWH2 effective interaction leads to near degeneracy of the prolate $K=1/2$ and oblate $K=3/2$ HF intrinsic states, with energy $E_K \simeq -16.77$ MeV. The corresponding quadrupole moments are $15.16 b^2$ and $-12.61 b^2$ for the prolate and oblate HF states respectively. Because of the small energy 'gaps' at the neutron fermi surface, the oblate solution of ^{51}Ti did not converge in the usual iterative procedure. The above $K=3/2$ oblate HF state was thus obtained by specific choice of the k -values

Table 43

Structural and spectral details of the occupied and a few unoccupied proton and neutron orbitals of the PROLATE $K=1/2$ HF intrinsic state of ^{51}Ti . The energy and quadrupole moments of this HF intrinsic state is -16.77 MeV and 15.16 b² respectively. For other details see caption for table 1.

	k	e_k (MeV)	q_k (b ²)	$c_{\frac{1}{2}k}$	$c_{\frac{3}{2}k}$	$c_{\frac{5}{2}k}$	$c_{\frac{7}{2}k}$
P R O T O N S	1/2	-8.66	3.77	0.118	-0.259	-0.125	0.950
	-1/2	-8.64	3.86	0.127	-0.271	0.141	0.944
	3/2	-7.45	1.86		-0.095	-0.126	0.987
	-3/2	-7.18	1.87		-0.101	0.119	0.988
	5/2	-6.10	-0.31			-0.059	0.998
N E U T R O N S	1/2	-4.98	3.69	0.114	-0.247	-0.116	0.955
	-1/2	-5.11	3.87	-0.142	-0.261	0.177	0.938
	3/2	-3.30	1.69		-0.076	-0.069	0.995
	-3/2	-3.12	1.83		-0.098	0.105	0.990
	5/2	-1.82	-0.35			-0.038	0.999
	-5/2	-1.97	-0.35			0.040	0.999
	7/2	-1.02	-3.0				1.0
	-7/2	-1.07	-3.0				1.0
	1/2	1.74	3.14	-0.455	0.752	0.375	0.295
	-1/2	1.06	2.83	0.492	0.748	-0.290	0.337
	3/2	3.39	-1.85		0.992	0.098	0.082
	1/2'	3.43	0.61	0.590	0.611	-0.527	0.024

Table 44

Structural and spectral details of the occupied and a few unoccupied proton and neutron orbitals of the OBLATE $K=3/2$ HF intrinsic state of ^{51}Ti . The energy and quadrupole moments of this HF intrinsic state is -16.66 MeV and -12.61 b^2 . For other details see caption for table 1.

	k	e_k (MeV)	q_k (b^2)	$c_{\frac{1}{2}k}$	$c_{\frac{3}{2}k}$	$c_{\frac{5}{2}k}$	$c_{\frac{7}{2}k}$
P R O T O N S	7/2	-8.58	-3.0				1.0
	-7/2	-8.19	-3.0				1.0
	5/2	-6.88	-0.86			0.177	0.984
	-5/2	-6.63	-0.95			-0.212	0.977
	3/2	-6.13	0.12		0.243	0.028	0.970
N E U T R O N S	7/2	-4.50	-3.0				1.0
	-7/2	-4.87	-3.0				1.0
	5/2	-2.58	-0.89			0.187	0.982
	-5/2	-2.88	-0.77			-0.144	0.986
	3/2	-1.77	0.32		0.199	0.046	0.979
	-3/2	-2.03	0.21		0.232	-0.001	0.973
	1/2	-1.60	0.88	0.105	0.203	0.043	0.973
	-1/2	-1.63	0.95	-0.085	0.202	-0.002	0.976
	3/2	2.36	-1.30		0.970	-0.148	-0.190
	-3/2	1.87	-1.11		0.962	0.146	-0.229
	1/2	1.97	-1.21	0.747	0.615	0.130	-0.215
	5/2	3.67	-2.11			0.982	-0.187
	1/2	4.31	2.86	-0.603	0.756	-0.241	-0.082

of the single particle orbits. Such features were also observed for the nucleus ^{49}Ti .

The structural and spectral details of the single particle states of the prolate and oblate HF states of ^{51}Ti are summarized in tables 43 and 44. Notice that in the prolate HF intrinsic state the $k=1/2$ orbital corresponding to the odd neutron has about 44% admixture of the fp shell states other than the $p_{3/2}$ state.

For the description of ^{51}Ti nucleus, we have included in the calculation additional three lowest 1p-1h excited intrinsic states. The details of these states are given in table 45.

Table 45

K-values and energies of the prolate and oblate HF states of ^{51}Ti and of the one particle-one hole excited intrinsic states included in the present calculation.

Shape	Hole k_i	Particle k_m	K	E_K (MeV)
Prolate	(HF STATE)		1/2	-16.77
	n 1/2	n 3/2	3/2	-15.13
	n -7/2	n -1/2	7/2	-15.06
Oblate	(HF STATE)		3/2	-16.66
	n 3/2	n 1/2	1/2	-16.25

It is clear from the table that the prolate $K=3/2$ intrinsic state at -15.13 MeV is obtained by the excitation of the odd neutron from the $k=1/2$ orbital to the unoccupied $k=3/2$ orbital. At only 40 keV from this $k=3/2$ unoccupied orbital is the orbit with $k=1/2$. Therefore the odd neutron excitation to this $k=1/2$ orbital would lead to an intrinsic $K=1/2$ state very close (at about 40 keV) to the $K=3/2$ intrinsic state at -15.13 MeV. However, in the present calculation we have not included this additional intrinsic state.

All the intrinsic state included in the present calculation have a dominant $T=7/2$ isospin.

2.1.2 Energy Spectrum of Projected States and their Non-orthogonality.

The states $\psi_{MK}^J(\eta)$ of definite angular momentum have been projected from the five intrinsic states of table 45. The energy spectrum of these states is displayed in fig.21. From these projected states, an orthogonalized set of basis states $\phi_M^J(\nu)$ is obtained by the procedure discussed in chapter 2.

It is seen that the overlaps of the states projected from the prolate $K=7/2$ 'hole' intrinsic state at -15.06 MeV with all the other corresponding projected states are small. The extent of the 'smallness' of these overlaps is

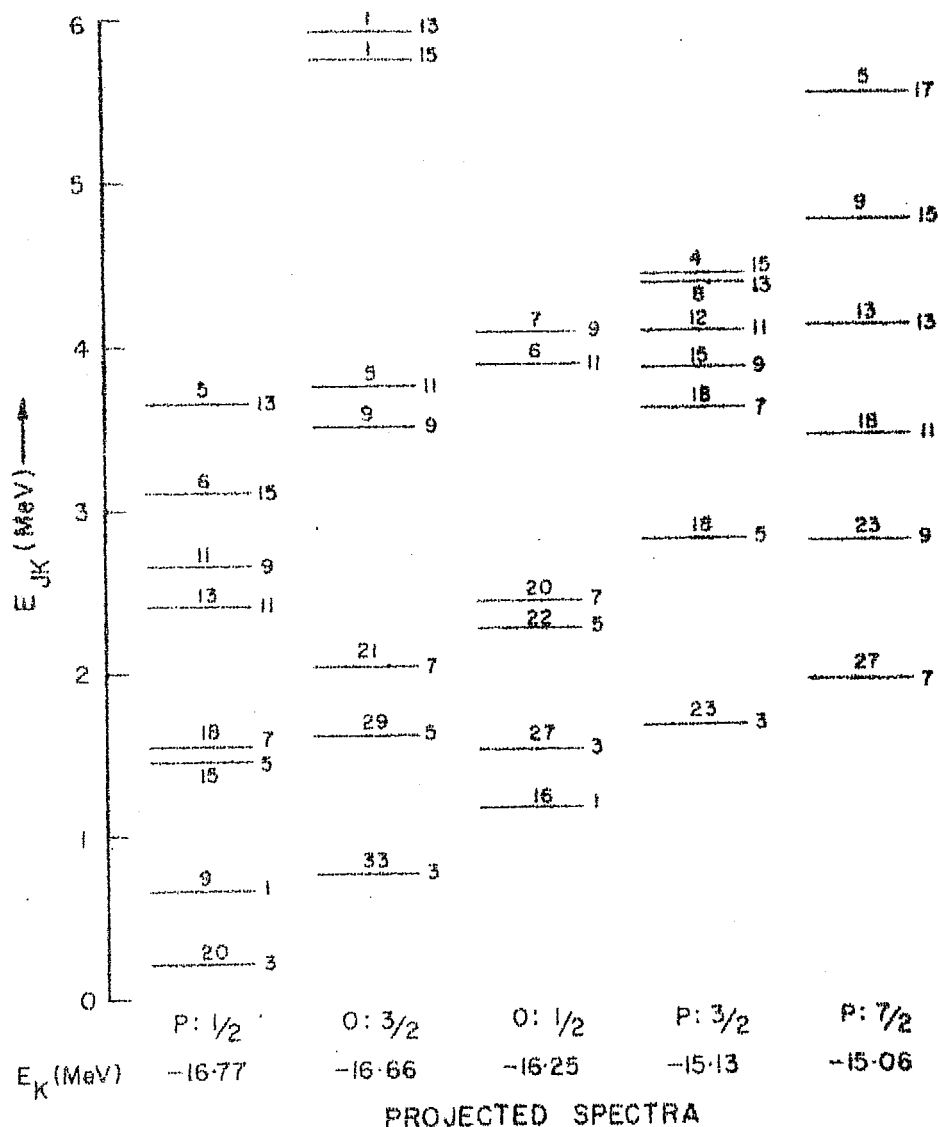
^{51}Ti


Fig.21

Energy spectra of the states with definite angular momentum projected from the prolate (P) and oblate (O) intrinsic states in ^{51}Ti . The K-values and energies of these intrinsic states are given at the bottom. For the projected states the numbers on the right are their 2J values while those on the top are their intensities in their intrinsic states.

Table 46

The overlap matrix of the $J=9/2$ states projected from the five intrinsic states $\chi_K(\eta)$ at energies $E_K(\eta)$ (in MeV) of ^{51}Ti . P and O refer to prolate and oblate shapes.

K	P $\frac{1}{2}$	O $\frac{3}{2}$	O $\frac{1}{2}$	P $\frac{3}{2}$	P $\frac{7}{2}$
E_K	-16.77	-16.66	-16.25	-15.13	-15.06
P $\frac{1}{2}$	1.0	-0.365	0.363	0.241	-0.004
O $\frac{3}{2}$		1.0	0.327	-0.662	0.003
O $\frac{1}{2}$			1.0	-0.284	-0.045
P $\frac{3}{2}$				1.0	0.007
P $\frac{7}{2}$					1.0

illustrated in column P:7/2 in table 46 for the $J=9/2$ state. It is therefore likely that there might exist in ^{51}Ti the band of states projected from this 'hole' $K=7/2$ intrinsic state, if the mixing due to Hamiltonian is weak.

The mutual overlaps between the states projected from the other intrinsic states of table 45 are, in general, large. However, for the states with $J=1/2, 3/2, 5/2$ and $7/2$ projected from the prolate and oblate HF states alone, these overlaps are larger.

2.2 COMPOSITE SPECTRUM AND COMPARISON WITH THE EXPERIMENT

The composite spectrum of ^{51}Ti has been obtained by

^{51}Ti

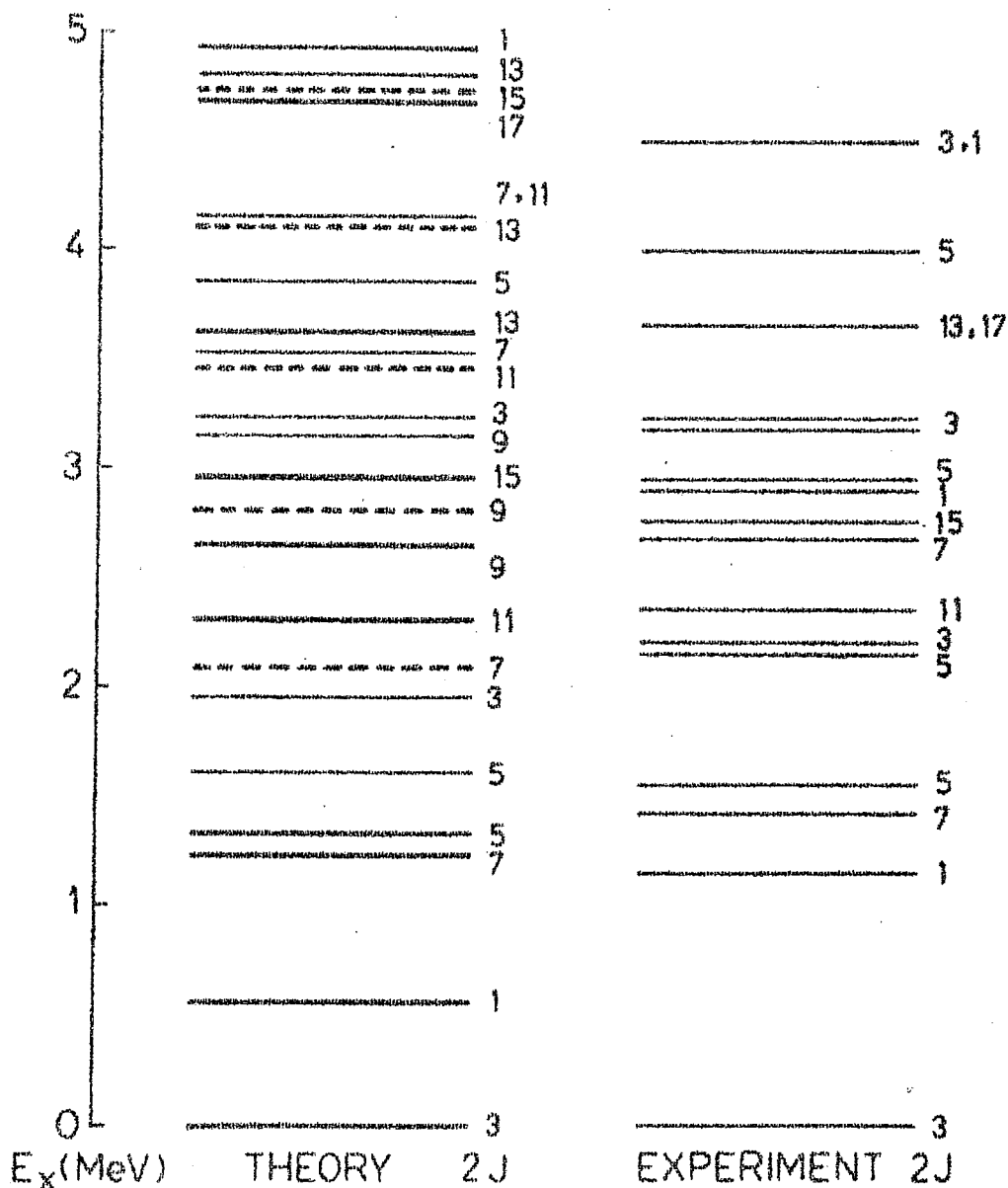


Fig. 22

Comparison of the calculated and observed spectrum of ^{51}Ti . In the theoretical spectrum, the states drawn in thick lines belong dominantly to the prolate HF $K=1/2$ intrinsic state. The ones in dotted lines are predominantly those projected from the prolate $K=7/2$ 'hole' intrinsic state. Other states have a complex structure.

diagonalizing the Hamiltonian in the basis of its orthonormalized states $\phi_M^J(\nu)$ constructed from the states of definite J projected from the five intrinsic states.

In fig.22 is compared¹⁵⁾ the experimental and the calculated spectrum of ^{51}Ti .

The agreement between the two is reasonable. There exist calculated counterpart with right sequence for almost all the observed states upto about 3 MeV excitation. These calculated states, however, are in general depressed compared to the experimental spectrum. The worst discrepancy occurs for the states with $J=1/2, 5/2$ and $7/2$ which are about 600 keV lower than the observed counterparts. The high spin states with $J=11/2, 13/2$ and $15/2$ are in very good agreement with their observed²⁾ energies. The $J=9/2$ and $17/2$ states at 2.65 and 4.67 MeV do not have observed counterparts. For the observed 3.64 MeV level with probable $J=(13/2, 17/2)$ our calculation favours a $J=13/2$ assignment.

2.3 BAND STRUCTURE

Inspite of the prolate-oblate near degeneracy and the tendency for $(f_{7/2})^8$ subshell closure, the set of states drawn in thick lines in fig.22 can to a large extent be regarded as the states projected from the prolate HF $K=1/2$

intrinsic state. The average 'band mixing' in all these states is about 5% except for the $J=5/2$ state at 1.32 MeV which has about 43% admixture of other states orthogonal to that projected from the $K=1/2$ HF intrinsic state.

The states indicated by thick dotted lines in fig.22 are the ones that are predominantly those projected from the prolate $K=7/2$ 'hole' intrinsic state. The average band mixing to these states is about 2%. We have identified our calculated $J=7/2$ band head of this $K=7/2$ band with the observed $J=7/2$ state at 2.67 MeV. This latter state has been strongly excited in (t,p) reaction⁷⁾ and has been found to have a dominant $(f_{7/2})^{-1} (p_{3/2})^2$ structure.

For other states no data is available. The observed $J=1/2$ state at 2.90 MeV does not have a calculated counterpart. It is expected that this state would be reproduced when the prolate $K=1/2$ intrinsic state which is only 40 keV higher than the $K=7/2$ 'hole' intrinsic state is included in the calculation.

2.4 ELECTROMAGNETIC PROPERTIES

No data is available on the electromagnetic properties of ^{51}Ti . We have calculated $B(E2)$, $B(M1)$, $(E2/M1)$ mixing ratios, lifetimes and branching ratios for the low-lying states of this nucleus. Effective charges $e_p=1.32e$ and e_n

$e_n = 0.89e$ are used. For M1 transitions values of free nucleon g -factors are used.

In table 47 are presented our DCM results on $B(E2)$, $B(M1)$ and $(E2/M1)$ mixing ratios for the transitions between the states drawn in thick lines in fig.22. These values are small compared to the similar transitions in the $^{45,47}\text{Ti}$ isotopes, and reflects the lack of collectivity for this nucleus. However, the $B(M1)$ values for the transition $1/2 \rightarrow 3/2$, $5/2 \rightarrow 3/2$ and $13/2 \rightarrow 15/2$ are large.

Table 47

Calculated electromagnetic properties of the states drawn in thick lines in fig.22 of ^{51}Ti . The suffixes for a J-value in cols.1 and 2 indicate the number of that J-state in ascending energy in fig.22.

$2J_i$	$2J_f$	$B(E2)$ $e^2 \text{fm}^4$	$B(M1)$ $(\text{n.m.})^2$	$E2/M1$
1_1	3_1	155	1.56	+0.09
7_1	3_1	106		
5_1	3_1	74	0.07	-0.43
	1_1	32		
	7_1	3	1.56	-0.003
11_1	7_1	126		
9_1	7_1	9	0.02	-0.21
	5_1	77		
15_1	11_1	101		
13_1	11_1	2.5	0.10	-0.05
	9_1	114		
	15_1	2.6	1.30	+0.01

In contrast to the transitions between members of the 'ground state band', the transitions between the members of the excited $K=7/2$ band predicted by our calculation are large. These are given in table 48. As shown in first half of table 49 these states have hindered $B(E2)$ and $B(M1)$ values for transitions to the members of the 'ground state band' and to other low-lying states. It is therefore likely that these members of the $K=7/2$ band may be identified by their hindered transitions.

Table 48

Calculated $B(E2)$ and $B(M1)$ values for the transitions between the members of the $K=7/2$ 'hole' band predicted to exist in the spectrum of ^{51}Ti

$2J_i$	$2J_f$	$B(E2)$ $e^2 \text{fm}^4$	$B(M1)$ $(n,m.)^2$
9_2	7_2	269	0.61
11_2	7_2	58	
	9_2	258	1.04
13_2	9_2	102	
	11_2	212	1.36
15_2	11_2	125	
	13_2	174	1.46

values

The $B(E2)$ and $B(M1)$ for transitions from the low-lying $J=5/2$ and $3/2$ states calculated at 1.59 and 1.94 MeV to the other states are given in the second half of table 49.

Table 49

Calculated $B(E2)$ and $B(M1)$ values for transitions from the states J_i to the states J_f in ^{51}Ti . The values for the transitions between the members of the 'ground state band' and the $K=7/2$ band are given in Part I of the table. Those from other low-lying states are listed in Part II of the table.

I				II			
$2J_i$	$2J_f$	$B(E2)$ $e^2_{\text{fm}}{}^4$	$B(M1)$ (n.m.) 2	$2J_i$	$2J_f$	$B(E2)$ $e^2_{\text{fm}}{}^4$	$B(M1)$ (n.m.) 2
7_2	3_1	0.61		5_2	3_1	2.76	0.01
	7_1	3.23	0.009		1_1	73	
	5_1	0.002	0.004		7_1	53	0.12
	5_2	0.101	0.002		5_1	43	0.96
9_2	7_1	0.56	0.004	3_2	3_1	20	0.13
	5_1	0.52			1_1	14	0.32
	5_2	1.36			7_1	2	
11_2	7_2	0.0008		5_1			
	9_1	0.28	0.02			30	2.45

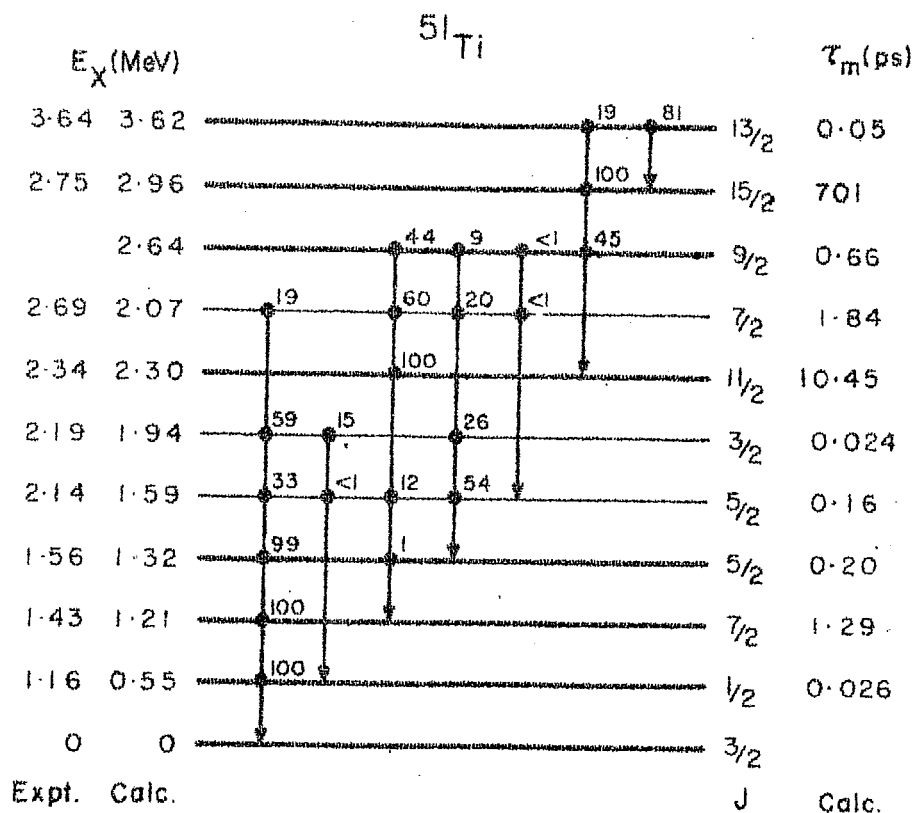


Fig.23

The calculated mean lifetimes and branching ratios for the transitions between the low-lying states in ^{51}Ti . The states drawn in thick line are those belonging dominantly to the prolate HF K=1/2 intrinsic state of ^{51}Ti . The numbers on the top of the states are the branching intensities for the transitions from a state marked with a filled circle to the state where the vertical arrow ends.

In fig.23 are given the branching intensities and the mean lifetimes of its some of low-lying states upto about 3 MeV in ^{51}Ti . We have associated our calculated states with the corresponding observed states to calculate these decay properties. The ground state moments are predicted to be $Q_{3/2} = -13.0 \text{ efm}^2$, $\mu_{3/2} = -1.11 \text{ (n.m.)}$

It would be interesting to undertake an experimental investigation of the decay properties of the low-lying states in this nucleus.

REFERENCES

1. M.N. Rao and J. Rapaport, Nucl.Data Sheets B3(1970) 37.
2. S.E. Arnell, C.G. Mattsson and O.Skeppstedt, Phys. Scrip. 6 (1972) 222.
3. J.H. Bjerregaard, P.F. Dahl, O. Hansen and L.G. Sidenius, Nucl.Phys. 51 (1964) 641.
4. P.D. Barnes, C.K. Bockelman, O. Hansen and A. Sperduto, Phys. Rev. 136 (1964) B438.
5. P. Wilhjelm, O.Hansen, J.R. Comfort, C.K. Bockelman, P.D. Barnes and A. Sperduto, Phys. Rev.166 (1968) 1121.
6. D.C. Kocher and W. Haeberli, Nucl. Phys. A196 (1972) 225.
7. R.N. Glover, A. Denning and G. Brown, Phys. Lett.27B (1968) 434.
8. J.R. Maxwell and W.C. Parkinson, Phys. Rev. 135 (1964) B82.
9. H. Chnuma, Nucl. Phys. 88 (1966) 273.
10. J. Vervier, Nucl. Phys. 78 (1966) 497.
11. H. Horie and K. Ogawa, Proc. Theo.Phys.46 (1971) 439.
12. M. Divadeenam and W.P. Beres, Phys. Lett. 30B (1969)598.
13. D. Larner, Phys. Rev.C2 (1970) 522.
14. A.K. Dhar and K.H. Bhatt, Proceedings of the International Topical Conference on Effective Interactions and Operators, Tucson, ed.by. B.R. Barrett, Vol.1,p.8 (1975).
15. A.K. Dhar, D.R. Kulkarni and K.H. Bhatt, Nucl.Phys. and Solid State Phys. 16B (1973) 146.

PART IV

VANADIUM ISOTOPES

Chapter 7: STRUCTURE OF ^{47}V

Chapter 8: STRUCTURE OF ^{48}V

Chapter 9: STRUCTURE OF ^{49}V

Chapter 10: STRUCTURE OF ^{51}V

INDEX

VANADIUM ISOTOPES

SECTION HEADINGS		Page Nos.			
CHAPTERS		7	8	9	10
1.	INTRODUCTION	221	240	266	295
1.1	Experimental Data	221	240	266	295
1.2	Previous Calculations	221	242	267	296
2.	PRESENT CALCULATIONS	222	243	268	299
2.1	Calculation of Energy Spectrum	222	243	268	300
2.2	Comparison of the Calculated and Experimental Spectrum	228	248	273	305
2.3	Band Structure	231	250	275	308
2.4	Electromagnetic Properties	231	252	276	308
2.5	Negative Parity States		259		
	REFERENCES	238	264	292	315

STRUCTURE OF VANADIUM ISOTOPES

In this part we shall discuss the spectrum and electromagnetic properties of the nuclei $^{47,48,49,51}\text{V}$. Lot of experimental data both on high-spin states and decay properties in these nuclei has become available very recently through the advent of heavy-ion reactions.

We have performed DCM calculations for these isotopes of vanadium, using the same effective interaction as for the study of titanium isotopes. We shall present for each of these nuclei our DCM results in comparison with the experiment and other calculated results.

For the E2 transitions, effective charges $e_p = 1.25e$, $e_n = 0.47e$ and $e_p = 1.32e$, $e_n = 0.89e$ are used. The former charges were obtained recently by Kuo and Osnes in a microscopic calculation for some of the fp shell nuclei. For the study of M1 transitions, free nucleon g-factors are used.

CHAPTER 7

THE NUCLEUS ^{47}V

1. INTRODUCTION

1.1 Experimental Data

The level structure of ^{47}V has been investigated by a variety of experiments¹⁻¹⁶⁾ involving the reactions $^{46}\text{Ti}(^3\text{He}, d)$, $^{46}\text{Ti}(d, n)$, $^{46}\text{Ti}(p, n)$, $^{46}\text{Ti}(p, \gamma)$, $^{46}\text{Ti}(p, n\gamma)$, $^{50}\text{Cr}(p, \alpha)$, $^{40}\text{Ca}(^{12}\text{B}, 2pn)$ and $^{31}\text{P}(^{19}\text{F}, p2n)$. The ground state spin and parity $3/2^-$ has been identified by Rosner and Pullen⁶⁾ in stripping reaction and by Redi and Graber⁸⁾ by atomic-beam technique. The first $5/2^-$ and $7/2^-$ states of this nucleus occur at 88 and 148 keV respectively.

1.2 Previous Calculations

The nucleus ^{47}V , like ^{45}Ti , provides an example of the failure of the $(f_{7/2})^n$ configuration model¹⁷⁾ calculation, according to which the first $J=3/2^-$ state in ^{47}V occurs¹⁸⁾ at about 0.75 MeV. In fact the $(f_{7/2})^7$ shell model calculation fails to explain even the broad features of ^{47}V level scheme. The $J=15/2^-$ level in ^{47}V , observed by Blasi et al¹⁵⁾ at 2.615 MeV does not occur in this pure shell model calculation upto about 3.5 MeV.

In the RPC model calculation of Malik and Scholz¹⁹⁾ intrinsic states corresponding to either strong negative ($\beta \approx -0.4$) or strong positive ($\beta > 0.5$) deformations were required to reproduce reasonably the ground state triplet in ^{47}V . In the recent RPC calculations²⁰⁾ in which j^2 terms have been treated slightly more carefully, intrinsic states with $\beta \approx 0.22$ have been found to give qualitative agreement with the experimental spectrum of ^{47}V .

2. PRESENT CALCULATIONS

We shall first present the details²¹⁾ of the spectrum of low-lying states in ^{47}V and then proceed to the study of electromagnetic properties of these states. We have also identified on the basis of decay properties, the calculated states that can be regarded as the counterparts of the observed states. MWH2 effective interaction and ^{41}Ca single-particle energies are used in the calculations.

2.1 THE CALCULATION OF THE ENERGY SPECTRUM

2.1.1 Intrinsic States

2.1.1.1 Hartree-Fock Intrinsic States

Axially symmetric prolate and oblate HF intrinsic states of ^{47}V have been obtained in the $(fp)^7$ configuration

Table 50

Structural and spectral details of the occupied and some of the lowest unoccupied proton and neutron orbitals of the PROLATE $K=3/2$ HF state of ^{47}V ($E_{\text{HF}} = -19.30$ MeV, $Q_{\text{HF}} = 24.92$ b²) For other details see caption for table 1.

	k	e_k (MeV)	q_{k2} (b ²)	$c_{\frac{1}{2}k}$	$c_{\frac{3}{2}k}$	$c_{\frac{5}{2}k}$	$c_{\frac{7}{2}k}$
P R O T O N S	1/2	-7.48	4.35	0.146	-0.366	-0.127	0.910
	-1/2	-7.60	4.75	-0.199	-0.412	0.199	0.867
	3/2	-4.77	2.28		-0.184	-0.201	0.962
	-3/2	-5.27	2.30		-0.187	0.212	0.959
	5/2	-1.71	-0.26			-0.089	0.996
	1/2	-1.43	3.52	-0.512	0.502	0.591	0.367
N U C L E O N S	1/2	-7.09	4.52	0.172	-0.379	-0.176	0.892
	-1/2	-6.64	4.55	-0.178	-0.380	0.183	0.889
	3/2	-4.60	2.27		-0.181	-0.202	0.962
	-3/2	-3.87	2.21		-0.170	0.183	0.968
	5/2	-1.69	-0.24			-0.098	0.995
	-5/2	-1.30	-0.26			0.091	0.996
	1/2	-0.44	2.94	-0.496	0.585	0.470	0.437

Table 51

Structural and spectral details of the occupied and some of the lowest unoccupied proton and neutron orbitals of the OBLATE $K=5/2$ HF state of ^{47}V ($E_{\text{HF}} = -17.02$ MeV, $Q_{\text{HF}} = -15.05$ b²). For other details see caption for table 1.

	k	e_k (MeV)	q_k (b ²)	$c_{\frac{1}{2}k}$	$c_{\frac{3}{2}k}$	$c_{\frac{5}{2}k}$	$c_{\frac{7}{2}k}$
P R O T O N S	7/2	-6.18	-3.0				1.0
	-7/2	-6.55	-3.0				1.0
	5/2	-3.89	-1.02			0.232	0.973
	-5/2	-4.32	-1.00			-0.227	0.974
	3/2	-2.62	-0.24		0.291	0.170	0.942
	1/2	-1.62	0.51	0.069	0.281	0.055	0.956
N E U T R O N S	7/2	-5.99	-3.0				1.0
	-7/2	-5.55	-3.0				1.0
	5/2	-3.80	-0.98			0.221	0.975
	-5/2	-3.12	-1.05			-0.241	0.970
	3/2	-2.18	-0.04		0.257	0.121	0.959
	-3/2	-1.86	-0.16		0.285	-0.107	0.953
	1/2	-1.32	0.40	0.102	0.293	0.037	0.950

space. The prolate $K=3/2$ HF intrinsic state is lower ($E_K = -19.30$ MeV, $Q_K = 24.92$ b²) than the oblate $K=5/2$ intrinsic state ($E_K = -17.02$ MeV, $Q_K = -15.05$ b²) by about 2.3 MeV.

In tables 50 and 51 are presented the spectral and structural details of the occupied and a few lowest unoccupied proton and neutron orbitals of the prolate and oblate HF states of ⁴⁷V. It is seen from table 50 that the proton and neutron energy 'gaps' at the fermi surface are about 3.06 and 2.2 MeV respectively. It is therefore expected that the 1p-1h excited intrinsic states generated from the prolate HF state of ⁴⁷V would lie about 2-3 MeV above the HF state.

2.1.1.2 One Particle-One Hole Excited Intrinsic States

We have considered for the present calculation, intrinsic states upto about 4 MeV excitation relative to the prolate HF state. Six 1p-1h excited intrinsic states were found to lie within this chosen energy interval. The details of these are summarized in table 52 wherein for completeness we have also given the K-values and energies of the prolate and oblate HF intrinsic states.

Except for the intrinsic states with $K=1/2$ at -15.60 and -14.85 MeV, all other intrinsic states of table 52 have

Table 52

Energies and K-values of the prolate, oblate HF and 1p-1h excited intrinsic states of ^{47}V .

Shape	Hole k_1	Particle k_m	K	E_K (MeV)
Prolate	(HF STATE)		3/2	-19.30
	n -3/2	n -5/2	1/2	-16.96
	p -1/2	p -3/2	1/2	-16.78
	n 3/2	n 5/2	5/2	-16.64
	p 3/2	p 5/2	5/2	-16.49
	p 3/2	p 1/2	1/2	-15.60
	n -3/2	n -1/2	5/2	-15.30
	n 3/2	n 1/2	1/2	-14.85
Oblate	(HF STATE)		5/2	-17.01

dominant isospin $T=1/2$. The amplitude of isospin components with $T \geq 3/2$ in these intrinsic states is negligibly small. The above $K=1/2$ intrinsic state at -15.60 MeV is obtained by the excitation of the odd proton from the occupied $k=3/2$ orbit to the unoccupied $k=1/2$ orbit. Since there is no neutron occupying a similar $k=1/2$ orbit this $K=1/2$ intrinsic state is expected to have large admixture of isospin components with $T \geq 1/2$. For this reason we have included in our calculation the intrinsic states with $K=1/2$ and $5/2$ at -14.85 and -15.30 MeV, in which the neutrons are excited from the $k=\pm 3/2$ orbit to the $k=\pm 1/2$ orbital. It is hoped that the

linear combination of these states would yield the wave function that would have definite isospin.

2.1.1.3 Energy Spectra and Nonorthogonality of the Projected States

In figs.24 and 25 are plotted the energy spectra of the states of definite angular momenta J projected from the different intrinsic states of table 52. These are plotted according to the increasing energies of their intrinsic states. It is seen that none of the states projected from the intrinsic states other than the prolate $K=3/2$ HF state, lies below 3 MeV. It is therefore expected that the observed ground state band of ^{47}V would be reasonably well described by the states projected from the prolate $K=3/2$ HF state alone.

It may be noticed from fig.24, col.1 ($P:3/2$) that the states with $J=3/2-5/2-7/2$ projected from the prolate $K=3/2$ intrinsic state are already in reasonable agreement with the observed ground state triplet of states in ^{47}V . It may be pointed out that our prolate HF intrinsic state of ^{47}V corresponds to deformation $\beta \sim 0.17$. In the RPC calculation of Haas et al²⁰⁾ intrinsic states corresponding to $\beta \sim 0.22$ were considered for the calculations. In contrast, in the RPC calculations of Malik and Scholz¹⁹⁾ intrinsic states

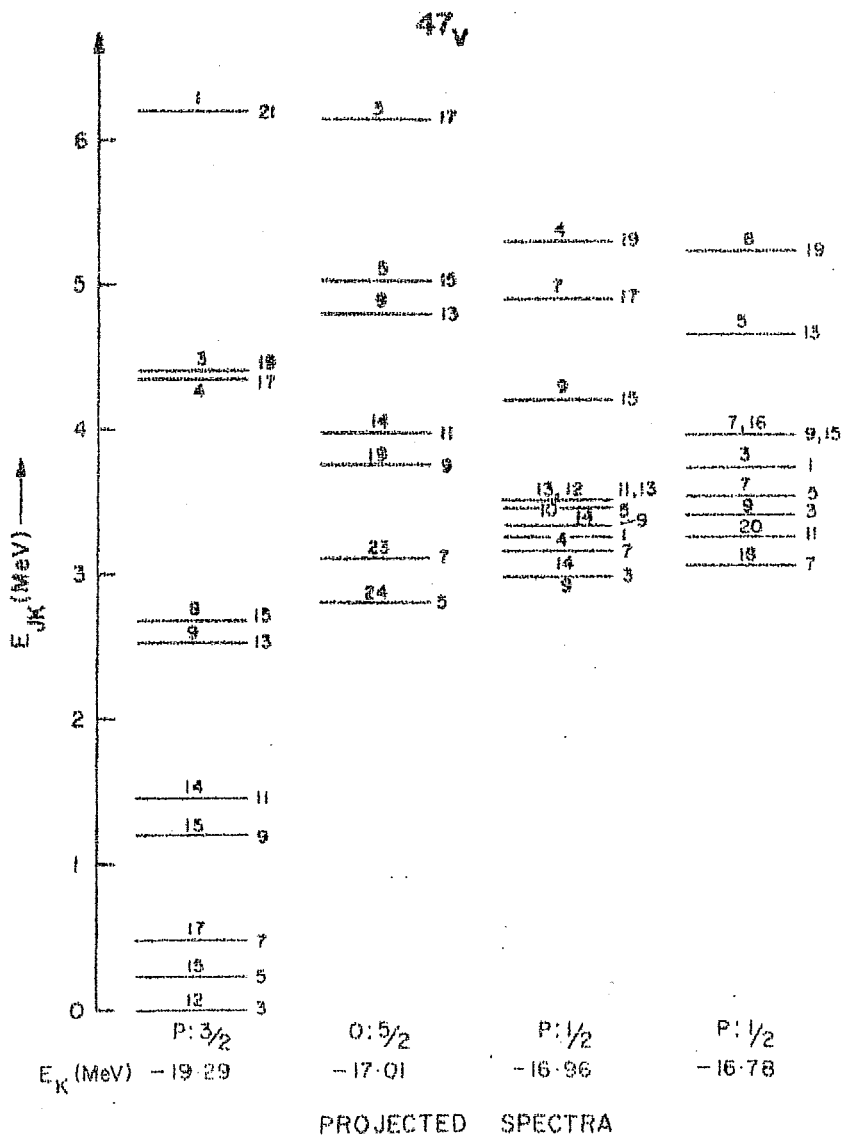


Fig.24

Energy spectrum of the states projected from the prolate (P) and oblate (O) intrinsic states of ^{47}V . The energies and K-values of these intrinsic states are given at the bottom. The numbers on the right of the projected states are their $2J$ values while those on the top are their intensities in their intrinsic states.

Energy level diagram for the $^{100}\text{Mo}(^{100})\text{Mo}$ reaction. The vertical axis is labeled E_K (MeV) and ranges from 3 to 6. The horizontal axis represents different states. The diagram shows several energy levels with their corresponding spin and parity (P) values. The levels are labeled with numbers 1 through 15. The P values are: $1/2$, $5/2$, $5/2$, $1/2$, $1/2$, $1/2$, $1/2$, $1/2$, $1/2$, $1/2$, $1/2$, $1/2$, $1/2$, $1/2$, $1/2$. The levels are arranged in a way that shows the progression of energy levels for different states.

PROJECTED SPECTRA

五子學

The energy spectrum of the states projected from the prolate (P) intrinsic states of ^{47}Ti . These spectra are plotted relative to the energies of the states in fig.24. For other details see caption of fig.24.

with large deformation $\beta > 0.5$ were found necessary to reproduce this triplet of states.

The overlaps $N_{K\gamma}^J, K'\gamma'$ (eq.(35)) of the states of definite angular momentum projected from the different intrinsic states are, in general, not large enough to lead to an overcomplete basis, nor are they so small as to result in a set of excited states that would belong predominantly to a definite intrinsic state.

The composite spectrum of ^{47}V is finally obtained by diagonalizing the Hamiltonian matrix in the basis of projected states after taking care of their nonorthogonality.

2.2 COMPARISON OF THE CALCULATED AND OBSERVED SPECTRUM

In fig.26 the DCM calculated spectrum of ^{47}V is compared with its observed spectrum. The correspondences that exist between the observed and calculated spectra are:

(i) The calculated Yrast band of states, drawn in thick lines in fig.26 is in good agreement with the observed¹⁵⁾ band upto $J=15/2^-$ at 2.61 MeV. However, the calculated $J=13/2^-$ state at 2.22 MeV does not have an experimental counterpart. It is indeed surprising that this state is not observed in the heavy-ion reaction of Blasi et al¹⁵⁾, although a higher $J=15/2^-$ member of the band is populated.

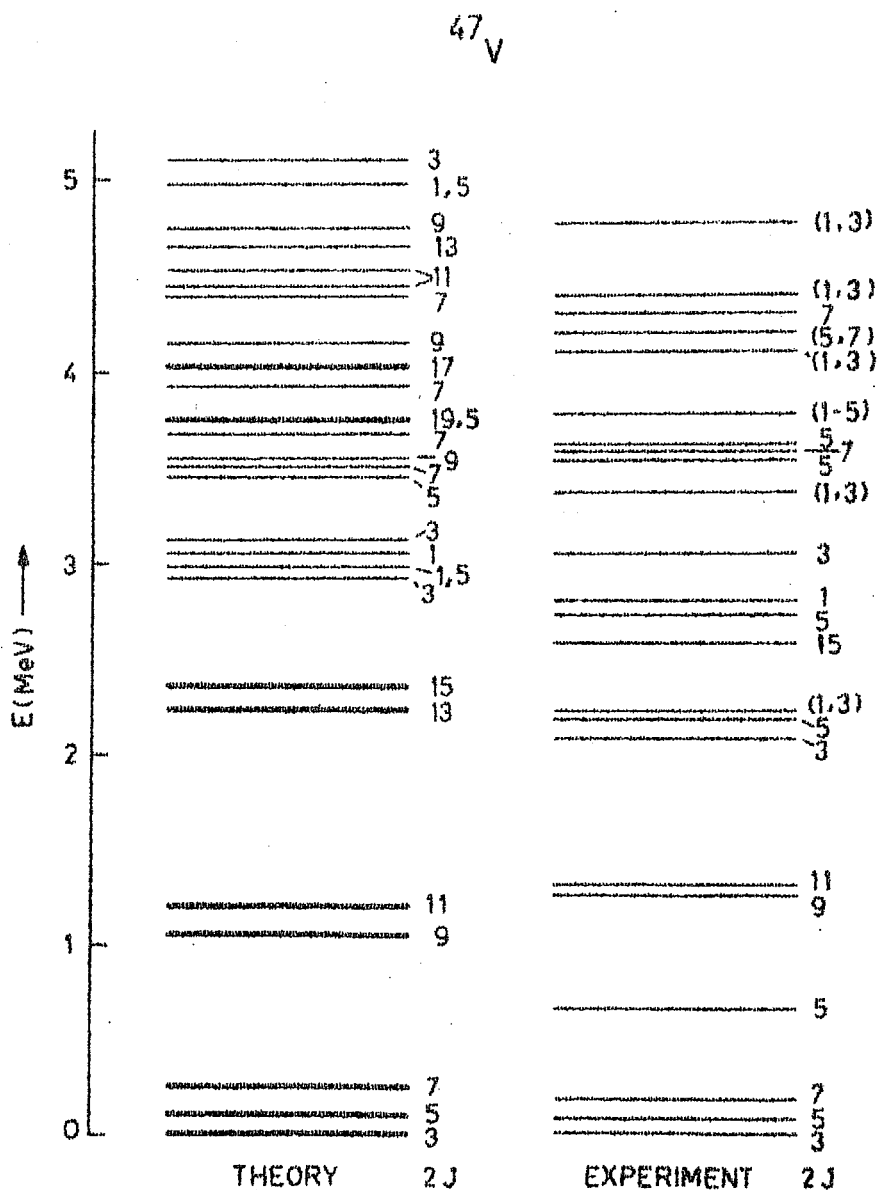


Fig.26

Comparison of the theoretical and the experimental spectrum of ^{47}V . The states drawn in thick lines are the members of the ground state band.

The non-observation of this $J=13/2^-$ state perhaps implies that it might be occurring either very close to the $J=15/2^-$ state or above it. The $J=17/2$ and $19/2$ members of the band are predicted to occur at 4.02 and 3.76 MeV respectively.

(ii) In the experimental spectrum states with $J=5/2^-$ and $3/2^-$ occur¹²⁾ at 0.66 and 1.97 MeV. Our calculation does not reproduce these states. Also the RPC calculation of Haas et al²⁰⁾ fails to reproduce them. On the basis of the single particle energy gaps of the prolate and oblate HF states of ^{47}V , (see tables 50 and 51) we do not anticipate any intrinsic state that would give a $J=5/2^-$ state at 0.66 MeV. We feel that these state might be the 'intruder' states arising by p-h excitations from ^{40}Ca core. This is quite likely in view of the existence of a $J=3/2^+$ state at only 260 keV excitation in ^{47}V .

(iii) A triplet of states with $J=3/2^-$, $5/2^-$ and $(1/2^-$ or $3/2^-)$ is observed to exist at 2.083, 2.176 and 2.212 MeV. Decay properties of these states are studied by (p, γ) reaction. In the calculated spectrum we have a corresponding triplet of states with $J=3/2-5/2-1/2$ at 2.92, 2.98 and 2.99 MeV respectively. We shall later show that the decay properties of these calculated $J=1/2$ and $3/2$ states are in good agreement with those measured for the corresponding observed states. However, the calculated $J=5/2$ state at 2.98 MeV does

not have decay properties similar to that observed for the observed state at 2.176 MeV. Thus we do not have a corresponding calculated state for the $J=5/2^-$ state at 2.176 MeV. The RPC calculation²⁰⁾ also does not reproduce this $J=5/2^-$ state in ^{47}V .

It thus appears that the calculated $J=1/2$ and $3/2$ members of this triplet occur about 800 keV higher than the experimental one. It may be recalled that in ^{45}Ti also we suggested the existence of an excited triplet, which is also found to be about 800 keV higher than its two likely observed members.

(iv) In the present calculated spectrum, the third $J=5/2$ state occurs at 3.45 MeV. The observed one occurs at 2.72 MeV.

(v) The calculated $J=1/2$ and $3/2$ state at 3.06 and 3.13 MeV agree well with those observed at 2.77 and 3.06 MeV.

(vi) Beyond 3 MeV excitation, there occur many low-spin states in the observed spectrum which do not have calculated counterparts. As is seen from table 52, in the present DCM calculation only four $J=1/2$ and five $J=3/2$ states that can be projected from $K=1/2$ and $3/2$ intrinsic states are included. Thus the present DCM calculation is not expected to provide a description of the low-spin states

observed above 3 MeV. It is however likely that by expanding the configuration space to include other p-h excited $K=1/2$ and $3/2$ intrinsic states a good description of $J=1/2$ and $3/2$ states too may be obtained. Such a feature is well demonstrated by our calculation²²⁾ for the description of only $J=1/2$ and $3/2$ states in ^{47}Ti .

The other higher-spin states predicted by our calculations above 3 MeV are not yet observed.

2.3 BAND STRUCTURE

The states of the composite spectrum have been analysed for the possible band structures. The Yrast band of states, with $J=3/2$ upthrough $19/2$, plotted in thick lines, is found to be belonging dominantly to the prolate $K=3/2$ HF intrinsic state. The average 'band mixing' in these states is only about 6%. The other states have a complex structure.

2.4 ELECTROMAGNETIC PROPERTIES

The electromagnetic properties of the low-lying states of ^{47}V have been studied by the heavy-ion reactions ^{40}Ca (^{10}B , 2pn) at 25 MeV by Elasi et al¹⁵⁾ and ^{31}P (^{19}F , p2n) at 47 MeV by Toulmonde et al¹⁶⁾ by (p, γ) reaction of Willmes¹¹⁾ and Albinsson and Dubois⁹⁾ by (p, n γ) reaction of Schulz and Toulmonde¹³⁾ and Thompson et al¹⁴⁾. The data is available

on $B(E2)$, $B(M1)$, $(E2/M1)$ mixing ratios, lifetimes and branching ratios for the transitions mostly between the members of the ground state band.

We have calculated the electric properties of the low-lying states of ^{47}V using the Kuo-Osnes²³⁾ effective charges $e_p = 1.25e$, $e_n = 0.47e$ and the charges $e_p = 1.32e$, $e_n = 0.89e$. The magnetic properties are calculated by using free nucleon g -factors. We shall also present our DCM results in comparison with the RPC model and experimental results.

2.4.1 $B(E2)$, $B(M1)$ Values and $(E2/M1)$ Mixing Ratios

These are presented respectively in tables 53, 54 and 55 for the decays between the members of the ground state band. The calculated values do not agree with the observed values mainly because the observed values are, in general, very uncertain. This prevents any meaningful conclusions about the results of the present calculation.

It is seen that the $B(E2)$ values as obtained in RPC calculation are similar to our values calculated with Kuo-Osnes charges. However, significant differences between DCM and RPC results occur for the $B(M1)$ and $(E2/M1)$ mixing ratios; more particularly for the transitions between the high-spin states of the ground state band.

Table 53

$B(E2, J_i \rightarrow J_f)$ values in $e^2 fm^4$ for the transitions within the ground state band of ^{47}V .

J_i	J_f	Expt ^a	DCM [*]	DCM ⁺	RPC ^b
5/2	3/2		342	198	253
7/2	3/2	> 25 312 \pm 121 ^d	147	86	110
	5/2		148	147	160
9/2	5/2	161 \pm 91 ^c	203	116	157
	7/2	141 \pm 81 ^c 907 \pm 504 ^c	124	70	96
11/2	7/2	200 $^{+100}_{-80}$	254	147	188
	9/2		112	67	
13/2	9/2		270	156	198
	11/2		62	34	47
15/2	11/2	> 110	278	160	210
	13/2		60	36	
17/2	13/2		275	161	
	15/2		35	19	
19/2	15/2		253	145	
	17/2		31	18	

* $e_p = 1.32e$, $e_n = 0.89e$

a. Ref.15

c. Ref.14

+ $e_p = 1.25e$, $e_n = 0.47e$

b. Ref.20

d. Ref.16

Table 54

$B(M1, J_i \rightarrow J_f)$ values in $(n.m.)^2$ for transitions between the members of the ground state band in ^{47}V .

J_i	J_f	Expt ^a	DCM	RPC ^c
5/2	3/2	> 0.084 0.07 ± 0.01	0.22	0.07
7/2	5/2	$> 0.29^b$ 0.45 ± 0.09	0.34	0.36
9/2	7/2	0.072 ± 0.039 0.0036 ± 0.002	0.26	0.09
11/2	9/2		0.66	
13/2	11/2		0.20	0.09
15/2	13/2		0.90	
17/2	15/2		0.14	
19/2	17/2		1.05	
a. Ref. 14.		b. Ref. 15.	c. Ref. 20	

Table 55

$(E2/M1)$ mixing ratios for the transitions within the ground state band of ^{47}V .

J_i	J_f	Expt	DCM	RPC
5/2	3/2	-0.10 ± 0.06	-0.02	-0.05
7/2	5/2		-0.01	-0.01
9/2	7/2	-0.41 ± 0.05 -4.7 ± 1.0	-0.15	-0.31
13/2	11/2		-0.10	-0.24
15/2	13/2		-0.02	
17/2	15/2		-0.14	

2.4.2 Branching Ratios and Lifetimes

In fig.27 are presented the experimental and calculated mean lifetimes and branching intensities for the transitions between the low-lying states in ^{47}V . We have associated the calculated states with the corresponding observed states for the calculation of these decay properties. First we shall concern ourselves with the ground state band indicated by thick lines in the figure and then the other states.

The agreement between theory and experiment for the ground state band upto $J=11/2$ at 1.29 MeV is good. However, the mean lifetime of the $J=5/2$ state observed at 88 keV is not well reproduced.

It however appears that this discrepancy might not be removed even by including other higher p-h excited intrinsic states in the calculation. Blasi et al¹⁵⁾ have observed a 100% decay of the $J=15/2^-$ state at 2.61 MeV to the $J=11/2$ state at 1.29 MeV. As already mentioned they have not observed any $J=13/2^-$ state below this $J=15/2^-$ state. Our calculation gives $J=13/2^-$ state at 2.22 MeV. Using the theoretical energy of this $J=13/2^-$ state, the $J=15/2^-$ state is found to decay with 52:48 percent branches to the $J=11/2$ and $13/2$ states at 1.29 and 2.22 MeV respectively, with a mean lifetime consistent with the measurements of

^{47}V

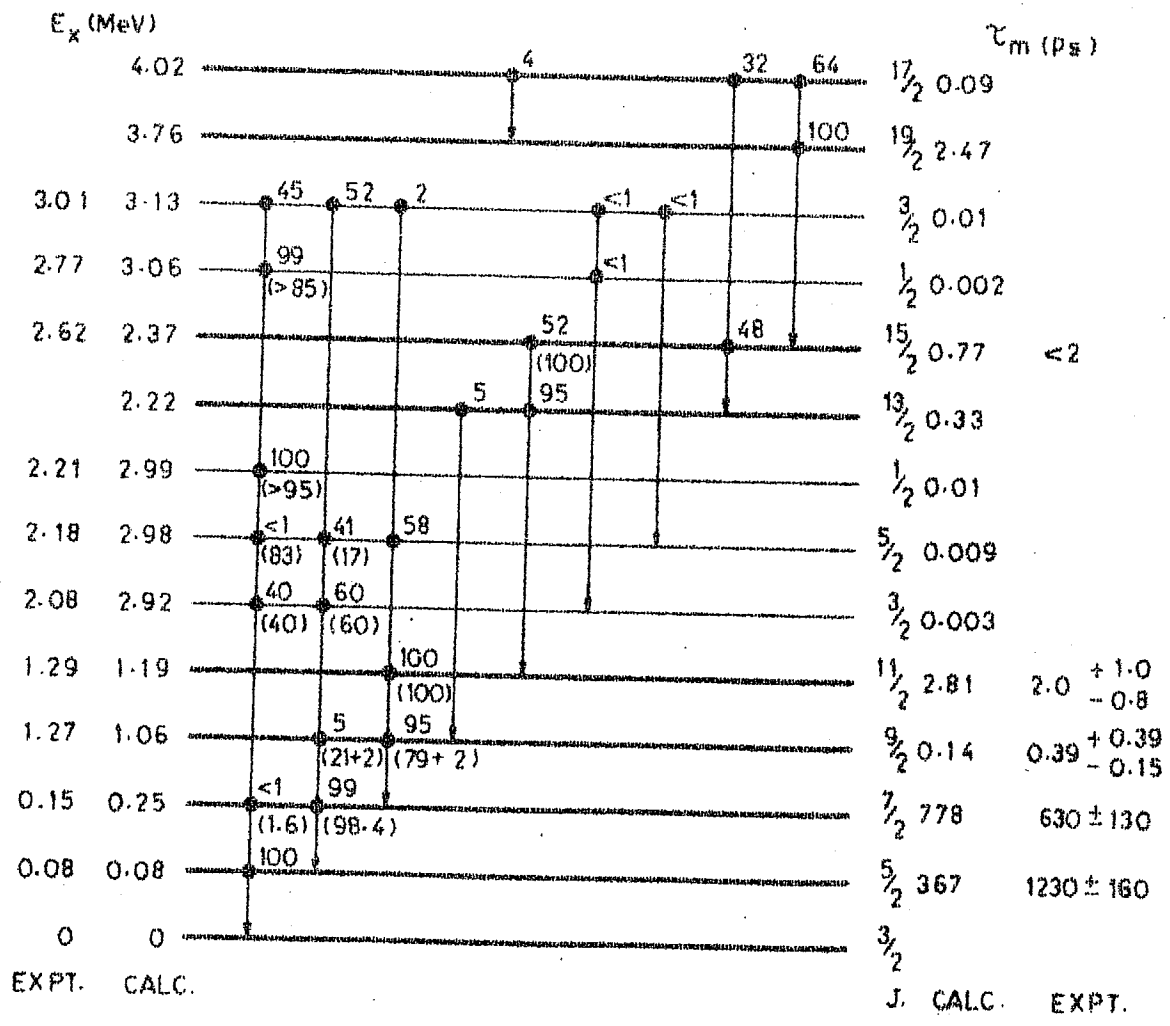


Fig.27

Comparison of the calculated and observed mean lifetimes and branching ratios in ^{47}V . The states drawn in thick lines are the members of the ground state band. The numbers in the parenthesis are the observed branching ratios while those on top are the corresponding calculated ones.

Blasi et al.¹⁵⁾. As already suggested, if in the experimental spectrum the $J=13/2^-$ state occurs above or in very close vicinity of the observed $J=15/2^-$ state, then our calculated $J=15/2^-$ state would decay by a 100% branch to the $J=11/2^-$ state at 1.29 MeV, in concurrence with the measurements of Blasi et al. The mean lifetime (1.5 ps) of the $J=15/2^-$ state would still be consistent with the observed¹⁵⁾ lifetime of less than 2 ps. It would be interesting to look for this missing $J=13/2^-$ states in ^{47}V .

Among the other states in fig.27, spins $3/2^-$; $5/2^-$, ($1/2^-$ or $3/2^-$) have been suggested for the levels observed at 2.08, 2.18 and 2.21 MeV. We have associated our triplet of states with $J=3/2^-$ - $5/2^-$ - $1/2^-$ at 2.92, 2.98 and 2.99 MeV with these observed levels. The corresponding branching intensities and lifetimes are given in figure 27. For the $J=3/2^-$ and $1/2^-$ states, the agreement is good, but for $J=5/2^-$, the decay pattern is entirely different from what is observed. Thus the association between the calculated and observed $J=5/2^-$ states is not favoured.

For the levels observed at 2.77 and 3.01 MeV, ($p,n\gamma$) reaction studies have led to definite spin assignments $1/2^-$ and $3/2^-$ respectively. The calculated branching ratio and mean lifetimes of these states when associated with our calculated $J=1/2^-$ and $3/2^-$ states at 3.06 and 3.13 MeV

respectively are given in fig.27. The branching ratio for the decay of the $J=1/2$ state agrees well with the observed value.

2.4.3 Static Moments

No experimental values are available either for the static electric quadrupole or the magnetic dipole moments in ^{47}V . In table 56, are compared the DCM calculated moments of the ground state triplet of ^{47}V , with those obtained in RPC model by Haas et al²⁰⁾ and Malik and Scholz¹⁹⁾. Inter-

Table 56

Static electric quadrupole and magnetic dipole moments of the ground state triplet of ^{47}V .

J	E_J keV	Q(efm ²)			μ (n.m.)		
		DCM*	RPC I ^a	RPC II ^b	DCM	RPC I ^a	RPC II ^b
3/2	0	16.75	17.4		2.12	2.96	
5/2	88	-7.77	-6.3		2.23	3.44	
7/2	146	-13.47	-16.9	10	2.90	4.82	4.71

* $e_p = 1.25e$, $e_n = 0.47e$. a. Ref.20 b. Ref.19.

esting discrepancy occurs for the sign of the quadrupole moment of the $J=7/2$ state as predicted by our calculation and that of Malik and Scholz. In general our static electric quadrupole moments are similar to those obtained by Haas et al, but the magnetic moments are slightly different.

REFERENCES

1. M.B. Lewis, Nucl. Data Sheets 4 (1970) 313.
2. W.E. Dorenbusch, J. Rapaport and T.A. Belote, Nucl. Phys. A102 (1967) 681.
3. C. St-Pierre, P.N. Maheshwari, D. Doutriaux and L. Lamar-
che, Nucl. Phys. A102 (1967) 433.
4. B. Cujec and I.M. Szoghy, Phys. Rev. 179 (1969) 1060.
5. V.V. Okorokov, V.M. Serezhin, V.A. Smotryaev,
D.L. Tolchenkov, I.S. Trostin, Yu.N. Cheblukov, V.S.
Zolotarev and V.S. Romanov, Sov. Jou. Nucl. Phys. 14 (1972)
275.
6. B. Rosner and D.J. Pullen, Phys. Rev. Lett. 18 (1967) 13;
Phys. Rev. 162 (1967) 1048.
7. G.J. McCallum, A.T.F. Ferguson and G.S. Mani, Nucl.
Phys. 17 (1960) 116.
8. O. Redi and M.A. Graber, Bull. Amer. Phys. Soc. 12 (1967) ,
474.
9. H. Albinsson and J. Dubois, Phys. Lett. 15 (1965) 260;
Ark. Fys. 34 (1967) 1.
10. G.J. McCallum and K.P. Pohl, Nucl. Phys. A157 (1970) 552.
11. H. Willmes, Phys. Rev. C1 (1970) 1972.
12. M. Schrader, K. Bucholz and H.V. Klapdor, Nucl. Phys.
A213 (1973) 173.
13. N. Schulz and M. Toulmonde, Nucl. Phys. A230 (1974) 401.

14. J.V. Thompson, R.A.I. Bell, L.E. Carlson and M.R.Najam, Aust.J.Phys.28 (1975) 251.
15. P. Blasi, T.Fazzini, A. Giannatiempo, R.B. Huber and C. Signorini, Il.Nuovo Cimento,15A (1973) 521.
16. M. Toulmonde, N. Schulz, J.C. Merdinger and P.Engelstein, Proc. Int. Conf.on Gamma-Ray Trans.Prob., Delhi, 1974, ed.S.C. Pancholi and S.L. Gupta (Delhi Univ.Press, to be published).
17. J.D. McCullen, B.F. Bayman and L. Zamick, Phys. Rev. 134 (1964) B515.
18. J.N. Ginocchio, Phys. Rev. 144 (1966) 952.
19. F.B. Malik and N. Scholz, in Nuclear Structure, ed. A. Hossain, H.A. Rashid and M.Islam (1967), North Holland: Amsterdam; Also Phys. Rev.147(1966)836.
20. B. Haas, P. Taras and J. Styczen, Nucl. Phys. A246 (1975) 141.
21. A.K. Dhar, S.B. Khadkikar, D.R. Kulkarni and K.H.Bhatt, Proc.Int.Conf. on Gamma-Ray Trans.Prob, Delhi, 1974, ed.by S.C. Pancholi and S.L.Gupta (Delhi Univ.Press, to be published).
22. A.K. Dhar, D.R. Kulkarni and K.H. Bhatt, Nucl. Phys. A238 (1975) 340.
23. T.T.S. Kuo and E. Osnes, Phys. Rev. C12 (1975) 309.

CHAPTER 8

THE NUCLEUS ^{48}V

1. INTRODUCTION

1.1 Experimental Data

The recent possibilities of the heavy-ion induced reactions have led to resurgence of interest in the studies of nuclear structure. The strong selective excitations of the nuclei by these reactions have unfolded new aspects of nuclear dynamics. One such study reported recently^{1,2)} is connected with the structure of ^{48}V via the reaction $^{34}\text{S}(^{16}\text{O}, \text{pn})$ induced by 32-36 MeV ^{16}O beam. The interesting result of this study are the observations of:

(i) the ground state positive parity band of states with $J^\pi = 4^+$ to 9^+ , and

(ii) very low-lying negative parity rotation-like band of states with $J^\pi = 1^-$ to 7^- . It has been suggested that this band arises due to the $d_{3/2}$ proton excitation to the fp shell.

The mean lifetimes, branching ratios and transition strengths for the decays between the low-lying states of ^{48}V have been measured by Haas et al.³⁾ in their study of $^{34}\text{S}(^{16}\text{O}, \text{pn}\gamma)$ reaction at 34 MeV incident beam energy.

Samuelson et al⁴⁾ measured gamma-ray excitation functions using $^{46}\text{Ti}(\alpha, p n \gamma)$ reaction to populate high-spin states of ^{48}V . Their results indicated the existence of another well-defined negative parity band of states built on a 1.099 MeV state with $K=4^-$ upto a spin of 8^- . On the basis of lifetime measurements in ^{48}V , Haas et al³⁾ suggested $J^\pi = 5^+$ to 1.099 MeV level and thus contradicting the interpretation of Samuelson et al⁴⁾ that 1.099 MeV state is the 4^- band-head of a negative parity band. In a still recent investigation⁵⁾ of the lifetime measurements using recoil distance technique and $^{45}\text{Sc}(\alpha, n \gamma)$ reaction at 9.5 MeV α -beam, Brown et al assigned $J=4$ to the 1.099 MeV level, in concurrence with the measurements of Samuelson et al. They further showed that the observed transition strength for the 1.099 MeV $J=4$ state to the $J=4^+$ ground state supports either parity assignment for the 1.099 MeV level. Brown et al also measured $B(E2)$, $B(M1)$, branching and mixing ratios for transitions between the low-lying states of ^{48}V upto about 1.7 MeV.

Rickel et al⁶⁾ examined recently the levels in ^{48}V by performing $(p, n \gamma)$ reaction at 5.5-7 MeV and the heavy-ion induced reaction $^{34}\text{S}(^{16}\text{O}, p n \gamma)$ at 34 MeV and deduced spins, parities and $(E2/M1)$ mixing ratios for transitions between some of the states upto about 1.8 MeV excitation. Their

experiments too could not resolve the discrepancy in the spin and parity assignments of the 1.099 MeV level.

The states upto about 1.5 MeV in ^{48}V have also been studied previously by Huber et al⁷⁾ in the heavy-ion reactions $^{40}\text{Ca}(^{10}\text{B}, 2p)$ and $^{40}\text{Ca}(^{12}\text{C}, 3pn)$ induced by 25 MeV ^{10}B and 20-26 MeV ^{12}C beams. Besides the identification of some of the positive and negative parity states of ^{48}V , lifetimes, branching ratios and E2, M1 strengths were obtained.

Smith et al⁸⁾ have identified seven $J^\pi=1^+$ states upto about 5 MeV excitation in ^{48}V using $^{46}\text{Ti}(^3\text{He}, p)$ reaction. The decay of these states was determined by $(p\gamma)$ coincidence measurements. Recently Manthuruthil et al⁹⁾ performed $^{48}\text{Ti}(^3\text{He}, t)$ reaction at 25 MeV incident energy and identified 45 levels upto about 3 MeV excitation energy in ^{48}V . Guichard et al¹⁰⁾ performed $^{50}\text{Cr}(p, ^3\text{He})$ reaction at 44.7 MeV and observed 35 levels upto about 3.7 MeV in ^{48}V . Samuelson et al¹¹⁾ have also performed $^{48}\text{Ti}(p, n\gamma)$ ^{48}V reaction and measured branching and mixing ratios for the states upto about 2 MeV excitations. The other^{12,13,14)} experiments conducted for the study of ^{48}V involve the β -decay of ^{48}Cr , $^{50}\text{Cr}(d, \alpha)$, $^{46}\text{Ti}(^3\text{He}, p)$ and $^{47}\text{Ti}(^3\text{He}, d)$ reactions.

1.2 Previous Calculations

Complete (fp)⁸ shell model calculations for this nucleus

are not feasible because of the enormously large resulting matrices that need be diagonalized. However, regarding ^{48}V as the self-conjugate nucleus within the $f_{7/2}$ shell, $(\pi f_{7/2})^3 (\nu f_{7/2})^{-3}$ configuration calculations have been performed by Lawson¹⁵⁾ and by Brown et al⁵⁾. Reasonable agreement with the experimental spectrum of the low-lying states was obtained. In particular, the calculation¹⁵⁾ reproduces remarkably well the spectrum of 1^+ states observed by Smith et al⁷⁾. However, the "signature" selection rule which arises for electromagnetic transitions in such self-conjugate configurations is not well obeyed.

In the following sections we shall undertake a systematic investigation of the energy spectrum and electromagnetic properties of the low-lying positive parity states of ^{48}V , as obtained¹⁶⁾ in our DCM calculations. We also discuss in a semi-quantitative way the $K=1^-$ negative parity band of states in ^{48}V , observed by Haas et al¹⁾.

2. PRESENT CALCULATIONS

2.1 CALCULATION OF THE ENERGY SPECTRUM

2.1.1 Intrinsic States

Axially symmetric HF calculations were performed¹⁶⁾ for ^{48}V using the MWH2 interaction. The lowest HF state is prolate

Table 57

Structural and spectral details of the occupied and some of the lowest unoccupied proton and neutron orbitals of the PROLATE HF state of ^{48}V ($E_{\text{HF}} = -21.08$ MeV, $Q_{\text{HF}} = 23.35$ b²). For other details see caption for table 1.

	k	e_k (MeV)	q_{k2} (b ²)	$c_{\frac{1}{2}k}$	$c_{\frac{3}{2}k}$	$c_{\frac{5}{2}k}$	$c_{\frac{7}{2}k}$
P R O T O N S	1/2	-7.73	4.09	0.113	-0.327	-0.116	0.931
	-1/2	-7.65	4.45	-0.161	-0.367	0.177	0.899
	3/2	-5.64	2.21		-0.180	-0.166	0.969
	-3/2	-5.71	2.25		0.182	0.185	0.966
	5/2	-3.37	-0.21			-0.121	0.993
	-5/2	-3.04	-0.22			-0.103	0.995
	1/2	-1.76	3.71	-0.529	0.533	0.576	0.323
	1/2	-6.67	4.27	0.134	-0.351	-0.134	0.917
	-1/2	-6.60	4.27	-0.156	-0.332	0.181	0.912
	3/2	-4.40	2.09		-0.151	-0.148	0.977
N E U T R O N S	-3/2	-4.31	2.21		-0.170	0.184	0.968
	5/2	-1.89	-0.24			-0.103	0.995
	-5/2	-1.97	-0.23			0.107	0.994
	1/2	-0.28	3.47	-0.516	0.543	0.554	0.364
	-1/2	0.02	2.82	0.501	0.668	-0.374	0.403
	7/2	0.31	-3.0				1.0

Table 58

Structural and spectral details of the occupied and some of the lowest unoccupied proton and neutron orbitals of the OBLATE HF state of ^{48}V ($E_{\text{HF}} = -19.21$ MeV, $Q_{\text{HF}} = -14.75$ b²). For other details see caption for table 1.

	k	e_k (MeV)	q_k (b ²)	$c_{\frac{1}{2}k}$	$c_{\frac{3}{2}k}$	$c_{\frac{5}{2}k}$	$c_{\frac{7}{2}k}$
P R O T O N S	7/2	-6.73	-3.0				1.0
	-7/2	-6.97	-3.0				1.0
	5/2	-4.78	-0.92			0.196	0.981
	-5/2	-4.87	-0.96			-0.212	0.977
N E U T R O N S	3/2	-3.57	-0.08		0.259	0.161	0.952
	1/2	-2.59	0.66	0.060	0.252	0.087	0.962
	7/2	-5.80	-3.0				1.0
	-7/2	-5.74	-3.0				1.0
N E U T R O N S	5/2	-3.94	-0.90			0.192	0.981
	-5/2	-3.26	-0.95			-0.208	0.978
	3/2	-2.21	0.02		0.245	0.124	0.962
	-3/2	-2.20	0.06		0.240	-0.102	0.965
S	1/2	-1.76	0.48	0.081	0.282	0.059	0.954
	3/2	1.35	-1.23		0.958	-0.181	0.221

with $K=4$ and has an energy $E_K = -21.08$ MeV. In this HF state the three protons occupy the orbits with $k_p = (\pm 1/2, \pm 3/2)$ and the five neutrons occupy the orbits with $k_n = (\pm 1/2, \pm 3/2, \pm 5/2)$. The oblate HF state with $K=4$ occurs at -19.21 MeV. The details of some of the single particle orbits of the *and oblate* prolate_A HF states are presented in tables 57 and 58.

In addition to these two HF states, the lowest seven intrinsic states obtained by 1p-1h excitation from them are included in the calculation. The particular particle-hole excitations for these states are listed in table 59 together with the energies $E_K(\gamma)$ of these intrinsic states. In these

Table 59

List of intrinsic states, obtained by 1p-1h excitations from the HF states of ^{48}V , included in the calculation.

Shape	Hole k_i	Particle k_m	Intrinsic	
			K	E_K (MeV)
Prolate	(HF STATE)		4	-21.08
	p +3/2	p -3/2	1	-20.68
	n +5/2	n +3/2	2	-19.47
	n +5/2	n -1/2	1	-19.11
	n -3/2	n -5/2	3	-18.98
	p -1/2	p -3/2	3	-18.90
	p +1/2	p -3/2	2	-18.67

Oblate	(HF STATE)		4	-19.21
	p +5/2	p -5/2	1	-18.88

nine intrinsic states there are two states each with $K=4$, 3 and 2 and three states with $K=1$. The total energy spread of these nine intrinsic states is about 2.5 MeV.

2.1.2 Projected States and their Nonorthogonalization

The states of definite angular momentum J are projected from each of the intrinsic states listed in table 59. The energy spectra of these projected states is exhibited in figs. 28 and 29. The projected states obtained from different intrinsic states are, in general, not orthogonal to each other. The mutual overlaps between the states of definite J projected from different intrinsic states are large, yet not too large, to render the basis space overcomplete. An interesting case occurs for the states projected from the prolate $K=2$ 1p-1h excited intrinsic state at -19.47 MeV (see table 59). The overlaps of almost all the states projected from this intrinsic state with the other states are found to be small. It is therefore expected that the orthonormalization would not alter drastically. the states projected from the above prolate $K=2$ band, from their unperturbed positions. This might then lead to the existence of the $K=2$ band of states in the spectrum of ^{48}V , if the Hamiltonian does not mix very strongly the various bands. Earlier we have predicted¹⁷⁾ the existence of similar low-lying $K=1/2$ band of states in odd Ti isotopes and ^{49}Cr .

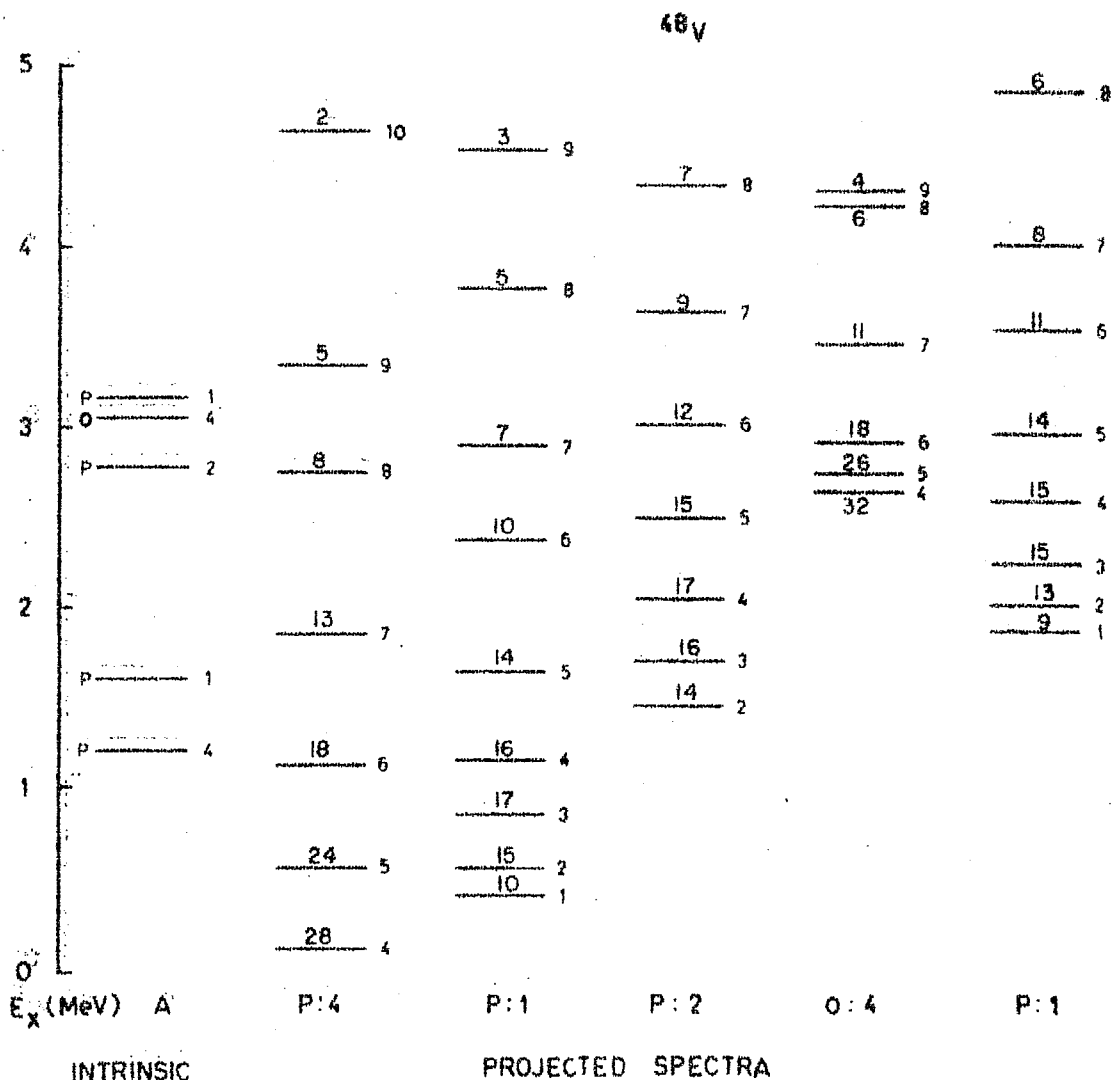


Fig.28

Energy spectra of prolate (P) and oblate (O) intrinsic states of ^{48}V and of the states with definite angular momentum projected from them. The energies of intrinsic states are plotted at A where numbers on the right are their K-values. The numbers on the right of projected states are their J values while those on the top are their intensities in their intrinsic states.

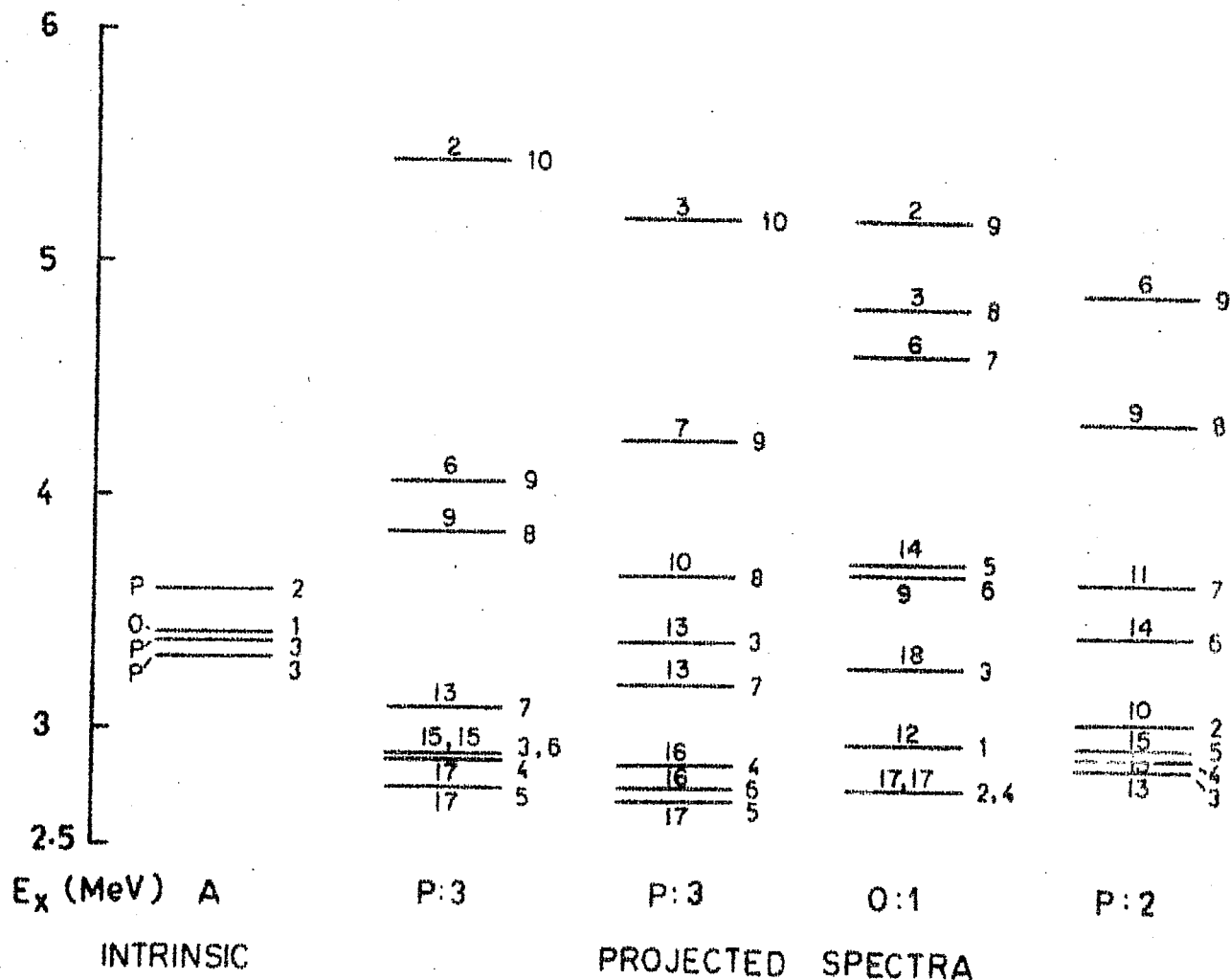


Fig.29

Energy spectra of the states projected from the prolate (P) and oblate (O) intrinsic states of ^{48}V . All these spectra are plotted relative to the energies of the states in fig.28. For other details see caption of fig.28.

The spectrum of ^{48}V is finally obtained by diagonalizing the Hamiltonian in the basis of orthonormalized states obtained above. The calculated spectrum is compared with the experiment in the next section.

2.2 COMPARISON WITH THE EXPERIMENTAL SPECTRUM

The calculated spectrum is compared with the experimental spectrum in fig.30. The agreement between the two upto about 2 MeV is good. **Notable** differences that exist in the experimental and calculated spectra are:

(i) The calculated second $J=2^+$ state at 0.72 MeV does not have an observed counterpart at that energy. Instead the second $J=2^+$ state is observed at 1.52 MeV and has no corresponding calculated state at that energy.

(ii) In the experimental spectrum a level at 775 keV has been observed and assigned spins $J=3^+, 5^+$ by Huber et al⁷⁾. However, Manthuruthil et al⁹⁾ find the existence of this level somewhat uncertain. We do not have any state in the calculated spectrum that would correspond to this level.

(iii) In the experimental spectrum a state at 1.099 MeV is observed^{3,4,5)}. Haas et al³⁾ have assigned a $J=5^+$ to this level, while the recent measurements of Samuelson et al⁴⁾ suggest a $J=4^-$ to this level. The $J=4$ assignment is

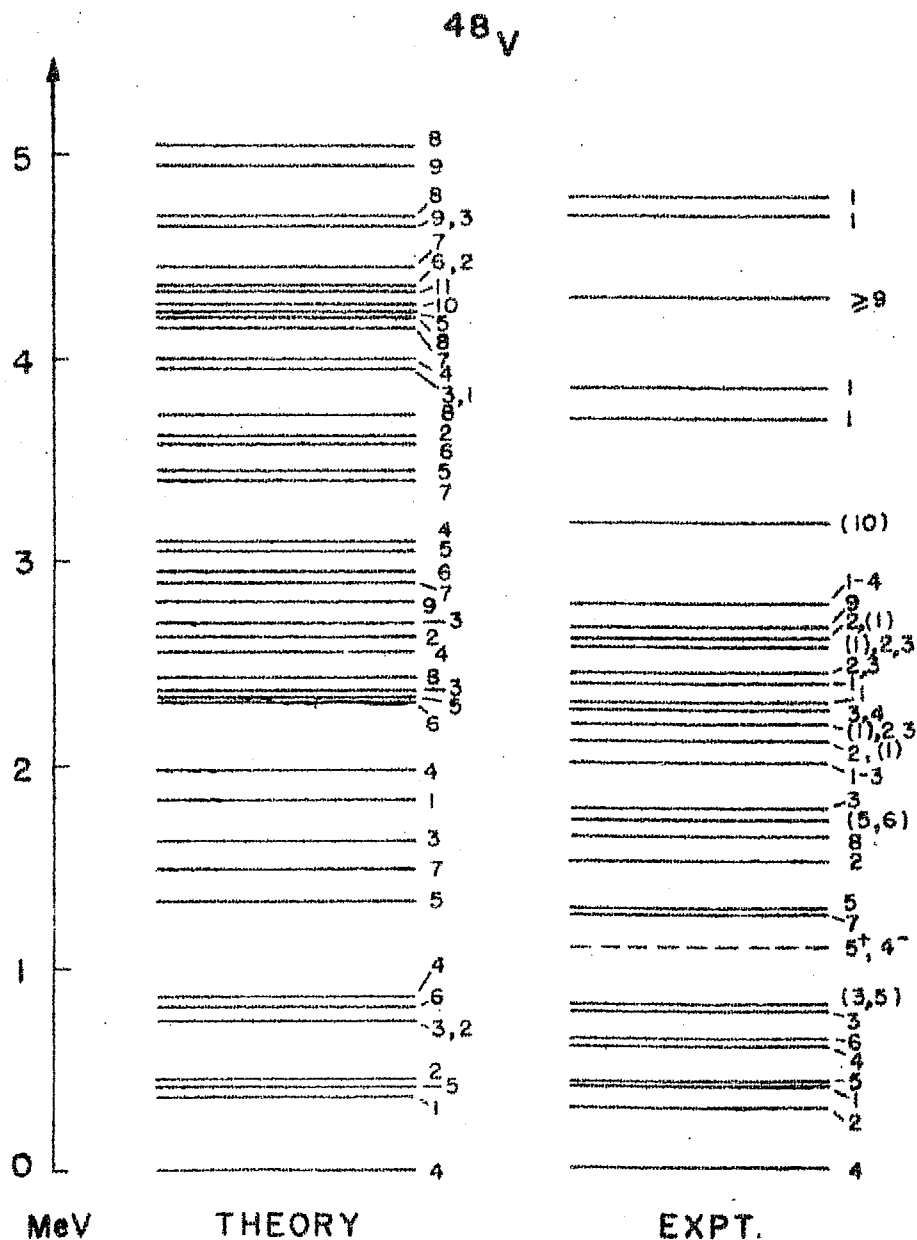


Fig.30

Comparison of the calculated and experimental spectrum of ^{48}V . In the experimental spectrum the state drawn in broken line does not have a unique spin and parity assignment.

also made by Brown et al⁵⁾. If the 5^+ assignment of Haas et al is correct there would be an additional 5^+ state in the experimental spectrum compared to the calculated one. Later on we shall show that the electromagnetic properties of the calculated 5^+ states at 1.32 MeV are similar to those of the observed state at 2.16 MeV and not to those of the 1.099 MeV level. Thus our calculations do not favour a 5^+ assignment to the 1.099 MeV level. There would, however, be no discrepancy between the experiment and the present calculation if the 1.099 MeV level has a negative parity.

(iv) The first $J=8^+$ state is calculated to be at 2.41 MeV. Experimentally a $J=(8^+)$ state is observed at 1.65 MeV. It should be noted in this connection that the $(f_{7/2})^8$ calculation of Brown et al⁵⁾ shows that the positions of the high-spin states with $J \geq 8$ change by more than an MeV when the effective matrix elements deduced from ^{48}Sc are used compared to those obtained with the ^{42}Sc matrix elements. Interestingly enough the observed states with $J=8$ and 10 are in better agreement with those calculated with ^{48}Sc interaction while those with $J=7,9$ and probably 11 agree better with those obtained by ^{42}Sc . For the high-spin states our spectrum is more like the $(f_{7/2})^8$ spectrum obtained with ^{42}Sc interaction.

(v) A tentative second 6^+ state is observed at 1.69 MeV. The energy of our calculated second $J=6^+$ state that might correspond to this observed state is 2.30 MeV.

(vi) Smith et al.⁷⁾ have observed seven $J=1^+$ states upto about 5 MeV excitation in the spectrum of ^{48}V . Our calculation reproduces very well the lowest two $J=1^+$ states. It may be pointed out that in our basis space only three $K=1$ intrinsic states (see table 59) from which a $J=1$ state is projectable, are included. Therefore our present calculation is not expected to provide an adequate description of all the observed $J=1^+$ states in ^{48}V . A larger DCM calculation for the description of $J=1^+$ states including about ten $K=1$ intrinsic states is under progress and shall appear elsewhere.

In general the present calculation provides an improved spectrum of ^{48}V compared to that given by the $(f_{7/2})^n$ calculation.

2.3 BAND STRUCTURE OF THE CALCULATED STATES

Two bands are likely to exist in ^{48}V .

(i) The $K=4$ "ground state band". The calculated states with $J=4-10$ belonging to this band occur at 0.0, 0.44, 0.85, 1.53, 2.47, 2.85 and 4.32 MeV respectively. They are, to a

large extent, states projected from the prolate $K=4$ HF state. The average admixture of states projected from other intrinsic states is about 12 percent.

We have associated in fig.31 our calculated $K=4$ ground state band of states with observed^{2,5)} Yrast states with $J=4-9$ at 0.0, 0.428, 0.627, 1.255, 1.651 and 2.627 MeV respectively.

(ii) The excited $K=2$ band. The calculated states with $J=2-8$ belonging to this band occur at 0.77, 1.68, 2.03, 2.39, 3.01, 3.45 and 4.27 MeV respectively. The average 'band mixing' to these states is about 15 percent. It may be mentioned that for the $J=2$ state the admixture of other bands is about 40 percent.

There exist in the experimental spectrum the states with $J=2,3$ and 4 at 1.52, 1.78 and 2.26 MeV respectively. Our calculated $J=3$ and 4 members of the $K=2$ band are close in energy to these states but the calculated $J=2$ state is about 300 keV lower. However, its decay properties are similar to the observed 2^+ state at 1.52 MeV. It is therefore tempting to identify the above $2^+, 3^+$ and 4^+ states as the members of this excited $K=2$ band.

It should be mentioned that in the neighbouring nucleus ⁴⁹Cr also, the present interaction gives rise¹⁷⁾ to an

excited $K=1/2$ band which is lower by about 500 keV than the observed one. It is necessary therefore to improve the effective interaction to give proper band separations in these nuclei.

All the other calculated states of ^{48}V have a complex structure.

2.4 ELECTROMAGNETIC PROPERTIES

In this section we shall discuss the $B(E2)$, $B(M1)$, $(E2/M1)$ mixing ratios, branching ratios and mean lifetimes of the transitions between the low-lying states of ^{48}V . We have calculated $B(E2)$ values using two sets of effective charges (i) $e_p = 1.32e$ and $e_n = 0.89e$ and (ii) the Kuo-Osnes charges $e_p = 1.25e$ and $e_n = 0.47e$.

2.4.1 Transitions in the Ground State Band

2.4.1.1 $B(E2)$ and $B(M1)$ Values

In tables 60 and 61, the experimental^{3,5)} $B(E2)$ and $B(M1)$ values are compared with the results of our calculations and those of the $(f_{7/2})^8$ calculations⁵⁾.

The results of the present calculations of $B(E2)$ values are in better agreement with the experimental ones compared to those of the $(f_{7/2})^8$ calculation. Note in particular that for the $5 \rightarrow 4$ transition the latter calculation

Table 60

$B(E2, J_i \rightarrow J_f)$ values in $e^2 \text{fm}^4$ for transitions within the ground state band of ^{48}V .

J_i	J_f	Expt I ^a	Expt. II ^b	DCM ^c	DCM ^d	$(f_{7/2})^8$ ^a
5	4	120 ± 45	$100.5^{+81.9}_{-49.7}$	185	317	0.75
6	4	48 ± 5	$41.4^{+9.3}_{-8.3}$	35	60	49
	5	≤ 510	$202.5^{+128.5}_{-86.0}$	177	304	56
7	5			53	92	
	6			132	229	
8	6			90	157	
	7		≥ 44.04	69	124	
9	7		≥ 68.2	108	188	
	8		≥ 9.12	76	135	
10	8			107	190	
	9			43	77	

a. Ref.5. b. Ref.3. c. $e_p = 1.25e$, $e_n = 0.47e$

d. $e_p = 1.32e$, $e_n = 0.89e$.

gives an almost forbidden $B(E2)$. Thus the present calculations account for the breakdown of the "signature" selection rule¹⁵⁾ due to configuration mixing. The experimental $B(E2)$ values appear to favour the Kuo-Osnes effective charges.

Table 61

$B(M1, J_i \rightarrow J_f)$ values in $(n.m.)^2$ for transitions within the ground state band of ^{48}V .

J_i	J_f	Expt.I ^a	Expt.II ^b	DCM	$(f_{7/2})^8$ ^a
5	4	0.081 ± 0.013	0.079 ± 0.014	0.08	0.0
6	5	0.023 ± 0.004	0.029 ± 0.007	0.09	0.031
7	6	0.023	0.045	0.19	
8	7		0.526	0.13	
9	8		0.007	0.28	
10	9			0.08	
11	10			0.43	

a. Ref.5 b. Ref.3

Both the calculations reproduce well the observed hinderence of the $B(M1)$ values for the lowest two transitions.

2.4.1.2 Mixing Ratios, Branching Ratios and Lifetimes

The $(E2/M1)$ mixing ratios for the transitions between the states belonging to the ground state band are given in table 62. Our calculations reproduce well the observed ratios.

Table 62

(E2/M1) mixing ratios for transitions between the members of the ground state band in ^{48}V .

J_i	J_f	(E2/M1) mixing ratio		
		DCM ^a	DCM ^b	Expt ^c
5	4	0.17	0.22	0.13 \pm 0.03
6	5	0.07	0.10	0.14 \pm 0.02
7	6	0.14	0.18	0.05 \pm 0.07
8	7	0.07	0.10	0.08 \pm 0.05
9	8	0.13	0.18	0.34 \pm 0.04
10	9	0.32	0.43	

a. $e_p = 1.25e$, $e_n = 0.47e$. b. $e_p = 1.32e$, $e_n = 0.89e$

c. Ref.3.

The experimental and theoretical information on the branching ratios and mean lifetimes of the decay of the states in ^{48}V are summarized in fig.31. The members of the ground state band are plotted in thick lines. The B(E2) values obtained with the Kuo and Osnes effective charges have been employed in the calculations of branching ratios and mean lifetimes.

In general, the agreement between theory and experiment is good upto about 1.5 MeV. The first significant discrepancy occurs for the J=8 state where our calculations indicate an almost equal decay branch to the 6^+ (0.627 MeV)

48V

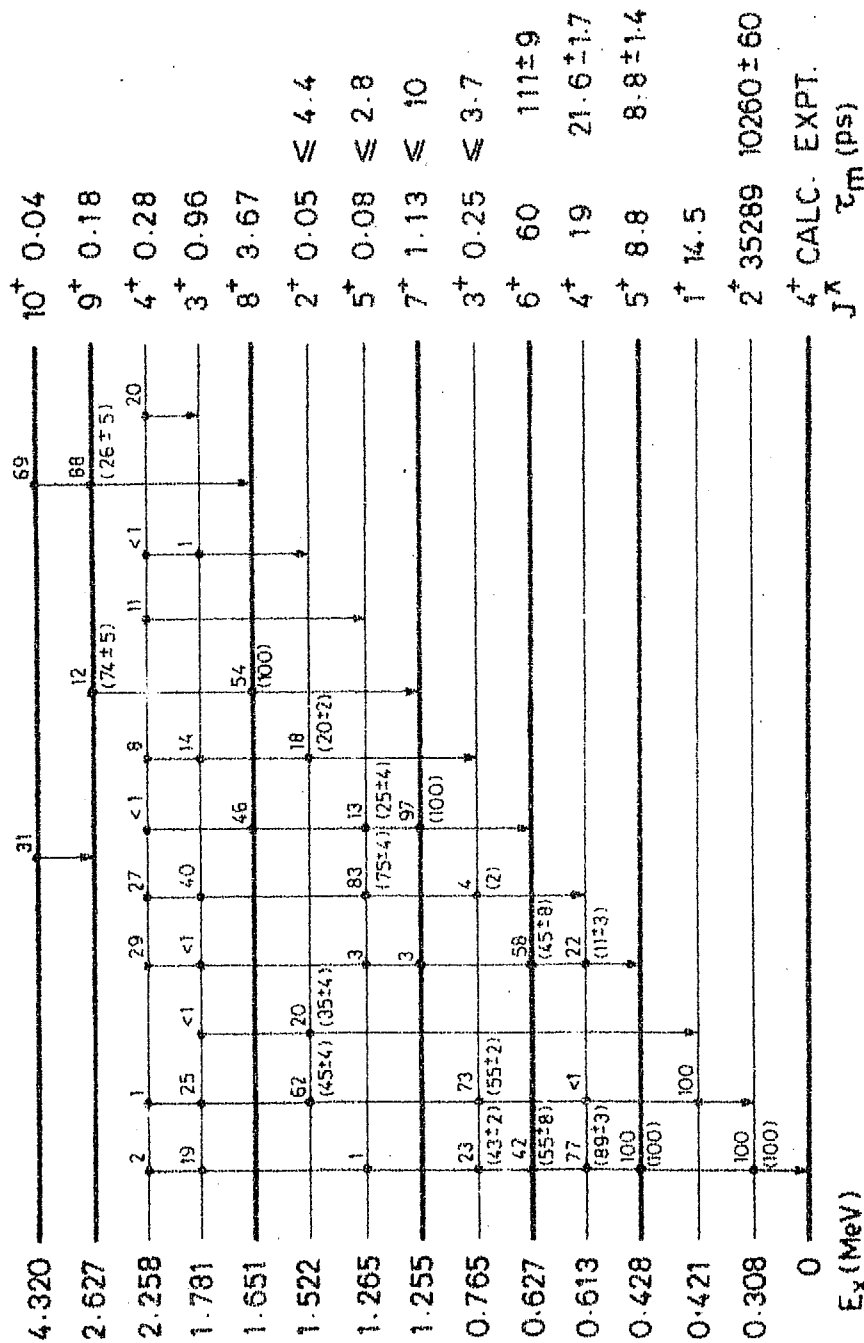


Fig.31

Mean lifetimes and branching ratios in ^{48}V . The states drawn in thick lines are the members of the ground state band. The excitation energies on the left are the observed energies.

and 7^+ (1.255 MeV) in contrast to the experimental 100 percent, dominantly M1, branch to the 7^+ state. Similarly the decay of 9^+ state at 2.627 MeV is not similar to the experimental one.

The calculated lifetimes of the low-lying states are in reasonable agreement with the observed ones. A significant discrepancy between the two is seen for the first 2^+ and the 6^+ states.

2.4.2 Electromagnetic Properties of other States

The $B(E2)$, $B(M1)$ values for the decays of other low-lying states not belonging to the ground state band are summarized in tables 63 and 64. The observed $B(E2)$ values for the $2_1 \rightarrow 4_1$ and $4_2 \rightarrow 4_1$ transitions are significantly larger than our calculated ones. On the other hand, the observed $B(M1)$ values are retarded compared to the experimental ones. The branching ratios and lifetimes of these states obtained in our DCM calculations are compared with the experiment in fig.31. We have associated our calculated $J=2^+$ state at 0.72 MeV of the $K=2$ excited band with the $J=2^+$ state observed at 1.522 MeV. The calculated branching ratios and mean lifetime of this calculated 2^+ state at that energy are in reasonable agreement with the experiment.

Table 63

Comparison of the calculated and experimental $B(E2, J_i \rightarrow J_f)$ values in $e^2 \text{fm}^4$ from the transitions from the states J_i not belonging to the ground state band of ^{48}V . The subscript for a particular state indicates the number of that state in ascending order of energy.

J_i	J_f	Expt ^a	DCM ^b	DCM ^c	$(f_{7/2})^8$ ^a
2 ₁	4 ₁	28.5±0.2	8	13	92
1 ₁	2 ₁		274	474	103
4 ₂	4 ₁	13.7±3.5	2	5	82
	5 ₁		7	10	99
3 ₁	4 ₁		0.2	0.03	2
	2 ₁	≥ 0.6	77	133	60
5 ₂	4 ₂	≥ 1.6	36	65	
	6 ₁		3	4	
2 ₁	2 ₁	≥ 0.6	20	37	

a. Ref.5.

b. $e_p = 1.25e$, $e_n = 0.47e$.

c. $e_p = 1.32e$, $e_n = 0.89e$.

Table 64

Comparison of the calculated and experimental $B(M1, J_i \rightarrow J_f)$ values in $(n.m.)^2$ for the transitions from the states J_i belonging to the ground state band.

J_i	J_f	Expt ^a	DCM ^b	$(f_{7/2})^8$ ^a
1 ₁	2 ₁		2.72	2.27
4 ₂	4 ₁	0.0098±0.0006	0.0097	0.0088
4 ₂	5 ₁		0.10	0.40
3 ₁	4 ₁	≥0.014	0.12	0
3 ₁	2 ₁	≥0.085	1.79	1.13
5 ₂	4 ₂	≥0.049	2.07	
5 ₂	6 ₁	≥0.016	0.34	

a. Ref.5

b. $e_p = 1.25e$, $e_n = 0.47e$.

As mentioned in subsec.2.2 our calculated $J=5^+$ state at 1.32 MeV has branching ratios and lifetime similar to the observed 5^+ state at 1.265 MeV and not to those of the observed 1.099 MeV state. The latter state (not plotted in fig.30) decays³⁾ only to the ground state with a lifetime of 6.5 ± 0.5 ps. Thus our calculations do not favour a positive parity for the 1.099 MeV level.

2.4.3 Static Moments

In table 65 are given the static electric quadrupole and magnetic dipole moments of the first few states in ^{48}V . The experimental data about the electric quadrupole moments is not available. The observed^{18,19)} magnetic moment of 4^+ ground state is well reproduced while that of 2^+ at 308 keV is smaller than the observed value.

Table 65

Static moments of some of the low-lying states in ^{48}V .

J	E_J keV	$Q(\text{efm}^2)$		μ (n.m.)	
		DCM ^a	DCM ^b	DCM	Expt ^c
4^+	0	39	50	1.78	1.63 ± 0.1
2^+	308	-8	-9	0.12	0.44 ± 0.19
1^+	421	8	10	-1.53	
5^+	428	16	21	2.52	

a. $e_p = 1.25e$, $e_n = 0.47e$. b. $e_p = 1.32e$, $e_n = 0.89e$.

c. Ref.18,19.

2.5 NEGATIVE PARITY STATES

As mentioned in subsec.1.1, negative parity rotational-band of states with $J=1^-$ to 7^- has been observed¹⁾ in the heavy ion reaction of Haas and Taras. Samuelson et al⁴⁾ also identified another odd parity rotational-band of states

built on $K=4^-$ in the spectrum of ^{48}V . The $J=4^-$ member of this latter band is shown to exist at 1.099 MeV level while the measurements of Brown et al⁵⁾ indicate $J=4$ of either parity for this state.

The observed¹⁾ moment of inertia parameter for the $K=1^-$ band is $\frac{\hbar^2}{2\mathcal{J}} = 56.7$ keV. From the $2^- \rightarrow 1^-$ transition the quadrupole moment Q_0 of the $K=1^-$ intrinsic state giving rise to this band was estimated by Haas and Taras¹⁾ to be $Q_0 = 0.79$ barn. They suggested that this band might arise from the excitation of a $d_{3/2}$ proton into fp shell.

In here we would like to present some evidence that seems to support this lp-lh interpretation of the $K=1^-$ band of states. In particular, we show that the three characteristic properties of the negative parity band, namely the K-value, the moment of inertia parameter and the value of the intrinsic quadrupole moment determined experimentally, are consistent with the lp-lh description of the negative parity band.

i) The K-values

The lowest energy lp-lh excited intrinsic state of ^{48}V corresponding to a proton excitation from the $d_{3/2}$ state to the fp shell is sketched in fig.32. In such an intrinsic state $k_p = \pm 3/2^+$ and $k_n = \pm 5/2^-$. This deformed coupling scheme

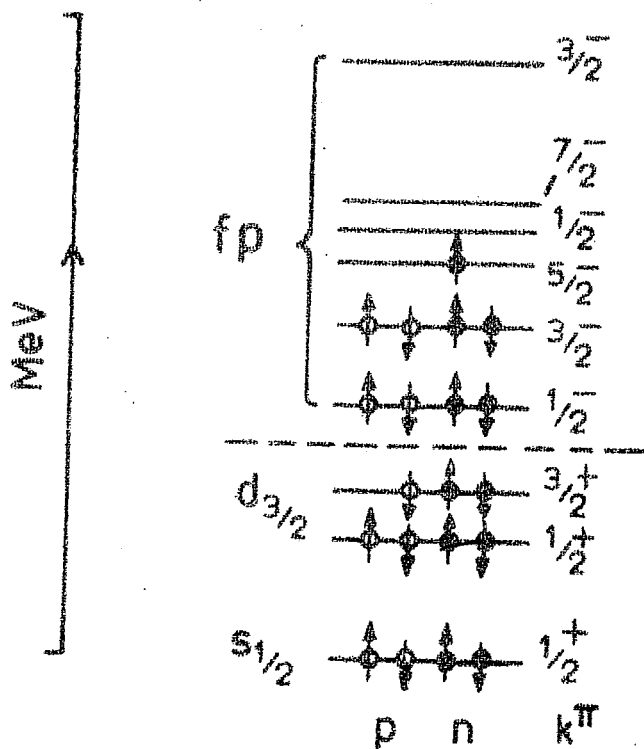


Fig. 32.

leads automatically to $K=1^-$ and 4^- intrinsic states and are thus consistent with the observations of the low-lying $1p-1h$ $K=1^-$ and a $K=4^-$ bands of states in the spectrum of ^{48}V .

ii) Moment of Inertia

It is clear from fig.32 that the $K=1^-$ intrinsic state of ^{48}V is obtained by creating a $d_{3/2}$ hole in the intrinsic state of the ground state band of ^{49}Cr . Physical considerations²⁰⁾ and general expressions for moment of inertia indicate that the moment of inertia for this $K=1^-$ band in ^{48}V would be approximately equal to that of the ground state band of ^{49}Cr .

We have performed²¹⁾ DCM calculations for the nucleus ^{49}Cr using the same interaction as for the description of positive parity states of ^{48}V . The calculated spectrum and the electromagnetic properties are in very good agreement with the experiment. The details of ^{49}Cr nucleus are presented in chapter 11, part V.

The ground state band of ^{49}Cr is highly collective but not strictly rotational. The average moment of inertia of the calculated spectrum of ^{49}Cr is $\frac{\hbar^2}{2\mathcal{I}} = 57.3 \text{ keV}$. This agrees very well with the experimental value of 56.7 keV observed for the $K=1^-$ band of ^{48}V .

iii) Intrinsic Quadrupole Moment

The electric quadrupole moment Q of the theoretical $1p-1h$ excited $K=1^-$ intrinsic state, sketched in fig.32 can be written as:

$$Q \approx e Q_o \approx e_p \left[q_p(\text{hole}) + Q_p(\text{Cr}) \right] + e_n Q_n(\text{Cr})$$

where e_p and e_n are the effective charges for the proton and neutron respectively. q_p corresponds to the mass quadrupole moment of the $k=3/2^+$ proton hole orbital. Q_p and Q_n are the corresponding moments arising due to the nucleons in the fp shell space. We have assumed, for the present calculation, the values of Q_p and Q_n to be the same as those

obtained for the lowest energy HF intrinsic state of ^{49}Cr . These values are $Q_p(\text{Cr}) = 0.47$ barn and $Q_n(\text{Cr}) = 0.48$ barn. Adding the contribution of the $d_{3/2}$ proton hole and taking Kuo and Osnes²²⁾ effective charges we obtain $(Q_o)_{\text{cal}} = 0.73$ barn. This is in good agreement with the experimental value $(Q_o) = 0.79$ barn measured by Haas and Taras.

To summarize, the present calculation accounts reasonably well for the collective features in the spectrum of the low-lying states of ^{48}V . It is nice to note that the model seems to incorporate the breakdown of the "signature" selection rule arising in the $(1f_{7/2})^8$ space. However, it fails to improve upon the spectrum of the high-spin states with $J \geq 8$ obtained in the simpler $(f_{7/2})^8$ calculation. This interesting anomaly is likely to provide useful information on the deficiency of the effective interaction.

REFERENCES

1. B. Haas and P. Taras, Phys.Rev.Lett.33 (1974) 105.
2. P. Taras, B. Haas and R. Vaillancourt, Nucl. Phys. A232 (1974) 99.
3. B. Haas, P. Taras, J.C. Merdinger and R. Vaillancourt, Nucl. Phys. A236 (1974) 405.
4. L.E. Samuelson, W.H. Kelly, F.M. Bernthal, R.A. Warner and Wm.C. McHarris, Preprint MSUCL-146 COO-1779-149.
5. B.A. Brown, D.B. Fossan, J.M. McDonald and K.A. Snover, Phys. Rev.C11 (1975) 1122.
6. D.G. Rickel , N.R. Roberson, C.P. Cameron, R.D. Ledford, S.G. Buccino and D.R. Tilley, Nucl. Phys. A256 (1976)152.
7. R.B. Huber, C. Signorini, W. Kutschera and H. Moringa, Il Nuovo Cimento 15A (1973) 501.
8. J.W. Smith, L. Meyer-Schutzmeister and G. Hardie, Phys. Rev.C8(1973) 2232.
9. J.C. Manthuruthil, C.P. Poirier and L. Meyer-Schutzmeister, Phys. Rev.C11 (1975) 1141.
10. A. Guichard, W. Benenson and H. Nann, Phys. Rev.C12 (1975) 806.
11. L.E. Samuelson, W.H. Kelly, R.A. Warner, Wm.C.Harris, E.M. Bernstein and R. Shamu, in Proc.Int.Conf.on Nucl. Phys.,Munich, 1973, Vol.I, ed.by J.de Boer and H.J.Mang (North Holland, Amsterdam, 1973) p.209.

12. R.K.Sheline and J.R. Wilkinson, Phys. Rev.99 (1955) 165.
13. W.E. Dorenbusch, T.A. Belote and J.Rapaport, Nucl. Phys. A109 (1968) 649.
14. W.E. Dorenbusch, T.A. Belote, J. Rapaport and K.C.Nair, Nucl.Phys. A112 (1968) 385.
15. R.D. Lawson, Nucl. Phys. A173 (1971) 17.
16. A.K. Dhar, D.R. Kulkarni and K.H. Bhatt, Nucl. Phys. and Solid State Phys. (India) 16B (1973) 146.
17. A.K. Dhar, D.R.Kulkarni and K.H. Bhatt, Nucl.Phys. A238 (1975) 340.
18. V.S. Shirley, Table of Nuclear Moments, in Hyperfine Interactions in Excited Nuclei, ed. G. Goldring and R. Kalish (Gordon and Beach Science Publishers, Inc. New York, 1971) p.1255.
19. B.K. Patnaik, S. Gangadharan and S.Jha, Cont.Int. Conf.on Properties of Nuclear States, Montreal, Canada, 1969, ed. M. Harvey, R.Y. Cussion, J.S. Geiger and J.M. Pearson, (Univ.Press, Montreal, 1969), p.90.
20. B.R. Mottelson, Course de l'Ecole d'Ete de Physique Theorique des Houches 1958 (Dunod, Paris, 1959).
21. A.K.Dhar, D.R. Kulkarni and K.H. Bhatt, Proceedings of Int.Conf.on Nucl.Structure and Spectroscopy, Amsterdam, 1974, eds.H.P. Blok and A.E.L.Dieperink, (Scholar's Press, Amsterdam, 1974) p.59.
22. T.T.S. Kuo and E. Osnes, Phys. Rev.C12 (1975) 309.

CHAPTER 9

THE NUCLEUS ^{49}V

1. INTRODUCTION

1.1 Experimental Data

There has been a growing experimental¹⁾ interest in the study of ^{49}V nucleus. This nucleus lies near the middle of the $f_{7/2}$ shell and is expected to show large collective features. Lot of experimental data on the level structure of this nucleus has become available very recently. The properties upto about 2.6 MeV in ^{49}V have been investigated²⁻¹²⁾ by various authors using the reactions (p, γ) , $(p, n\gamma)$, $(\alpha, p\gamma)$, $(^3\text{He}, d)$, (t, α) and (p, α) . The ground state band and some other high-spin states of ^{49}V have been observed by Sawa et al¹³⁾ in $^{46}\text{Ti}(\alpha, n)$ reaction studies. Recently Tabor and Zurmuhle¹⁴⁾ studied the structure of this nucleus by $(\alpha, p\gamma)$ reaction at $E_\alpha = 10$ MeV and obtained detailed information about the decay properties of the levels upto about 3 MeV excitation. Similar information upto about 3.5 MeV has been obtained by Haas et al¹⁵⁾ by using $(\alpha, p\gamma)$ and $(p, n\gamma)$ reactions at $E_\alpha = 10.6$ MeV and $E_p = 2.1$ MeV. The mean lifetimes of $J=5/2$ and $3/2$ members of the observed ground state triplet have been measured

by Currie¹⁶⁾ and Blasi et al. Recently these lifetimes were remeasured by Cheung and Mark¹⁷⁾ for the 91 keV $J=5/2^-$ level and by Vingiani et al⁶⁾ for the 153 keV $3/2^-$ level. Brown et al¹⁸⁾ measured the lifetime of 1021 keV $11/2^-$ and 2261 keV $15/2^-$ levels in ^{49}V excited in (α, p) reaction. The lifetime measurement of $J=15/2^-$ state observed at 1.022 MeV is recently made by Haas et al¹⁹⁾. Lifetimes of various levels upto about 2.5 MeV excitation energy have recently been measured by doppler-shift attenuation method by Rosza et al²⁰⁾ and Kiuru²¹⁾. Britz et al²¹⁾ also measured the lifetimes of states upto about 3.25 MeV in ^{49}V . Measurements of gamma-ray intensities and spin assignments in ^{49}V have recently been made by Okon et al²²⁾ Tabor et al²³⁾ and by Jackson et al²⁴⁾ in β -decay study of ^{49}Cr .

1.2 Previous Calculations

Theoretically the nucleus ^{49}V has been studied²⁵⁾ by considering proton-neutron configuration $\pi(f_{7/2})^3 \nu(f_{7/2})^{-2}$. This calculation fails to reproduce the 153 keV $3/2^-$ member of the observed ground state triplet $(7/2-5/2-3/2)$. Instead the first $3/2^-$ state is obtained at about 0.80 MeV.

The RPC model calculations for ^{49}V have been made

by Malik and Scholz²⁶⁾, Tabor and Zurmuhle¹⁴⁾ and Haas et al^{15,27)}. Tabor and Zurmuhle consider intrinsic states corresponding to $\delta \sim 0.20$ while those used by Haas et al to $\delta \sim 0.17$. In contrast Malik and Scholz find intrinsic states corresponding to $\delta \sim -0.38$ necessary for the optimum agreement with the experiment. It may however be pointed out that the parameters C and D corresponding to the strengths of the $l.s$ and l^2 terms respectively as considered by Haas et al²⁷⁾ are $C = -1.60$ MeV, $D = -0.21$ MeV compared to $C = -2.91$ MeV and $D = -0.39$ MeV of Malik and Scholz. The agreement of these calculations with the experiment is only qualitative.

2. PRESENT CALCULATIONS

We have performed DCM calculations for the nucleus ^{49}V using MWH2 interaction. In subsec.2.1, we shall describe the spectrum calculations for ^{49}V . In subsec.2.2, the composite spectrum is compared with the experiment and the eigenstates analysed for possible band structure in subsec.2.3. The electromagnetic properties of the low-lying states would be discussed in subsec.2.4.

2.1 CALCULATIONS OF THE ENERGY SPECTRUM

2.1.1 Intrinsic States

The axially symmetric HF calculation for the nucleus ^{49}V gives prolate $K=3/2$ intrinsic state at -23.16 MeV and the oblate $K=5/2$ intrinsic state -21.43 MeV. The

intrinsic quadrupole moments of these states are 21.7 b^2 and -14.3 b^2 respectively. The structure, energies and quadrupole moments of the proton and neutron occupied and a few unoccupied single particle orbits of the prolate and oblate HF state are given in tables 66 and 67 respectively. It is seen from table 66 that the HF energy gaps at the proton and neutron fermi surfaces are about 2 MeV. It is therefore expected that the p-h excited intrinsic states of ^{49}V would lie above 1.5 MeV relative to the prolate HF state. Therefore the ground state band^(28,29) of ^{49}V might reasonably be described by projections from the HF intrinsic state alone, since the oblate $J=5/2$ intrinsic state too lies at about 1.73 MeV from the prolate $K=3/2$ state.

For the description of the excited states of ^{49}V and to examine the effects of the other higher p-h excited intrinsic states on the ground state band of ^{49}V projected from prolate intrinsic state, we have included in the present DCM calculation, four lowest 1p-1h excited intrinsic states. The details of these intrinsic states are presented in table 68 along with the energies and K-values of the HF intrinsic states from which they were obtained. Thus in all six intrinsic states were considered in this calculation. Of these two have $K=1/2$, one $K=3/2$ and three $K=5/2$ and the

Table 66

Structural and spectral details of the occupied and some of the lowest unoccupied proton and neutron orbitals of the PROLATE HF state of ^{49}V ($E_{\text{HF}} = -23.16$ MeV, $Q_{\text{HF}} = 21.71 \text{ b}^2$). For other details see caption for table 1.

	k	e_k (MeV)	q_k (b^2)	$c_{\frac{1}{2}k}$	$c_{\frac{3}{2}k}$	$c_{\frac{5}{2}k}$	$c_{\frac{7}{2}k}$
P R O T O N S	1/2	-7.93	3.73	0.066	-0.275	0.084	0.955
	-1/2	-7.83	4.16	-0.124	-0.325	0.163	0.923
	3/2	-6.13	2.15		-0.175	-0.135	0.975
	-3/2	-6.57	2.17		-0.178	0.145	0.973
	5/2	-4.11	-0.19			0.133	0.991
	1/2	-2.07	4.12	-0.542	-0.512	0.622	0.240
N E U T R O N S	1/2	-6.61	3.98	0.111	-0.302	-0.128	0.938
	-1/2	-6.15	4.01	-0.117	-0.303	0.138	0.936
	3/2	-4.83	2.10		-0.153	-0.148	0.977
	-3/2	-4.16	2.02		-0.141	0.128	0.982
	5/2	-2.58	-0.22			-0.116	0.993
	-5/2	-2.19	-0.22			0.112	0.994
	7/2	-0.36	-3.0				1.0
	1/2	-0.02	3.53	-0.520	0.607	0.505	0.326
	1/2	2.26	1.14	0.131	0.665	-0.729	0.099

Table 67

Structural and spectral details of the occupied and some of the lowest unoccupied proton and neutron orbitals of the OBLATE HF state of ^{49}V . ($E_{\text{HF}} = -21.43$ MeV, $Q_{\text{HF}} = -14.26$ b²). For other details see caption for table 1.

	k	e_k (MeV)	q_k (b ²)	$c_{\frac{1}{2}k}$	$c_{\frac{3}{2}k}$	$c_{\frac{5}{2}k}$	$c_{\frac{7}{2}k}$
P R O T O N S	7/2	-7.08	-3.0				1.0
	-7/2	-7.57	-3.0				1.0
	5/2	-5.32	-0.89			0.186	0.983
	3/2	-4.15	0.07		0.225	0.161	0.961
	1/2	-3.20	0.81	0.046	0.226	0.111	0.967
	7/2	-6.01	-3.0				1.0
N E U T R O N S	-7/2	-5.54	-3.0				1.0
	5/2	-4.11	-0.81			0.159	0.987
	-5/2	-3.39	-0.89			-0.186	0.983
	3/2	-2.57	0.21		0.207	0.113	0.971
	-3/2	-2.23	0.12		0.228	-0.103	0.968
	1/2	-1.62	0.80	0.058	0.233	0.034	0.970
	3/2	1.41	-1.42		0.965	-0.189	-0.184

Table 68

Energies and K-values of various intrinsic states included in the calculation of ^{49}V spectrum.

Shape	Hole k_1	Particle k_m	K	E_K (MeV)
Prolate	(HF STATE)		3/2	-23.16
	p -1/2	p -3/2	1/2	-21.61
	n -5/2	n -7/2	1/2	-21.48
	p 3/2	p 5/2	5/2	-21.32
	n 5/2	n 7/2	5/2	-21.32
<hr/>				
Oblate	(HF STATE)		5/2	-21.43

total energy spread of these intrinsic states is 1.84 MeV.

All these intrinsic states have dominant $T=3/2$ isospin,

with an extremely small admixture of $T > 3/2$ isospin

components.

2.1.2 Energy Spectra and Nonorthogonality of the Projected States

In fig.33 are plotted the energy spectra of the states of definite angular momenta projected from the six intrinsic states of ^{49}V . Also given for each of the projected states is the intensity $|a_{JK}|^2$ of that state in its corresponding intrinsic state. A noticeable difference is in the spectrum

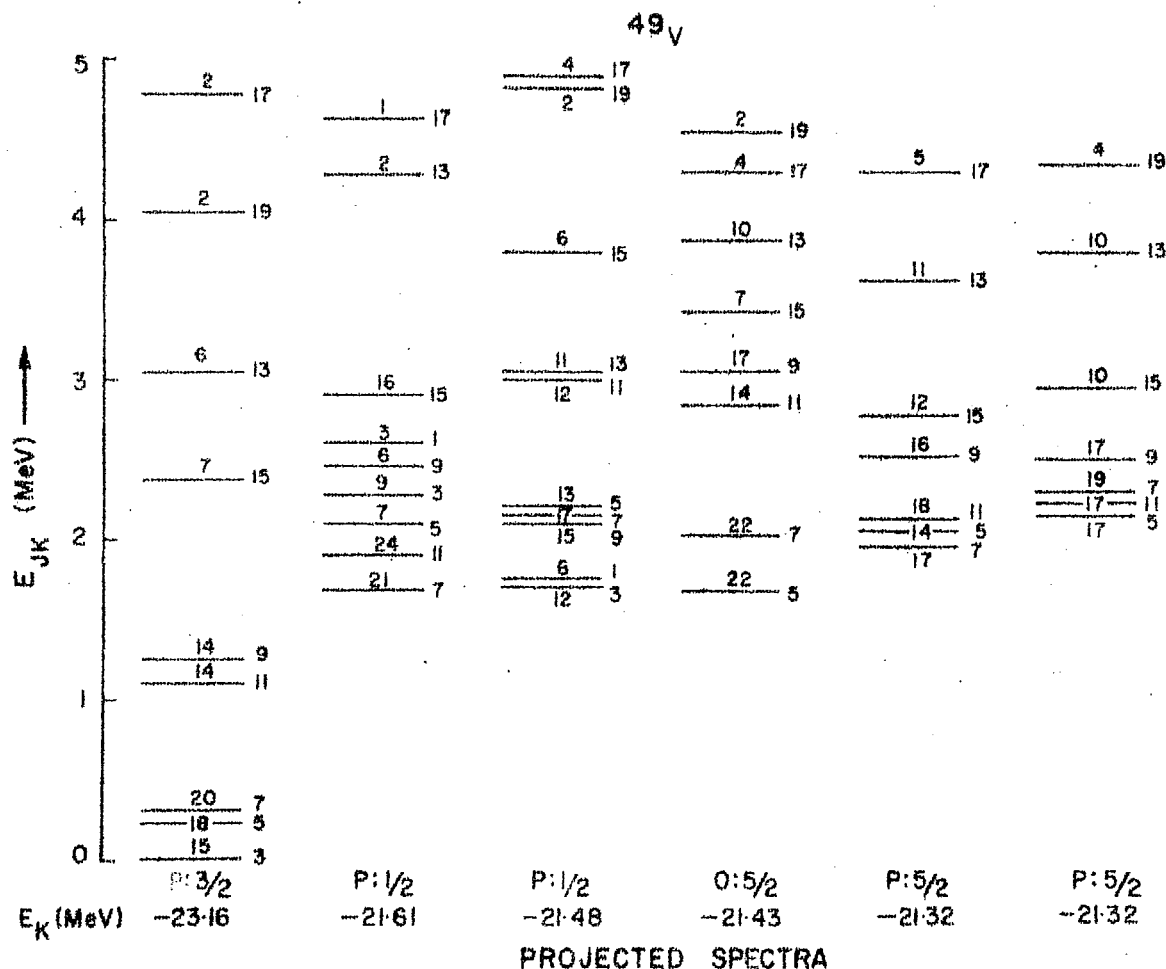


Fig.33

Energy spectra of the states with definite angular momentum projected from the prolate (P) and oblate (O) intrinsic states in ^{49}V . The energies and K-values of the intrinsic states are given at the bottom. For the projected states the numbers on the right are their $2J$ values while those on the top are their intensities in their intrinsic states.

of states projected from the $K=1/2$ intrinsic state at -21.48 MeV, compared to similar $T=3/2$ states projected from the $K=1/2$ intrinsic state of ^{47}Ti (fig.8, col.P:1/2) which were found to cluster in doublets.

The overlaps $N_{K\eta, K'\eta'}^J$ of the states projected from different intrinsic states are in general large, yet not too large to result in an overcomplete basis space.

The Hamiltonian matrix is finally diagonalized in the basis of states projected from these six intrinsic states of ^{49}V , after taking care of their nonorthogonality. The composite calculated spectrum is compared with the experiment in the next section.

2.2 CALCULATED VS OBSERVED SPECTRUM

In fig.34 are compared the experimental and theoretical spectra of ^{49}V . The agreement between the two upto about 2.5 MeV is very good. The correspondences that occur between the two are:

(i) The calculated Yrast band of states with $J=3/2^-$, upto $J=15/2^-$ at 2.15 MeV is in very good agreement with the observed spectrum except that the $J=3/2$ and $7/2$ states have flipped in the calculated spectrum. The $J=13/2$, $17/2$ and $19/2$ members of the band are not yet observed.

^{49}V

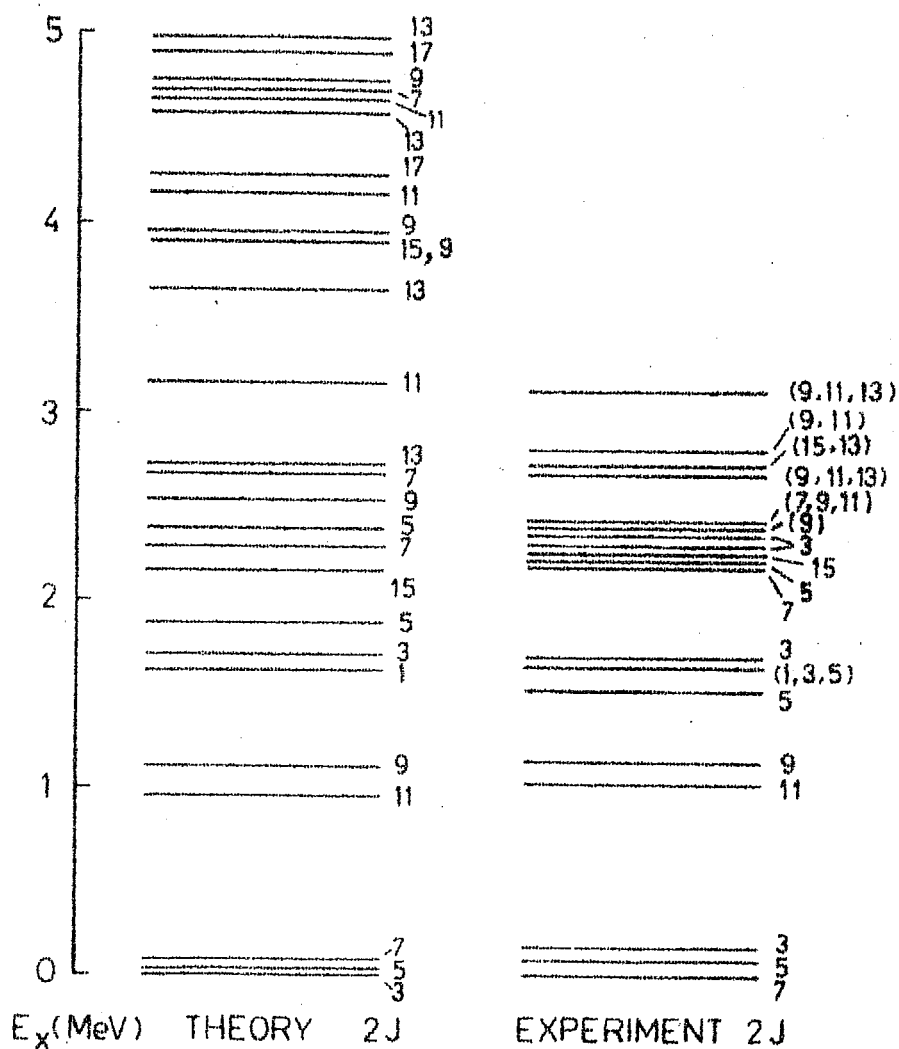


Fig. 34

Comparison of the theoretical and the experimental spectrum of ^{49}V .

The RPC calculation of Tabor and Zurmuhle¹⁴⁾ also reproduces well this band of states upto $J=11/2$ but the calculated first $J=15/2$ state is found to be about 700 keV higher than the observed state. In contrast the RPC calculation of Haas et al¹⁵⁾ provides a qualitative agreement.

It might be mentioned that our microscopic calculation gives rise to the prolate HF intrinsic state corresponding to $\delta \approx 0.11$ while that needed by Tabor and Zurmuhle correspond to $\delta \approx 0.20$.

(ii) The triplet of states observed about 1.5-1.75 MeV is well reproduced by our DCM, and RPC calculation of Tabor and Zurmuhle¹⁴⁾. These calculations favour a $J=1/2^-$ for the level observed at 1.64 MeV with probable $(1/2^-, 3/2^-, 5/2^-)$ spin assignment. The RPC calculation of Haas et al^{15, 27)} fails to reproduce the $1/2^-$ and $5/2^-$ members of this triplet.

(iii) Among the bunch of seven states observed about 2.18 to 2.41 MeV, there occur two states with $J=3/2^-$ at 2.26 and 2.31 MeV. We do not have any $J=3/2^-$ state in the calculated spectrum about 2 to 3 MeV. The present DCM calculation includes only three $J=3/2$ states. The first two calculated $3/2^-$ states are in agreement with the observed ones. Expansion of the basis space to include higher p-h

excited $K=1/2$ and $3/2$ states from which $J=1/2$ and $3/2$ states are projectable would be necessary to describe the low-spin states of ^{49}V .

The other five observed higher spin states are reasonably well reproduced within 2.2 to 2.65 MeV by the present calculation. We shall later make the association between these calculated and observed states, on the basis of the agreement of their calculated and observed decay properties. The RPC calculations do not explain these states.

(iv) In the experimental spectrum, there occurs a triplet of high-spin states at about 2.75 MeV and also a state at 3.13 MeV. Many probable spin assignments are made. In the calculated spectrum we have a $J=13/2$ state at 2.72 and an $11/2$ state at 3.15 MeV.

(v) Beyond 3 MeV, no experimental data is available.

2.3 BAND STRUCTURE

The states of the composite spectrum in ^{49}V have been analysed for the possible band structures. The Yrast band of states with $J=3/2-19/2$ is found to belong dominantly to that projected from the prolate $K=3/2$ intrinsic state. The average band mixing in all these states is about 6 per cent. The $J=1/2$ and $3/2$ states of the calculated triplet

about 1.75 MeV and the second $J=7/2$ state at 2.27 MeV are found to be mainly (96,97,87% respectively) the states projected from the prolate $K=1/2$ intrinsic state at -21.48 MeV. All other states are found to have a complex structure.

2.4 ELECTROMAGNETIC PROPERTIES

Detailed experimental information is available on the decay properties of the levels in ^{49}V . The information exists on $B(E2)$, $B(M1)$, $(E2/M1)$ mixing ratios, branching ratios and mean lifetimes of the low-lying states upto about 3 MeV.

We have compared in the tables our results (labelled DCM) with the experimental results of Haas et al^{15,27)} (Expt.I) and of Tabor and Zumuhle¹⁴⁾ (Expt.II) and with their corresponding RPC results labelled RPC I and RPC II respectively.

2.4.1 B(E2) Values

These are given in table 69 for the transitions between the members of the ground state band of states and in table 70 for the transitions from the states not belonging to the ground band. Kuo-Sones³⁾ effective charges $e_p = 1.25e$ and $e_n = 0.47e$ are employed.

Table 69

Comparison of the theoretical and experimental $B(E2)$ values for transitions within the ground state band of ^{49}V .

J_i	J_f	$B(E2, J_i \rightarrow J_f) \text{ in } e^2 \text{ fm}^4$					
		Expt. I ^a	Expt. II ^b	DCM ^c	DCM ^d	RPC I ^a	RPC II ^b
5/2	7/2			280	171	136	
3/2	7/2	197±20		245	146	146	254
	5/2			354	206	220	
11/2	7/2	144±28	172±59	206	120	123	211
9/2	7/2	58±33	106±28	72	38	49	111
	5/2	83±44	126±17	140	77	96	173
	11/2			113	70	55	
15/2	11/2	279±128	< 71	291	127	137	
13/2	11/2			31	15		
	9/2	295 ⁺²³⁰ ₋₁₂₅		181	105	120	
	15/2			42	26	29	
19/2	15/2			161	87		
17/2	13/2			54	33		
	15/2			11	5		
	19/2			26	0.82		

a. Ref. 15. b. Ref. 14. c. $e_p = 1.32e$, $e_n = 0.89e$. d. $e_p = 1.25e$, $e_n = 0.47e$.

Table 70

Comparison of the theoretical and experimental $B(E2)$ values for transitions from the states J_i at energies E_i to the states J_f at energies E_f in ^{49}V .

$E_i(\text{keV}), J_i$	$E_f(\text{keV}), J_f$	$B(E2, J_i \rightarrow J_f)$ in $e^2\text{fm}^4$		
		Expt. I ^a	DCM ⁺	RPC I ^a
1514, 5/2	0, 7/2		3.6	0.65
	90, 5/2	$> 0.3, < 435$	2.9	4.1
	153, 3/2	570^{+595}_{-260}	0.23	1.9
1643, 1/2	90, 5/2		128.6	
	153, 3/2		13.2	2.5
1661, 3/2	90, 5/2	< 122	5.7	22
	153, 3/2		0.40	8.9
	1643, 1/2		84.2	
2182, 7/2	0, 7/2		0.12	0.06
	90, 5/2	$4.2^{+8.8}_{-3.7}$	0.22	5.5
	1155, 9/2		0.42	14.5
	1661, 3/2		106.0	
2235, 5/2	0, 7/2		0.09	
	90, 5/2		3.10	
	1155, 9/2		32.4	
	1514, 5/2		123.0	

a. Ref. 15. $+ e_p = 1.25e, e_n = 0.47e$.

For the ground state band the $B(E2)$ values are also calculated with the charges³¹⁾ $e_p = 1.32e$ and $e_n = 0.89e$. These values are given in column 5 of table 69.

The experimental values of Haas et al^{15, 27)} and Tabor and Zurmuhle¹⁴⁾ are not similar. Besides, both the experimental values are uncertain.

Our DCM values are in reasonable agreement with the experiment. As seen from table 69, there does not seem to be a unique preference for either of the sets of effective charges. The RPC values of Haas et al¹⁵⁾ (RPC I) and their experimental values (Expt. I) are similar to the DCM values obtained with effective charges $e_p = 1.25e$, $e_n = 0.47e$. In contrast the calculated (RPC II) and experimental value (Expt. II) of Tabor and Zurmuhle¹⁴⁾ appear to be in optimum agreement with DCM results, using $e_p = 1.32e$, $e_n = 0.89e$.

In general, however, the $B(E2)$ values for the transitions between the members of the ground state band in ^{49}V appear to be large. The $B(E2)$ values in table 70 for the transitions from other states to the members of the ground state band are, in general, very small.

2.4.2 $B(M1)$ Values

These are given in tables 71 and 72 for the transitions between the members of the ground state band and other states upto 2.7 MeV in ^{49}V .

Table 71

Comparison of the experimental and calculated $B(M1)$ values for transitions within the ground state band of ^{49}V .

J_i	J_f	$B(M1, J_i \rightarrow J_f) \text{ in } (\text{n.m.})^2$				
		Expt. I ^a	Expt. II ^b	DCM	RPC ^a	RPC II ^b
5/2	7/2	0.12 ± 0.01	0.12 ± 0.01	0.21	0.37	0.57
3/2	5/2	0.004 ± 0.0005	0.0035 ± 0.0001	0.02	0.001	0.036
9/2	7/2	0.012 ± 0.005	0.016 ± 0.004	0.06	0.003	0.004
	11/2	< 0.90	0.65 ± 0.16	0.50	0.67	0.87
13/2 ^c	11/2		$(0.034^{+0.019}_{-0.010})$	0.0006		
	15/2	$0.39^{+0.41}_{-0.19}$	$2.4^{+1.3}_{-0.7}$	0.89	0.85	
17/2	15/2			0.15		
	19/2			0.70		

a. Ref. 15. b. Ref. 14. c. 2727 keV level of Ref. 14.

Table 72

Comparison of the experimental and calculated $B(M1)$ values for transitions from the states J_i at energies E_i to the states J_f at energies E_f in ^{49}V .

E_i (keV)	J_i	E_f (keV)	J_f	$B(M1, J_i \rightarrow J_f) \text{ in (n.m.)}^2$			
				Expt. I ^a	Expt. II ^b	DCM	RPC I ^a RPC II ^b
1514,	5/2	0,	7/2	$0.11^{+0.11}_{-0.05}$	> 0.38	0.76	0.08 1.50
		91,	5/2	$> 0.004, < 0.10$	> 0.16	0.03	0.37 0.81
		153,	3/2	$0.23^{+0.20}_{-0.09}$	> 0.90	1.03	1.09 0.08
1643,	1/2 ^c	153,	3/2	$0.34^{+0.14}_{-0.08}$	> 0.55	1.59	0.70 2.34
1661,	3/2	91,	5/2	$0.59^{+0.68}_{-0.30}$	$0.41^{+0.31}_{-0.13}$	1.56	1.37 0.40
		153,	3/2	$0.37^{+0.48}_{-0.19}$	$0.26^{+0.20}_{-0.08}$	0.84	0.72 0.12
2182,	7/2	0,	7/2	< 0.01	$0.026^{+0.016}_{-0.010}$	0.08	0.03
		91,	5/2	$0.16^{+0.10}_{-0.05}$	$0.074^{+0.041}_{-0.02}$	0.67	0.71
		1155,	9/2	$0.36^{+0.26}_{-0.16}$	$0.22^{+0.14}_{-0.08}$	1.12	1.29
2235,	5/2 ^c	0,	7/2		$(0.064^{+0.1}_{-0.03})$	0.09	
		91,	5/2		$0.25^{+0.39}_{-0.10}$	0.79	
2353,	9/2 ^c	0,	7/2		$(0.052^{+0.03}_{-0.01})$	0.57	
		1021,	11/2		$0.21^{+0.12}_{-0.06}$	0.61	

-contd-

Table 72 (contd)

E_i, J_i (keV)	E_f, J_f (keV)	$B(M1, J_i \rightarrow J_f) \text{ in } (n.m.)^2$			
		Expt. I ^a	Expt. II ^b	DCM	RPC I ^a RPC II ^b
2408, 7/2 ^c	0, 7/2		> 0.30	0.81	
	1155, 9/2		> 0.34	0.06	
2671, 11/2 ^c	1021, 11/2		> 0.79	1.76	
2727, 13/2 ^c	1021, 11/2		(0.03 ^{+0.02} _{-0.01})	0.001	
	2262, 15/2		2.4 ^{+1.3} _{-0.7}	1.02	

a. Ref. 14. b. Ref. 15. c. Spin assigned in this work.

The experimental $B(M1)$ values as given by Haas et al¹⁹⁾ and Tabor and Zurmuhle¹⁴⁾, for the transitions between the members of the ground state band (table 71) are similar. In contrast, the experimental values of Tabor and Zurmuhle and Haas et al given in table 72 for the transitions between the other low-lying states in ^{49}V are not similar and have large errors. In many cases only lower limits of $B(M1)$ values are known. In our DCM calculations values of free nucleon g -factors for the proton and neutron are used. The calculated results are in semi-quantitative agreement with the experiment. A careful remeasurement of $B(M1)$ values would be desirable.

2.4.3 (E2/M1) Mixing Ratios

These are given in table 73 for the transitions between the low-lying states upto about 2.73 MeV. The experimental and RPC values are of Haas et al¹⁵⁾. In our DCM results, $B(E2)$ values obtained with effective charges $e_p = 1.25e$, $e_n = 0.47e$ are used.

The DCM results are in agreement with both the experiment and RPC values. Significant discrepancies occur for the transitions $5/2^-$ (1514 keV) \rightarrow $3/2^-$ (153 keV) and $7/2^-$ (2183 keV) \rightarrow $7/2$ (g.s) for which the opposite signs of (E2/M1) mixing ratios are obtained in RPC and DCM calculations.

Table 73

Comparison of the experimental and calculated (E2/M1) mixing ratios for transitions between the low-lying states in ^{49}V .

E_i, J_i (keV)	E_f, J_f (keV)	(E2/M1) mixing ratios		
		DCM ^a	RPC I ^b	Expt. I ^a
90, 5/2	0, 7/2	-0.02	-0.01	
153, 3/2	90, 5/2	-0.04	0	
1155, 9/2	0, 7/2	-0.24	-1.3	$-0.78^{+0.18}_{-0.22}$, -0.68 ± 0.08
1514, 5/2	0, 7/2	0.02	0.03	
	90, 5/2	-0.12	-0.04	> 0.06 , < 1.23
	153, 3/2	0.01	-0.02	0.57 ± 0.05
1643, 1/2	153, 3/2	0.04	0.07	
1661, 3/2	90, 5/2	-0.02	-0.05	0.04 ± 0.09
	153, 3/2	0.01	0.04	
2183, 7/2	0, 7/2	-0.02	0.03	
	90, 5/2	0.01	0.05	0.09 ± 0.04
2235, 5/2	0, 7/2	-0.02		-0.17 ± 0.12 ; > 23 ; < -6.3
	90, 5/2	-0.04		-0.04 ± 0.14
2353, 9/2	0, 7/2	0.06		0.54 ± 0.23
	1021, 11/2	0.05		0.19 ± 0.16
2408, 7/2	0, 7/2	0.008		-0.02 ± 0.15
	1155, 9/2	-0.01		
2671, 11/2	1021, 11/2	0.01		0.16 ± 0.08 ; -0.73 ± 0.13
2727, 13/2	1021, 11/2	-2.18		
	2262, 15/2	0.02		

* $e_p = 1.25e$, $e_n = 0.47e$. a. Ref. 14. b. Ref. 15.

2.4.4 Mean Lifetimes

These are given in table 74. Different experiments have led to different values with large errors. Our DCM results appear to be in reasonable agreement with the experimental and RPC values, except for the $J=3/2$ state at 153 keV. For this state, the DCM calculated mean lifetime is a factor of about 3 smaller than the experiment⁶⁾. The RPC value²⁷⁾ is about twice the observed value. The discrepancy in the DCM value appears to be because of large $B(M1)$ value for the $3/2 \rightarrow 5/2$ transition.

We have also summarized in fig.35 the results of our lifetime calculations along with some of the observed values of table 74 with which they seem to be in optimum agreement.

It may be pointed out that, as seen from fig.34, there occur observed states with many probable spin assignments about 2.5 MeV. We have suggested possible spin assignments for these levels (marked with an open circle in fig.35) on the basis of overall agreement of the calculated and observed decay properties of these states. Thus in fig.35 such states are labelled by definite spin as assigned by us. We shall discuss this in some detail in the following subsection.

Table 74
Comparison of experimental and calculated mean lifetimes of the low-lying states
in ^{49}V .

Energy keV	J	τ_m (ps)					
		DCM ⁺	RPC [*]	Expt. I ^a	Expt. II ^b	Expt. III ^c	Expt. IV ^d
91	5/2	368	210	450 \pm 30	430 \pm 20 ^f	330 \pm 20 ^g	
153	3/2	8631	50000	28700 \pm 500 ^e			
1021	11/2	6.2	5.9	6.3 ^{+3.9} _{-2.5}	4.3 ^{+1.9} _{-1.1}	> 5	5.1 \pm 1.0 ^h
1155	9/2	0.53	2.6	1.65 ^{+0.48} _{-0.34}	1.06 \pm 0.15	4.3 ^{+5.6} _{-2.1}	> 0.4
1514	5/2	0.011	0.014	0.045 ^{+0.021} _{-0.018}	< 0.014		0.045 ^{+0.03} _{-0.02}
1643	1/2	0.011	0.025	0.05 \pm 0.02	< 0.03		0.06 \pm 0.03
1661	3/2	0.006	0.008	< 0.04	0.023 \pm 0.01	0.016 ^{+0.012} _{-0.008}	0.025 \pm 0.005
2183	7/2	0.007	0.007	< 0.08	0.048 \pm 0.017	0.031 \pm 0.010	
2235	5/2	0.005		< 0.05	0.018 \pm 0.011	0.021 \pm 0.008	0.03 ^{+0.030} _{-0.015}
2263	15/2	2.2	2	0.93 ^{+0.55} _{-0.28}	> 3.84	0.064 ^{+0.025} _{-0.016}	0.045 ^{+0.030} _{-0.015} , 3.5 ^h
2363	9/2	0.006		< 0.07	0.048 \pm 0.017		
2408	7/2	0.003		< 0.03	< 0.011	< 0.01	
2670	11/2	0.005		< 0.03	< 0.016		
2727	13/2	0.40		0.35 ^{+0.15} _{-0.11}	0.138 ^{+0.058} _{-0.049}		

⁺ $e_p=1.25e$, $e_n=0.47e$.

^{*} Ref. 27. a. Ref. 15. b. Ref. 14. c. Ref. 20. d. Ref. 21

e. Ref. 6. f. Ref. 17. g. Ref. 22. h. Ref. 18.

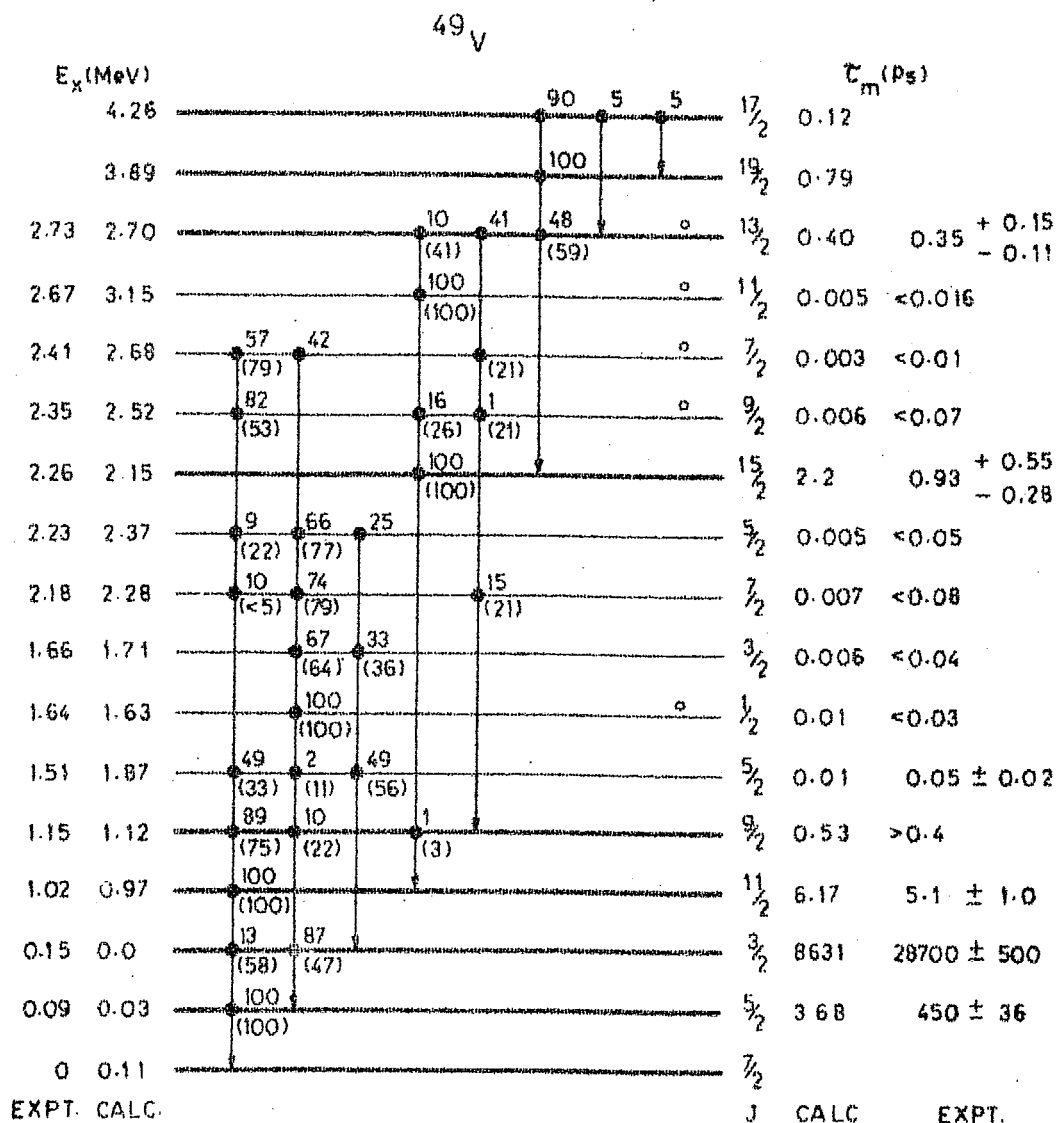


Fig.35

Comparison of the calculated and observed mean lifetimes and branching ratios in ^{49}V . The numbers on the top of the states are the calculated decay intensities while those below in brackets are the corresponding observed ones. The states drawn in thick lines are the members of the ground state band. For the states marked with open circles, the spin assignments have been made in this work. For a discussion of these states see subsec.2.4.5.

2.4.5 Branching Ratios

These are given in fig.35. The states drawn therein by thick lines belong to the ground state band. We have associated our calculated states with the corresponding observed states for calculations of these decay properties. The DCM calculated branching intensities are given on top of a state, marked with a filled circle, from which the decay is considered to the state where the arrow ends. The observed^{4,14,15)} values are given immediately below in parenthesis. The agreement between the two is in general good. For the $J=3/2^-$ state observed at 0.15 MeV our calculated branches are in disagreement with the corresponding observed branches, mainly because of the disagreement in the $B(M1)$ values.

For some of the observed levels (indicated by an open circle) unique spin assignments have not been made. In fig. 35 we have suggested spin assignments to some of these levels on the basis of the overall agreement of energy, branching ratios and lifetimes of our calculated states, with those of the corresponding observed states. We shall now discuss some of these states.

1.64 MeV Level

This level is assigned¹⁴⁾ $J=1/2^-, 3/2^-$ or $5/2^-$ and is

observed to decay only to $J=5/2^-$ member of the ground state triplet with a mean lifetime of less than 0.03 ls. In the calculated spectrum (fig.34) the only state that has decay properties consistent with these observations is the $J=1/2^-$ at 1.63 MeV. The calculated lifetime for its 100% branch to 91 keV $5/2^-$ state is 0.01 ps. Thus we suggest $J=1/2^-$ for this 1.64 MeV observed level.

2.35 MeV Level

Tentative spin assignments ($9/2^-$, $11/2^-$) are made by Tabor and Zurmuhle¹⁴⁾. They observed its decay, $57.5 \pm 4.8\%$ and $42.5 \pm 4.8\%$ to the $J=7/2$ ground state and $J=11/2^-$ state at 1.021 MeV respectively. Mean lifetime of 0.048 ± 0.017 ps is measured. In contrast to these observations, Haas et al¹⁵⁾ observed its decay branches 53:21:26 to $J=7/2$, $11/2$ and $9/2$ at 0.0, 1.021 and 1.155 MeV, with a mean lifetime of less than 0.07 ps. Thus these two measurements for this observed level are not similar.

Our calculated $J=9/2$ state at 2.52 MeV has decay properties in reasonable agreement with the observed decay properties of the 2.35 MeV level.

2.41 MeV Level

This level is assigned $7/2^-$ or $9/2^-$ by Tabor and Zurmuhle¹⁴⁾ and is observed to have 83:17 percent decay

branches to $7/2$ ground state and $9/2$ at 1.155 MeV respectively. Haas et al¹⁵⁾ observed similar decay intensities but assigned $7/2^+$, $9/2^-$ or $11/2^-$ spin values. The decay properties of our calculated $J=7/2^-$ state at 2.68 MeV are in qualitative agreement with those of the observed 2.41 MeV level.

There does not occur any other $J=7/2$, $9/2$ or $11/2$ state in the calculated spectrum that has decay properties similar to those of the 2.41 MeV observed level. Also, in the experimental spectrum no other $J=7/2$ state is observed. It is thus likely that the calculated 2.68 MeV $J=7/2$ state may be the one corresponding to 2.41 MeV observed level.

2.67 MeV Level

This state is excited in (α, n) reaction of Sawa et al¹³⁾ and (α, p) reaction of Haas et al¹⁵⁾. Spins $9/2^-$ or $11/2^-$ are suggested. Tabor and Zurmuhle¹⁴⁾ have suggested spins $9/2^-$, $11/2^-$ or $13/2^-$.

Our calculated $J=11/2^-$ state at 3.15 MeV is the only state that has decay properties, as seen from fig.35, in agreement with the observed properties.

2.73 MeV Level

This state is assigned $13/2^-$ or $15/2^-$ by Sawa et al¹³⁾

and by Tabor and Zurmuhle¹⁴⁾. Branching intensities 59:41 percent for the decays to 2.26 and 1.02 MeV state are observed¹⁴⁾ with a mean lifetime of $0.138^{+0.058}_{-0.049}$ ps. Haas et al¹⁵⁾ have assigned $J=15/2^-$ for this observed level. Mean lifetime of $0.35^{+0.15}_{-0.11}$ ps is measured for its 100% decays to the 2.63 MeV level.

Thus the experimental data for this level is conflicting.

Our calculated $J=13/2^-$ member of the ground state band at 2.70 MeV has decay properties in reasonable agreement with the measurements of Tabor and Zurmuhle. We would like to assign $J=13/2^-$ for this level.

2.4.6 Static Moments

Table 75

Static moments of the ground state triplet in ^{49}V .

J	E_J keV	$Q(\text{efm}^2)$			μ (n.m.)				
		DCM ⁺	RPCI ^a	MS ^c	Expt	DCM	RPCI ^a	RPCII ^b	MS ^c
7/2	0	-10.6	-12.4	10	4.46 ± 0.05^d	4.0	5.09	5.45	4.71
5/2	90	-9.7	-5.9			2.87	3.45		
3/2	153	15.7	13.8		2.37 ± 0.12^e	2.42	3.00		

+ $e_p = 1.25e$, $e_n = 0.47e$.

a. Ref. 27, 15. b. Ref. 14. c. Ref. 32. d. Ref. 33. e. Ref. 6

In table 75 are given the static electric quadrupole and magnetic dipole moments of the ground state triplet of states in ^{49}V . The quadrupole moments are not measured so far. The RPC values of the quadrupole moments are in general smaller than ours but are of the same phase. Malik and Scholz³²⁾ on the other hand predict the sign opposite to ours for the ground state quadrupole moment. Our magnetic moments are in much better agreement with the observed values than the RPC values.

REFERENCES

1. S.Raman, Nucl. Data Sheets 4 (1970) 397.
2. J.C. Legg, D.G. Megli, D.R. Abraham, L.D. Ellsworth
S. Hechtel, Phys. Rev. 186 (1969) 1138.
3. P. Blasi, P.R. Maurenzig, R.A. Ricci, N. Taccetti,
R. Giacomich, M. Lagonegro and G.Poiani, Nuo.Cim.51B
(1967) 241.
4. P. Blasi, M. Mando, P.R.Maurenzig and N. Taccetti,
Nuo.Cim.4A (1971) 61.
5. J.G. Malan, E. Barnard, J.A.M. deVilliers, J.W. Tepel
and P. Van der Merwe, Nucl. Phys. A195 (1972) 596.
6. G.B. Vingiani, C. Rossi-Alvarez, A. Buscemi, F. Brando-
lini and F. Cervellera, Phys. Lett.40B (1972) 638.
7. J.N. Mo, B. Cujec, R. Dayras, I.M. Szoghy and M.Toule-
monde, Nucl. Phys. A147 (1970) 129.
8. G. Brown, A. MacGregor and R. Middleton, Nucl. Phys.
77 (1966) 385.
9. C.St.Pierre, P.N. Maheshwari, D. Doutriaux and
L. Lamarche, Nucl. Phys. A102 (1967) 433.
10. D. Bachner, R. Santo, H.H Duhm, R.Bock and S.Hinds,
Nucl.Phys. A106 (1968) 577.
11. D.J. Pullen, B. Rosner and O. Hansen, Phys. Rev.177(1969)
1568.

12. B. Cujec and I.M. Szoghy, Phys. Rev.179 (1969) 1060.
13. Z.P. Sawa, J. Blomqvist and W. Gullholmer, Nucl.Phys. A205 (1973) 257.
14. S.L. Tabor and R.W. Zurmuhle, Phys. Rev.C10 (1974) 35.
15. B. Haas, J. Chevallier, J. Britz and J. Styczen, Phys. Rev. C11 (1975) 1179.
16. W.M. Currie, Nucl. Phys. 47 (1963) 551.
17. H.C. Cheung and S.K. Mark, Nucl.Phys.A176 (1971) 219.
18. B.A. Brown, D.B. Fossan, J.M. McDonald and K.A. Snover, Phys. Rev. C9 (1974) 1033.
19. B. Haas, J. Chevallier, N. Schulz, J. Styczen and M. Toulemonde, Phys. Rev. C11 (1975) 280.
20. C.M. Rosza, R.G. Arnes, B.J. Bruner, S.E. Caldwell and J.W. Smith, Bull.Am. Phys. Soc. 17 (1972) 536.
21. A. Kiuru, Z. Phys. 251 (1972) 93.
J. Britz, J. Chevalier, B. Haas and J. Styczen, Proc. of the Int.Conf.Nucl.Phys. Munich, 1973, ed.by J.de Boer and H.J. Mang (North Holland/American Elsevier, 1973) Vol.I, P.210.
22. O.B. Okon, H. Bakhru, M.K. Dewanjee and I.L. Preiss, Phys. Rev. C7 (1973) 239.
23. S.L. Tabor, L.K. Fifield, K.G. Young Jr. and R.W. Zurmuhle, Phys. Rev. C10 (1974) 1484.
24. S.V. Jackson, E.A. Henry and R.A. Meyer, Phys. Rev. C12 (1975) 2094.
25. J.D.McCullen, B.F.Bayman and L.Zamick, Phys.Rev.134(1964) B515.

26. F.B. Malik and W. Scholz, *Phys. Rev.* 150 (1966) 919.
27. B. Haas, P. Taras and J. Styczen, *Nucl. Phys.* A246 (1975) 141.
28. A.K. Dhar, D.R. Kulkarni and K.H. Bhatt, *Proceedings of the International Conference on Nuclear Structure and Spectroscopy, 1974*, ed. H.P. Blok and A.E.L. Dieperink (Scholar's Press, Amsterdam, 1974), p.59.
29. A.K. Dhar, S.B. Khadkikar, D.R. Kulkarni and K.H. Bhatt, *Proceedings of the International Conference on Gamma-Ray Transition Probabilities, Delhi, 1974*, ed. by S.C. Pancholi and S.L. Gupta (Delhi Univ. Press, to be published).
30. T.T.S. Kuo and E. Osnes, *Phys. Rev.* C12 (1975) 309.
31. A.K. Dhar, unpublished.
32. F.B. Malik and W. Schoz, *Phys. Rev.* 147 (1966) 836; 153 (1967) 1071; 176 (1968) 1355.
33. V.S. Shirley, *Hyperfine Interactions in Excited Nuclei*, Rehovot, Vol.4, ed. G. Goldring and R. Kalish (Gordon and Breach, Paris, New York, 1971) p.1262.

CHAPTER 10

THE NUCLEUS ^{51}V

1. INTRODUCTION

1.1 Experimental Data

The nucleus ^{51}V has been studied¹⁾ by stripping reactions $^{48}\text{Ti}(\alpha, p)$, $^{50}\text{V}(d, p)$, $^{50}\text{Ti}(^3\text{He}, d)$, pick-up reactions $^{52}\text{Cr}(d, ^3\text{He})$, $^{52}\text{Cr}(t, \alpha)$, $^{53}\text{Cr}(d, \alpha)$ inelastic scattering experiment involving the reactions $^{51}\text{V}(e, e')$, $^{51}\text{V}(n, n')$, $^{51}\text{V}(n, n'\gamma)$, $^{51}\text{V}(p, p')$, $^{51}\text{V}(d, d')$ and $^{51}\text{V}(\alpha, \alpha')$ and by Coulomb excitation. Horoshko et al²⁾ examined this nucleus by the reaction $^{48}\text{Ti}(\alpha, p\gamma) ^{51}\text{V}$ at 14 MeV and by the Coulomb excitation of ^{51}V by ^{32}S ions at 60 MeV, and deduced the energy spectrum, $B(M1)$, $B(E2)$, $(E2/M1)$ mixing ratios and branching ratios for decays between some of the low-lying states of this nucleus. Goodman and Donahue³⁾ also measured the electromagnetic properties of the low-lying states upto about 2.7 MeV in ^{51}V populated in $^{48}\text{Ti}(\alpha, p\gamma)$ reaction at 9.2 MeV incident energy. Lifetimes of some of the excited states were measured by doppler-shift attenuation method. A number of measurements⁴⁾ have been made for the determination of the lifetime of its first excited state at 0.32 MeV. The lifetime of the $J=15/2^-$ state at 2.70 MeV in ^{51}V

has recently been measured by Poletti et al⁵⁾ following the reaction $^{48}\text{Ca} (^6\text{Li}, 3n)$ at 26 MeV incident beam energy. The high spin states of ^{51}V upto about 6.25 MeV have been measured by Gogelein et al⁶⁾ in the heavy ion induced reaction $^{48}\text{Ca} (^7\text{Li}, 4n) ^{51}\text{V}$ and upto about 4 MeV by Harrach⁷⁾ in (n, γ) reaction.

1.2 Previous Calculations

Theoretically, the nucleus ^{51}V has been considered to have a relatively simple shell model structure with three protons outside ^{48}Ca closed core. The $(f_{7/2})^3$ calculations^{8,9)} have been reasonably successful in describing the spectrum of the low-lying states of this nucleus. Using $(f_{7/2})^3$ wave functions, Brown et al¹⁰⁾ calculated the proton effective charges that would be necessary to fit the observed $B(E2)$ values between the low-lying states of ^{51}V having a dominant $(f_{7/2})^3$ structure. These effective charges vary between $e_p = 1.72 \pm 0.04e$ to $1.94 \pm 0.07e$. In the pure $(f_{7/2})^3$ configuration, the $M1$ strengths are strictly forbidden. However $M1$ transitions, though hindered, have been observed²⁾ in ^{51}V (as also in ^{43}Ca , ^{53}Mn which have a similar $(f_{7/2})^{\pm 3}$ structure according to MBZ model). This indicates the necessity of other fp shell configurations for the description of low-lying states in ^{51}V . Auerbach¹¹⁾ and Lips and McEllistrem¹²⁾ performed extended calculation for ^{51}V to

include besides pure $(f_{7/2})^3$ configuration the $(f_{7/2}^2 p_{3/2})$ configuration. The interaction matrix elements were determined by a least squares fit of calculated to observed level energies. Lips and McEllistrem¹²⁾ also included $(f_{7/2}^2 f_{5/2})$ configuration by taking the matrix elements involving the $f_{5/2}$ orbit from a surface delta interaction and from the effective interaction of Kuo and Brown. Considerable improvement over the $(f_{7/2})^3$ configuration calculation was obtained.

Horoshko et al²⁾ performed $(fp)^3$ shell model calculation for ^{51}V . ^{48}Ca was regarded as the closed core and the corresponding Kuo-Brown two body effective interaction¹³⁾ employed. The spectrum and transitions rates were well accounted for. Proton effective charges $e_p = 1.57e$ was used in the calculation of E2 transition rates.

It must be pointed out that in all these shell model calculations, except the one based on pure $(f_{7/2})^3$ configuration, the calculated states do not have definite isospin. Osnes and Warke^{14,15)} constructed good isospin states in the $(f_{7/2})^{11}$ and $[(f_{7/2})^{10} (p_{3/2})]$ configuration and showed that although the E2 transition rates between the levels dominated by pure $(f_{7/2})^n$ configuration are only weakly affected, the M1 transitions are rather strongly affected by this configuration mixing.

Scholz and Malik¹⁶⁾ performed RPC calculation for ^{51}V . The calculated spectrum is found to be in qualitative agreement with the experiment for large deformation parameters $\beta = -0.32$ and for $\beta = 0.20$. The calculated $B(M1)$ values are in significant disagreement with the observed values.

It is seen that two opposing features about the structure of ^{51}V emerge from the observed^{2,3)} $B(E2)$ and $B(M1)$ values for the transitions between the low-lying states of this nucleus. The highly retarded $M1$ transitions in ^{51}V indicate the dominance of the $(f_{7/2})^{11}$ configuration. On the other hand the large proton effective charges needed in the $(f_{7/2})^{11}$ configuration to fit the observed $B(E2)$ values suggest a substantial deformation. It is therefore of interest to see if the calculations using HF theory can explain these apparently contradictory features of ^{51}V structure.

The HF theory takes into account partially the effects of field producing components of the effective interaction between the nucleons as well as the role of the single particle energies in determining the dominant configurations. It is therefore likely that the deformed HF calculations, within $(fp)^{11}$ space, with a "suitable" effective interaction (like MWH2) might lead to the HF intrinsic state of smaller deformation with dominant $f_{7/2}$ component. It is, however, commonly felt that the projected HF theory is likely to be useful only for the nuclei with large deformations and hence

well defined ground state shapes. It thus appears that for a "mildly" deformed nucleus like ^{51}V the projected HF calculations would not describe well its low-lying observed states. It is therefore of interest to examine the nucleus ^{51}V in the framework of DCM calculations and see how far the observed data can be explained.

2. PRESENT CALCULATION

The present study of ^{51}V is primarily motivated to see how well our DCM calculations can account for the observed^{2,3,6,7)} properties of the Yrast band of states in this nucleus. Thus the present aim is somewhat conservative than what we had for the description of other fp shell nuclei.

Our limited aim in the description of ^{51}V is due to the limitations of the chosen MWH2 interaction¹⁷⁾. It is already mentioned in Chapter 1 that although this interaction reproduces the spherical HF solution for ^{56}Ni and is consistent with the experimental data on $B(E2, 0^+ \rightarrow 2^+)$ transitions in even-even nuclei it fails to reproduce the single particle or hole energies with respect to closed ^{56}Ni ; for instance in ^{57}Ni , this interaction gives $1f_{5/2}$ state lower than $2p_{3/2}$ single particle state. It is therefore expected that the observed states that have dominant contributions arising from the excitations of particles from the

$f_{7/2}$ subshell, would not be correctly described by the chosen MWH2 interaction. However, such defects in the interaction are not very serious for the description of states belonging dominantly to $(f_{7/2})^n$ configuration.

2.1 STRUCTURE OF HARTREE FOCK STATES OF ^{51}V

The deformed HF calculations in $(fp)^{11}$ configuration space, with MWH2 interaction gives¹⁸⁻²⁰⁾ near degenerate multiple solutions for ^{51}V . The prolate $K=3/2$ and the oblate $K=5/2$ HF intrinsic states have energy $E_K = -25.4$ MeV and quadrupole moments $Q_K \sim \pm 11 b^2$. In addition, the interaction yields a highly deformed prolate $K=3/2$ HF intrinsic state at -24.1 MeV with $Q_K = 31.5 b^2$.

In the lowest energy prolate and oblate HF intrinsic states the neutron $(f_{7/2})^8$ sub-shell is almost full. The structure of this prolate $K=3/2$ intrinsic state corresponds to deformation δ_1 sketched in fig.36. The details of the structure of the occupied and a few unoccupied single particle prolate and oblate intrinsic states are given in tables 76 and 77 respectively. It is seen that the HF energy gaps for the proton is smaller than for the neutron.

It is interesting to compare the intrinsic quadrupole moments of ^{51}V obtained in the $(fp)^{11}$ and $(f_{7/2})^{11}$ configuration spaces.

Table 76

Structural and spectral details of the occupied and some of the unoccupied proton and neutron orbitals of the PROLATE HF state of ^{51}V ($E_{\text{HF}} = -25.35$ MeV, $Q_{\text{HF}} = 11.04$ b 2). For other details see caption for table 1.

	k	e_k (MeV)	q_k (b 2)	$c_{\frac{1}{2}k}$	$c_{\frac{3}{2}k}$	$c_{\frac{5}{2}k}$	$c_{\frac{7}{2}k}$
P R O T O N S	1/2	-7.92	2.87	0.036	-0.124	-0.045	0.991
	-1/2	-7.60	3.24	-0.079	-0.171	0.127	0.974
	3/2	-6.69	1.70		-0.064	-0.097	0.993
	5/2	-5.67	-0.34			-0.045	0.999
	7/2	-5.00	-3.0				1.0
	1/2	-1.56	4.35	-0.413	0.490	0.760	0.110
N E U T R O N S	1/2	-5.75	3.23	0.072	-0.178	-0.084	0.978
	-1/2	-5.29	3.24	-0.075	-0.178	-0.097	0.976
	3/2	-4.58	1.77		-0.079	-0.104	0.991
	-3/2	-3.98	1.70		-0.070	0.083	0.994
	5/2	-3.06	-0.35			-0.041	0.999
	-5/2	-2.68	-0.36			0.033	0.999
	7/2	-2.05	-3.0				1.0
	-7/2	-1.85	-3.0				1.0
	1/2'	1.27	3.93	-0.485	0.692	0.494	0.204
	1/2''	2.85	1.31	-0.217	-0.655	0.722	0.041

Table 77

Structural and spectral details of the occupied and some of the unoccupied proton and neutron orbitals of the OBLATE HF state of ^{51}V ($E_{\text{HF}} = -25.41$ MeV, $Q_{\text{HF}} = -10.66 \text{ b}^2$). For other details see caption of table 1.

	k	e_k (MeV)	q_k (b^2)	$c_{\frac{1}{2}k}$	$c_{\frac{3}{2}k}$	$c_{\frac{5}{2}k}$	$c_{\frac{7}{2}k}$
P R O T O N S	7/2	-7.65	-3.0				1.0
	-7/2	-8.19	-3.0				1.0
	5/2	-6.36	-0.79			0.150	0.989
	-5/2	-6.81	-0.75			-0.136	0.991
	3/2	-5.77	0.47		0.152	0.110	0.982
	1/2	-5.33	1.44	0.020	0.120	0.052	0.991
	5/2	-1.05	-2.21			0.989	-0.150
N E U T R O N S	7/2	-5.81	-3.0				1.0
	-7/2	-5.35	-3.0				1.0
	5/2	-4.20	-0.69			0.111	0.994
	-5/2	-3.45	-0.75			-0.136	0.991
	3/2	-3.00	0.59		0.138	0.063	0.988
	-3/2	-2.65	0.53		0.154	-0.052	0.987
	1/2	-2.39	1.23	0.038	0.162	0.005	0.986
	-1/2	-2.39	1.22	-0.041	0.161	-0.020	0.986
	3/2	1.91	-1.70		0.974	-0.191	-0.124
	1/2	2.49	-1.49	0.721	0.663	0.144	-0.138

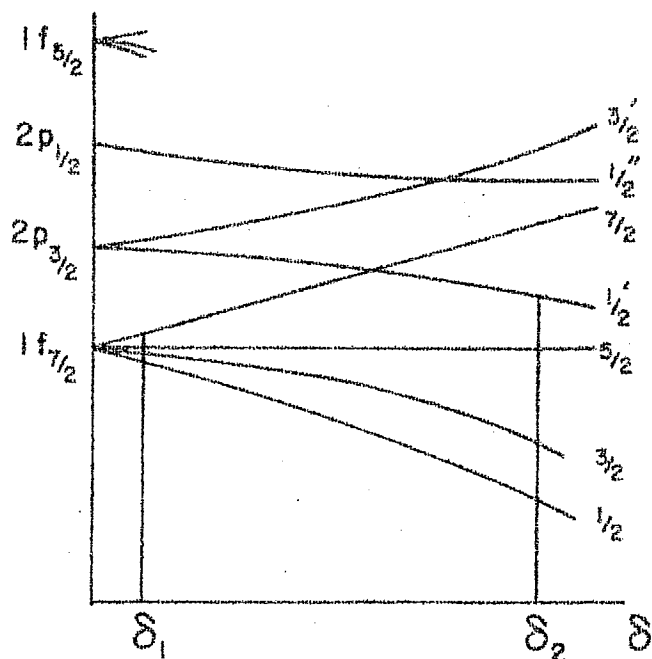


Fig. 36.

It is seen from table 76 that in $(fp)^{11}$ configuration the amplitude of the fp shell states other than the $f_{7/2}$ state in the prolate $K=3/2$ HF intrinsic state is quite small. The quadrupole moments of the proton and neutron orbitals are listed in column 3 of table 76. The corresponding proton and neutron quadrupole moments in the $(f_{7/2})^{11}$ configuration can be obtained by regarding the components in the occupied proton and neutron orbitals of table 76 to be

$$c_{jk} = \begin{cases} 1 & \text{if } j=7/2 \\ 0 & \text{if } j \neq 7/2 \end{cases}$$

The total contribution to the mass quadrupole moment Q due to protons and neutrons in these configurations is given in the table below.

Q	$(fp)^{11}$	$(f_{7/2})^{11}$
$Q_P(b^2)$	7.8	5.6
$Q_N(b^2)$	3.2	0.0
$Q(b^2)$	11.0	5.6

It is seen that in the $(fp)^{11}$ configuration not only proton contribution is larger than that in $(f_{7/2})^{11}$ configuration, but the neutrons also contribute substantially to the mass quadrupole moment of the lowest energy prolate $K=3/2$ HF intrinsic state of ^{51}V . Thus the HF state of ^{51}V besides having dominant $f_{7/2}$ component in its wave function, also brings in sizeable quadrupole moment necessary for the description of $B(E2)$ values observed between its dominant $(f_{7/2})^{11}$ multiplet of states.

The inappropriateness of the present effective interaction is reflected in the structure of first unoccupied $k=1/2$ orbit for the protons in table 76. Its major component is $f_{5/2}$ and not $p_{3/2}$ as expected on the basis of systematics of the single particle energies.

The highly deformed $K=3/2$ intrinsic state has the neutron occupancy ($\pm 1/2$, $\pm 3/2$, $\pm 5/2$, $\pm 1/2'$) and corresponds to an almost asymptotically deformed structure of ^{51}V . This is indicated in fig.36 by δ_2 .

2.2 "SPHERICAL" STATES IN ^{51}V

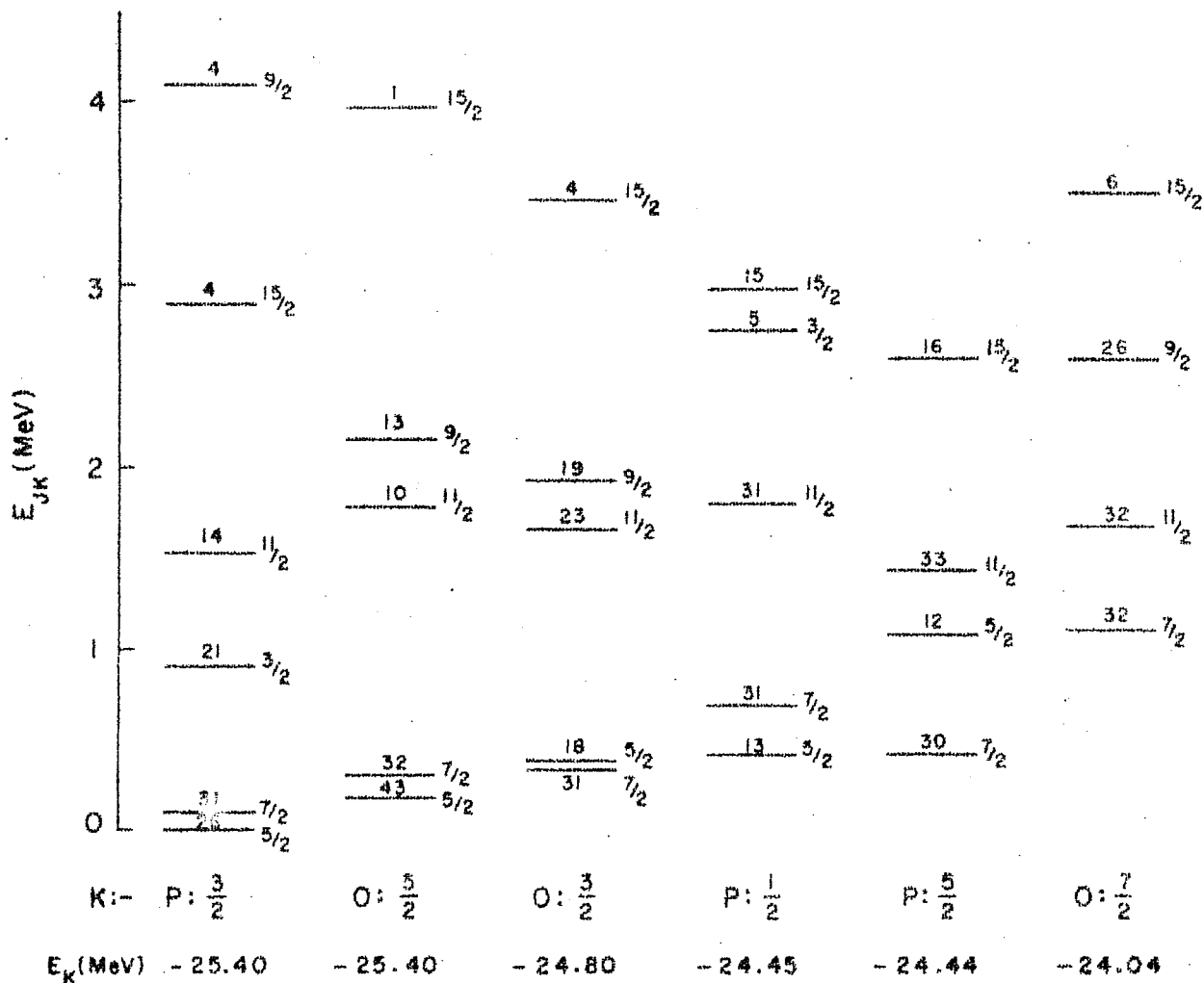
2.2.1 THE ENERGY SPECTRUM

For the description of the "spherical states" that have a dominant $(f_{7/2})^{11}$ component of ^{51}V we have included in the present calculation four additional proton excited intrinsic states based on the lowest energy prolate and oblate HF states of ^{51}V . The details of these intrinsic states along with the energies and K-values of prolate and oblate HF states are given in table 78. For all the six states of

Table 78

Energies and K-values of the intrinsic states included in the calculation of 'spherical' states of ^{51}V .

Shape	Hole k_i	Prolate k_m	K	E_K (MeV)
Prolate	(HF STATE)		3/2	-25.4
	p -1/2	p -3/2	1/2	-24.45
	p 3/2	p 5/2	5/2	-24.44
Oblate	(HF STATE)		5/2	-25.4
	p 5/2	p 3/2	3/2	-24.8
	p -7/2	p -5/2	7/2	-24.04



PROJECTED SPECTRA

Fig.37

Energy spectra of the states projected from prolate (P) and oblate (O) intrinsic states of ^{51}V . The K -values and energies of these intrinsic states are given at the bottom. The numbers on the right of projected states are their J values while those on the top are their intensities in their corresponding intrinsic states.

table 78, isospin $T=5/2$ is the dominant component while the components with $T \gg 7/2$ are negligibly small.

In the $(f_{7/2})^{11}$ configuration of ^{51}V there exists only one state of each angular momentum. It is therefore expected that the states projected from either of the intrinsic states of table 78 would provide an adequate description of the "spherical" states of ^{51}V . This is almost true except for the $J=9/2$ and $3/2$ states projected from the prolate and oblate intrinsic states of table 78.

In fig.37 we have plotted the energy spectrum of the states projected from the different intrinsic states of table 78. The number on top of each of these states is the intensity $|a_{JK}|^2$ of that state in its corresponding intrinsic state.

It is interesting to observe from this figure that in spite of the $(f_{7/2})^{11}$ dominance in these intrinsic states, none of the prolate ($P:3/2, P:1/2$ or $P:5/2$) intrinsic states contains $(f_{7/2})^3 J=9/2$ state. The $J=9/2$ state projected from the prolate $K=3/2$ HF intrinsic state is at 4.10 MeV with 4 percent intensity. This $J=9/2$ state has $(f_{7/2})^2 P_{3/2}$ dominant structure. In a similar manner the oblate intrinsic states do not contain any $(f_{7/2})^3 J=3/2$ state. In contrast to these the $(f_{7/2})^3 J=9/2$ state is contained in the oblate states ($O:5/2$ or $O:3/2$) while the $(f_{7/2})^3 J=3/2$ state is

contained only in the prolate $K=3/2$ ($P:3/2$) intrinsic state.

It is thus clear that for the overall description of the dominant $(f_{7/2})^{11}$ multiplet of states in ^{51}V , it is necessary to consider the mixing of both prolate and oblate projected states. Neither of them by themselves alone would provide the agreement with the experimental spectrum of ^{51}V .

As a consequence of the $(f_{7/2})^{11}$ configuration in the intrinsic states of table 78, the states projected from these various intrinsic states have about 96% overlap with each other. This renders the basis space highly overcomplete. We shall, however, later show that the inclusion of the p-h excited intrinsic state of table 78, improves appreciably the energies of the $J=9/2$ and $15/2$ states and also slightly the agreement for M1 transitions. The Hamiltonian matrix is diagonalized in the basis of states projected from the six intrinsic states of table 78, after taking care of their nonorthogonality.

The spectrum so obtained is compared with the experiment^{2,3,6,7)} in fig.38A. The agreement between the two upto $J=15/2$ at 2.70 MeV is good except that the $7/2$ and $5/2$ states have flipped in the calculated spectrum. Above 2.5 MeV there exist in the experimental spectrum the states that do not have dominant $(f_{7/2})^3$ structure.

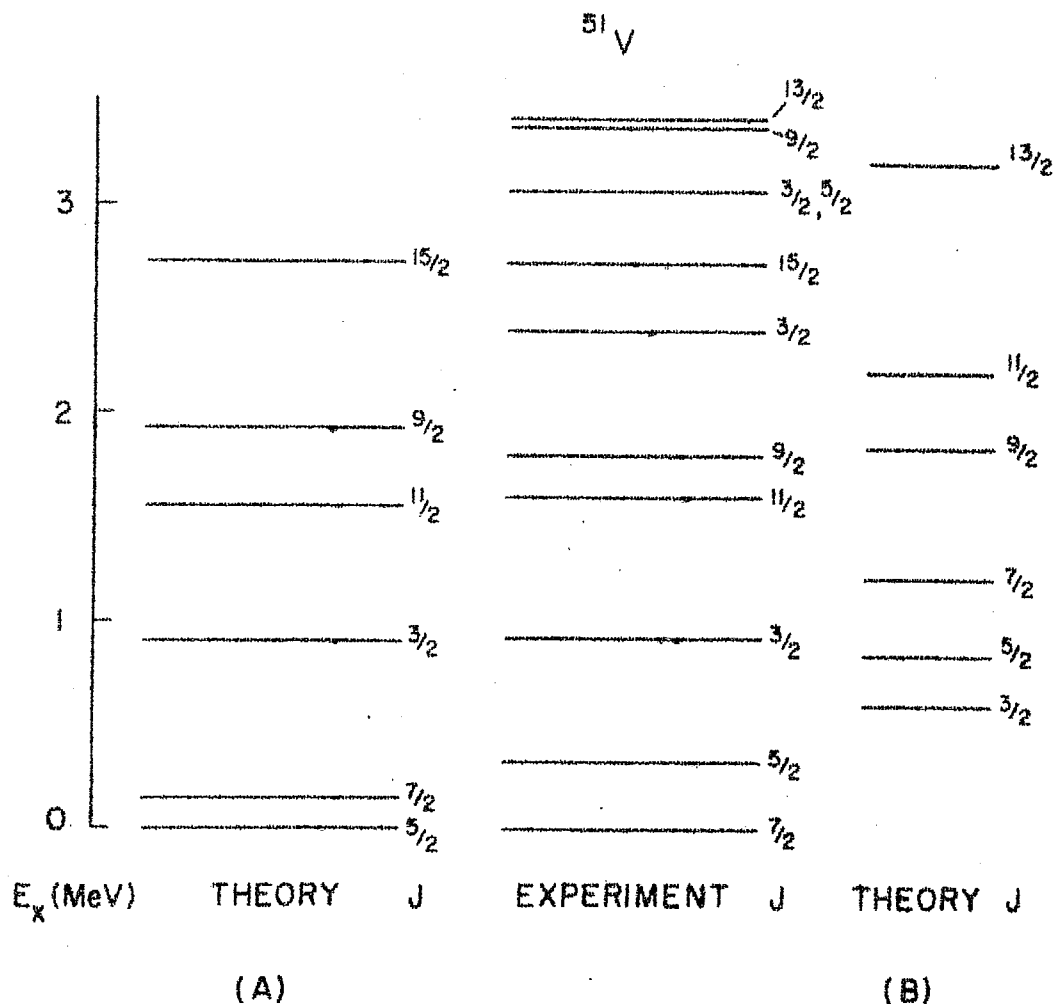


Fig.38

Comparison of the theoretical and the experimental spectrum of ^{51}V . At A are plotted the "spherical" states of ^{51}V . See subsec.2.2 for a discussion on these states. A highly deformed $K=3/2$ band of states that is predicted to exist, is plotted at B. See subsec.2.3 for a discussion on this band.

It might be mentioned that the band mixing calculation¹⁸⁻²⁰⁾ involving prolate and oblate HF states alone also provide a reasonable agreement with the experimental spectrum of ^{51}V . The only major discrepancy occurs for the $J=9/2$ and $15/2$ states which are reproduced 300 keV higher than their observed energies.

2.2.2 ELECTROMAGNETIC TRANSITIONS

We shall now present the results of the electromagnetic properties of the states of ^{51}V described above. For the E2 transitions, effective charges²¹⁾ $e_p=1.32e$, $e_n=0.89e$ and Kuo-Osnes charges²²⁾ $e_p=1.25e$, $e_n=0.47e$ are used, while for M1 transitions free nucleon g-factors for the proton and neutron are considered. We have also compared our full DCM results with the results of only prolate-oblate (labelled PO) mixing calculations and also with the $(f_{7/2})^3$ and $(fp)^3$ calculation and RPC calculation of Scholz and Malik.

2.2.2.1 B(E2) Values

These are given in table 79. Our DCM calculated values in col,5, obtained with effective charges $e_p=1.32e$, $e_n=0.89e$ are in remarkable agreement with the experiment^{2,3)}. Kuo-Osnes charges provide only a qualitative agreement. The $(fp)^3$ calculation of Horoshko et al²⁾ uses $e_p=1.57e$ while

Table 79

Comparison of calculated and experimental $B(E2)$ values for transitions between the low-lying states in ^{51}V .

J_i	J_f	$B(E2, J_i \rightarrow J_f) e^2 \text{fm}^4$					
		expt ^a	PO [*]	DCM [*]	DCM ⁺	(fp) ^{3a}	(f _{7/2}) ^{3a}
5/2	7/2	154±7.6 ^b	160.6	164.4	125.2	169	174.6
3/2	7/2	72±13 ^b	79.5	78.7	61.0	70.9	61.2
	5/2	107±9	93.0	92.2	70.0	106.7	44.9
11/2	7/2	78±14 ^b	88.0	90.0	68.3	80.4	79.3
9/2	7/2	27.5±6.3 ^b	24.0	19.6	13.8	26.8	29.5
	5/2	27.5±6.6 ^b	35.0	24.7	17.6	19.3	27.6
	11/2		59.3	47.3	36.0		
15/2	11/2	66±5 ^c	78.0	63.6	47.5		

a. Ref.2. b.Ref.3. c.Ref.10. * $e_p=1.32e$, $e_n=0.89e$
 + $e_p=1.25e$, $e_n=0.47e$.

in (f_{7/2})¹¹ calculation²⁾ $e_p=1.77e$ is required. The $B(E2)$ value for 3/2→5/2 is poorly described by the pure (f_{7/2})¹¹ calculation. The $B(E2)$ values given in column 4 (labelled PO) are similar to those obtained in the DCM calculation.

It is interesting to note that the deformation brought in by the HF intrinsic state helps substantially in reproducing the $B(E2)$ values in ^{51}V with the reasonable effective charges $e_p = 1.32e$, $e_n = 0.89e$. These charges were found to give good agreement²³⁾ for the E2 transitions in other fp shell nuclei as well.

2.2.2.2 $B(M1)$ Values

These are given in table 80. The $B(M1)$ values in ^{51}V are highly hindered and are strictly forbidden in $(f_{7/2})^3$ configuration. Our DCM calculation provides an improved agreement with the experiment²⁾ than the PO or $(fp)^3$ calculations²⁾.

Table 80

Comparison of calculated and experimental $B(M1)$ values for transitions between the low-lying states in ^{51}V .

J_i	J_f	$B(M1, J_i \rightarrow J_f) \times 10^4 (\text{n.m.})^2$					
		Expt. ^a	PO	DCM	$(fp)^3$ ^a	RPC ^b $\beta = -0.32$	RPC ^c $\beta = 0.20$
5/2	7/2	49 \pm 4	14.7	42	12.7	0.36	2100
3/2	5/2	{ 36 \pm 0.18 ^c 29 \pm 4	78	50	2.02	1200-4900	8900
9/2	7/2	4.7 \pm 1.6	0.7	5.2	1.96	370	350
	11/2		38	6.4			

a. Ref. 2.

b. Ref. 16

c. Ref. 24

The RPC calculations¹⁶⁾ with large deformation give M1 values of about two to three orders of magnitude large. This disagreement of the RPC results with the experiment is mainly due to the fact that the collective model is inherently incapable of taking into account the geometrical effects which forbid M1 transitions in $(f_{7/2})^n$ configurations. The microscopic DCM calculation reproduces the quadrupole collectivity and also the M1 hinderences.

2.2.2.3 (E2/M1) Mixing Ratios

These are given in table 81. The experimental²⁾ values have large errors. Our values are in general agreement with the observed values.

Table 81
Comparison of E2/M1 mixing ratios in ^{51}V .

J_i	J_f	Mixing ratios		
		$(\alpha, p \gamma)$ Ref. 2	DCM [*]	$(fp)^3$ Ref. 2
5/2	7/2	$-0.32^{+0.30}$	-0.54	-0.94
		-0.57		
		-0.47 ± 0.03		
3/2	5/2	$-8.8^{+4.1}$	-0.63	-3.7
		$-\infty$		
		-0.33 ± 0.11		
9/2	7/2	$+3.75^{+0.76}$	+2.93	+5.4
		-0.58		
11/2			0.42	

* $e_p = 1.32e$, $e_n = 0.89e$.

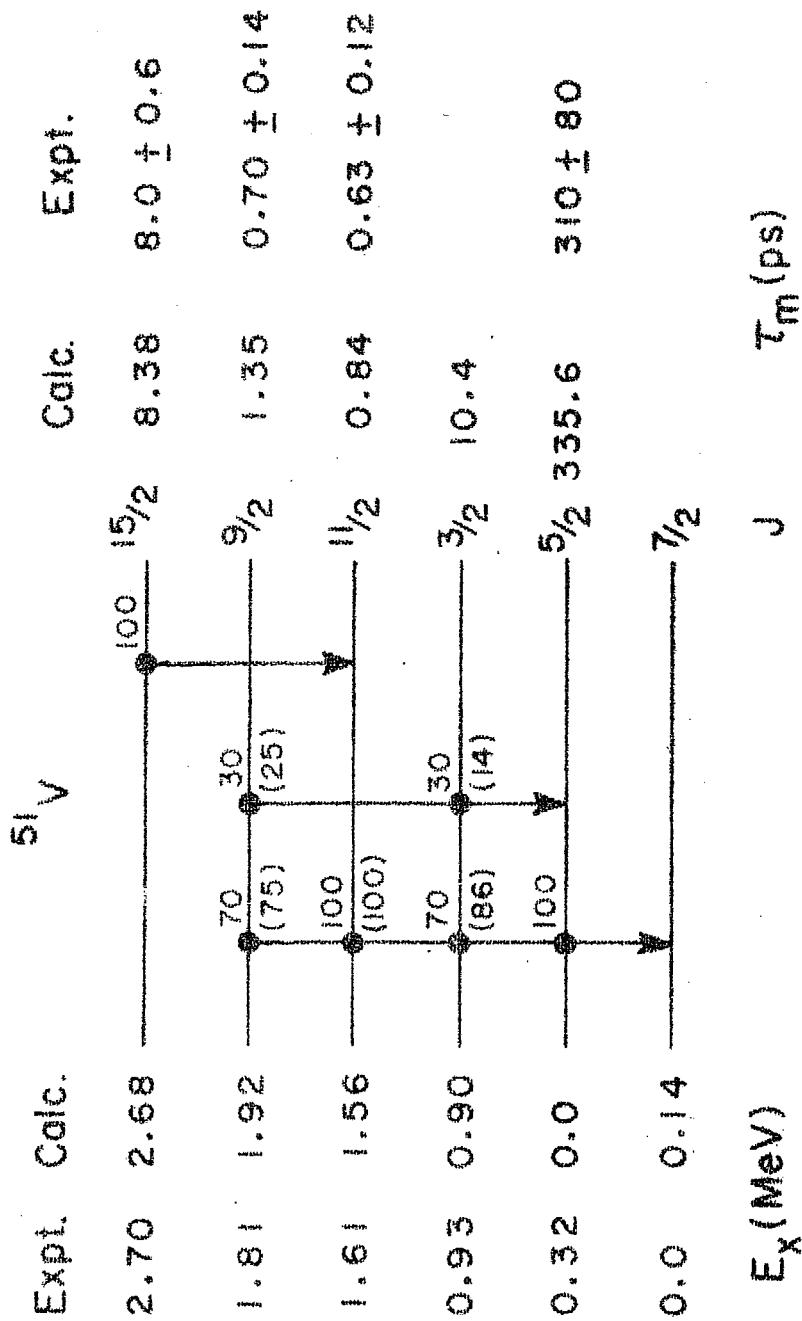


Fig.39

Mean lifetimes and Branching ratios for the transitions between the "spherical" states of ^{51}V . The observed decay intensities are given in parenthesis below the level while the calculated ones are given at the top.

2.2.2.4 Branching Ratios and Mean Lifetimes

These are presented in fig.39. Good agreement between the experimental^{2-5,25)} and calculated values is obtained.

2.2.2.5 Static Moments

These are presented in table 82. The calculated results are in agreement with the experimental²⁶⁻²⁸⁾ values.

Table 82

Static moments of the first few states in ^{51}V

J	E_J MeV	$Q(e\text{ fm}^2)$				μ (n.m.)		
		Expt. ^a	DCM [*]	(fp) ^{3d}	(f _{7/2}) ^{3d}	Expt.	DCM	(fp) ^{3d}
7/2	0	-5.2 \pm 1.0	-6.0	-6.4	-6.8	5.148	5.11	5.52
5/2	0.32		-14.8	-13.0	-19.0	4.2 \pm 0.7 ^b	3.52	3.84
						3.86 \pm 0.03 ^c		
3/2	0.93		13.7				1.88	

* $e_p = 1.32e$, $e_n = 0.89e$. a.Ref.26. b.Ref.27.c.Ref.28.d.Ref.2

2.3 THE HIGHLY DEFORMED EXCITED $K=3/2$ BAND

As mentioned in subsec.2.1 the MWH2 interactions gives rise to an excited prolate $K=3/2$ HF intrinsic state with quadrupole moment $Q_K = 31.5\text{ b}^2$ at only 1.25 MeV above the

less deformed prolate HF $K=3/2$ intrinsic state of ^{51}V .

The states with definite angular momenta projected from this highly deformed $K=3/2$ intrinsic states are almost orthogonal to the states projected from other intrinsic states listed in table 78 used for the calculations of the "spherical states" in ^{51}V . These projected states are also not altered from their unperturbed positions by the mixing due to Hamiltonian of the states projected from this intrinsic state and those of table 78.

The spectrum of this band^{18,19)} of states in ^{51}V is plotted in fig.38B. The experimental spectrum of ^{51}V does not contain such states so low in energy. It is likely that the chosen effective interaction does not reproduce correctly the position of the band head and that such a collective band may indeed exist at a somewhat higher energy.

Table 83

Calculated $B(E2)$ and $B(M1)$ values for transitions between the members of the prolate $K=3/2$ excited band in ^{51}V .

$J_i \rightarrow J_f$	$B(E2)^*$ $e^2 \text{ fm}^4$	$B(M1)$ $(\text{n.m.})^2$
5/2 → 3/2	614.71	0.27
7/2 → 3/2	258.30	
→ 5/2	399.22	0.41
9/2 → 5/2	372.0	
→ 7/2	240.41	0.37
11/2 → 7/2	444.01	
→ 9/2	186.22	0.55
13/2 → 9/2	460.46	
→ 11/2	115.51	0.37

* $e_p = 1.32e$, $e_n = 0.89e$.

In table 83 are presented the $B(E2)$ and $B(M1)$ values for the intraband transitions between the members of this excited band. It is seen that these transitions are quite large compared to those for the 'ground state band'. Because of the near purity of these states, the crossover transitions from the members of this band to those with the dominant $(f_{7/2})^3$ multiplet, are extremely hindered. Thus the $J=3/2$ member of this highly deformed band may be observed as an isomeric state.

REFERENCES

1. M.N.Rao and J.Rapaport, Nucl. Data Sheets B3 (1970) 37
(All references to previous experiments are given herein).
2. R.N. Horoshko, D. Cline and P.M.S. Lesser, Nucl.Phys.
A149 (1970) 562.
3. A.S. Goodman and D.J. Donahue, Phys. Rev.C5 (1972) 875.
4. E.N. Shipley, R.E. Holland and F.J. Lynch, Phys.Rev.182
(1969) and references therein.
5. A.R. Poletti, B.A. Brown, D.B. Fossan, P.Gorodetzky,
J.J. Kolata, J.W. Olness and E.K. Warburton, Phys.Rev.
C10(1974) 997.
6. H. Gogelein, R. Huber and C. Signorini, Proceedings of
the International Conference on Nuclear Physics, Munich,
1973, ed. J.de Boer and H.J. Mang (North Holland,
Amsterdam/American Elsevier, New York, 1973) Vol.I,
P.176.
7. D. Harrach, Proceedings of the International Conference
on Nuclear Physics, Munich, 1973, ed.J.de Boer and H.J.
Mang, (North Holland, Amsterdam/American Elsevier, 1973)
Vol.I, P.175.
8. R.D. Lawson and J.L. Uretsky, Phys. Rev. 106 (1957) 1369.
9. J.D. McCullen, B.F. Bayman and L. Zamick, Phys. Rev.
134 (1964) B515.
10. B.A. Brown, D.B. Fossan, J.M. McDonald and K.A. Snover,
Phys.Rev.C9 (1974) 1033.

11. N. Auerbach, Phys. Lett. 24B (1967) 260.
12. K. Lips and M.T. McEllistrem, Bull. Am. Phys. Soc. 14 (1969) 1205.
13. T.T.S. Kuo and G.E. Brown, Nucl. Phys. A114 (1968) 241.
14. E. Osnes and C.S. Warke, Nucl. Phys. A154 (1970) 331.
15. E. Osnes, Proceedings of the Topical Conferences on the Structure of $1f_{7/2}$ nuclei, ed. R.A. Ricci (Editrice Compositori, Bologna, 1971) P.79.
16. W. Scholz and F.B. Malik, Phys. Rev. 147 (1966) 836.
17. J.B. McGrory, B.H. Wildenthal and E. Halbert, Phys. Rev. C2 (1970) 186.
18. A.K. Dhar, S.B. Khadkikar, D.R. Kulkarni and K.H. Bhatt, Proceedings of the International Conference on Gamma-ray Transition Probabilities, New Delhi, 1974, ed. S.C. Pancholi and S.L. Gupta (Delhi Univ. Press, to be published).
19. A.K. Dhar, S.B. Khadkikar, D.R. Kulkarni and K.H. Bhatt, Nucl. Phys. and Solid State Phys. (India) 17B (1974) 246.
20. A.K. Dhar, S.B. Khadkikar, D.R. Kulkarni and K.H. Bhatt, Proceedings of the International Conference on Self Consistent Field Theories in Nuclei, Trieste, 1975, ed. by G. Ripka, p.83.
21. A.K. Dhar, unpublished.
22. T.T.S. Kuo and E. Osnes, Phys. Rev. C12 (1975) 309.

23. A.K. Dhar and K.H. Bhatt, to appear in Nucl.Phys.'A' and Phys.Rev.'C'.
24. P.G. Bizzetti, Proceedings of the Topical Conference on the Structure of $1f_{7/2}$ Nuclei, 1971, ed. R.A. Ricci (Editrice Compositori, Bologna, 1971), p.393.
25. Nuclear Level Schemes A=45 Through A=257 (Academic Press, Inc. New York and London, 1973).
26. W.J. Childs, Phys. Rev. 156 (1971) 71.
27. I.Y. Krause, Phys. Rev. 129 (1963) 1330.
28. L. Keszthelyi, I. Demeter, Z. Szoskefalvi-Nagy, L. Varga and Z. Zamori, Nucl. Phys. A120 (1968) 540.

PART V

CHAPTER 11

STRUCTURE OF ^{49}Cr

INDEX

CHAPTER 11

STRUCTURE OF ^{49}Cr

1.	INTRODUCTION	318
1.1	Experimental Data	318
1.2	Previous Calculations	319
2.	PRESENT CALCULATIONS	319
2.1	Calculation of Energy Spectrum	319
2.2	Comparison of the Calculated and Observed Spectrum	323
2.3	Electromagnetic Properties	325
	REFERENCES	341

CHAPTER 11

STRUCTURE OF ^{49}Cr

1. INTRODUCTION

1.1 Experimental Data

The nucleus ^{49}Cr is the maximally quadrupole deformed odd-A nucleus in the 1f-2p shell. The ground state band of this nucleus has been populated by Sawa et al.¹⁾ in (α, n) reaction studied at $E_\alpha = 14.2$ MeV and by Blasi et al.²⁾ by performing the heavy-ion induced reactions $^{40}\text{Ca}(^{12}\text{C}, 2pn)$ and $^{40}\text{Ca}(^{14}\text{N}, \alpha p)$ at 20-62 MeV ^{12}C beam and 28-62 MeV ^{14}N beam energies. Blasi et al.²⁾ have also provides some information on decay modes, lifetimes and mixing ratios of some of the members of the ground state band and other high-spin states of this nucleus. Bluementhal et al.³⁾ studied the (α, γ) angular correlation in $^{50}\text{Cr}(^3\text{He}, \alpha \gamma) ^{49}\text{Cr}$ reaction to determine the spins of the excited states and measured the branching ratios for the decays of various observed levels. They also deduced (E2/M1) mixing ratios for some of the transitions in ^{49}Cr . Zurmuhle et al.⁴⁾ in their $(p, n\gamma)$ reaction made lifetime measurements of levels below 3 MeV excitation in ^{49}Cr , using doppler-shift attenuation and recoil-distance methods. Zurmuhle et al also deduced from these measurements in combination with known mixing ratios,

the $B(E2)$, $B(M1)$ values for the transitions between the first four members of ^{49}Cr spectrum.

1.2 Previous Calculations

The $(f_{7/2})^9$ configuration model calculation for ^{49}Cr have been performed by Ginocchio⁵⁾. The agreement of this calculation with the observed spectrum is not very good. The other calculations for this nucleus are of Malik and Scholz⁶⁾, Zurmuhle et al⁴⁾ and recently of Haas et al⁷⁾ all based on RPC model.

We have performed DCM calculations based on projected HF theory for the nucleus ^{49}Cr . MWH2 effective interaction^{8,9)} and ^{41}Ca single particle energies are used. In this chapter we shall discuss first the energy spectrum and then the electromagnetic transition probabilities between the low-lying states of this nucleus. We shall also compared our results with those obtained in RPC model calculations.

2. PRESENT CALCULATIONS

2.1 CALCULATION OF THE ENERGY SPECTRUM

2.1.1 The Intrinsic States

Both prolate and oblate HF intrinsic states $\chi_K(?)$ have been obtained for the nucleus ^{49}Cr . The single-particle

states with $|k| = 1/2, 3/2$ and $5/2$ are occupied in the prolate HF $K=5/2$ intrinsic state. The energy of this intrinsic state is -26.89 MeV. The states with $|k| = 7/2, 5/2$ and $3/2$ are occupied in the oblate HF state at -24.10 MeV.

In addition to these HF states, the lowest four one particle-one hole excited intrinsic states based on prolate and oblate HF states have been included in the calculation. These are listed in table 84.

Table 84

K-values and energies E_K of the prolate and oblate HF states of ^{49}Cr and of the intrinsic states obtained by lp-lh excitations from these HF states. For other details see caption for fig.3.

Shape	Hole k_i	Prolate k_m	K	E_K (MeV)
Prolate	(HF STATE)		5/2	-26.89
	n 5/2	n 1/2'	1/2	-25.97
	n -3/2	n -5/2	3/2	-24.35
	p -3/2	p -5/2	3/2	-24.06
<hr/>				
Oblate	(HF STATE)		3/2	-24.10
	n 3/2	n 1/2	1/2	-23.19

The HF state and the intrinsic states obtained by exciting the odd neutron, have isospin $T=1/2$. Therefore angular momentum states projected from these intrinsic states

would have good isospin. For the intrinsic states involving the excitation of a paired nucleon, the $T=3/2$ isospin component is significantly large leading to considerable isospin mixing in the projected states. The isospin components with $T \geq 5/2$ are negligibly small in all these intrinsic states. In our calculations, we have considered intrinsic states involving similar excitation of a paired proton and separately of a paired neutron as well. This would result in the final spectrum of wave functions which would be expected to have a definite isospin.

It should be mentioned that the MWH2 interaction chosen for the present calculation produces prolate HF intrinsic state of ^{49}Cr corresponding to the deformation $^{9)} \delta \simeq 0.15$. This is in contrast to the RPC calculation of Zurmuhle et al $^{4)}$, and of Haas et al $^{7)}$ where intrinsic states corresponding to a large deformation $\delta = 0.24$ have been considered.

2.1.2 Energy Spectrum and Nonorthogonality of the Projected States

The states $\psi_{MK}^J(\gamma)$ with definite angular momentum have been projected from each of the six intrinsic states $\chi_K(\gamma)$ included in this calculation. Except for the states projected from the prolate $K=5/2$ HF and $K=1/2$ excited intrinsic states, all other projected spectra show a considerable departure from $J(J+1)$ sequence. It is found that

none of the angular momentum states projected from the intrinsic states other than the prolate $K=5/2$ and $1/2$ states, lies below about 3.5 MeV. It is therefore expected that the low-lying negative parity states of ^{49}Cr would be, to a large extent, those corresponding to the prolate $K=5/2$ and $1/2$ intrinsic states alone.

The states $\psi_{MK}^J(\eta)$ projected from different intrinsic states $\chi_K(\eta)$ are, in general, not orthogonal to each other. However, of particular interest are the states projected from the prolate $K=1/2$ excited intrinsic state obtained by odd neutron excitation from the $k=5/2$ single particle orbital to the $k=1/2'$ unoccupied orbital of the prolate HF state. All the angular momentum states (upto $J=19/2$) projected from this $K=1/2$ intrinsic state have very small overlaps with all other states of definite J projected from other intrinsic states. This indicates the possibility of the existence of a well defined band of states projectable from this $K=1/2$ intrinsic state. This is quite analogous to ^{47}Ti wherein a similar $K=1/2$ band of states has been predicted to exist.

2.1.3 Composite Spectrum

The composite spectrum of ^{49}Cr has been obtained by diagonalizing the Hamiltonian in the basis of orthonormalized

states projected from the six intrinsic states mentioned above. The resulting spectrum is plotted in fig.40. It turns out that the states projected from the prolate $K=5/2$ HF intrinsic state and the $K=1/2$ 1p-1h excited intrinsic state mix very weakly with the other projected states. The other projected states are mixed considerably by the Hamiltonian.

2.2 COMPARISON OF THE CALCULATED AND OBSERVED SPECTRUM

In fig.40 we have compared the calculated and observed spectrum of ^{49}Cr . In the calculated spectrum the states drawn in thick lines are the members of the ground state band^{10,11}). Except for the $J=15/2$ state at 3.05 MeV the average band mixing in the calculated ground state band upto $J=17/2$ state at 4.23 MeV is only about 2 percent. For the $J=15/2$ and $19/2$ states at 3.05 and 4.40 MeV, the intensity of the $J=15/2$ and $19/2$ states projected from the $K=5/2$ HF state is about 62 and 29 percent respectively.

The states drawn in thick dotted lines in the calculated spectrum belong to the $K=1/2$ band. The band mixing due to Hamiltonian is extremely small for all the members of this band upto $J=19/2$.

The other states drawn in thin lines have a complex structure with large band mixing.

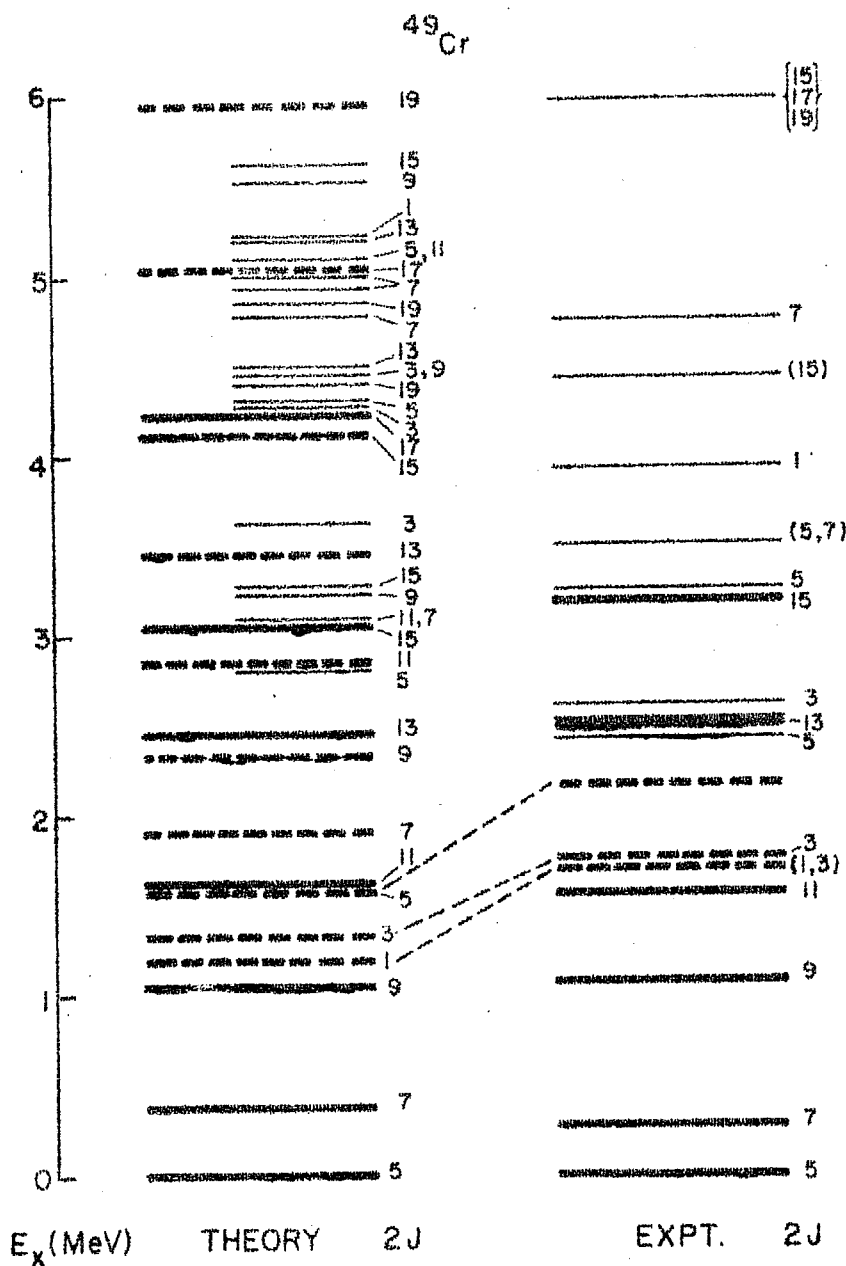


Fig. 40

Comparison of the calculated and the experimental spectrum of ^{49}Cr . The states drawn in thick lines are the members of the ground state band; those in dotted lines are the members of the $K=1/2$ band. More complex states are drawn in thin half lines.

The spectrum of the experimental ground state band observed by Blasi et al²⁾ and Sawa et al¹⁾, drawn in thick lines in fig.40 agrees very well with our calculated one. It is surprising that although Blasi et al²⁾ have observed high-spin states upto about 6 MeV, they have not reported the $J=17/2$ member of the ground state band expected to occur at 4.23 MeV.

It is likely that the observed $J=1/2$ and $3/2$ states at 1.70 and 1.74 MeV, drawn in thick dotted lines, may correspond to the calculated $J=1/2$ and $3/2$ members of the $K=1/2$ band. The decay properties of the observed state at 2.17 MeV, which we shall soon discuss, suggest that this state may be the $J=5/2$ member of the $K=1/2$ band. It thus appears that the calculated $K=1/2$ band is shifted downward by about 500 keV compared to the experiment.

There is no experimental information which allows us to identify in the observed spectrum the other members of the $K=1/2$ band. For the same reason it is not possible to suggest a correspondence between the remaining calculated and experimental states, except for the states observed²⁾ at 4.37 and 5.97 MeV with $J=15/2$ and $(15/2^-, 17/2^-, 19/2^-)$ as probable spin assignments.

A significant discrepancy between the experimental and calculated spectrum is that the calculated spectrum does

not have a $J=3/2$ state corresponding to the observed $3/2$ state at 2.61 MeV. This discrepancy may be removed if the configuration space is enlarged to include about 10 intrinsic states for each J . This expectation is supported by the fact that in ^{47}Ti , a calculation¹²⁾ in the space of ten projected states for each J , reproduces quite well the spectrum of the $J=1/2$ and $3/2$ states upto 6 MeV excitation.

2.3 ELECTROMAGNETIC PROPERTIES

In this section we shall discuss^{11,13)} the electromagnetic properties of the low-lying states of ^{49}Cr . For the calculation of electric properties, effective charges $e_p = 1.32e$ and $e_n = 0.89e$ while for magnetic properties, values of free nucleon g -factors are used.

We shall compare the results of our DCM calculation, with the available experimental data and also with those of the RPC calculations.

2.3.1 Ground State Band

This band of states is shown by thick lines in fig.40. The experimental¹⁻⁴⁾ information on $B(E2)$, $B(M1)$, $(E2/M1)$ mixing ratio, branching ratio and lifetimes for transitions within this band has been obtained for the states upto $J=11/2$. In addition to the DCM results, we have also given for compari-

Table 85

B(E2) values in $e^2 \text{fm}^4$ for transitions within the ground state band of ^{49}Cr .

$J_i \rightarrow J_f$	Present				RPC	
	Expt. ^a	DCM [*]	PHF [*]	DCM ⁺	Haas ^b et al	Zurmuhle ^a et al
7/2 5/2	302 \pm 79	431	462	354	290	377
9/2 5/2	160	124	128	103	86	129
7/2	310 $^{+260}_{-110}$	349	384	289	251	379
11/2 7/2	133 $^{+66}_{-110}$	207	214	172	150	185
9/2	505 $^{+620}_{-230}$	251	291	204	189	293
13/2 9/2		254	265	210	191	
11/2		182	218	149	145	
15/2 11/2		204	295	170	243	
13/2		81	169	63	108	
17/2 13/2		305	309	249	241	
15/2		63	129	50	86	
19/2 15/2		92	317	78		
17/2		18	105	14		

* $e_p = 1.32e$, $e_n = 0.89e$. + $e_p = 1.5e$, $e_n = 0.5e$.

a. Ref. 4

b. Ref. 7

son the $B(E2)$ and $B(M1)$ values obtained with the wave functions projected from the $K=5/2$ HF state. These results are listed as PHF in the tables.

2.3.1 $B(E2)$ Values

These are listed in table 85. The DCM values, in col.4, obtained with the effective charges¹⁴⁾ $e_p=1.32e$ and $e_n=0.89e$ are little larger than the observed values which have large errors. On the other hand the DCM values obtained by using $e_p=1.5e$ and $e_n=0.5e$ and listed in col.6, appear to be in a better agreement with the experimental values. The RPC calculated $B(E2)$ values obtained by Haas et al⁷⁾ are somewhat smaller than our values while those of Zurmuhle et al⁴⁾ are quite similar to our values. It may, however, be recalled that in these RPC calculations intrinsic states corresponding to deformation $\delta=0.24$ have been found to give optimum agreement for the observed spectrum and $B(E2)$ values. In contrast our intrinsic states correspond to $\delta \sim 0.15$.

2.3.1.2 $B(M1)$ Values

These are given in table 86. The experimental values are of Zurmuhle et al⁴⁾. The calculated $B(M1)$ values are large and therefore it is expected that the members of the ground state band of ⁴⁹Cr would decay preferentially by $M1$ mode. This is in agreement with the heavy-ion reaction

measurements of Blasi et al.²⁾ who found that all the γ -rays emitted upto 3.19 MeV $J=15/2$ state showed a M1 shape. The calculated $B(M1)$ value of 0.36 (n.m.)^2 for the $7/2 \rightarrow 5/2$ transition is almost twice its observed⁴⁾ value. Otherwise the agreement between our DCM results and the experiment is good.

Table 86

$B(M1)$ values in $(\text{n.m.})^2$ for transitions within the ground state band of ^{49}Cr .

$J_i \rightarrow J_f$	Expt. ^a	DCM	PHF	RPC	
				Hass ^b et al	Zurmuhle ^a et al
7/2 5/2	0.15 ± 0.04	0.36	0.40	0.15	0.06
9/2 7/2	$0.40^{+0.20}_{-0.10}$	0.59	0.58	0.24	0.18
11/2 9/2	0.57 ± 0.20	0.70	0.69	0.38	0.34
13/2 11/2		0.72	0.72	0.34	
15/2 13/2		0.74	0.80	0.54	
17/2 15/2		0.35	0.74	0.36	
19/2 17/2		0.43	0.86		

a. Ref.4.

b. Ref.7.

Except for the $17/2 \rightarrow 15/2$ and $19/2 \rightarrow 17/2$ transitions, all other $B(M1)$ values obtained in the DCM calculations are not very different from their PHF results. The RPC

calculated $B(M1)$ values obtained by Haas et al⁷⁾ and Zurmuhle et al⁴⁾ are significantly different from our results.

2.3.1.3 (E2/M1) Mixing Ratios

These are given in table 87. The observed values are of Sawa et al¹⁾ and of Zurmuhle et al⁴⁾. The agreement between

Table 87

(E2/M1) mixing ratios for transitions between the members of the ground state band of ⁴⁹Cr.

$J_i \rightarrow J_f$	(E2/M1)		
	Expt. ^a	DCM	RPC ^c
7/2 → 5/2	+0.14±0.02	+0.08	+0.10
9/2 → 7/2	+0.21±0.03 +0.19±0.04 ^b	+0.17	+0.22
11/2 → 9/2	+0.05±0.03 +0.12±0.03 ^b	+0.08	+0.09
13/2 → 11/2	+0.03±0.03	+0.12	+0.16
15/2 → 13/2		+0.06	+0.08
17/2 ^d → 15/2		+0.12	
19/2 ^d → 17/2		+0.01	

a.Ref.1. b.Ref.4. c.Ref.7.d.Theoretical excitation energy.

the DCM calculated and observed values is on the whole good. That the mixing ratios for all the transitions is less than +0.20 is also supported by the observations of Blasi et al²⁾. The calculated value of +0.07 in comparison to the observed

value of $+0.14 \pm 0.02$ for the $7/2 \rightarrow 5/2$ transition is because our calculated $B(M1)$ values for this transition is about twice the observed $B(M1)$ value. For the $13/2 \rightarrow 11/2$ transition the experimental value is smaller than the calculated value.

2.3.1.4 Branching Ratios

In fig.41 are compared the experimental^{3,4)} and calculated branching ratios for the low-lying states of ^{49}Cr . The DCM calculated branching ratios are given on top of the level from which the transitions are considered. The corresponding experimental ratios are given in parenthesis below the level. Of interest, here, are the branching ratios for transitions between the members of the ground state band drawn in thick lines in fig.41.

The agreement between the calculated and observed branching ratios for the decays upto $J=11/2$ at 1.56 MeV is very good. It is seen that the dominant decay mode of all the members of the ground state band is of $M1$ character. This is in qualitative concurrence with the measurements of Blasi et al²⁾.

The branching ratios obtained by the RPC calculations⁷⁾ are similar to ours.

2.3.1.5 Mean Lifetimes

The lifetimes of some of the transitions between the

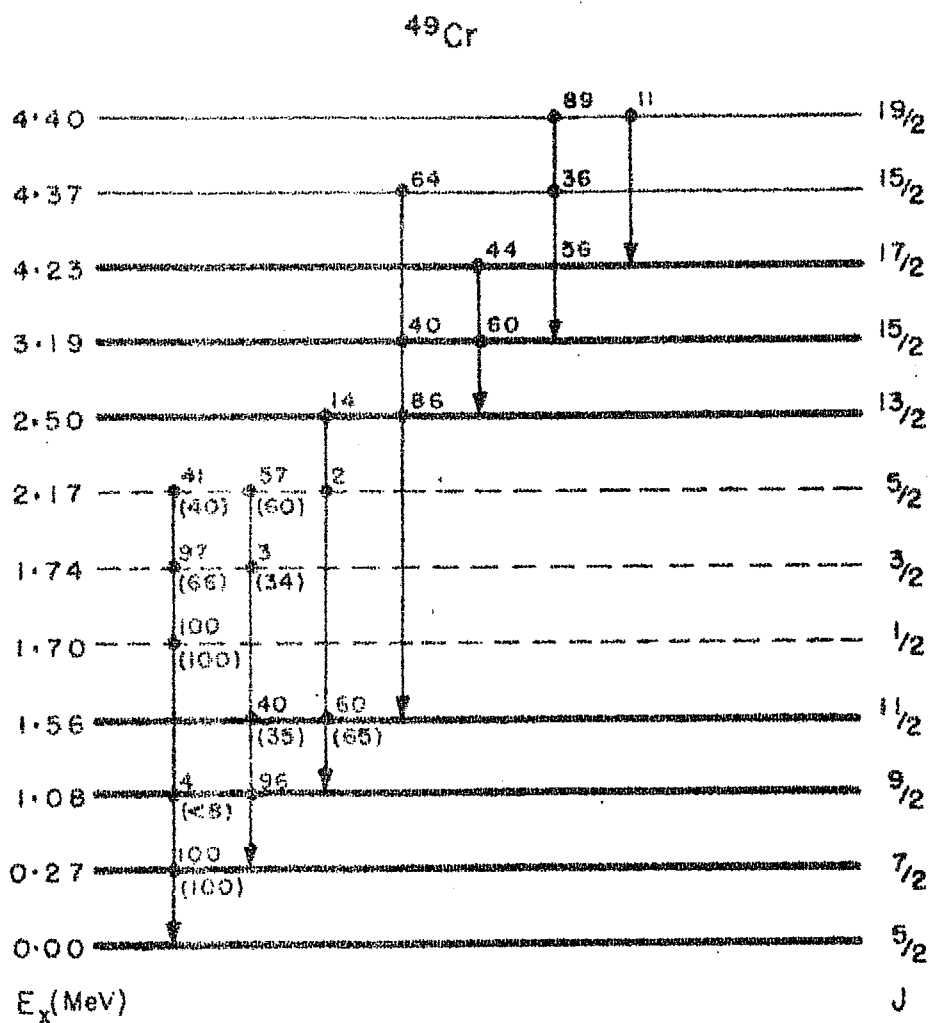


Fig.41

Calculated and experimental branching intensities in ^{49}Cr . The states drawn in thick lines belong to the ground state band. Those in dotted lines belong to the excited $K=1/2$ band. The numbers on the top are the calculated decay intensities while those below in parenthesis are the corresponding experimental values.

low-lying states of ^{49}Cr have been measured by Zurmuhle et al.⁴⁾. In table 88 are compared our DCM calculated mean lifetimes with the observed and RPC results. For the $7/2 \rightarrow 5/2$ transition our calculated value is very small compared to RPC or experimental value. This is because our $B(M1)$ value for this transition is larger than the observed $B(M1)$ value.

Table 88

Mean lifetime of the members of the ground state band of ^{49}Cr .

J	τ (ps)		
	Expt ^a	DCM	RPC ^b
7/2	19 ± 5^c	8	19
9/2	0.26 ± 0.09	0.17	0.40
11/2	$0.59^{+0.30}_{-0.12}$	0.44	0.72
13/2		0.08	0.16
15/2		0.14	0.16
17/2 ^d		0.08	0.03

a. Ref. 2. c. Ref. 7. c. See also Ref. 4.

d. Theoretical excitation energy.

2.3.1.6 Static Moments

In table 89 are given the static electric quadrupole and magnetic dipole moments of the first three states of ^{49}Cr . Experimental measurements of the quadrupole moments

Table 89

Static moments of first few states of ^{49}Cr .

J	E_J MeV	$Q(\text{efm}^2)$		$\mu(\text{n.m.})$		
		DCM	RPC ^a	Expt. ^b	DCM	RPC ^a
5/2	0.0	39.3	32	$\pm 0.48 \pm 0.01$	-0.52	-1.22 ^c
7/2	0.27	7.7	5.6		0.45	-0.92
9/2	1.09	-10.4			1.51	
a. Ref. 7.		b. Ref. 15, 16.		c. See also Ref. 4.		

are not yet available. Our calculations predict the ground state quadrupole moment of about 39 efm^2 .

The magnitude of the ground state magnetic moment is measured by Sanner et al¹⁵⁾ and Jonsson et al¹⁶⁾ using atomic beam resonance technique. Our calculated value is in very good agreement with the observed value. RPC model results of Haas et al⁷⁾ and Zurmuhle et al⁴⁾ give a considerably larger value. It would be interesting to measure the sign of the ground state magnetic moment and its quadrupole moment. For the $J=7/2$ state at 0.27 MeV, our calculation predicts a positive magnetic moment of 0.45 (n.m.). This is in contrast to the predictions of RPC model calculations⁷⁾.

2.3.2 Excited $K=1/2$ Band

In fig. 42 we present the results of our DCM calculations of the $B(E2)$ and $B(M1)$ values for the transitions between the

CAPTION FOR FIGURE 42

Spectrum and transitions within the $K=1/2$ band in ^{49}Cr . This band is split into two sub-bands on the basis of pure E2 transitions. The magnitude of $B(E2)$ values (in $e^2\text{fm}^4$) obtained in the DCM calculation are given along the side of thick arrows. The $B(E2)$ and $B(M1)$ (in $(\text{n.m.})^2$) values for the transitions between these sub-bands are given above and below the thin arrows respectively.

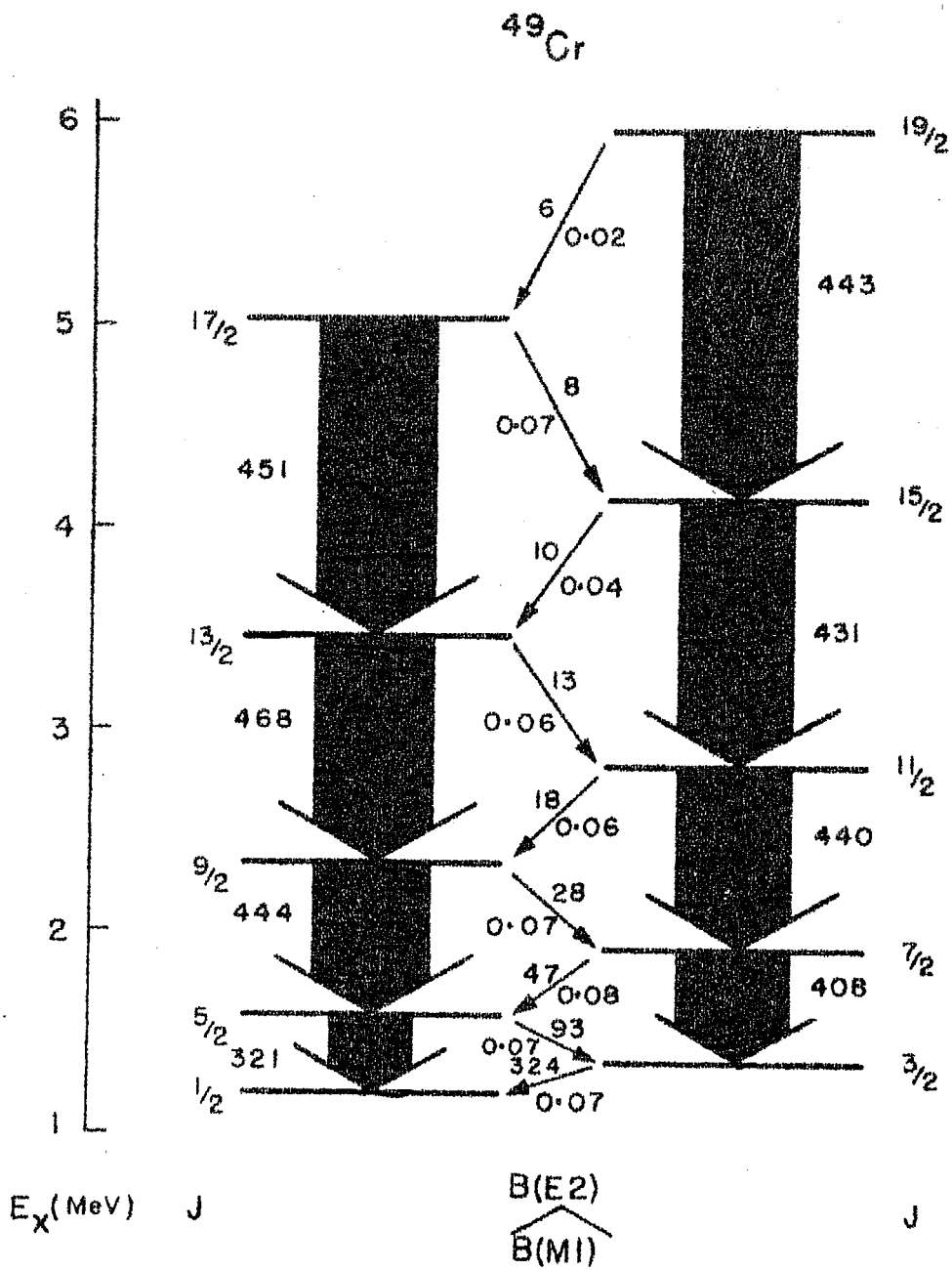


Fig.42

members of the $K=1/2$ band. The band splits into two bands: one with spins $J=1/2, 5/2, 9/2, 13/2$ and $17/2$ and the other with $J=3/2, 7/2, 11/2, 15/2$ and $19/2$. The $B(E2)$ values for transitions between the members of these sub-bands are large and have roughly the same value except the $B(E2)$ for the $5/2 \rightarrow 1/2$ transition. The $E2$ as well as $M1$ transitions between these two sub-bands are weak. Here the $B(M1)$ values are approximately the same for all the transitions except for the $19/2 \rightarrow 17/2$ and for the $15/2 \rightarrow 13/2$ transitions. Another significant exception is the large $B(E2)$ value of $324 \text{ e}^2 \text{ fm}^4$ for the $3/2 \rightarrow 1/2$ transition.

Unfortunately no experimental information on these transitions is yet available. It is not possible therefore to identify the members of this band on the basis of their intraband transitions.

2.3.3 Interband Transitions

In this section we attempt to identify in the experimental spectra the states belonging to the $K=1/2$ band on the basis of their decay properties to the member of the ground state band. According to our calculations these decays should be highly hindered. In table 90 we have listed the $B(E2)$ and $B(M1)$ values for transitions from the $J=1/2-9/2$ states of the $K=1/2$ band to the $J=5/2-11/2$ states of the $K=5/2$ ground state band.

Table 90

Calculated $B(E2)$ and $B(M1)$ values for the transitions between some of the members of the $K=1/2$ band and the ground state band of ^{49}Cr .

E_i^{cal} (MeV)	E_f^{expt}	J_i	J_f	$B(E2)$ $e^2 \text{fm}^4$	$B(M1)$ (n.m.) ²
1.20	0.0	1/2	5/2	2.55	
1.34	0.0	3/2	5/2	0.88	0.0041
	0.27		7/2	1.53	
1.58	0.0	5/2	5/2	0.24	0.002
	0.27		7/2	1.20	0.004
	1.08		9/2	1.02	
1.90	0.0	7/2	5/2	0.01	0.000006
	0.27		7/2	0.21	0.0066
	1.08		9/2	1.02	0.0093
2.33	0.27	9/2	7/2	0.17	0.001
	1.08		9/2	0.78	0.0069
	1.56		11/2	0.84	0.0083

Zurmuhle et al.⁴⁾ have found that the 1.70, 1.74 and 2.17 MeV levels (indicated by dotted line in fig. 41) decay weakly to the 5/2 and 7/2 members of the ground state band which we now discuss. The decay properties of the states are similar to those of the calculated $J=1/2, 3/2$ and $5/2$ members of the $K=1/2$ band.

The 1.70 MeV state decays only to the $J=5/2$ ground

state. If a $J=1/2$ assignment is assumed for this level, Zurmuhle et al.⁴⁾ find that $B(E2)$ value is less than 0.95 W.U. Our calculated $B(E2)$ value for the transition from the $J=1/2$ state of the $K=1/2$ band to the $J=5/2$ ground state is 0.2 W.U.

The $J=3/2$ state at 1.74 MeV decays both to the $J=5/2$ and $7/2$ members of the ground state band with 66:34 branching. Zurmuhle et al.⁴⁾ have observed a retardation of about 10^{-4} or 10^{-5} in $B(M1)$ values for the $3/2 \rightarrow 5/2$ ground state transition. Similarly in case of the $B(E2)$ value the retardation of either about 7×10^{-4} or about 0.75 W.U. is observed. The calculated $B(M1)$ and $B(E2)$ values for the corresponding decays of the $J=3/2$ member of the $K=1/2$ band are about 10^{-3} and 0.08 W.U.

It may however be pointed out that in contrast to the observed⁴⁾ branching ratios from the $J=3/2$ state at 1.742 MeV, our calculated $J=3/2$ state, at that energy, decays with a 97% branch to the $J=5/2$ ground state. This discrepancy is however not serious since the $B(M1)$ and $B(E2)$ values are extremely hindered and such hindered transitions would not be reproduced very accurately by our calculations. In order to reproduce the observed 66 and 34 percent branches of the $J=3/2$ level the calculated $B(M1)$ value for the $3/2 \rightarrow 5/2$ transition should be 0.0001 (n.m.)^2 compared to our

value of 0.0041 (n.m.)^2 . The mean lifetime of the calculated $J=3/2$ state is obtained to be 2.5 ps. This compares well with the observed lifetime of about 4 ps.

Zurmuhle et al.⁴⁾ have observed a state of unassigned spin at 2.17 MeV. This state is observed to decay with a 40 and 60 percent branch to the ground and first excited state of ^{49}Cr . The mean lifetime of this state is measured to be about 4.5 ps. We have associated in turn our calculated $J=5/2, 7/2$ and $9/2$ members of the $K=1/2$ band and also the $J=5/2$ state calculated at 2.75 MeV, with the observed 2.17 MeV level. The only calculated state that fits well with the decay modes of the 2.17 MeV is the $J=5/2$ member of the $K=1/2$ band. As shown in fig.41 this state at that energy decays with 41 and 57 percent branches in excellent agreement with the experiment. The calculated mean lifetime of this state is 1.1 ps. We therefore suggest that the 2.17 MeV observed level has $J=5/2$ and is the third member of the $K=1/2$ band.

It appears from these considerations that the observed states at 1.70, 1.74 and 2.17 MeV may be the $J=1/2, 3/2$ and $5/2$ members of the $K=1/2$ band. As shown in fig.40 the calculated band is shifted downwards by about 500 keV compared to the observed band. Such relative shifts between the calculated and observed excited bands also occur¹⁷⁾ in the sd shell.

The other members of the $K=1/2$ band do not yet have the experimental counterparts. It would be interesting to undertake an experimental investigation of this band of states built on the $K=1/2$ intrinsic state.

2.4 OTHER STATES

Among the low-lying states of ^{49}Cr observed upto about 3 MeV (see fig.40) excitation, we have thus far, discussed all the states except the ones observed⁴⁾ at 2.433 MeV with $J=5/2^-$, 2.504 MeV of unassigned spin and 2.614 MeV with $J=3/2^-$. Zurmuhle et al⁴⁾ have studied the decay properties of these states. Among other states, Blasi et al²⁾ have observed γ -decay from the levels at 4.367 MeV with tentative spin assignment ($15/2^-$) and from the 5.966 MeV level with probable spin assignment ($15/2^-$, $17/2^-$, $19/2^-$).

We have attempted to identify in the calculated spectrum the states that have decay properties similar to the above observed states.

2.433 MeV Level

Zurmuhle et al⁴⁾ have assigned $J=5/2$ for this level with an observed lifetime > 4 ps. This state has branching values 43:17:40 for the decays to $J=5/2^-$ ground state, $J=7/2^-$ at 0.272 MeV and to $J=3/2^+$ at 1.982 MeV. Thus the

decay intensities for transitions from this state to the negative parity states are in the ratio 2.5:1.

It is tempting to associate the calculated $J=5/2$ state at 2.79 MeV with this observed level. A difficulty of this association is that the calculated state decays with 25:75 percent branches to the ground and first excited states of ^{49}Cr with a lifetime of 31 fs.

2.504 MeV Level

No spin assignment have been made for this level. Lifetime of less than 12 fs is measured⁴⁾. This level has 80:20 percent branches to the ground and first excited state.

We have associated, in turn, each of our calculated state with $J=7/2, 9/2, 5/2, 11/2$ and $7/2$ at 1.90, 2.33, 2.79, 2.82 and 3.07 MeV respectively with this observed level at 2.504 MeV. The calculated $J=7/2$ state at 3.07 MeV has the corresponding branching ratios of 86:4 and lifetime of 39 fs. In fact this is the only state which provides a reasonable agreement with the decay properties of the observed 2.504 MeV level. Hence, we suggest a $J=7/2$ assignment to the 2.504 MeV observed level.

2.614 MeV Level

This level is assigned⁴⁾ $J=3/2^-$. We do not have a corresponding $J=3/2^-$ state about 2.6 MeV, in our calculated spectrum.

4.367 MeV Level

This level with a tentative $J=(15/2^-)$ is observed by Blasi et al²⁾ in the heavy-ion reaction measurements. They have suggested that this state is not a member of the ground state band and observed its decay to $J=15/2^-$ and $13/2^-$ members of the ground state band. The latter decay is weak. The $4.367 \text{ MeV} \rightarrow J=15/2$ at 3.19 MeV transition is observed to have a large quadrupole component. Mean lifetime greater than 0.6 ps is measured for this level.

In the calculated spectrum (fig.40), we have high-spin states with $J=15/2$, $17/2$ and $19/2$ within 4 to 5 MeV relative excitation energy. The $J=19/2$ assignment to the 4.367 MeV level is ruled out by the observed 4.367 MeV $J=13/2$ state decay. The $J=15/2$ state at 4.13 MeV , shown by dotted line, is the member of the $K=1/2$ band and decays with a 75 percent branch to the $J=11/2$ state of the $K=1/2$ band with a mean lifetime of 0.15 ps . This is in consistent with the observed decay pattern of the level under study.

The 4.23 MeV $J=17/2$ state of the ground state band, drawn in thick line, decays with 44 and 56 percent branches to the $J=13/2$ and $15/2$ members of the ground state band. The corresponding mean lifetime is 0.08 ps. Thus although the decay properties of the $J=17/2$ state calculated at 4.23 MeV are somewhat similar to the decay properties of the 4.367 MeV level, the lifetimes do not agree. It is thus not possible at this stage to associate the calculated $J=15/2$ or $17/2$ state uniquely with this observed ($15/2^-$) state.

REFERENCES

1. Z.P. Sawa, J. Blomqvist and W. Gullholmer, Nucl.Phys. A205 (1973) 257.
2. P. Blasi, R.B. Huber, W.Kutschera and C. Signorini, Proceedings of the International Conference on Nuclear Physics, Munich, 1973, ed.by J.de Boer and H.J. Mang (North Holland, Amsterdam/American Elsevier, New York, 1973) Vol.I, p.211.
3. D.A. Blumenthal, R.W. Zurmuhle and D.P. Balamuth, Phys. Rev. C4 (1971) 415.
4. R.W. Zurmuhle, D.A. Hutcheon and J.J. Weaver, Nucl.Phys. A180 (1972) 417.
5. J.N. Ginocchio, Phys. Rev.144 (1966) 952.
6. F.B. Malik and W. Scholz, Phys. Rev. 150 (1969) 919; 153 (1967) 1071.
7. B. Haas, P. Taras and J. Styczen, Nucl. Phys. A246 (1975) 141.
8. J.B. McGrory, B.H. Wildenthal and E.C. Halbert, Phys. Rev.C2 (1970) 186.
9. B.E. Chi, Nucl.Phys. 83 (1966) 97.
10. A.K. Dhar, D.R. Kulkarni and K.H. Bhatt, Proceedings of the International Conference on Nuclear Structure and Spectroscopy, Amsterdam, 1974, ed.by H.P. Blok and A.E.L. Dieperink (Scholar's Press, Amsterdam, 1974) Vol.I, p.59.

11. A.K. Dhar and K.H. Bhatt, Nucl. Phys. and Solid State Phys.(India) 18B (1975)
12. A.K. Dhar, D.R. Kulkarni and K.H. Bhatt, Nucl.Phys. A238 (1975) 340.
13. A.K. Dhar, D.R. Kulkarni, S.B. Khadkikar and K.H. Bhatt, Proceedings of the International Conference on Gamma-Ray Transition Probabilities, New Delhi, 1974, ed.by S.C. Pancholi and S.L. Gupta (Delhi Univ.Press, to be published).
14. A.K. Dhar, unpublished.
K.H. Bhatt, invited talk, Proceedings of the International Conference on Gamma-Ray Transition Probabilities New Delhi, 1974, ed.by S.C. Pancholi and S.L. Gupta, (Delhi Univ.Press, to be published).
15. L. Sanner, R. Djay, J.O. Jonsson, I. Lindgren, M. Olsmats, A. Rosen, B. Wannberg and K.E. Adelroth, Arkiv for Phys. 30 (1965) 540.
16. J.O. Jonsson, L. Sanner and B. Wannberg, Phys. Scrip.2 (1970) 16.
17. D.R. Kulkarni and S.P. Pandya, Nucl. Phys. and Solid State Phys. (India) 17B (1973) 153.

Appendix II

E2 Transitions in Even-Even Isotopes of Ti, Cr and Fe.

We present here very briefly the results¹⁾ of our E2 transitions in the ground state bands of states of the nuclei Ti ($A=44,46,48,50$), Cr ($48,50,52$) and Fe ($52,54$). The ground state bands have been obtained by projecting out states of good angular momenta from the lowest energy, less-deformed HF intrinsic states of these nuclei. MWH2 interaction is used. As already mentioned in chapter 1, this interaction gives for ^{52}Cr , HF state with more deformation slightly lower than the one with smaller deformation. However, the observed ground state band of ^{52}Cr corresponds to the states projected from the less deformed HF state. The calculated spectrum of the ground state band in these nuclei is in general found²⁾ to be compressed compared to the experimental one.

In table A-1 are given the contributions M_p and M_n (given by eq.45) of the protons and neutrons to the reduced matrix elements for the transitions between the first few members of the ground state bands of the nuclei under study. The $B(E2)$ values is then given by:

$$B(E2, J_i \rightarrow J_f) = \frac{1}{2J_i+1} | M_p e_p + M_n e_n |^2$$

where e_p and e_n are the corresponding proton and neutron

Table A-1

Proton and neutron reduced matrix elements (M_p and M_n) for the E2 transitions within the members of the ground state bands of states in even-even Ti, Cr and Fe isotopes.

Z	A	$2 \rightarrow 0$	$4 \rightarrow 2$	$6 \rightarrow 4$	$8 \rightarrow 6$
22	44	$12.00(e_p + e_n)$	$18.89(e_p + e_n)$	$22.69(e_p + e_n)$	$24.57(e_p + e_n)$
	46	$11.79e_p + 16.48e_n$	$18.62e_p + 26.16e_n$	$22.52e_p + 32.54e_n$	$24.23e_p + 37.56e_n$
	48	$10.58e_p + 14.51e_n$	$17.04e_p + 22.64e_n$	$20.08e_p + 28.63e_n$	$19.73e_p + 34.45e_n$
	50	$11.49e_p + 3.91e_n$	$15.96e_p + 5.87e_n$	$15.17e_p + 7.40e_n$	$6.26e_p + 19.42e_n$
44	48	$17.04(e_p + e_n)$	$27.06(e_p + e_n)$	$33.50(e_p + e_n)$	$38.08(e_p + e_n)$
	50	$15.89e_p + 15.09e_n$	$25.06e_p + 24.13e_n$	$30.55e_p + 30.40e_n$	$34.07e_p + 35.43e_n$
	52	$14.30e_p + 4.41e_n$	$21.18e_p + 7.64e_n$	$24.08e_p + 12.10e_n$	$25.75e_p + 16.06e_n$
26	52	$14.03(e_p + e_n)$	$22.05(e_p + e_n)$	$26.75(e_p + e_n)$	$29.49(e_p + e_n)$
	54	$13.16e_p + 3.31e_n$	$18.82e_p + 6.83e_n$	$18.25e_p + 12.47e_n$	

effective charges. The harmonic oscillator length parameter needed in the evaluation of M_p and M_n are deduced from the relation $\hbar\omega = 41A^{-1/3}$ MeV.

In table A-2 are compared the experimental³⁻⁸⁾ and calculated $B(E2)$ values for the transitions within the ground state bands of even-even Ti, Cr and Fe nuclei. In calculation I (Cal.I) effective charges $e_p=1.5e$ and $e_n=0.5e$ were used while in calculation II(Cal.II) effective charges obtained by a least squares fit between the calculated and experimental $B(E2)$ values for the $2 \rightarrow 0$ transitions were used. The best fitted values of the charges were obtained to be:

$$e_p = (1.32 \pm 0.16) e$$

and

$$e_n = (0.89 \pm 0.18) e$$

These values are similar to those obtained by Bohr and Mottelson⁹⁾ ($e_p=1.21e$, $e_n=0.79e$) in a macroscopic calculation but are slightly larger than those obtained by Kuo and Osnes¹⁰⁾ ($e_p=1.25e$, $e_n=0.47e$) in a microscopic calculation.

In general, the agreement between the calculated

Table A-2.

Comparison of the experimental and calculated $B(E2)$ values for transitions between the ground state bands of states in even-even Ti, Cr and Fe isotopes. In calculation I (Cal.I) effective charges $e_p = 1.5e$, $e_n = 0.5e$ are used while in calculation II (Cal.II) least squares fitted effective charges $e_p = 1.32e$, $e_n = 0.89e$ are used.

Nucleus		$2 \rightarrow 0$	$4 \rightarrow 2$	$6 \rightarrow 4$	$8 \rightarrow 6$
^{44}Ti	Expt.	$157 \pm 22^{4)}$	$280 \pm 60^{4)}$	$157 \pm 22^{4)}$	
		$120 \pm 30^{5)}$	$252 \pm 75^{7)}$		
	Cal.I	115	159	158	142
	Cal.II	141	194	193	173
^{46}Ti	Expt.	$160 \pm 34^{3)}$			
		$217 \pm 17^{5)}$	$177 \pm 20^{6,7)}$	$150 \pm 80^{6)}$	
	Cal.I	134	187	193	179
	Cal.II	183	254	265	252
^{48}Ti	Expt.	$140 \pm 28^{3)}$			
		$151 \pm 18^{5)}$	$95 \pm 22^{6,7)}$	$53 \pm 5^{4)}$	
	Cal.I	103	147	148	125
	Cal.II	145	202	208	189
^{50}Ti	Expt.	$66 \pm 8^{4)}$			
		$49 \pm 8^{5)}$	$60^{+14}_{-10}{}^{4)}$	$34.2 \pm 1.2^{4)}$	
	Cal.I	74	80	54	22
	Cal.II	70	77	57	38

- contd -

Table A-2 (contd)

Nucleus		$2 \rightarrow 0$	$4 \rightarrow 2$	$6 \rightarrow 4$	$8 \rightarrow 6$
^{48}Cr		$207 \pm 27^{8)}$	$317 \pm 176^{8)}$		
	Expt.	$350 \pm 100^{5)}$	$330 \pm 190^{5)}$		$> 320^{8)}$
	Cal. I	232	325	345	341
	Cal. II	284	397	421	417
^{50}Cr		$227 \pm 20^{4)}$			
	Expt.	$208 \pm 23^{5)}$	$160 \pm 20^{6,7)}$	$130 \pm 30^{6,7)}$	
	Cal. I	197	274	286	279
	Cal. II	237	331	349	344
^{52}Cr		$119 \pm 7^{4)}$			
	Expt.	$113 \pm 10^{5)}$	$82 \pm 17^{4)}$	$59.5 \pm 3.4^{4)}$	
	Cal. I	112	141	137	128
	Cal. II	104	134	139	137
^{52}Fe	Cal. I	158	216	221	205
	Cal. II	192	264	269	250
^{54}Fe		$102 \pm 4^{4)}$	$78 \pm 16^{4)}$		
	Expt.	$108 \pm 10^{5)}$	147	$39.8 \pm 0.5^{4)}$	
	Cal. I	92	111	87	
	Cal. II	83	106	95	

and experimental values is good. However the calculated $B(E2)$ values for the transitions between the higher members are slightly larger than the observed ones. It is likely that the DCM calculation for these nuclei may improve upon these results.

REFERENCES

1. A.K. Dhar, D.R. Kulkarni, S.B. Khadkikar and K.H. Bhatt, Proceedings of the International Conference on Gamma-Ray Transition Probabilities, Delhi (1974) ed.by. S.C. Pancholi and S.L.Gupta (Delhi Univ.Press, to be published).
2. A.K. Dhar - Unpublished.
3. P.H. Stelson and L. Grodzins, Nucl. Data 1H (1965) 2.
4. B.A. Brown, D.B. Fossan, J.M. McDonald and K.A. Snover, Phys. Rev.C9 (1974) 1033.
5. W. Kutschera, R.B. Huher, C. Signorini and P. Blasi, Nucl. Phys. A210 (1973) 531.
6. W. Dehndardt, O.C. Kistner, W. Kutschera and H.J. Sann, Phys. Rev. C7 (1973) 1471.
7. W. Kutschera - Private Communication.
8. B. Haas, P. Taras, J.C. Merdinger and R. Vaillancourt, Nucl. Phys. A238 (1975) 253.
9. A. Bohr and B.R. Mottelson, Nuclear Structure (Benjamin, New York, to be published), Vol.II, Chap.6; as quoted by B.A. Brown et al, Ref.4 above.
10. T.T.S. Kuo and E. Osnes, Phys. Rev. C12 (1975) 309.